Transforming Linseed Stalk Residue into Crystalline Nanocellulose as a Nanofiller for Polylactic Acid-Based Bio nanocomposite Filament in Fused Deposition Modeling 3D Printing

Kibrom Feleke Gebru

A Dissertation Submitted to the Department of Mechanical Engineering, College of Mechanical, Chemical and Materials Engineering

Presented in Fulfillment of the Requirement for the Degree of Doctor of Philosophy (Ph.D.) in Manufacturing Engineering

Office of Graduate Studies, Adama Science and Technology University

June, 2025

Adama, Ethiopia

Transforming Linseed Stalk Residue into Crystalline Nanocellulose as a Nanofiller for Polylactic Acid-Based Bio nanocomposite Filament in Fused Deposition Modeling 3D Printing

Kibrom Feleke Gebru

Supervisors:

Main Supervisor: Ganesh Thothadri (Assoc. Prof.)
Co–Supervisor: Habtamu Beri (Assoc. Prof.)

A Dissertation Submitted to the Department of Mechanical Engineering, College of Mechanical, Chemical and Materials Engineering

Presented in Fulfillment of the Requirement for the Degree of Doctor of Philosophy (Ph.D.) in Manufacturing Engineering

Office of Graduate Studies Adama Science and Technology University

June, 2025
Adama, Ethiopia

DECLARATION

I hereby declare that this PhD dissertation "***Transforming Linseed Stalk Residue into Crystalline Nanocellulose as a Nanofiller for Polylactic Acid-Based Bio nanocomposite Filament in Fused Deposition Modeling 3D Printing***" is my original work. That is, it has not been presented for the award of any academic degree, diploma or certificate in any other university. All sources of materials used for this thesis have been duly acknowledged through appropriate citations.

Kibrom Feleke Gebru

Name of student	Signature	Date

RECOMMENDATION

I/We, the supervisor (s) of this dissertation, hereby certify that I/We have read and revised the dissertation entitled *"**Transforming Linseed Stalk Residue into Crystalline Nanocellulose as a Nanofiller for Polylactic Acid-Based Bio nanocomposite Filament in Fused Deposition Modeling 3D Printing**"* prepared under my/our guidance by Kibrom Feleke Gebru, ID. No. PGR/18481/11 submitted in partial fulfillment of the requirements for the degree of Doctor of Philosophy (Ph.D.) in Manufacturing Engineering. Therefore, I/We recommend the submission of the dissertation.

Ganesh Thothadri (Assoc. Prof.)

Main Supervisor	Signature	Date

Habtamu Beri (Assoc. Prof.)

Co–Supervisor	Signature	Date

APPROVAL OF BOARD OF EXAMINERS

We, the undersigned, members of the board of examiners of the final open defense by Kibrom Feleke Gebru have read and evaluated his dissertation entitled "***Transforming Linseed Stalk Residue into Crystalline Nanocellulose as a Nanofiller for Polylactic Acid-Based Bio nanocomposite Filament in Fused Deposition Modeling 3D Printing***" and examined the candidate. This is therefore, to certify that the dissertation has been accepted in partial fulfilment of the requirement of the Degree of Doctor of Philosophy (Ph.D.) in Manufacturing Engineering.

Ganesh Thothadri (Assoc. Prof.)		
Main Supervisor	Signature	Date
Habtamu Beri (Assoc. Prof.)		
Co–Supervisor	Signature	Date
Chairperson	Signature	Date
Internal Examiner	Signature	Date
External Examiner 1	Signature	Date
External Examiner 2	Signature	Date

Finally, approval and acceptance of the dissertation is contingent upon submission of its final copy of the Office of Postgraduate Studies (OPGS) through the candidate's Department Graduate Council (DGC) and School Graduate Committee (SGC).

Department Head	Signature	Date
College Dean	Signature	Date
Postgraduate Dean	Signature	Date

ACKNOWLEDGEMENT

I would like to express my deepest gratitude to all those who have contributed to my journey in completing this dissertation.

First and foremost, I am thankful to Almighty God for protecting and helping me throughout this journey. Your strength and wisdom have been my constant source of inspiration, helping me navigate the challenges I faced along the way. Next, I am immensely thankful to my advisors, Dr. Ganesh Thothadri and Dr. Habtamu Beri, their guidance and support have been invaluable throughout this journey. Your insights and encouragement have inspired me to push the boundaries of my research.

I would also like to thank my doctoral committee members, for their constructive feedback and encouragement. Your expertise has greatly enhanced the quality of this work. Further, I acknowledge department of Mechanical Engineering, CoMCME, ASTU, Wachemo University and office of graduate studies ASTU that made this research possible. Moreover, I also thank department of Chemical Engineering, Materials Engineering, Chemistry, Physics and Biology for their laboratory support, cooperation and facilitation. I would like to express my deepest gratitude to Professor Hirpa G. Lemu and Dr. Wakshum Mekonnen for their greatest support for the SEM, TEM, and HRTEM characterization of at Faculty of Science and Technology, University of Stavanger, Stavanger, Norway, and Dr. Adil Murtaza, State Key Laboratory for Mechanical Behavior of Materials, School of Physics, Xi'an Jiaotong University, Xi'an, China.

Finally, I am grateful to my family for their unwavering support and encouragement, thank you for believing in me and for your patience during the long years of research. I would like to extend my appreciation to my colleagues and friends, who provided a supportive environment and shared in both the challenges and triumphs of this journey. This dissertation is the culmination of many contributions, and I am sincerely thankful to everyone who played a part in it.

TABLE OF CONTENTS

LIST OF FIGURES

LIST OF TABLES

ABBREVIATIONS AND ACRONYMS

3D	Three Dimension
3DP	Three-Dimensional Printing
4D	Four Dimension
ABS	Acrylonitrile Butadiene Styrene
Adj MS	Adjusted Mean Square
Adj SS	Adjusted Sum of Squares
AFM	Atomic Force Microscopy
AHP	Alkaline Hydrogen Peroxide
AM	Additive Manufacturing
ANOVA	Analysis of Variance
AR	Aspect ratio
ASA	Acrylonitrile Styrene Acrylate
ASME	American Society of Mechanical Engineers
BCNW	Bacterial Cellulose Nano Whiskers
BET	Brunauer–Emmett–Telle
CAD	Computer–Aided Design
CF	Carbon Fiber
CFRC	Continuous Fiber Reinforced composite
CI	Cellulose Type One
CI	Confidence Interval
CII	Cellulose Type Two
CIII	Cellulose Type Three
CIV	Cellulose Type Four
CMC	Crystalline Micro Cellulose
CMF	Cellulose Microfibrils
CNC	Crystalline Nano Cellulose
CNF	Cellulose Nanofibers
CNT	Carbon Nanotubes
CrI	Crystallinity Index
DCM	Dichloromethane
DF	Degree of Freedom
DLS	Dynamic Light Scattering
DMA	Dynamic Mechanical Analysis
DMF	Dimethylformamide
DoE	Design of Experiment

DTA	Differential Thermal Analysis
DTG	Derivative Thermogravimetry
EDS	Energy Dispersive X–ray Spectroscopy
EG	Ethylene glycol
ENDO	Endothermic
ER	Extractives Removal
EVOH	Ethylene Vinyl Alcohol
EXO	Exothermic
EXP	Experimental
FAO	Food and Agriculture Organization
FAOSTAT	Food and Agriculture Organization Statistics
FDM	Fused Deposition Modeling
FEG/SEM	Field Emission Gun Scanning Electron Microscope
FFF	Fused Filament Fabrication
FRP	Fiber Reinforced Polymer
FTIR	Fourier Transform Infrared Spectroscopy
GF	Glass Fiber
GHG	Green Huse Gas
GO	Graphene Oxide
HDPE	High–Density Polyethylene
HIPS	High Impact Polystyrene
HR	Hemicellulose Removal
HRTEM	High Resolution Transmission Electron Microscope
Iα	Alpha Cellulose I
Iβ	Beta Cellulose I
L/D	Length to Diameter Ratio
LDPE	Low–Density Polyethylene
LR	Lignin Removal
MCC	Microcrystalline Cellulose
MFC	Micro Fibrillated Cellulose
MFI	Melt Flow Index
MWCNT	Multi–Walled Carbon Nanotubes
NC	Nano Cellulose
NCC	Nanocrystalline Cellulose
NFC	Nano Fibrillated Cellulose
NGO	Non–Governmental Organization

NMR	Nuclear Magnetic Resonance
OA	Orthogonal Array
OM	Optical Microscope
PA11	Polyamide 11
PA12	Polyamide 12
PA6	Polyamide 6
PA6,6	Polyamide 6,6
PAEK	Polyaryletherketone
PAN	Polyacrylonitrile
PANI	Polyaniline
PBT	Polybutylene Terephthalate
PC	Polycarbonate
PCL	Polycaprolactone
PE	Polyethylene
PEEK	Polyether Ether Ketone
PEI	Polyetherimide
PES	Polyether Sulfone
PET	Polyethylene Terephthalate
PETG	Polyethylene Terephthalate Glycol
PEVA	Polyethylene Vinyl Acetate
PI	Prediction Interval
PLA	Polylactic Acid
PLGA	Poly (lactic–co–glycolic acid)
PMMA	Polymethyl Methacrylate
POM	Polyoxymethylene
PP	Polypropylene
PPS	Polyphenylene Sulfide
PPSU	Polyphenyl Sulfone
PRED	Prediction
PS	Polystyrene
PSU	Polysulfone
PTFE	Polytetrafluoroethylene
PVA	Polyvinyl Alcohol
PVC	Polyvinyl Chloride
RF	Raw Fiber
RT	Retting Time

S/N	Signal to Noise Ratio
SAN	Styrene Acrylonitrile
SE	Standard Error
Seq SS	Sequential Sum of Squares
SS/NMR	Solid–State Nuclear Magnetic Resonance
SSA	Specific Surface Area
TAPPI	Technical Association of the Pulp and Paper Industry
TEMPO	Tetramethylpiperidine–oxyl
Tg	Glass Transition Temperature
TGA	Thermogravimetric Analysis
THF	Tetrahydrofuran
Tm	Melting Temperature
TPE	Thermoplastic Elastomer
TPS	Thermoplastic Starch
TPU	Thermoplastic Polyurethane
UHMWPE	Ultra–High–Molecular–Weight Polyethylene
UV	Ultraviolet
WAXS	Wide–Angle X–ray Scattering
XPS	X–ray Photoelectron Spectroscopy
XPS	X–ray Photoelectron Spectroscopy
XRD	X–ray Diffraction

ABSTRACT

Agricultural crop residues are non-consumable components of crops that remain after the harvest of the primary agricultural product. Globally, agricultural practices generate vast quantities of crop residues annually. Among the agricultural crops, linseed (Linum usitatissimum), also known as flaxseed, is an important oilseed crop mainly cultivated for its seed. While the seeds are widely used, the residual stalks generated after seed harvesting remains underutilized in most regions, often viewed as agricultural waste rather than a resource. Traditionally, these residues have been disposed of through open burning, contributing to environmental issues such as air pollution, greenhouse gas emissions, and soil degradation. However, increasing awareness of sustainability, climate change, proper waste management and resource optimization has driven interest in the valorization of agricultural residues to value added resources. In light of the escalating demand for environmentally sustainable, biodegradable and high–performance filament materials in the FDM based 3D printing, Bio nanocomposite materials become the best alternatives to synthetic polymers and polymer composite materials. Therefore, this study investigates the conversion of linseed stalk residue into CNC, which used as a nano filler in PLA filament for FDM 3D printing. The study encompasses raw linseed stalks were subjected to varying durations of water retting to determine the optimal condition for fiber extraction. Fibers that have been retted under different conditions, were evaluated for their tensile and physical properties using single-fiber tensile testing and OM. The optimally extracted fibers were further treated through a series of chemical treatments including dewaxing, alkalization, and bleaching to investigate the effects of these treatments on their physical, chemical, and thermal properties, analyzed using FTIR and TGA/DTG. MC was extracted through multistep pretreatment processes and subjected to acid hydrolysis and post-treatment processes to isolate CNC. Both MC and CNC samples were characterized using FTIR, SEM/TEM, XRD, and TGA/DTG/DTA. PLA/CNC nanocomposites were then formulated with varying CNC loadings through solvent casting. The resulting Bio nanocomposites were characterized to evaluate structural, chemical composition, morphological, and thermal properties using FTIR, SEM, XRD, and TGA/DTG/DSC. PLA/CNC-coated filaments were prepared and used to fabricate test specimens via FDM 3D printing. Finally, the PLA/CNC filaments and printed parts were evaluated for tensile performance and fracture morphology in comparison to neat PLA, using a UTM and SEM analysis to assess the mechanical enhancements achieved through CNC reinforcement. The results reveal that water retting for a duration of 216 h at ambient temperature optimizes the quality of fiber. The extracted fiber has a potential cellulose content of 68% for cellulose extraction and a purified MC with 70% yield was obtained through a multistep pretreatments processes for CNC isolation. The isolated rod–like CNC demonstrated notable physical attributes, specifically a yield of 79.87%, a diameter of 7.06 nm, a length of 66.14 nm, and an aspect ratio of 10.02, accompanied by commendable crystallinity and thermal stability. In the context of the nanocomposite, CNC was effectively integrated into PLA at a concentration of 3% compared to 1% and 5 %, which enhanced dispersion and compatibility, thereby leading to property improvements. Finally, the PLA/CNC–coated filament was effectively printed, resulting in enhanced tensile strength and elongation of the 3D printed PLA/CNC composite, with values recorded at 26.72 MPa and 28.87%, respectively. The study underscores the environmental and technological advantages of utilizing biodegradable bio-nanocomposites by recycling agricultural crop residue into value added bio based nano filler. The integration of nanotechnology through compatible, renewable nanofiller not only enhances the performance of Bio nanocomposites but also aligns with the principles of sustainable development. These advancements promote the use of entirely biobased, high-performance composite materials in FDM 3D printing, supporting the transition towards a circular bioeconomy.

KEYWORDS: *linseed stalk-residue, crystalline nanocellulose, polylactic acid, Bio nanocomposite, filament, fused deposition modeling, 3D printing*

CHAPTER 1

INTRODUCTION

1.1. Background of the Study

According to (Wastemanaged, 2024), the amount of waste produced by agriculture worldwide is estimated to be 1.3–2.1 billion tons per year. Agricultural waste encompasses a wide variety of materials produced by farming operations. These can be divided into agro–industrial waste, for example, bagasse and peels (banana, orange, onion, potato), livestock wastes and crop residues (Duque-Acevedo et al., 2020). Agricultural crop residues include the leftover stalks, leaves, seed pods, stems, straws, husks, weeds and roots from crops constitute after harvesting (A. P. Gupta et al., 2023). This waste is unavoidable and in many cases, it is left and burned on the field (Timogarden, 2016; Wastemanaged, 2024). This residue accounts for 80% of the crop (Businesswaste, 2024). In Ethiopia the gross crop residue potential is estimated around 69.6 to 105.5 million tons and the average national potential of recoverable agricultural residues is approximately 57.7 million tons per year. This indicating that 66% of the gross residue is available for recovery (Tolessa, 2023).

Linseed (*Linum usitatissimum*), a fibrous plant that is grown commercially in areas with milder climates, is one of the various agricultural crop residues (Saleem et al., 2020). It has a long and significant history, particularly in the context of textiles, and it is mentioned several times in the Bible. The use of linseed for producing linen, a textile derived from the flaxseed plant, dates back to ancient times. The history of linseed as a fiber for textiles is deeply intertwined with ancient agricultural practices and cultural significance, particularly in biblical times. Its references in the Bible highlight both its practical uses and its symbolic importance in ancient society (Kozłowski et al., 2020).

Linseed, also known as oilseed (flaxseed), is cultivated especially for its seeds. However, the breeding flax fiber type is grown primarily for fiber extraction (Jhala et al., 2010). The phenotypes and physiology of both species are significantly different. Linseed can grow to a height of 40 to 60 cm and has a high branching stem, while flax fiber can grow to 80 to 120 cm and have a lower branching stem (Zuk et al., 2015). Linseed and fibrous flax produce varying quantities of seed, stalk and fiber. For example, linseed produces 20 dt/ha of seed, 30dt/ha of stalk and 15% fiber yield. While flax fiber produces 85 dt/ha of stalk, 5 dt/ha of seed and 30% fiber yield (Praczyk et al., 2021). Linseed with a straw yield of 5.1 t/ha and a

25–30% fiber yield is also reported, so indicating it could be a large substantial source of fiber fiber (Khan et al., 2021).

Global linseed cultivation reached nearly 4 million metric tons in 2022, of which 66% was generated exclusively by Russia and Kazakhstan. India and China accounted for an additional 10.5% of the worldwide linseed output, and 13% of global production was secured by Canada and the United States of America (FAOSTAT, 2024). The aggregate harvested area of all linseed cultivating nations collectively exceeded 4.5 million hectares (Selge et al., 2024). Currently, some countries that have recognized this large potential, started utilizing effectively by research and development. For instance, France, the United States, Canada, Italy, and England play significant roles in flax fiber research on a global scale. The key research domains include fiber production, quality, and utilization in composites, textile manufacturing, chemical constituent analysis, and the extraction of valuable compounds such as cellulose, nanocellulose, hemicellulose, lignin, and pectin for various applications. Currently, in addition to flax fiber, the utilization of straw from the linseed crop has become a prominent research area, focusing on the valorization of agricultural crop residues (S. Gao et al., 2023).

In Ethiopia, only the linseed type is available. It is cultivated in almost all parts of the country, primarily for its seeds, which are used for oil production (Ali et al., 2014; Tolessa, 2023). Ethiopia produces an average of 84,000 tons of linseed annually, cultivated across approximately 82,000 hectares. According to (FAOSTAT, 2024), this positions Ethiopia as the seventh-largest linseed producer globally and the leading producer in Africa, accounting for over 86% of the continent's total linseed output, followed by Egypt and Tunisia. From the annual linseed seed production, an estimated 126,000 tons of stalk residue are generated, of which approximately 63,000 tons are considered practically recoverable each year (Tolessa, 2023). However, many farmers burn stubble to clear fields for the next crop after harvest. Improper disposal practices of crop residues, such as open-field burning, contribute to the emission of greenhouse gases (GHGs), including carbon dioxide (CO_2), nitrous oxide (N_2O), and methane (CH_4), thereby posing significant risks to both human health and the natural environment (Elbasiouny et al., 2019). Effectively managing agricultural crop residues is not just about efficient disposal. Effective management of agricultural crop residues involves a strategic hierarchy that prioritizes waste prevention, minimization, reuse, and recycling. Practices such as composting and biogas generation transform waste into valuable resources, while energy recovery methods further enhance sustainability. When necessary, environmentally safe disposal methods, including controlled incineration or

landfilling, are employed. This comprehensive approach not only reduces environmental impact but also contributes to maintaining soil health and ensuring long-term agricultural productivity, aligning with sustainable farming practices (Abubakar et al., 2022).

Globally, best practices for agricultural crop residue utilization focus on promoting sustainable agriculture and minimizing environmental impacts through circular bioeconomy strategies. Key approaches include bioenergy and biofuel generation, biogas production, biochar creation, and combustion for energy. Residues are also utilized in composting, soil mulching, animal feed supplementation, and the development of eco-friendly building materials, biofertilizers, and other value-added products (Koul et al., 2022; Sachdev, 2024). From the innovative waste management techniques that prioritize recycling, reduction, and reuse, recycling agricultural crop residues is a valuable practice that contributes to sustainable farming by transforming waste into valuable resources such as cellulose, hemicellulose, lignin and pectin (Sarkar et al., 2020; Tiwari et al., 2024). The extraction of lignocellulosic biomass components from crop residues could significantly elevate the value derived from agricultural waste (Mohite et al., 2022).

Among the components of lignocellulosic biomass, cellulose stands out as the most abundant and industrially valuable biopolymer. It makes up the majority of total biomass (30–50%) (Hayes, 2013), making them promising sources for cellulose extraction. Cellulose is a linear polysaccharide consisting of glucose units linked by β-1,4-glycosidic bonds and is primarily located in the primary and secondary cell walls of plants (De Avila Delucis et al., 2021). With the growing emphasis on sustainable and renewable resources, cellulose has garnered significant interest in material science. Particularly, due to its high tensile strength, superior film-forming properties, biodegradability, non-toxicity, and biocompatibility, it has found wide application in the paper, textile, water filtration, and composite material industries (Seddiqi et al., 2021).

Beyond traditional applications, the process of deconstructing cellulose into nanocellulose enhances its surface area, crystallinity, and reactivity, making it a valuable advanced material for various high-performance applications. This deconstruction, often achieved through methods like mechanical, chemical and biological approaches (Tarchoun et al., 2024). Nanocellulose in general exhibits properties such as biodegradability, high tensile strength, lightweight nature, renewability, and excellent barrier and rheological behavior, making it suitable for reinforcing biopolymers, especially in green composite materials. Its applications span across biodegradable packaging, biomedical scaffolds, drug delivery systems, electronics, rheology modifiers, and 3D printing filaments (Qureshi et al., 2024).

Nanocellulose is generally categorized into three main types, such as cellulose nanocrystals (CNCs), cellulose nanofibers (CNFs), and bacterial nanocellulose (BNCs), based on the source material and extraction methods. Their properties such as particle size, crystallinity, and morphology vary depending on the cellulose origin, extraction conditions, and any pre or post treatment processes (Chaka, 2022). Among the types of nanocellulose, cellulose nanocrystals (CNCs) are rigid, rod-like crystalline nanomaterials, relatively small diameters typically measuring 1 to 10 nm in diameter and possessing high aspect ratio between 5 and 50 (TAPPI, 2020). These contribute to their high surface area, low density, high degree of crystallinity and mechanical strength (Agbakoba et al., 2023). CNCs are typically extracted from the crystalline regions of natural cellulose by selectively hydrolyzing the amorphous domains, resulting in highly ordered crystalline structures. Among the various chemical methods available, sulfuric acid (H_2SO_4) hydrolysis is the most widely employed technique for this purpose (Akinjokun et al., 2021; Beyan et al., 2021; Gabriel, Wondu, et al., 2021). CNCs are increasingly used in packaging, filtration, hydrogels, construction, textiles, paper and pulp, composites, implants, electronics, sensors, cosmetics, paints and coating applications (Ul-Islam et al., 2016). Among the potential applications, cellulose nanocrystals (CNCs) serve as effective reinforcing agents in PLA bionanocomposites, enhancing thermal, mechanical, and barrier properties for advanced applications (M. P. Arrieta et al., 2017).

Polylactic acid (PLA) is a bio-based thermoplastic polyester that has gained significant attention as a sustainable alternative to traditional petroleum-based plastics. It is synthesized from renewable resources, including corn starch, sugarcane, and other carbohydrate-rich biomass (A. Ahmad et al., 2020; Ioannidou et al., 2022). PLA is distinguished by its biodegradability, biocompatibility, and commercial scalability (Ioannidou et al., 2022). With global plastic production surpassing 368 million tons each year, the resulting accumulation of plastic waste has escalated into a major environmental concern. In this context, PLA presents a promising alternative due to its ability to biodegrade under industrial composting conditions, thereby mitigating long-term environmental impact (Ramezani Dana et al., 2023).

Currently, polylactic acid (PLA) is the most commonly utilized biopolymer in 3D printing, primarily because of its low melting temperature, reduced thermal shrinkage, and minimal warping during processing (J. C. Tan et al., 2020). It is especially preferred for both desktop and industrial FDM printers because of its relatively low processing temperature (approximately 180–220°C), excellent layer adhesion, low tendency to warp, and minimal release of harmful fumes during printing. It does not require a heated bed, although moderate

heating (approximately 50–60°C) can improve adhesion and surface finish. Furthermore, PLA offers excellent dimensional accuracy and a smooth surface appearance, which are highly desirable for prototyping, educational models, artistic objects, and end-use parts (Alexandre et al., 2020). Nevertheless, the overall performance of pure PLA is constrained by its brittleness, slow crystallization rate, and low melt strength, particularly when subjected to repeated extrusion cycles (Trivedi, Gupta, et al., 2023; Khouri et al., 2024).

The ability to tailor the properties of FDM–printed parts through the selection of filament materials opens new possibilities for the design and optimization of functional components. Different types of fillers (reinforcements), such as carbon, metal, ceramic, cellulose or hybrid–based fillers in the form of continues and short fibers, micro and particle are incorporated into pure polymer filaments to improve the properties of FDM printed parts (Angelopoulos et al., 2021). The growing demand for sustainable and bio-based materials has spurred significant interest in developing eco-friendly, 3D-printable biopolymer composites. PLA-based bio nanocomposites reinforced with nanocellulose exhibit favorable physical and mechanical properties, along with biocompatibility and potential biodegradability, making them well-suited for FDM 3D printing and aligned with circular bio economy principles (Holden et al., 2023).

In light of these considerations, the valorization of linseed stalk residue into crystalline nanocellulose and its application in PLA-based bio nanocomposite filaments for FDM 3D printing presents a promising multi-purpose approach addressing both environmental and performance challenges. It not only addresses agricultural waste management challenges, but also contributes to the development of high-performance, biodegradable Bio nanocomposite materials for advanced applications while maintaining environmental sustainability. This study, therefore, aims to transform linseed stalk residue into crystalline nanocellulose and to explore its potential as a nanofiller for PLA-based Bio nanocomposite filament in Fused Deposition Modeling (FDM) 3D printing.

1.2. Statement of the Problem

Polylactic acid (PLA), a bio-based thermoplastic polyester derived from renewable resources such as corn starch, sugarcane, and carbohydrate-rich biomass, has emerged as a leading sustainable alternative to conventional petroleum-based plastics. Its biodegradability, biocompatibility, and commercial scalability make it particularly attractive in addressing the escalating global plastic waste crisis. PLA has become the most widely used biopolymer in

Fused Deposition Modeling (FDM) 3D printing due to its low melting point, minimal warping, ease of processing, and excellent dimensional accuracy.

Despite these advantages, the inherent material limitations of pristine PLA such as brittleness, low thermal resistance, slow crystallization rate, and poor melt strength restrict its use in load-bearing and high-performance applications. These issues become more pronounced during repeated thermal cycles in additive manufacturing processes. To enhance PLA's performance, researchers have incorporated various reinforcements, including short and continuous fibers, micro- and nanoparticles, and hybrid fillers. These additives originate from both inorganic and organic sources such as carbon nanotubes, graphene, metal oxides, ceramics, cellulose fibers, lignin, and chitin. While inorganic fillers are effective in enhancing the mechanical and thermal performance of biopolymers, they often pose significant challenges such as poor compatibility with the polymer matrix, reduced biodegradability, high processing temperatures, and increased viscosity. These issues hinder the development of fully sustainable and processable bio composites, limiting their applicability in eco-friendly manufacturing and end-of-life disposal. Organic fillers, particularly nanocellulose, offer a promising bio-based solution due to their renewable origin, lightweight nature, biodegradability, compatibility and reinforcing potential.

Crystalline nanocellulose (CNC) is a highly promising bio-filler for improving the mechanical properties of PLA composites, due to its high surface area and stiffness. However, conventional CNC sources like wood pulp and forest biomass are limited by high extraction costs, low cellulose content, and environmental concerns such as deforestation and land use competition. In contrast, agricultural residues offer a more sustainable and efficient alternative. These residues are rich in cellulose, have fewer non-cellulosic components, and are abundantly available as underutilized biomass. Leveraging them not only addresses the drawbacks of traditional sources but also provides a dual benefit by reducing agricultural waste and transforming it into high-value nanomaterials. This strategy aligns with circular bioeconomy goals by minimizing environmental impact, promoting resource efficiency, and adding value to agricultural practices.

Despite the growing interest in bio composites for FDM 3D printing, challenges persist in compounding and filament preparation. Incorporating bio-based fillers into PLA is often limited by poor dispersion, agglomeration, and thermal instability during processing. Natural filler variability and the sensitivity of biopolymers to heat and shear further complicate the process. Common methods such as dry mixing, solvent blending, and melt compounding, which require careful optimization to maintain filament quality and structural integrity.

Additionally, extrusion processes often face issues like thermal degradation and inconsistent flow, limiting the scalability and performance of bio-composite filaments.

To address these challenges, in the area of continuous fiber–reinforced composites (CFRCs), different printing techniques have been utilized such as in-nozzle impregnation, out-of-nozzle impregnation, and the use of pre-impregnated fibers. Additionally, recent innovations have introduced more integrated and flexible approaches, such as 3D printers capable of combining compounding and extrusion in a single system, in-situ reinforcement deposition during printing, and the layering of polymer filaments on woven reinforcement materials. While these methods show promise in enhancing performance and process efficiency, they remain at an early stage of development and are not yet widely adopted or fully optimized. Therefore, there is a clear need to explore and refine advanced composite filament production and 3D printing strategies that overcome existing limitations.

1.3. Objective

1.3.1. General objective

The main objective of the study is transformation of linseed stalk residue into crystalline nanocellulose as a nanofiller for polylactic acid (PLA)-based bio nanocomposite filament in fused deposition modeling (FDM) 3D printing.

1.3.2. Specific objectives

The specific objectives of the study are:

1. Extract fiber from linseed stalks by determining the optimum retting time to evaluate the effect of retting degree on physical and tensile properties of the extracted fibers.
2. Optimize multi–step extraction process parameters for the non-cellulosic components removal to evaluate the treatment effect on physical, chemical and thermal properties of the treated fibers.
3. Isolate crystalline nanocellulose (CNC) and analyze its crystallinity, morphology, surface functionality, and thermal stability to determine its potential as a nanofiller in polylactic acid (PLA).
4. Fabricate PLA/CNC Bio nanocomposites with varying CNC weight percentages to determine the optimal CNC loading for enhanced composite performance.
5. Develop PLA/CNC Bio nanocomposite coated filaments for FDM 3D printing to evaluate the tensile properties, surface morphology, and fracture behavior of the printed samples.

1.4. Significance of the Study

This study holds holistic significance across multiple domains, including agricultural crop residue management, nanotechnology, and Bio nanocomposite-based 3D printing. It offers environmental benefits, strengthens economic value chains, and provides valuable insights for future research and development in sustainable materials. Environmentally, it addresses a critical challenge in agricultural crop residue management by offering a value-added pathway for biomass that is often discarded or burned. By utilizing plant-based sources such as linseed stalks instead of conventional forest-derived or mineral-based materials, the study promotes sustainable sourcing of cellulose. Furthermore, the incorporation of CNC into biodegradable polymers like poly-lactic acid (PLA) replaces traditional inorganic fillers, thereby supporting the development of fully biodegradable bioplastics. This advancement not only enhances the environmental profile of 3D printed materials but also contributes to reducing plastic pollution, lowering greenhouse gas emissions, and fostering a circular bioeconomy.

In terms of research and development, the study significantly expands the scientific understanding of biomass valorization. It demonstrates that, beyond cellulose, linseed stalks contain a range of valuable compounds such as pectin, hemicellulose, and lignin, all of which have high potential for industrial applications in pharmaceuticals, food technology, and green chemistry. Additionally, the research emphasizes the versatility of cellulose and its derivatives, which go far beyond their role as reinforcing agents in polymer composites. These materials can be employed in film formation, biogas production, drug delivery systems, wound dressings, water purification membranes, aerogels, rheology modifiers, and smart responsive materials. By highlighting such applications, the study provides valuable insights that can guide future research into the utilization of other agricultural residues and inspire innovation in Bio nanocomposite-based 3D printing for advanced, high-performance, and sustainable uses.

Economically, the study outlines a clear and scalable value chain that adds worth at every stage of processing. Starting from raw linseed stalks, value is incrementally introduced through fiber extraction, cellulose purification, and nanocellulose isolation. Each stage produces intermediate or final products with distinct commercial potential. This process opens new income opportunities for farmers, who can monetize what is typically considered waste, either by directly supplying raw stalks or by engaging in fiber extraction. At the same time, small-scale enterprises and local industries can further process cellulose into high-

value CNC products, enabling local economic development and encouraging entrepreneurship in the bio-based materials sector. The model presented in this research is adaptable to a wide range of crop residues, making it a viable strategy for fostering rural economic growth while contributing to global sustainability goals.

1.5. Scope of the Study

This study focuses on the valorization of linseed stalk residues into value-added crystalline nanocellulose (CNC) for use in polylactic acid (PLA) Bio nanocomposites intended for fused deposition modeling (FDM) 3D printing, covering a comprehensive workflow from raw material processing to final product evaluation. The research begins with optimizing water retting duration for efficient fiber extraction and proceeds to refine chemical treatments for removing non-cellulosic components, enhancing the quality of the extracted fibers. Crystalline nanocellulose (CNC) is then isolated through acid hydrolysis and characterized to assess its suitability as a nanofiller. PLA/CNC composites are fabricated using solvent casting with varying CNC loadings and evaluated for thermal, morphological, and structural properties to determine optimal reinforcement levels. Finally, composite filaments are prepared through surface coating and used in FDM printing to examine mechanical performance and surface characteristics of the printed parts. Overall, the study integrates material extraction, nanocellulose production, composite formulation, filament preparation, and 3D printing to promote the sustainable valorization of agricultural waste in advanced manufacturing.

Linseed stalks were selected over other agricultural residues due to their high cellulose yield, underutilized status, regional availability, and potential to generate valuable products at multiple stages of processing, including fiber, micro cellulose, and CNC. Polylactic acid Polylactic acid (PLA) was selected as the matrix material because it is biodegradable, non-toxic, has a relatively low processing temperature, and is widely available in industrial markets. Moreover, it demonstrates excellent compatibility with cellulose-based fillers, making it more suitable for FDM applications compared to alternative biopolymers. However, PLA has inherent limitations such as brittleness, low thermal resistance, and moderate mechanical strength, which necessitate the incorporation of suitable fillers to enhance its structural, thermal, and mechanical properties for broader functional applications. CNC was chosen as the reinforcing nanofiller for the PLA matrix due to its nanoscale dimensions, large surface area, and strong interfacial bonding capacity. These properties allow CNC to significantly enhance mechanical performance at low filler loadings

without negatively affecting the extrusion or printing process, unlike other cellulose-based reinforcements such as continuous fibers, short fibers, or microcrystalline cellulose.

The fiber extraction process was carried out using water retting, which was selected over methods because of its lower environmental impact, cost-effectiveness, and ability to preserve the structural integrity of cellulose. By optimizing the retting duration, the process enabled the selective degradation of non-cellulosic components, leading to the production of high-quality fibers with favorable physical and mechanical properties.

CNC was subsequently isolated from the extracted fibers through sulfuric acid hydrolysis. This method was employed due to its efficiency in removing amorphous regions of cellulose and in producing CNC with high crystallinity and smaller size. Additionally, this process introduced sulfate half-ester surface groups, which improved the dispersion of CNC within the PLA matrix and enhanced interfacial adhesion.

For the preparation of the PLA/CNC composites, solvent casting was used to achieve uniform dispersion of CNC in the PLA matrix under room temperature conditions. This approach minimized the risk of thermal degradation for both the PLA and the CNC. A novel surface coating technique was employed to prepare the composite filaments, as an alternative to conventional melt extrusion. This strategy was intended to reduce repeated thermal processing cycles that can negatively alter the structural and functional characteristics of CNC. Finally, the PLA/CNC Bio nanocomposite filament was used in 3D printing through the FDM process, which was selected for its accessibility, cost-efficiency, and strong compatibility with PLA.

1.6. Limitation of the Study

While this research provides foundational insights into the valorization of linseed stalk residue for CNC-reinforced PLA composites in FDM 3D printing, several limitations warrant acknowledgment. Firstly, the linseed stalk residue was sourced exclusively from a single geographical location. This constraint raises concerns about the representativeness of the feedstock, as variations in soil composition, climatic conditions, or agricultural practices could alter the fiber's structural and chemical properties.

Although the Bio nanocomposite was developed using bio-based constituents of PLA and CNC, and the degradation rate and mechanism of PLA under industrial compositing conditions is well known, the biodegradability of the Bio nanocomposite after the addition of CNC was not experimentally validated. This could help to check whether the addition of

CNC affects the biodegradability or not. Consequently, it limiting the development of evidence-based end-of-life disposal strategies for users and policymakers.

Furthermore, while the composites were 3D-printed, some the printing process parameters were not systematically optimized. This oversight may have compromised the mechanical performance and structural integrity of printed specimens. The evaluation of 3D-printed samples focused narrowly on tensile properties, surface morphology, and fracture behavior. Some additional matrices for functional applications were not tested and evaluated, this restricting the understanding of how these composites would perform in real-world scenarios. Finally, although the raw material used for nanocellulose extraction is an underutilized waste with significant availability, the costs associated with feedstock procurement and laboratory-scale production were not analyzed. This omission limits a comprehensive cost-benefit analysis for scaling CNC extraction, filament production, and 3D printing applications

1.7. Structure of the Dissertation

The structure of the PhD dissertation and the contents of each chapter are as follows:

Chapter 1: Introduction; This chapter provides a comprehensive introduction to the study, detailing the background, objectives, significance, scope, and limitations of the research. It sets the stage for understanding the context and importance of the investigation.

Chapter 2: Literature Review; This chapter presents a structured review of literature related to cellulose, nanocellulose, and their use in polymer composites, particularly in Fused Deposition Modeling (FDM) 3D printing. It begins with an overview of cellulose types, sources, and nomenclature, followed by a discussion on the properties, extraction methods, and applications of micro- and nanocellulose. The integration of nanocellulose into polymer matrices is examined with emphasis on composite fabrication methods, interfacial interactions, and processing factors. Special focus is given to polylactic acid (PLA), including its synthesis, properties, and role in Bio nanocomposites. The chapter also outlines FDM 3D printing fundamentals, filament material selection, and factors influencing filament and printed part performance. Key characterization techniques are reviewed, and the chapter concludes with a summary, challenges (gaps) and future research directions relevant to the study.

Chapter 3: Materials and Methods; This chapter outlines the materials, methodology, and approaches, samples and sampling techniques, data collection and analysis methods and experimental procedures utilized in the study. It emphasizes the preparation,

characterization, testing and analytical techniques employed throughout the research, providing a clear framework for replicability.

Chapter 4: Results and Discussion: this chapter presents the main findings of the study, organized in tabular and graphical formats. This section includes a detailed discussion of the results, offering scientific justifications and interpretations to elucidate the significance of the findings.

Conclusions, Recommendation and Future outlooks: The conclusion section summarizes the key findings of the study, drawing together the main insights derived from the research. It highlights how the objectives were met, the implications of the results, and their significance in the context of the existing literature. Following the conclusions, the recommendation section offers practical suggestions based on the findings of the study and the future outlooks section recommends future research directions, practical applications, methodological improvements, interdisciplinary approaches and sustainability practices.

CHAPTER 2

LITERATURE REVIEW

2.1. Introduction

This chapter provides a comprehensive review of the literature relevant to cellulose, nanocellulose, and their applications in polymer composites, with a particular focus on Fused Deposition Modeling (FDM) 3D printing technology. The discussion begins with an overview of cellulose, including its types, nomenclature, and primary sources, followed by the properties and potential applications of nanocellulose. Various extraction methods for obtaining fiber, micro-cellulose and nanocellulose are explored in detail. The available methods for fiber extraction are generally classified into retting and mechanical extractions. Similarly, the extraction methods of micro and nanocellulose are categorized as mechanical, biological, and chemical techniques alongside pretreatment and post-treatment processes.

Subsequently, the chapter delves into the integration of nanocellulose into polymer matrices, emphasizing the factors affecting composite properties, manufacturing techniques, and the role of nanocellulose dispersion and interfacial adhesion. Special attention is given to PLA, a biodegradable polymer widely used in Bio nanocomposite applications, outlining its types, synthesis methods, physicochemical properties, industrial relevance and limitations.

Additionally, the chapter covers the fundamentals of FDM technology, the selection and characteristics of filament materials including pure polymers, polymer composites and reinforcement materials ranging from short, micro and nano sizes. Factors affecting the properties of polymer composite filaments and printed samples. The properties and potential applications of printed polymer and its composite parts. Characterization techniques for fibers, nanocellulose, and PLA-based nanocomposites are reviewed to provide insights into material performance and behavior. Finally, summery, challenges and future opportunities are reported. This review not only supports the experimental direction of the current study but also contributes to the broader understanding on thematic area of the study.

2.2. Overview of Cellulose

Cellulose, the most prevalent organic polymer on Earth, serves as a fundamental building block in plant cell walls, providing structural support and rigidity. Composed of linear chains of glucose units linked by β–1,4–glycosidic bonds, as shown in **Figure 1.** This biopolymer exhibits remarkable versatility, making it a valuable resource across various industries. With

growing concerns about environmental sustainability and the depletion of fossil fuels, cellulose has emerged as a promising alternative to synthetic polymers (de Avila Delucis et al., 2021).

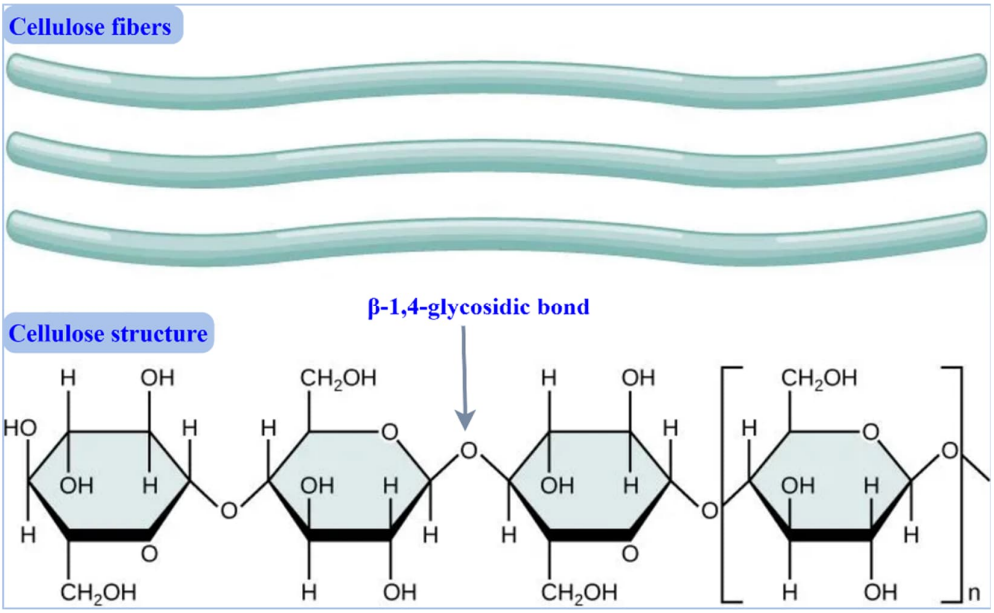

Figure 1. Chemical structure of cellulose (Trache et al., 2020b)

Cellulose can be sourced from a diverse array of materials, including wood, non–wood plants, and particularly agricultural residues. Each source presents unique chemical compositions and physical properties that influence the characteristics of the extracted cellulose (Lalita Chopra, 2022; Elfaleh et al., 2023). Wood, primarily derived from trees, provides a high yield of cellulose but raises challenges related to sustainability and deforestation. Non–wood plants, such as grasses and herbs, offer alternative sources that often have faster growth cycles. However, agricultural waste such as straw, husks, and other by–products represent a particularly advantageous source of cellulose. Utilizing these waste materials not only enhances resource efficiency but also addresses pressing waste management issues, making agricultural residues a key focus in cellulose research (Jampílek et al., 2020; Ventura-Cruz et al., 2021).

The chemical composition of cellulose varies significantly among different sources, typically comprising cellulose, hemicellulose, lignin, and other components. Lignin, a complex polymer that provides rigidity and resistance to microbial attack, is prevalent in wood and can hinder the extraction of pure cellulose. In contrast, agricultural waste often contains lower lignin content, facilitating cellulose extraction. Understanding these

compositional differences is crucial for optimizing extraction techniques and improving the quality of the cellulose produced (R. K. Mishra et al., 2018; Katakojwala et al., 2020).

2.2.1. Types and nomenclatures of cellulose materials

Plant bast fibers are primarily composed of cellulose, which is organized into various structural units, including elementary fibers, cellulose macro–fibrils, and cellulose microfibrils (Trache et al., 2020b), as shown in **Figure 2**.

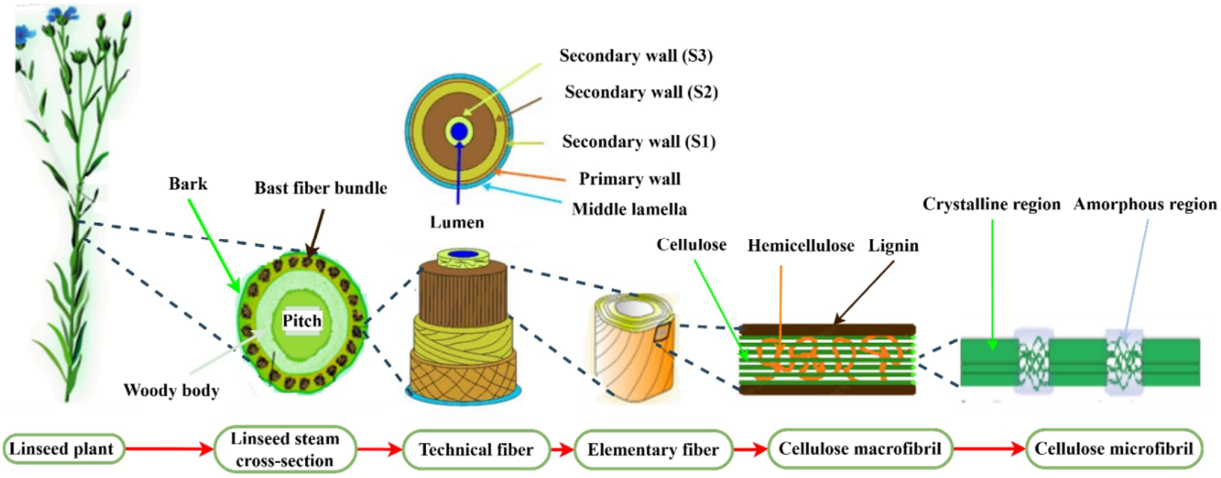

Figure 2. Multistep schematic representation of the bast fiber structure (Adapted from (Trache et al., 2020b))

Elementary fibers are extracted mainly from the secondary cell wall (S2), which is composed of cellulose macro–fibrils arranged in specific orientations within the plant cell wall. The macrofibril cellulose, which is a larger aggregate of microfibrils, is composed mainly of cellulose, hemicellulose and lignin constituents, which contribute to the overall structural integrity of the fiber. The smallest structural units, microfibrils, are composed of cellulose chains that include both crystalline and amorphous regions and are crucial for the strength and flexibility of bast fibers (Réquilé et al., 2018; Woigk et al., 2019).

Micro and nanocellulose are categorized into various subtypes based on their morphology, size, functional properties, and methods of production, all of which are largely influenced by the cellulose source and processing parameters. A range of terms has been used to describe these different forms. To address this, the Technical Association of the Pulp and Paper Industry (TAPPI) recently introduced standardized terminology and definitions for cellulose nanomaterials under WI 3021, primarily based on their dimensional characteristics (Kargarzadeh, Ioelovich, et al., 2017a). The nomenclature, abbreviations, and dimensions applicable to each subgroup are shown in **Figure 3**.

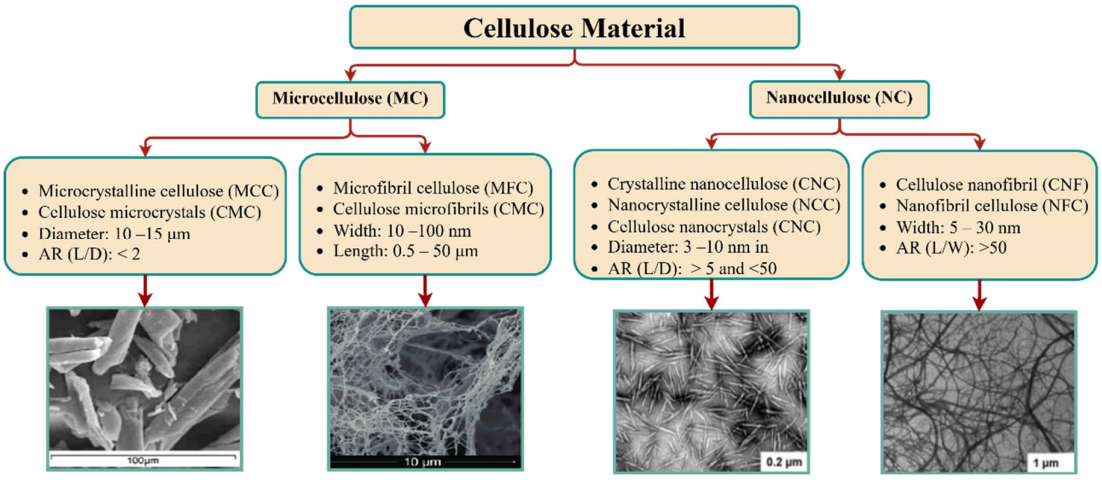

Figure 3. Standard terms for micro/nanocellulose (Adapted fromTAPPIW13021(TAPPI, 2020)

The term cellulose nanocrystal (CNC) is synonymous with the terms nanocrystalline cellulose (NCC) and crystalline nanocellulose (CNC). Similarly, cellulose nanofibrils (CNFs) with nanofibril cellulose (NFC), microcrystalline cellulose (MCC) with cellulose microcrystals (CMC) and microfibril cellulose (MFC) with cellulose microfibrils (CMC) have been used (TAPPI, 2020).

2.3. Sources of Cellulose

2.4. Natural fibers can be derived from a wide variety of plant, animal, and bacterial sources. The origin of the material plays a crucial role, as it significantly influences both the yield and the characteristics of the extracted cellulose (Lalita Chopra, 2022; Elfaleh et al., 2023). Numerous plant-based materials have been explored for cellulose extraction, including wood, non-wood sources, and agricultural crop residues, as illustrated in **Figure 4** (Shaghaleh et al., 2018).

Nonwood lignocellulose plants such as hemp, flax, jute, ramie, kenaf, bamboo, sisal, and cotton (Shaghaleh et al., 2018) are among the others. With the increasing demand for sustainable and biodegradable materials, interest in new sources of cellulose in addition to wood and nonwood sources, such as agricultural residues and byproducts such as corncob, rice husk, wheat straw, teff straw sugarcane bagasse and coffee husk is increasing (Jampílek et al., 2020; Ventura-Cruz et al., 2021).

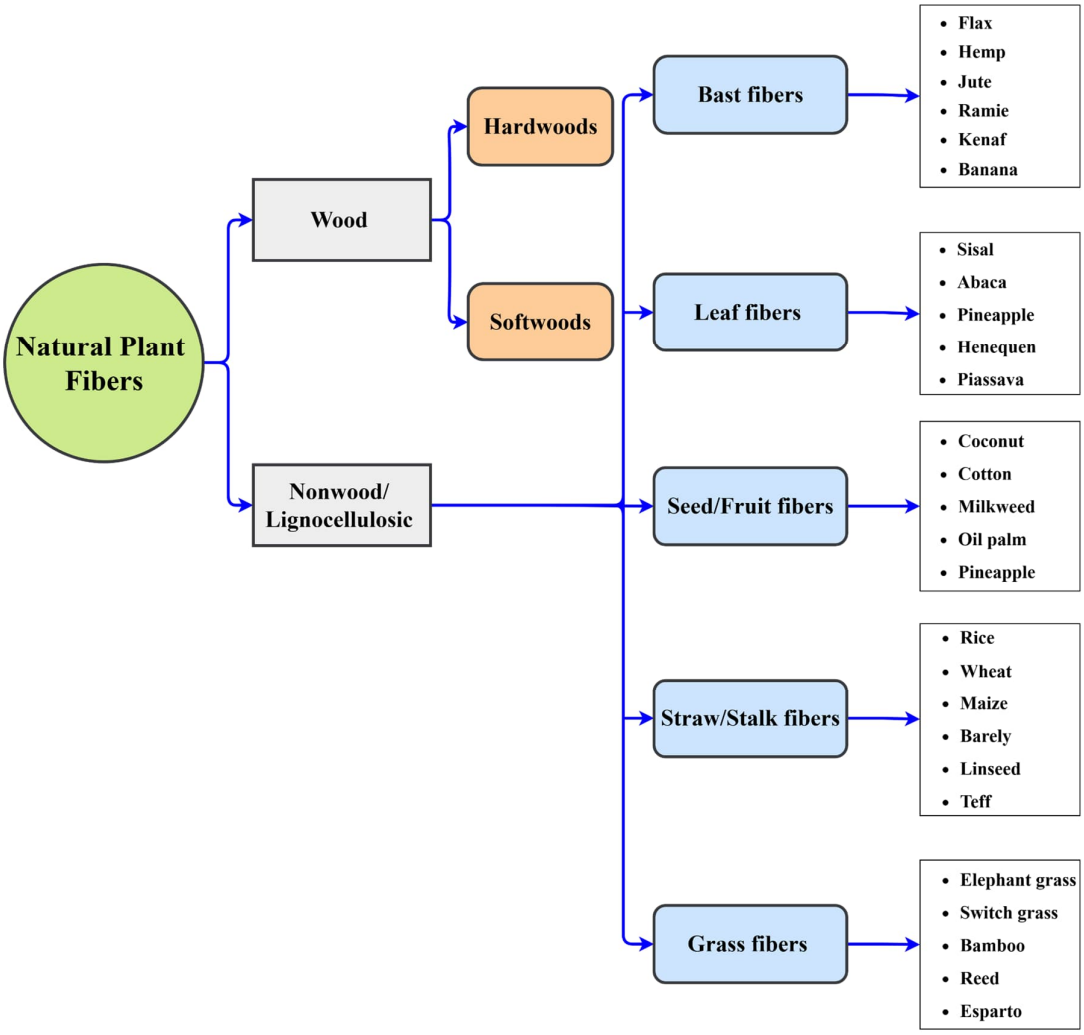

Figure 4. Classification of natural plant fibers as sources of fiber and cellulose (Adapted from (Shaghaleh et al., 2018)

2.4.1. Agricultural byproducts

Renewable materials have attracted increasing attention due to their positive environmental impact and sustainability (Ventura-Cruz et al., 2021). Among them, agricultural crop residues are abundant and offer a promising alternative for producing value-added products. Cellulose can be extracted from these lignocellulosic resources and utilized as a natural reinforcing agent in the development of bio nanocomposites (Gabriel, Belete, et al., 2021b). The growing interest in cellulose derived from agricultural residues is attributed to its distinctive properties, which are largely influenced by the source material and the extraction techniques employed (M. Islam et al., 2023).

As illustrated in **Figure 5**, cellulose has been successfully extracted from various agricultural waste materials, and its extraction processes and resulting properties have been thoroughly

studied and characterized. Some of the reported studies on corncob (Harini et al., 2020; Sartika et al., 2023), rice husk (M. Islam et al., 2023), wheat straw (S. Yu et al., 2022; C. Zhang et al., 2022), teff straw (Gabriel, Belete, et al., 2021b) and coffee husk (Zeleke et al., 2022; Karunakaran et al., 2023) are among the others.

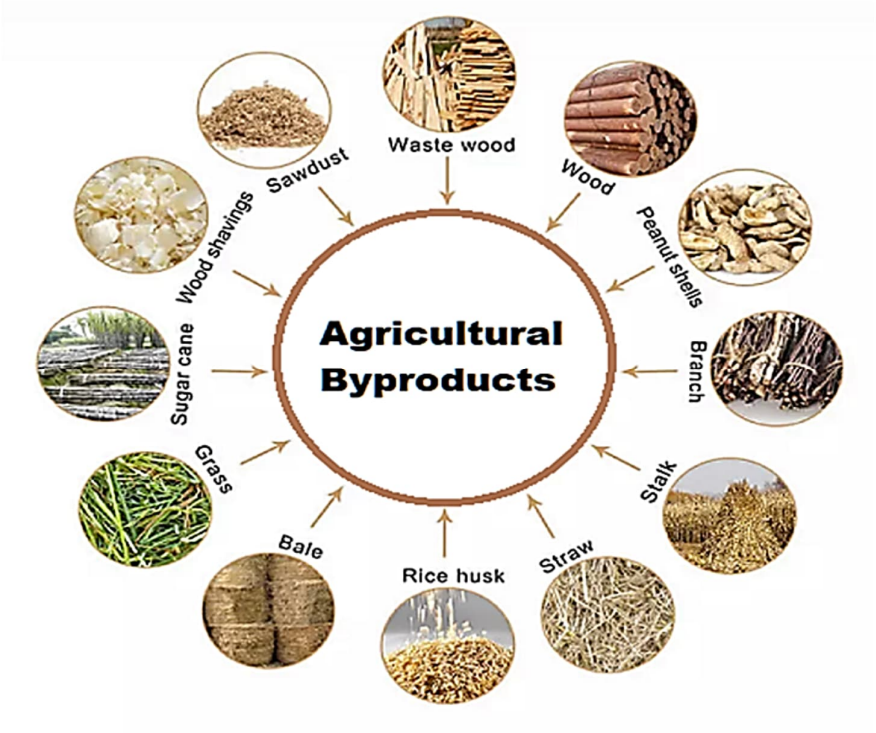

Figure 5. Various agricultural byproducts as sources of cellulose (M. Islam et al., 2023).

Lignocellulosic residues serve as a renewable source of cellulose, which is essential for producing micro and nanocellulose. Ongoing research focuses on developing efficient methods to obtain cellulose derivatives with tailored properties for various applications, while also aiming to optimize these processes for economic viability and environmental sustainability (Ventura-Cruz et al., 2021). Lignocellulosic materials, often derived as byproducts from industrial or agricultural activities, are generally abundant and low-cost. However, their composition varies by source, requiring detailed analysis, as properties like crystallinity, thermal stability, and chemical makeup are influenced by their origin (R. K. Mishra et al., 2018; Katakojwala et al., 2020).

Some of the studied and reported agro–industrial wastes used as alternative sources of cellulose such as khat waste (Gabriel, Wondu, et al., 2021), enset fibers (Beyan et al., 2021), corn cob (Ditzel et al., 2017), corn stover (Fonseca et al.), rice straw (P. Lu et al., 2012) (Srithongkham et al., 2012), maize stalk residue (A. Mtibe et al., 2015), sugarcane bagasse (A. Kumar et al., 2014b) and others as shown in **Table1**. The specific distribution of these

components can vary depending on the type of waste and its origin, influencing their suitability for different industrial processes and sustainable applications (S. Nayak et al., 2015; Gabriel, Belete, et al., 2021a; Kulshreshtha et al., 2021).

Table 1. Chemical compositions of different agricultural wastes (Gabriel, Belete, et al., 2021a)

Source	Cellulose (%)	Hemicellulose (%)	Lignin (%)
Oat straw	39	27	18
Teff straw	37	27	18
Barley straw	38	35	16
Sugarcane bagasse	40	23	18
Bean hulls	52	26	10
Coconut husk fiber	25	12	40
Corncob	45	35	15
Corn husks	29	40	11
Corn Stover	38–40	24–26	7–19
Cotton stalk	52	25	10.70
Nut shells	25–30	25–30	30–40
Mango seeds	55	21	24
Olive tree pruning	30–40	24–27	18–23
Pineapple leaf fiber	75	13	10
Pine	47	20	27
Pistachio shells	54	20	25
Poplar	49	24	20
Raw banana fiber	70	20	6
Rice straw	30–35	25–35	12–23
Sorghum bagasse	34–45	18–27	14–21
Soy hulls	48	24	6
Coffee hull	36	15	18
Spruce	43	30	28
Sugarcane bagasse	40–50	20–24	25–30
Switchgrass	30–50	5–20	10–40
Sunflower	37	21	17
Wheat straw	30–38	20–50	15–23
Enset fiber	60	22	13

Typically, these residues are composed of varying proportions of cellulose, lignin, hemicellulose, and extractives. Cellulose generally constitutes the largest fraction, often ranging from 30% to 50% of the total biomass, and is a primary source of fermentable sugars for biofuel production. Lignin, a complex and robust polymer, usually comprises 15% to 35% of agricultural waste, providing structural rigidity but also presenting challenges for enzymatic degradation. The hemicellulose content varies widely, typically between 20% and 35%, and is crucial for breakdown into fermentable sugars. Extractives, including fats, waxes, and resins, represent a relatively small yet significant portion, often ranging from

approximately 5% to 10%, affecting the physical properties and potential applications of these materials.

Among the chemical compositions, cellulose is a renewable and biodegradable polymer and it has emerged as a promising material for the development of eco–friendly alternatives. Due to its availability, sustainability, biocompatibility, good film–forming capacity, active surface area, and nontoxic nature (Arantes et al., 2020; Romão et al., 2022). The benefit and application of cellulose can be further expanded when cellulose chains are bundled together forming highly ordered domains that can be subsequently extracted as micro and nano particles (Foster et al., 2018a; Trache et al., 2020a).

2.4.1.1. Linseed crop and its byproducts

Linseed (*Linum usitatissimum*), a fibrous plant that is grown commercially in areas with milder climates, is one of the various agricultural crop residues (Saleem et al., 2020). It has a long and significant history, particularly in the context of textiles, and it is mentioned several times in the Bible. The use of linseed for producing linen, a textile derived from the flaxseed plant, dates back to ancient times. The history of linseed as a fiber for textiles is deeply intertwined with ancient agricultural practices and cultural significance, particularly in biblical times. Its references in the Bible highlight both its practical uses and its symbolic importance in ancient society (Kozłowski et al., 2020).

Table 2. Summarized comparison of linseed and flax fiber crops

Characteristic	Linseed Crop	Fiber Flax
Primary use	Mainly for seed production	Mainly for fiber extraction
Plant height	40–60 cm	80–120 cm
Branching	Highly branched	Less branched
Stalk yield	30 dt/ha	85 dt/ha
Seed yield	20 dt/ha	5 dt/ha
Fiber yield	Approximately 15%	Approximately 30%

Linseed, also known as oilseed (flaxseed), is cultivated especially for its seeds. However, the breeding flax fiber type is grown primarily for fiber extraction (Jhala et al., 2010). The phenotypes and physiology of both species are significantly different. Linseed can grow to a height of 40 to 60 cm and has a high branching stem, while flax fiber can grow to 80 to 120 cm and have a lower branching stem (Zuk et al., 2015). Linseed and fibrous flax produce varying quantities of seed, stalk and fiber. For example, linseed produces 20 dt/ha of seed, 30dt/ha of stalk and 15% fiber yield. While flax fiber produces 85 dt/ha of stalk, 5 dt/ha of seed and 30% fiber yield (Praczyk et al., 2021). Linseed with a straw yield of 5.1 t/ha and a

25–30% fiber yield is also reported, so indicating it could be a large substantial source of fiber fiber (Khan et al., 2021). The differences between linseed and fiber flax crops are summarized in **Table 2**.

2.4.1.2. Global linseed production

Global linseed cultivation reached nearly 4 million tons in 2022, of which 66% was generated exclusively by Russia and Kazakhstan. India and China accounted for an additional 10.5% of the worldwide linseed output, and 13% of global production was secured by Canada and the United States of America (FAOSTAT, 2024). The aggregate harvested area of all linseed cultivating nations collectively exceeded 4.5 million hectares (Selge et al., 2024). According to (FAOSTAT, 2024) report, the harvested areas and seed production volumes of the ten largest linseed growing counties in the world are shown in **Table 3**.

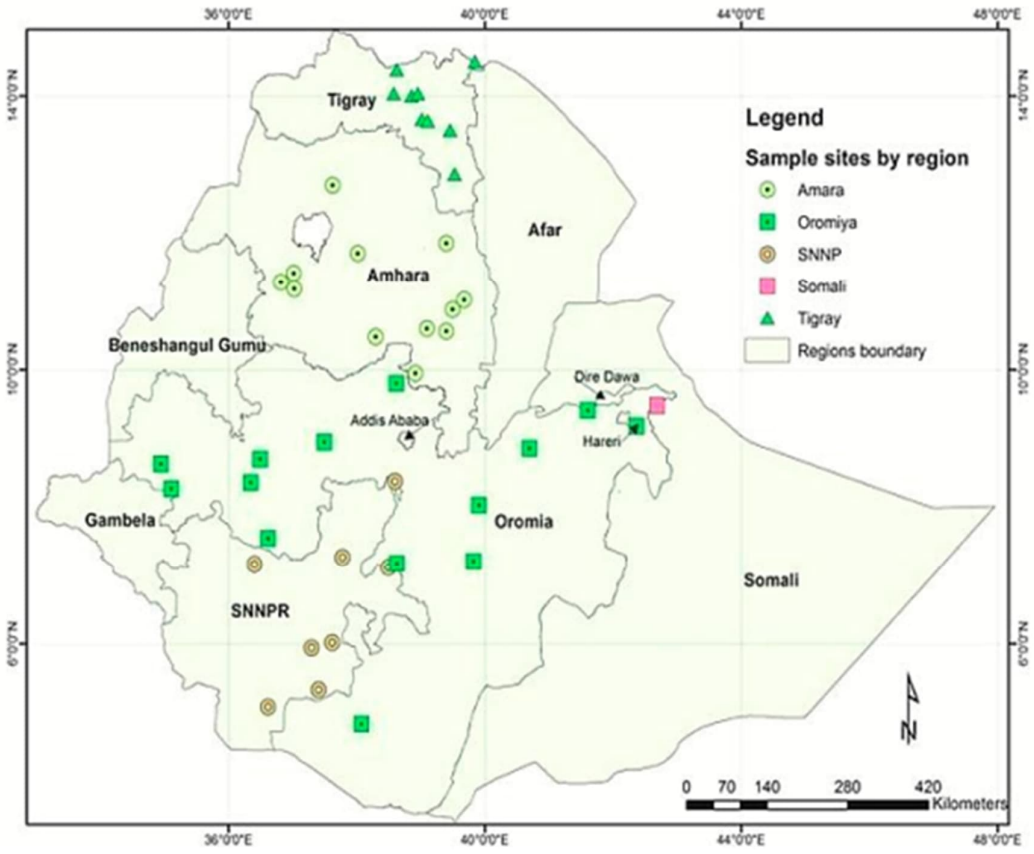

Figure 6. Map of Ethiopia showing the approximate linseed producer areas (Ali et al., 2014).

In Ethiopia, only the linseed type is available. It is cultivated in almost all parts of the country, primarily for its seeds, which are used for oil production as shown in **Figure 6** (Ali et al., 2014; Tolessa, 2023). Ethiopia produces an average of 84,000 tons of linseed annually, cultivated across approximately 82,000 hectares. According to (FAOSTAT, 2024), this

positions Ethiopia as the seventh-largest linseed producer globally and the leading producer in Africa, accounting for over 86% of the continent's total linseed output, followed by Egypt and Tunisia. From the annual linseed seed production, an estimated 126,000 tons of stalk residue are generated, of which approximately 63,000 tons are considered practically recoverable each year (Tolessa, 2023). The harvested areas and seed production volumes of top linseed producer countries in the world are shown in **Table 3** (FAOSTAT, 2024).

Table 3. Harvested areas and seed production volumes of counties in 2022 (FAOSTAT, 2024).

Country	Harvested Area [ha]	Production [t]
Russian Federation	2,040,500	1,767,000
Kazakhstan	1,345,000	845,500
Canada	312,000	473,000
China	225,000	290,000
India	197,000	126,500
USA	98,750	109,300
Ethiopia	82,000	84,000
Ukraine	32,300	27,500
France	29,000	50,800
United Kingdom	27,700	48,500
Worldwide Total	**4,533,200**	**3,974,000**

2.5. Properties of Nanocellulose

The size, shape, and other properties of nanocellulose, as well as its potential field of application, are influenced by differences in source selection, extraction methods, and subsequent chemical modifications (Kalia et al., 2011; Mohammadpour-Haratbar et al., 2024). Nanocellulose is valuable primarily for its ability to act as a reinforcing filler in composite materials. Therefore, to extract high-performance nanocellulose suitable for use in polymer composites, it is essential to thoroughly understand its structure and reinforcing capabilities. The resulting structure and properties of nanocellulose are significantly influenced by the treatment conditions applied during its extraction process (Mohammadpour-Haratbar et al., 2024).

Besides processing conditions, the type of plant source chosen can also impact the performance characteristics of nanocellulose. Factors such as botanical origin of the plant,

soil properties, climatic conditions, and age play a significant role in shaping the internal structure and chemical composition of the raw fibers (Kalia et al., 2011; Majeed et al., 2013). Nanocellulose possesses a range of distinctive properties that make it an attractive candidate for use as a reinforcing agent in polymer composites. Key attributes that promote its application in this role include the presence of abundant hydroxyl functional groups, a large specific surface area, higher aspect ratio, high crystallinity, excellent mechanical strength, and notable thermal stability (W. Zhang et al., 2011; M. T. Islam et al., 2013; Silvério, Neto, et al., 2013b).

2.5.1. Physical properties

Nanocellulose exhibits several outstanding physical properties that contribute to its versatility, including a high surface area, low density, and a high aspect ratio. Among these, the aspect ratio (defined as the ratio of length to diameter or width) is a critical factor that significantly affects the nanofiller's ability to enhance the mechanical performance of a polymer matrix (Tee et al., 2013; Amiralian et al., 2017). Nanofillers with aspect ratios greater than 30 tend to offer superior reinforcement compared to those with lower aspect ratios. In the case of nanocellulose, its aspect ratio can reach up to 100, depending on the plant source and the specific conditions used during its preparation (Rosa et al., 2010; Savadekar et al., 2012). For example, (Amiralian et al., 2017) reported nanocellulose with a high aspect ratio of 144, in which an extremophile, spinifex grass, was isolated via controlled acid hydrolysis and compared with other sources of cellulose via different acid hydrolysis methods. On the other hand, (Gabriel, Belete, et al., 2021a) reported nanocellulose isolated from different sources with different aspect ratios, such as teff straw (28), enset fiber (17), sugarcane bagasse (36) and coffee hull (25), with similar hydrolysis conditions.

Nanocellulose with a high aspect ratio is especially valuable for enhancing the performance of composite materials due to its nanoscale functional characteristics, entanglement behavior, and ability to form percolation networks (M. M. Reddy et al., 2013). A high aspect ratio in nanocellulose enhances its nanoscale effects, promoting strong interfacial interactions with the polymer matrix. This leads to efficient stress transfer between the nanocellulose and the matrix, potentially improving the overall properties of the polymer even at low filler concentrations (Rosa et al., 2010; Rebouillat et al., 2013). Fillers with a very high aspect ratio exhibit excellent flexibility, allowing them to form a complex entangled network within the matrix. This enhances reinforcement by increasing interactions with polymer chains, effectively restricting their mobility and improving the composite's

mechanical performance (Sahakaro, 2017). CNCs with a high aspect ratio tend to form a three-dimensional percolating network within the polymer matrix, primarily interconnected through hydrogen bonding. When well dispersed, this network significantly enhances both the mechanical strength and barrier properties of the polymer matrix (Ng et al., 2015a). In comparison to nanofibrils, nanocrystalline cellulose consists of shorter, rod-like particles with lower aspect ratios, which generally reduces their effectiveness in enhancing the mechanical and functional properties of polymer matrices (C. Chen et al., 2014).

Another key characteristic of nanocellulose is its specific surface area. Due to its nanoscale dimensions, nanocellulose exhibits a remarkably high surface area, which has been reported to exceed 100 m^2/g and can even reach several hundred m^2/g, depending on its form and preparation (Savadekar et al., 2012; M. T. Islam et al., 2013; Silvério, Neto, et al., 2013b). Various studies have reported the specific surface areas of nanocellulose isolated from different sources. For example, (P. Lu et al., 2012) reported nanocellulose isolated from rice straw (27 $m^2\ g^{-1}$), (Q. He, Y. Bai, et al., 2022b) from Chinese medicine residues (240 and 299 $m^2\ g^{-1}$), followed by different bleaching times, (F. Jiang et al., 2015) from tomato peels (101.8 $m^2\ g^{-1}$), (Michael Ioelovich, 2017) from sulfite pulp (170–200 $m^2\ g^{-1}$), kraft cellulose (150–170 $m^2\ g^{-1}$), flax cellulose (110–130 $m^2\ g^{-1}$) and cotton cellulose (70–100 $m^2\ g^{-1}$).

The large specific surface area of nanocellulose significantly enhances its interfacial interactions and bonding capability with compatible polymers, primarily through hydrogen bonding mechanisms (Ng et al., 2017). As the aspect ratio increases or the diameter decreases, the specific surface area of nanocellulose also increases. This elevated surface-to-volume ratio enhances the interaction with the polymer matrix at the nanoscale, improving surface reactivity and more effectively limiting the movement of polymer chains (Brinkmann et al., 2016; Ng et al., 2017). As a result of increased interfacial interactions and superior molecular-level distribution, composites can achieve improved performance with the use of relatively low amounts of filler (Rebouillat et al., 2013). The large surface area of nanosized celluloses often causes them to cluster together because of their pronounced hydrophilicity, especially upon drying. These aggregates are challenging to break apart, rendering aggregated nanocellulose unsuitable for efficient processing and for use as a reinforcing agent (Chu et al., 2020; Thakur et al., 2021). **Table 4** shows the summarized physical properties of nanocellulose isolated from different sources.

2.5.2. Chemical functional groups

The plentiful hydroxyl groups present on the surface of cellulose nanocrystals enable the formation of hydrogen bonds with hydrophilic polymer matrices and facilitate physical adhesion with nonpolar matrices, both of which contribute to improved reinforcement within the polymers (Kalia et al., 2011; Ng et al., 2015b). Hydrogen bonding between CNCs and compatible polymers creates strong interfacial interactions, facilitating efficient transfer of stress and load between the filler and matrix. This contributes to improved tensile strength and overall superior performance of the nanocomposites (Ng et al., 2015b; El-Wakil et al., 2016). The robust interface between the filler and matrix not only limits water molecule diffusion but also restricts polymer chain mobility at high temperatures, thereby improving thermal performance of the material (Idumah et al., 2021). Conversely, the plentiful hydroxyl groups on nanocellulose confer high chemical reactivity, enabling a wide range of chemical modifications. This makes it possible to enhance the compatibility and dispersion of nanocellulose within hydrophobic polymers through surface functionalization, thereby improving its performance as a reinforcing filler in polymer composites (Bangar et al., 2022). Moreover, the reinforcement provided by the rigid cellulosic network in polymers arises from strong hydrogen bonding among the hydroxyl groups of nanocellulose (Ng et al., 2015b; C. Peng et al., 2019).

FT–IR analysis can be used to detect the high concentration of hydroxyl groups on the surface of CNCs (Musino et al., 2021). The broad absorption bands observed between 3700 and 3000 cm^{-1} correspond to hydroxyl (O–H) stretching vibrations, which signify the presence of hydroxyl groups and extensive hydrogen-bonded networks (Trache et al., 2016). The intensity of these peaks increases progressively through the stages of fiber processing, from untreated fibers to alkalized fibers, bleached fibers, microfibrils, and finally nanocrystals (Ng et al., 2015b; Ilyas et al., 2017). This trend results from the increasing specific surface area as fiber size decreases, which exposes more hydroxyl groups on the surface (Jaffar et al., 2022). Consequently, the reinforcing capacity of cellulose fibers improves with each processing step due to the availability of more active sites for hydrogen bonding with the polymer matrix. Although CNCs contain fewer hydroxyl groups in their crystalline regions compared to CNFs, they may still provide superior reinforcement (Ng et al., 2015b; Ilyas et al., 2017; Jaffar et al., 2022).

Table 4. Physical properties of nanocellulose isolated form different sources

Source	Diameter/Width (nm)	Length (nm)	Aspect ratio	Shape	Reference
Teff straw	6.7 ± 2.08	193.06 ± 52.4	28.82	Needle–like	(Gabriel, Belete, et al., 2021a)
Enset fiber	8.88 ± 3.04	154.28 ± 36.7	17.32	Needle–like	
Sugarcane bagasse	5.16 ± 1.91	189.29 ± 49.9	36.68	Needle–like	
Coffee hull	7.268 ± 3.25	188.07 ± 25.8	25.88	Needle–like	
Khat waste	7.2–10.5	102–163	12.8–22.7	Needle–like	(Gabriel, Wondu, et al., 2021)
Cocoa pod husk	10–60	41–155	2.58–4.10	Rod–like	(Akinjokun et al., 2021)
Enset fibers	66	N/A	N/A	N/A	(Beyan et al., 2021)
Tea leaf fibers	7.97	N/A	N/A	Rod–like	(Abdul Rahman et al., 2017)
Pineapple leaf fiber	40–70	88–1100	3–16	N/A	(Mahardika et al., 2018)
Corn cob	28.2	N/A	N/A	Rod–like	(Ditzel et al., 2017)
Corn Stover	4.3–10.1	168–610	54.7	Rod–like	(Fonseca et al.)
Rice straw	11.2–30.7	117–270	23.1–45.4	N/A	(P. Lu et al., 2012)
Rice straw	12–48	56–779	4.66–16.22	N/A	(Srithongkham et al., 2012)
Rice straw	11.2	117	10.5	N/A	(Rivai et al., 2016)
Rice husk	39± 13	310 ± 160	10–20	Rod–like	(Collazo-Bigliardi et al., 2018)
Coffee husk	20 ± 4	310 ± 160	10–20	Rod–like	
Apple pomace	7.9 ±1.25	28 ±2.03	3.54 ±0.62	Needle–like	(Melikoğlu et al., 2019)
Sugarcane straw	6–10	120–240	20–24	Rod–like	(S. Lu et al., 2022)
Maize stalk residue	3–7	150–450	50–64	Rod–like	(A. Mtibe et al., 2015)
Coconut husk	8 ±3	172±88	22±8	Needle–like	(Nascimento et al., 2014)

Source	Diameter/Width (nm)	Length (nm)	Aspect ratio	Shape	Reference
Potato peel	10	410 ±181	41	Rod–like	(D. Chen et al., 2012)
Corncob	4.15 ±1.08	210.8±44.2	53.4±15	Needle–like	(Silvério, Flauzino Neto, et al., 2013)
Sugarcane bagasse	20–60	250–480	8–12.5	Rod–like	(A. Kumar et al., 2014b)
Soyhulls	4.43 ±1.20	122.7 ±39.40	29.41	Needle–like	(Flauzino Neto et al., 2013)
Oil palm trunk	4.28	176.20	41.16	N/A	(Lamaming et al., 2015)
Tomato peels	7.2 ±1.8	135 ±50	18.75 ±4.80	Rod–like	(F. Jiang et al., 2015)
Waste paper	3 –10	100 – 300	20 – 50	Rod–like	(Danial et al., 2015)
Onion skin	20 ±2	156 ±18	7.8 ±2.3	N/A	(Rhim et al., 2015)

N/A is parameter not available

2.5.3. Thermal properties

Lignocellulosic materials decompose thermally in three stages: moisture loss below 200°C, hemicellulose and partial lignin degradation between 180–350°C, and cellulose along with lignin breakdown from 350–500°C. Lignin decomposes slowly over a broad temperature range due to its complex structure (NorizanMohd Nurazzi et al., 2021). The thermal degradation of micro cellulose also occurs in three stages, but it shows improved thermal stability compared to raw fibers due to the elimination of non-cellulosic components. The first stage, around 200°C, involves moisture evaporation. The second stage, between 200–370°C, is associated with the breakdown of amorphous cellulose, while the third stage, from 370–520°C, corresponds to the decomposition of crystalline cellulose (Borsoi et al., 2016a). Nanocellulose typically undergoes thermal degradation in three primary stages. The first stage, occurring below 120°C, involves moisture evaporation (A. Kumar et al., 2014b; A. Mtibe et al., 2015). The second stage (120–300°C) corresponds to the degradation of amorphous cellulose regions, influenced by the cleavage of glycosidic bonds, the presence of sulfate half-ester groups, and the material's high surface area. The third stage (300–400°C) involves the breakdown of highly crystalline, non-sulfated nanocellulose. Additionally, some studies have reported a fourth stage, marked by the oxidation and decomposition of charred residues into lower molecular weight gases (A. Kumar et al., 2014b; A. Mtibe et al., 2015). Nanocellulose begins to degrade at a lower temperature than raw or micro cellulose, primarily because of its structural features such as the presence of sulfate half-ester groups, a greater number of chain ends, smaller dimensions, and higher surface area. These attributes enhance heat transfer and lower the energy required for thermal decomposition (Roman et al., 2004; W. Chen et al., 2011).

A slight reduction in the thermal stability of nanocellulose compared with that of micro cellulose was observed and reported by (Gabriel, Belete, et al., 2021a) for micro– and nanocellulose extracted from different sources, such as teff straw (207°C and 134°C), enset fiber (210°C and 133°C), sugarcane bagasse (199°C and 139°C), coffee hull (282°C and 134°C), and commercial cellulose (268°C and 142°C). On the other hand, some enhancements in the thermal stability of nanocellulose were observed, but with no negatively charged sulfate half ester groups, it was large in size, had a smaller specific surface area and was highly crystalline. For example, (Borsoi et al., 2016a) reported an increase in the onset decomposition temperature of cellulose whiskers (357°C) isolated from microcrystalline

cellulose with an onset decomposition temperature of 350°C. Similarly, (Amin et al., 2022) reported improved thermal stability of nanocellulose hydrolyzed with phosphoric acid with an onset degradation temperature of 280°C compared with micro cellulose powder (270°C) due to the presence of phosphate surface charges that do not promote dehydration reactions at low temperatures in comparison with sulfate groups. **Table 5** shows the thermal properties of nanocellulose isolated from various sources.

Table 5. Thermal properties of nanocellulose isolated from different cellulose sources

Source	T_{Onset} (°C)	T_{peak} (°C)	T_{Endset} (°C)	Reference
Khat waste	129	355[a]	470	(Gabriel et al., 2021)
Cocoa pod husk	250	332[a]	400	(Akinjokun et al., 2021)
Enset fibers	240	350[a]	395	(Beyan et al., 2021)
Pineapple leaf fiber	300	350[a]	450	(Mahardika et al., 2018)
Corn Stover	211	302[a]	390	(Fonseca et al., 2015)
Rice husk	261	301[a]	350	(Collazo et al., 2018)
Coffee husk	248	295[a]	380	
Apple pomace	150	187[a]	300	(Melikoğlu et al., 2019)
Sugarcane straw	150	253[a] and 356[b]	450	(S. Lu et al., 2022)
Maize stalk residue	170	190[a], 290[b] and 450[c]	470	(A. Mtibe et al., 2015)
Coconut husk	270	311[a]	380	(Nascimento et al., 2014)
Switch grass	145	280[a] and 450[b]	550	(Q. Wu et al., 2013)
Corncob	185	276[a] and 497[b]	424	(Silvério et al., 2013)
SCB	220	245[a], 300[b] and 400[c]	470	(A. Kumar et al., 2014b)
Soyhulls	170	294[a] and 518[b]	432	(Flauzino Neto et al., 2013)
Oil palm trunk	205	309[a]	500	(Lamaming et al., 2015)
Tomato peels	200	275[a]	340	(F. Jiang et al., 2015)
Onion skin	200	265[a] and 350[b]	370	(Rhim et al., 2015)
Teff straw	146	216[a] and 342[b]	430	
Enset fiber	112	215[a] and 348[b]	439	(Gabriel et al., 2021a)
Sugarcane bagasse	153	224[a] and 354[b]	430	
Coffee hull	152	216[a] and 355[b]	504	

[a, b and c] are the 1st, 2nd and 3rd peak decomposition temperatures, respectively.

The high thermal stability of nanocellulose is largely attributed to its highly crystalline structure, where cellulose chains are tightly packed and stabilized by strong hydrogen bonds (Kalia et al., 2011; Tonoli et al., 2012). These well-organized, three-dimensional crystalline networks resist thermal motion and do not easily allow bond rearrangement at elevated temperatures, which prevents the material from melting (Kalia et al., 2011; Tonoli et al., 2012). Due to its excellent thermal stability, nanocellulose has gained significant interest as a means of enhancing the thermal performance of polymers. However, its application is generally limited to polymers that are processed at temperatures below 200°C, as higher

temperatures may lead to the thermal degradation of the nanocellulose filler (Besbes et al., 2011; Srithep et al., 2013).

The thermal degradation of composites can be significantly delayed at elevated temperatures because nanocellulose increases the amount of heat energy needed to break down the polymer matrix (Trovatti et al., 2012). Incorporating nanocellulose into polymers also helps minimize thermal expansion and enhances the rate of heat dissipation (Trovatti et al., 2012; Y. Cao et al., 2013). This may promote broader use of biopolymer-based composites, which significantly benefit from economical approaches to improving their thermal stability (Johansson et al., 2012).

2.5.4. Structural and molecular properties

Key structural and molecular properties of nanocellulose such as crystallinity, crystal size, average molecular weight, and degree of polymerization can vary significantly based on the origin of the cellulose source and the extraction or processing conditions used (Rebouillat et al., 2013). The high crystallinity of nanocellulose stems from cellulose's fundamental chemical structure, in which each monomer contains three hydroxyl groups capable of forming numerous intra- and intermolecular hydrogen bonds. These strong interactions promote the tight packing of cellulose chains into well-organized crystalline structures (Hosakun et al., 2022; Parameswaranpillai et al., 2022).

The crystalline regions of cellulose are characterized by strong interchain hydrogen bonds, which greatly restrict their solubility in conventional organic solvents and water (Bingxin et al., 2015; Jarvis, 2023). Conversely, the amorphous, less-ordered areas of nanocellulose offer a more open structure that facilitates molecular interactions. This difference is important for comprehending cellulose's behavior across different applications (Bingxin et al., 2015; Jarvis, 2023). The crystalline structure of nanocellulose significantly influences the water uptake behavior of polymer composites. The tightly packed crystalline regions of nanocellulose limit their interaction with water molecules, in contrast with the hydrophilic surfaces rich in hydroxyl groups that promote water binding. This duality plays a crucial role in the overall water absorption characteristics of nanocellulose composites (Y.Y. Li et al., 2023). The crystalline structure of nanocellulose can greatly improve the barrier properties of hydrophilic polymers by forming complex, winding paths that hinder the diffusion of molecules like gases and water (X. Wang et al., 2023; Kramer et al., 2024). This effect is especially important for certain bio-based polymers such as PLA, TPS, and PHA, which

typically have inadequate gas and water vapor barrier performance for more demanding applications like food packaging and protective coatings (X. Wang et al., 2023; Kramer et al., 2024). Approaches to further enhance barrier properties are by incorporating highly crystalline nanocellulose. The high crystallinity of nanocellulose can strengthen the semi-crystalline polymer matrix by acting as a nucleating agent within the amorphous regions, thereby improving overall hardness of the material (Rejab et al., 2022; H. Wu et al., 2023; Xie et al., 2023). Highly crystalline nanocelluloses exhibit strong nucleation capabilities in reinforced polymers, providing abundant primary nucleation sites that promote the growth of crystallites and support the recrystallization of polymer chains at the interface (Ng et al., 2015b; H. Wu et al., 2023).

As a result, the crystal packing induced by CNCs within the matrix significantly increases the polymer's degree of crystallinity, leading to improved stiffness and rigidity of its crystalline structure (H. Wu et al., 2023). Among the structural properties, crystallinity index percentage of nanocellulose isolated from different sources was mostly calculated and reported, as shown in **Table 6**. The molecular weight and degree of polymerization of nanocellulose are key factors influencing the performance of polymer composites (Masruchin, 2023).

Generally, a higher molecular weight improves mechanical properties like tensile strength and modulus by forming a more interconnected network within the composite. However, it can also raise the viscosity, potentially hindering dispersion and causing agglomeration (Masruchin, 2023). For example, (Jinping Zhou et al., 2004) reported a molecular weight of micro cellulose of 3.22–12.86 × 10^4 g/mol extracted from cotton linters. A higher degree of polymerization enhances reinforcement efficiency and interfacial bonding by offering longer, higher molecular weight chains that interact more effectively with the polymer matrix, resulting in improved thermal stability and durability. However, during nanocellulose production, the degree of polymerization drops significantly, limiting its full mechanical performance potential (Fukuzumi et al., 2013). For example, (Corrêa et al., 2010) reported a decrease in the degree of polymerization of nanocellulose (67.5) compared with that of micro cellulose (144) extracted from curaua fibers. Similarly, (Xiong et al., 2012a) reported 219 and 144 degrees of polymerization for micro– and nanocellulose extracted from waste cotton fabrics, respectively. Therefore, largely preserving the degree of cellulose polymerization by controlling the processing conditions is highly desirable.

Table 6. Structural properties of nanocellulose isolated from different sources

Source	CrI (%)	Crystalline size (nm)	Reference
Enset fibers	80.91	1.56	(Beyan et al., 2021)
Rice straw	91.2	8.33	(P. Lu et al., 2012)
Coconut husk	82	5.0	(Nascimento et al., 2014)
Sugarcane bagasse	72.5	3.5	(A. Kumar et al., 2014b)
Soyhulls	73.5	2.73	(Flauzino N. net al., 2013)
Onion skin	27	1.76	(Rhim et al., 2015)
Teff straw	76.61	3.68	
Enset fiber	83.41	5.50	
SCB	82.60	5.36	(Gabriel et al., 2021a)
Coffee hull	80.86	5.04	
Khat waste	82.84	N/A	(Gabriel et al., 2021)
Cocoa pod husk	67.6	N/A	(Akinjokun et al., 2021)
Tea leaf fibers	83.1	N/A	(Abdul R. et al., 2017)
Pineapple leaf fiber	82.7	N/A	(Mahardika et al., 2018)
Corn cob	70.9	N/A	(Ditzel et al., 2017)
Corn Stover	43	N/A	(Fonseca et al.)
Rice straw	91.2	N/A	(Rivai et al., 2016)
Rice husk	90	N/A	(Collazo et al., 2018)
Coffee husk	92	N/A	
Apple pomace	78	N/A	(Melikoğlu et al., 2019)
Sugarcane straw	62.66	N/A	(S. Lu et al., 2022)
Maize stalk residue	72.6	N/A	(A. Mtibe et al., 2015)
Potato peel	85	N/A	(D. Chen et al., 2012)
Switch grass	69	N/A	(Q. Wu et al., 2013)
Corncob	83.7	N/A	(Silvério et al., 2013)
Oil palm trunk	63.91	N/A	(Lamaming et al., 2015)
Tomato peels	80.8	N/A	(F. Jiang et al., 2015)
Waste paper	75.9	N/A	(Danial et al., 2015)

N/A is parameter not available

For instance, (Henriksson et al., 2008) prepared nanocelluloses with varying degrees of polymerization (410, 580, and 820) from softwood pulp by controlling the enzyme concentration and (Fukuzumi et al., 2013) obtained nanocelluloses with different degrees of polymerization (250–400) by regulating the processing time of ultrasonic disintegration.

On the other hand, a higher degree of polymerization may also affect the crystallinity and size of nanocellulose (Jie Zhou et al., 2022; Masruchin, 2023). Therefore, these benefits must be balanced against potential challenges in processing and compatibility, especially in terms of hydrophilic and hydrophobic interactions. Achieving an optimal balance of molecular weight and degree of polymerization is key to maximizing the effectiveness of nanocellulose in composite materials (Jie Zhou et al., 2022).

2.6. Potential Applications of Nanocellulose

2.7. Nanocellulose has attracted widespread attention in recent decades due to its renewable nature, unique surface chemistry, impressive physical characteristics, and favorable biological traits such as biocompatibility, biodegradability, and non-toxicity (Seddiqi et al., 2021). Leveraging these attributes, researchers are now designing innovative and multifunctional materials to address diverse needs in areas like medicine, energy, environment, agriculture, and material engineering. Its potential applications span a wide range of industries, including packaging, filtration, construction, textiles, electronics, cosmetics, and coatings, as illustrated in **Figure 7** (Ul-Islam et al., 2016; Chaka, 2022). The suitability of a material for a particular application is determined by how closely its properties match the technical requirements and standards of that application (Abdel-Hakim et al., 2023). Nanocelluloses (NCs), in particular, are ideal for sensing technologies due to their abundance, biocompatibility, versatility, and ability to interact with a wide range of molecules through numerous functional groups (Abdel-Hakim et al., 2023).

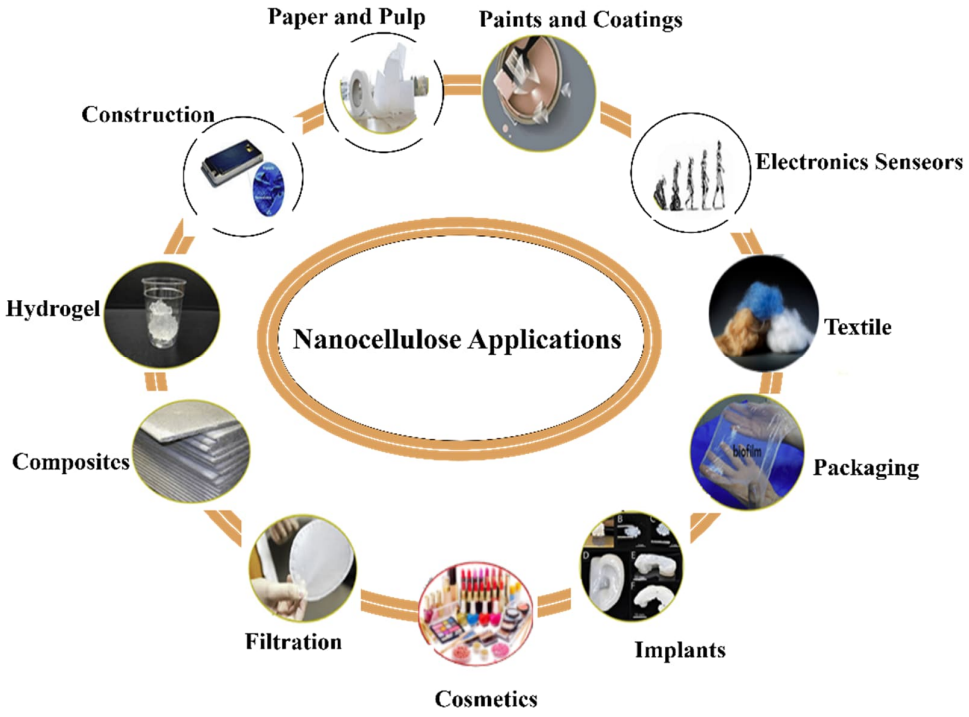

Figure 7. Potential applications of nanocellulose in various fields (Adapted from (Ul-Islam et al., 2016; Chaka, 2022).

A study by (Weishaupt et al., 2017) reported protein-nanocellulose paper for sensing copper ions at the nano- to micromolar level. Another study on a potential sensor for water–soluble

gases from rice husk–derived cellulose nanofibers was reported by (Shahi et al., 2021). Another report by (Kafy et al., 2015) developed cellulose/graphene nanocomposites as multifunctional electronic and solvent sensor materials.

Nanocellulose and its composites can be used in the electronics industry because of their enhanced flexibility and conductivity (Abdel-Hakim et al., 2023). (J. Han et al., 2019) reported the nanocellulose–templated assembly of polyaniline in natural rubber–based hybrid elastomers toward flexible electronic conductors. A study by (W. Yang et al., 2018) reported that flexible cellulose nanofibril film substrates with highly smooth surfaces and high transparency are attractive for next–generation flexible transparent electrical device applications. Moreover, (Zheng et al., 2017) reported nanocellulose–mediated hybrid polyaniline electrodes for high–performance flexible supercapacitors.

Owing to their high strength and stiffness, NC–based composites can be used for load–bearing walls, roof systems, staircases, and subflooring or as bio foam in insulation (Abdel-Hakim et al., 2023). For example, (Missio et al., 2022) reported green and sustainable foams that were stronger, lighter, and more resistant to fire produced by nanocellulose crosslinking. Cellulose nanocomposites have potential applications in the paper and cardboard industries, where they can be used as strengthening agents. Cellulose nanocomposites can increase the bond strength between cellulosic fibers and thus increase the mechanical properties of these materials. The burst strength, smoothness, density, and barrier properties of paper and cardboard can also be improved by the incorporation of nanocomposites (Abdel-Hakim et al., 2023). (Barbash et al., 2020) presented the application of nanocellulose isolated from nonwood plants to improve the quality of paper and cardboard. In addition, (Perdoch et al., 2022) studied the influence of different nanocellulose structures for paper reinforcement.

Due to their excellent biocompatibility, low toxicity, unique structural and surface properties, and favorable mechanical and rheological characteristics, nanocellulose (NC) and its composites stand out as advanced materials for medical applications (Tang et al., 2015). Crystalline nanocellulose (CNC), in particular, exhibits antimicrobial properties, strong water retention, and mechanical strength, making it ideal for use in wound healing dressings (Ghafari et al., 2019). Overall, NC is applied in various biomedical fields, including drug delivery, surgical treatments like skin and burn dressings, dental implants and scaffolds, eye-related devices such as contact lenses and retinal prostheses, and biosensing technologies (Abdel-Hakim et al., 2023). (Tang et al., 2015) reported the potential of PVA–doped bacterial nanocellulose tubular composites for artificial blood

vessels. Similarly, a novel bilayer scaffold from a nanocellulose–based aerogel for skin tissue engineering applications was reported by (Ghafari et al., 2019).

Nanocellulose and its composites play a significant role in the creation of packaging films. Owing to their nontoxicity, renewability, and ecologically beneficial qualities, these materials are flexible and strong enough to resist damage caused by heat, chemicals and microorganisms. In addition, it is transparent enough to allow food quality control upon storage (Abdel-Hakim et al., 2023). Spherical nanocellulose was used to prepare green composites with PLA for food packaging applications (F. Lu et al., 2016), and (Heidarbeigi et al., 2021) mixed CNCs with low–density polyethylene (LDPE) for packing applications with enhanced gas permeability.

Nanocellulose and its composite are promising candidates for water purification applications because they are biodegradable, nontoxic, and sustainable nanofillers with outstanding mechanical properties, high aspect ratios, large surface areas, and, most importantly, chemically tunable surfaces (Abdel-Hakim et al., 2023). (W. Zhu et al., 2022) presented a nanocellulose/Zn–MOF–based catalytic filter for water purification via an oxidation process, and (Ashori et al., 2019) reported cellulose nanocrystal–reinforced polyether sulfone nanocomposite membranes via an electrospinning technique for water purification.

Nanocellulose–based nanocomposites can also be implemented in fire extinguishers (Asyraf et al., 2020) and automotive components (Ilyas et al., 2020; Ilyas et al., 2021) because of their high thermal stability and tensile strength. Nanocellulose holds significant promise for applications in flexible electronics, smart materials, 3D printing, and various medical and energy-related technologies. Additionally, microcrystalline cellulose is widely utilized in diverse fields, serving roles such as abrasives in cosmetics, adsorbents, anti-caking agents, bulking agents, viscosity enhancers in aqueous systems, binders, emulsion stabilizers, slip modifiers, and texturizers (Norrrahim et al., 2021).

2.8. Extraction Methods and Procedures

2.8.1. Extraction of Fiber and Cellulose Macrofibril

The first stage of fiber processing involves extracting fibers from plant stalks or stems. This requires separating the outer fiber bundles by breaking the bonds that connect them to the stem core, typically through a multistep process that isolates technical fibers, elementary fibers, as well as cellulose macro fibrils and microfibrils (Réquilé et al., 2018; Woigk et al.,

2019), as shown in **Figure 2**. Generally, two main techniques namely, mechanical and retting extractions are employed for this purpose (C. H. Lee et al., 2020), as shown in **Figure 8.**

2.8.1.1. Mechanical extraction

Mechanical extraction relies on physical forces to break the bonds between the fiber and the plant core. During this process, plant stalks are fed into a decorticator, where they are broken down using compressive, shear, or impact forces (C. H. Lee et al., 2020). Various types of decorticators such as crushing rollers, hammer mills, ball mills, and drop weights are employed for this purpose. After decortication, a cleaning step is carried out to separate the loosened fibers from the remaining mixture of fiber-bound core fragments and fine particles (C. H. Lee et al., 2020). However, a major challenge of this method is the difficulty in precisely controlling the applied mechanical forces (Bos, 2004; C. H. Lee et al., 2020). Furthermore, mechanical extraction often results in fibers of inconsistent lengths and is generally associated with high operational costs (P. M. Tahir et al., 2011; C. H. Lee et al., 2020).

2.8.1.2. Retting extraction

Retting is a complex process, and its effectiveness largely depends on the type of retting method used and the specific processing conditions. If the fibers are under-retted, separation is inefficient, while over-retting can weaken the fibers (Preisner et al., 2014; C. H. Lee et al., 2020).

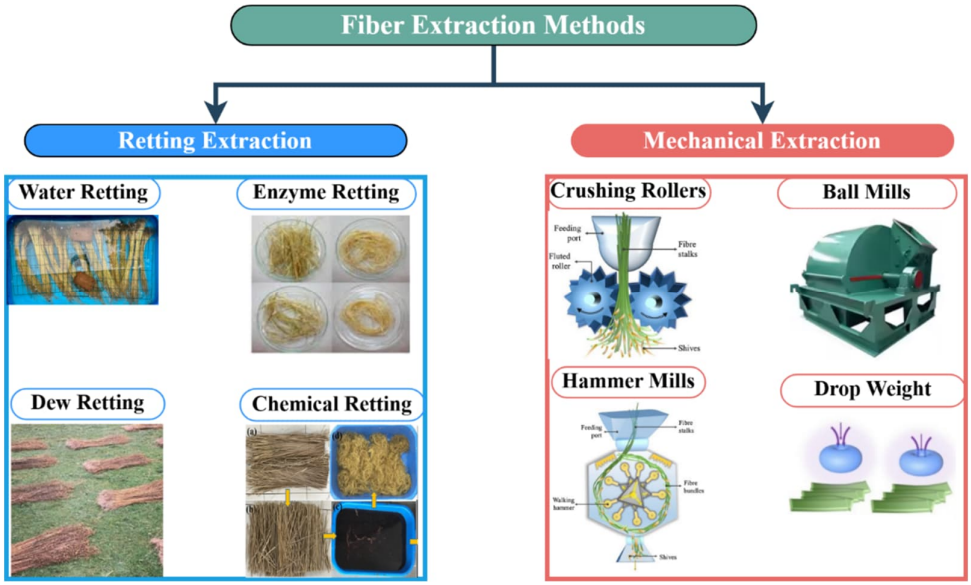

Figure 8. Fiber extraction methods (Adapted from (C. H. Lee et al., 2020)

During retting, fiber bundles originating from the phloem are separated by breaking down surrounding components like hemicellulose, lignin, and pectin. This is primarily a biological process, where enzymes degrade the non-cellulosic substances binding the fibers, resulting in isolated cellulosic fibers. With the exception of chemical retting, all retting methods rely on enzymatic activity to facilitate fiber extraction fibers (Preisner et al., 2014; C. H. Lee et al., 2020). Water retting and dew retting involve biological methods to degrade the substances that bind fiber bundles. Water retting utilizes anaerobic bacteria to produce pectinase enzymes, which help break down fiber-binding components, but this process often leads to serious environmental problems such as water pollution, foul odors, and wastewater contamination (Akin et al., 2004; C. H. Lee et al., 2020). Dew retting, on the other hand, relies on fungi from the soil that colonize bast stems. Although it is less harmful to the environment and more cost-effective, dew retting is slow, yields inconsistent results, and is highly influenced by local climatic conditions (Speri, 2011; C. H. Lee et al., 2020). Chemical retting provides faster and more controlled fiber extraction, but it is costly and can negatively affect the fiber's color and tensile strength (C. H. Lee et al., 2020). In search of improved methods, researchers have turned to enzyme retting, which uses specific enzymes under gentle conditions without harmful chemicals. This method can produce fibers of similar quality to those obtained by water retting. However, prolonged exposure to enzyme mixtures, especially those containing cellulase, can weaken the fibers, making it critical to carefully control the retting time (C. H. Lee et al., 2020). Comparisons of different extraction techniques are summarized in the table shown in **Table 7** (C. H. Lee et al., 2020) .

2.8.2. Extraction of micro and nanocellulose

The extraction of micro and nanocellulose is a rather complicated process, often involving several steps of mechanical, chemical, and biological approaches, each with distinct advantages and challenges, as shown in **Figure 9**. Recent studies highlight innovative techniques that enhance yield, properties and sustainability while minimizing environmental impact (Tarchoun et al., 2024).

2.8.2.1. Mechanical extraction

In mechanical extraction, the native structure of cellulose fibers is disrupted, breaking them down into nanofibrils (NFCs) or microfibril bundles (MFCs), typically with diameters between 10 and 100 nanometers and lengths in the micrometer range (Kargarzadeh, Ahmad, et al., 2017). A variety of mechanical methods are available for isolating cellulose nanofibrils

(CNFs) or cellulose microfibrils (CMFs) from different raw materials, including high-pressure homogenization, steam explosion, microdissection, grinding, cryo-crushing, and high-intensity ultrasonication (Chaka, 2022; D. Tahir et al., 2022).

2.8.2.2. Biological extraction

Biological methods, including enzymatic, bacterial, and fungal treatments, offer a more environmentally friendly alternative to chemical processes by selectively breaking down lignin and hemicellulose (Cleverton L Pirich et al., 2020). Enzymatic hydrolysis uses specific enzymes to isolate cellulosic fibers with low energy input and minimal environmental impact. Despite being eco-friendly, this method is slower and more costly. Common enzymes used include cellobiohydrolases, endoglucanases, xylanases, and ligninases (Zinge et al., 2020).

2.8.2.3. Chemical extraction

The extraction of nanocellulose via chemical techniques typically involves several steps to isolate and refine cellulose fibers into nanoscale dimensions. The extraction steps involved pretreatment, treatment and posttreatment (Kargarzadeh, Ioelovich, et al., 2017a). Various studies utilized and reported different methods and chemicals to isolate nanocellulose from different sources as shown in **Table 8**.

Table 7. Comparisons of different fiber extraction methods (C. H. Lee et al., 2020).

Extraction methods	Advantages	Disadvantages	Retting duration
Water retting	• Produces retted fibers with great uniformity and high quality	• Putrid odor, environmental problems, and high–water consumption, requires intense treatment on wastewater	7–14 days
Dew retting	• Pectin materials could easily be removed	• Product contaminated with soil, restriction to certain climatic change, inconsistent quality, and reduced strength	2–3 weeks
Enzymatic retting	• Specific properties can be achieved for different applications by varying retting period and type of enzymes used and the process is cleaner and faster	• Low fiber strength	12–24 hours
Chemical retting	• The smooth and clean surface can be obtained, consistency within a short period	• Deterioration of fiber strength when the chemical concentration, temperature and time are higher, as well as it has a high processing cost and unfavorable color	60–75 minutes
Mechanical extraction	• High quantities of the short fiber shall be yielded in a short period	• Lower fiber quality and high cost	N/A

Pre–treatment methods

The purpose of implementing these pretreatments is mainly to remove impurities such as wax, lignin, pectin, and hemicelluloses and to facilitate partial breakdown of cellulosic fibers (Vishnu et al., 2019). Various pretreatment processes and chemicals used to isolate nanocellulose, specifically dewaxing, delignification, alkalization and bleaching, have been reported in the literature. Mixtures of toluene–ethanol (Chime et al., 2022; Lalita Chopra, 2022), benzene–ethanol (Guo et al., 2021) and ethanol–water (Bangar et al., 2023) are commonly used as solvents for dewaxing cellulose fibers to remove impurities and extractives (wax, pectin). Toluene–ethanol is a commonly used and reported solvent for dewaxing, among other methods (Akinjokun et al., 2021; Beyan et al., 2021). The most commonly used chemical solutions for the delignification of cellulose fibers to remove lignin are alkaline hydrogen peroxide, hydrogen peroxide, sodium hypochlorite, sodium chlorite and mixtures of chlorine reagents with hydrogen peroxide, alkalinity and acids (Ventura-Cruz et al., 2020; Assefa et al., 2023).

Chlorine reagents are still used in most delignification and bleaching treatments, considering their remarkable oxidation of residual polymeric lignin with little destruction of the polymeric chain of polysaccharides (P. Lu et al., 2012; Abdul Rahman et al., 2017; Akinjokun et al., 2021). (A. Mtibe et al., 2015) uses $NaClO_2$ and NaClO, as reported by (Melikoğlu et al., 2019) (Danial et al., 2015). For effective delignification and bleaching processes, some studies have reported mixtures of chlorine reagents with hydrogen peroxide, alkaline reagents and acids (Fonseca et al.; Mahardika et al., 2018; Beyan et al., 2021). However, the environmental efficacy of chlorine reagents is high (Beroual et al., 2021). To reduce this problem, alkaline hydrogen peroxide and hydrogen peroxide are used and recommended (Srithongkham et al., 2012; Nascimento et al., 2014; Ditzel et al., 2017; Saha et al., 2019).

The delignified fibers are further treated during the alkalization process via the use of widely used chemicals such as NaOH (Yuliasmi et al., 2019; Noori et al., 2021) and KOH (R. Ray et al., 2020; Trembus et al., 2022) to remove hemicelluloses. Some studies also reported a mixture of NaOH with KOH, H_2O_2, Na_2SO_3, acetic acid and formic acid (Gabriel, Wondu, et al., 2021) and a mixture of acetic acid with HCl acid (Ditzel et al., 2017). To obtain highly purified cellulose, the alkalized cellulose fibers should be further bleached with H_2O_2 (Mahmoud et al., 2021; Rizwan et al., 2021).

Hydrolysis treatment methods

Hydrolysis is the primary technique employed for extracting micro- and nanocellulose, where the amorphous regions of cellulose are removed, crystalline linkages between fibrils are separated, and crystalline nanocellulose (CNCs) is released through a controlled chemical process most commonly acid hydrolysis (K.-H. Lin et al., 2019). This method uses strong mineral acids to break down purified cellulose, with key parameters such as temperature, duration, acid concentration, and mixing ratio carefully regulated to ensure effective CNC isolation (Kargarzadeh, Ioelovich, et al., 2017a).

For hydrolysis, various types of mineral acids can be utilized, such as sulfuric (H_2SO_4) (K.-H. Lin et al., 2019), hydrochloric (HCl) (Noremylia et al., 2022), nitric (HNO_3) (Mohomane et al., 2022), phosphoric (H_3PO_4) (Soleimani et al., 2022), maleic ($C_4H_4O_4$) (S. Zhu et al., 2023), and formic (HCOOH) (J. Jiang et al., 2021) acids. Additionally, the combination of HCl with organic acids, such as acetic acid (CH_3COOH) (Beyene et al., 2020) and butyric acid ($C_4H_8O_2$) (J. Jiang et al., 2021), has also been reported. Among the mentioned mineral acids, the most commonly used acid to prepare CNCs is sulfuric acid (Akinjokun et al., 2021; Beyan et al., 2021; Gabriel, Wondu, et al., 2021). Sulfuric acid offers the advantage of introducing anionic sulfate ester groups onto the cellulose surface through esterification. These anionic groups create a negatively charged electrostatic layer on the nanocrystal surface, which enhances their stability and dispersion in aqueous solutions (Cleverton Luiz Pirich et al., 2019; Lim et al., 2021).

Post–treatment methods

The third stage of treatment, commonly known as posttreatment methods followed by acid hydrolysis for isolating CNCs, includes centrifugation, neutralization, dialysis, sonication and drying (Jordan et al., 2019; Kian et al., 2019). For the effective processing and commercialization of nanocellulose, dewatering and drying methods are crucial post–treatment steps (Q. Wang et al., 2019). The high thixotropic viscosity of the dilute suspension is a result of the large surface area, hydrophilic nature, and high water–holding capacity of the CNCs.

Therefore, dewatering and drying of CNCs via conventional methods may cause irreversible particle agglomeration, which prevents them from dispersing again upon rehydration due to the hydrogen bonding of the particles. Solvent evaporation, centrifugation, shear stress–aided dewatering, filtration, and pressing are some of the current methods utilized in nanocellulose dewatering to reduce obstacles. To properly dry the nanocellulose gel, a

drying step, such as an oven, spray, freeze, or supercritical CO_2 drying technique, is required after dewatering (Sinquefield et al., 2020). Freeze drying is a commonly used technique because of its low degree of irreversible particle agglomeration during drying (P. Lu et al., 2012; Mondragon et al., 2014b; Akinjokun et al., 2021).

Treatment conditions for nanocellulose isolation

The treatment conditions, such as concentration, mixing ratio, reaction time, temperature and number of repetitions, may vary across studies for successful extraction of pure cellulose from different sources as shown in the summarized **Table 9**. In their study, (Collazo-Bigliardi et al., 2018) performed alkali treatment using 4% sodium hydroxide, followed by bleaching with an acetate buffer and 1.7% sodium chlorite, and then subjected the material to acid hydrolysis with 64% sulfuric acid at 50°C for 40 minutes. Similarly, (Lamaming et al., 2015) used a dewaxing step with ethanol: toluene (1:2, v/v) for 6 hours, bleaching with sodium chlorite in an acidic medium (acetic acid, pH 4–5) at 70°C for 3 hours, alkalization with 6% KOH at 20°C for 24 hours, and acid hydrolysis in 210 mL of 64% sulfuric acid at 45°C for 1 hour.

(Gabriel, Wondu, et al., 2021) adopted a delignification method using 40% formic acid and 40% acetic acid at 90°C for 1.5 hours in a water bath, followed by a 2.5% NaOH treatment for 1 hour. For bleaching, a mixture of 20% formic acid, 20% acetic acid, and 7.5% hydrogen peroxide (in a 2:1:2 ratio) was applied at 90°C for 1.5 hours, followed by an additional step using 10% hydrogen peroxide in an alkaline medium at 70°C for 30 minutes, before carrying out hydrolysis with 64% sulfuric acid. (Akinjokun et al., 2021) followed a dewaxing process using ethanol: toluene (1:2) for 6 hours, then treated the sample with 4% NaOH at 80°C for 2 hours for alkalization. Bleaching was performed using a 1.7% sodium chlorite solution at 80°C for 4 hours, followed by hydrolysis in 64% sulfuric acid at 45°C for 1 hour with vigorous stirring.

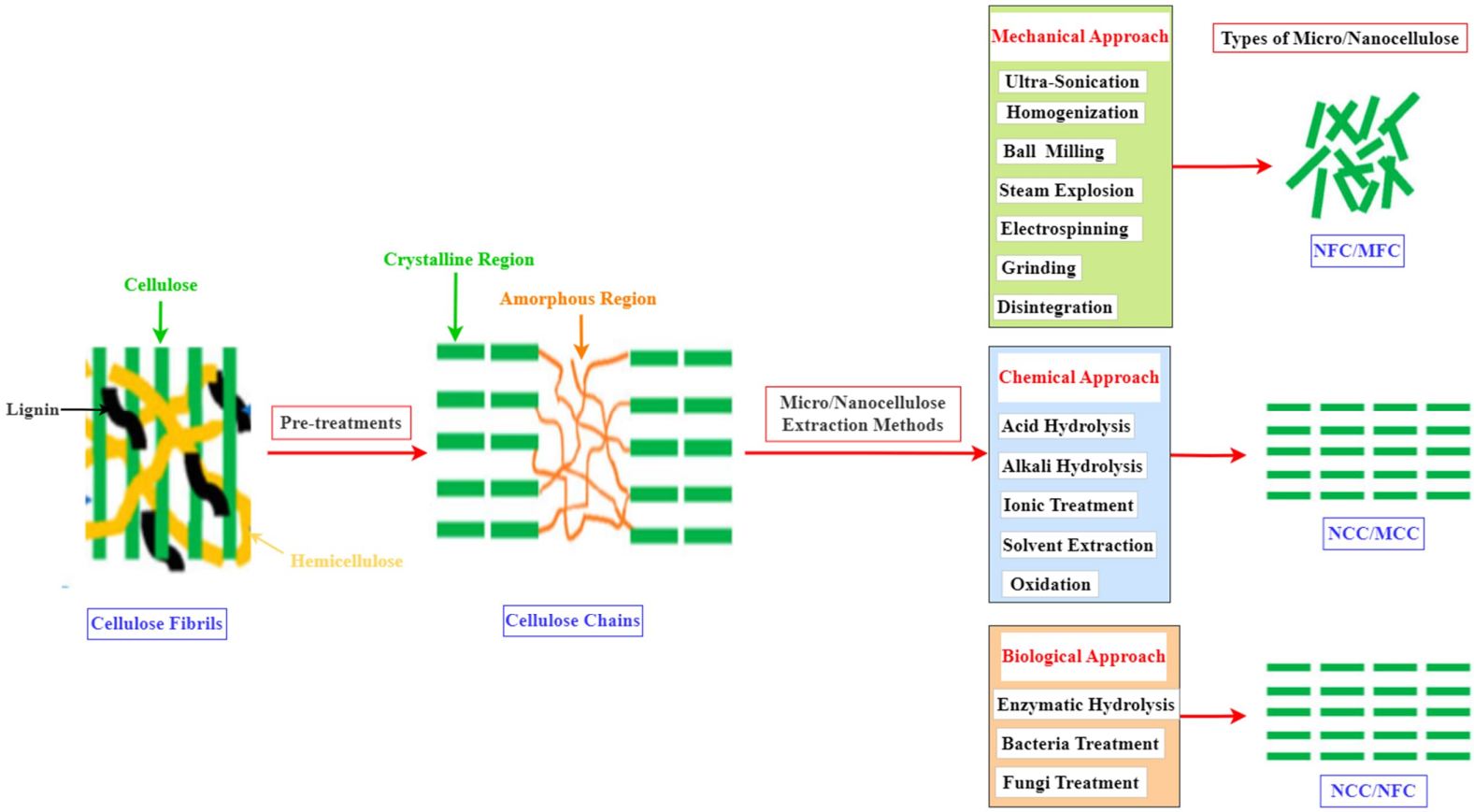

Figure 9. Schematic diagram of micro and nanocellulose extraction from lignocellulosic biomass (Adapted from (Chaka, 2022; D. Tahir et al., 2022).

Table 8. Nanocellulose isolation methods and procedures

Sources	Pretreatments			Hydrolysis treatments	Posttreatments	References
	Dewaxing treatments	**Alkali treatments**	**Delignification/ Bleaching treatments**			
Khat waste	N/A	Formic/acetic acids and NaOH	H_2O_2	H_2SO_4	Successive centrifugations, dialysis, homogenization and freeze drying	(Gabriel, Wondu, et al., 2021)
Cocoa pod husk	Toluene: ethanol	NaOH	$NaClO_2$	H_2SO_4	Centrifugations, dialysis, sonication and freeze drying	(Akinjokun et al., 2021)
Enset fibers	Toluene: ethanol	NaOH	Acetic acid /NaClO	H_2SO_4	Washing, dialysis and sonication	(Beyan et al., 2021)
Tomato peels	Toluene: ethanol	NaOH and H_2O_2	$NaClO_2$ and KOH	H_2SO_4	Centrifugations, sonication and freeze drying	(Assefa et al., 2023)
Tea leaf fibers	N/A	NaOH	$NaClO_2$	H_2SO_4	Centrifugations, dialysis and sonication	(Abdul Rahman et al., 2017)
Pineapple leaf fiber	N/A	NaOH	$NaClO_2$ /acetic acid	HCl	High–shear homogenization and ultrasonication	(Mahardika et al., 2018)
Corn cob	Acetosolv	Acetic and HCl acids	NaOH and H_2O_2	H_2SO_4	Repeated centrifugations, dialysis and homogenization	(Ditzel et al., 2017)

Sources	Pretreatments			Hydrolysis treatments	Posttreatments	References
	Dewaxing treatments	**Alkali treatments**	**Delignification/ Bleaching treatments**			
Corn Stover	NaOH and hot water	NaClO/buffer solution	NaOH and $NaClO_2$	H_2SO_4	Repeated centrifugations, dialysis and sonication	(Fonseca et al., 2015)
Rice straw	Toluene: ethanol	KOH	$NaClO_2$	H_2SO_4	Centrifugations, dialysis, sonication and freeze drying	(P. Lu et al., 2012)
Rice straw	N/A	NaOH	H_2O_2	HCl	High–shear homogenization	(Srithongkham et al., 2012)
Rice straw	Hexane: ethanol	NaOH and NaOH/Na_2SO_3	Nitric acid/$NaNO_2$ and NaClO	HCl	Neutralization, filtration and oven drying	(Rivai et al., 2016)
Rice husk	N/A	NaOH	$NaClO_2$/Buffer solution	H_2SO_4	Repeated centrifugation, dialysis and sonication	(Johar et al., 2012)
Rice and Coffee husk	N/A	NaOH	$NaClO_2$/Buffer solution	H_2SO_4	Repeated centrifugation, dialysis, neutralization, filtration and sonication	(Collazo-Bigliardi et al., 2018)
Kenaf fibers	N/A	NaOH	$NaClO_2$/Buffer solution	H_2SO_4	Repeated centrifugations and dialysis	(Zainuddin et al., 2013)
Apple pomace	HCl	NaOH	NaClO	H_2SO_4	Repeated centrifugations, dialysis, homogenization and freeze drying	(Melikoğlu et al., 2019)

Sources	Pretreatments			Hydrolysis treatments	Posttreatments	References
	Dewaxing treatments	**Alkali treatments**	**Delignification/ Bleaching treatments**			
Sugarcane straw	Ethanol	NaOH	$NaClO_2$	H_2SO_4	Washing, centrifugation and ultrasonication	(S. Lu et al., 2022)
Commercial cellulose	N/A	N/A	N/A	$Cr(NO_3)_3$	Centrifugations, dialysis and freeze drying	(Y. W. Chen et al., 2017)
Maize stalk residue	N/A	NaOH and KOH	$NaClO_2$	H_2SO_4 and mechanical blender and grinder	Centrifugation, dialysis and ultrasonication	(A. Mtibe et al., 2015)
Coconut husk	N/A	Acetic and HCl acids	H_2O_2 and NaOH	H_2SO_4	Repeated centrifugation, sonication cycles, and dialysis	(Nascimento et al., 2014)
Potato peel	N/A	NaOH	$NaClO_2$/acetate buffer	H_2SO_4	Repeated centrifugation and dialysis	(D. Chen et al., 2012)
Switch grass and cotton	Benzene: ethanol	KOH	$NaClO_2$	H_2SO_4	Centrifugation, dialysis and ultrasonication	(Q. Wu et al., 2013)
Corncob	N/A	NaOH	NaOH, $NaClO_2$ and acetic acid	H_2SO_4	Centrifugation, dialysis and ultrasonication	(Silvério, Flauzino Neto, et al., 2013)
Sugarcane bagasse	Benzene: methanol	KOH	$NaClO_2$	H_2SO_4	Successive centrifugation, dialysis and sonication	(A. Kumar et al., 2014b)

Sources	Pretreatments			Hydrolysis treatments	Posttreatments	References
	Dewaxing treatments	**Alkali treatments**	**Delignification/ Bleaching treatments**			
Sugarcane bagasse	Ultrasonicated in distilled water	NaOH and H_2O_2	NaOH and H_2O_2	H_2SO_4	Repeated centrifugations, ultrasonication and freeze drying	(Saha et al., 2019)
Soyhulls	N/A	N/A	NaOH, $NaClO_2$ and acetic acid	H_2SO_4	Centrifugation, dialysis and sonication	(Flauzino Neto et al., 2013)
Kenaf fiber	N/A	NaOH	NaOH, $NaClO_2$ and acetic acid	H_2SO_4	Repeated centrifugation, dialysis, ultrasonication and freeze–drying	(Kargarzadeh et al., 2012)
Mengkuang leaves	N/A	NaOH	$NaClO_2$	H_2SO_4	Repeated centrifugation, dialysis and sonication	(Sheltami et al., 2012)
Agave	N/A	NaOH	$NaClO_2$	H_2SO_4	Repeated centrifugation, neutralization and dialysis	(Rosli et al., 2013)
Commercial cotton linter pulp	N/A	N/A	N/A	H_2SO_4	Repeated centrifugation, neutralization, dialysis, ultrasonication and filtration	(Oun et al., 2015)
Oil palm trunk	Toluene: ethanol	KOH	$NaClO_2$	H_2SO_4	Centrifugation and dialysis	(Lamaming et al., 2015)
Tomato peels	Toluene: ethanol	NaOH and KOH	$NaClO_2$ and H_2O_2	H_2SO_4	Repeated centrifugation, dialysis, sonication, filtration	(F. Jiang et al., 2015)

Sources	Pretreatments			Hydrolysis treatments	Posttreatments	References
	Dewaxing treatments	**Alkali treatments**	**Delignification/ Bleaching treatments**			
					and freeze–drying	
Waste paper	Hot water	NaOH	NaClO	H_2SO_4	Centrifugation and dialysis	(Danial et al., 2015)
Onion skin	N/A	NaOH	$NaClO_2$, acetic acid and Na_2SO_3	H_2SO_4	Repeated centrifugation, dialysis, ultrasonication, and freeze–drying	(Rhim et al., 2015)
Beer industrial residues	N/A	NaOH and KOH	$NaClO_2$ and acetic acid	HCl	Repeated centrifugation, neutralization and ultrasonication	(Shahabi-Ghahafarrokhi et al., 2015)
Bamboo	$HNO_3/KClO_3$	N/A	N/A	H_2SO_4	Dialysis and freeze–drying	(Liu et al., 2010)
MCC	N/A	N/A	N/A	HBr	Repeated centrifugation, ultrasonication, and freeze–drying	(S.-Y. Lee et al., 2009)

N/A is parameter not available

Table 9. Different treatment conditions used for nanocellulose isolation

Sources	Chemicals	Treatment Conditions			References
		Concentration (%)	Temperature (°C)	Time (h)	
Various dewaxing treatments					
Cocoa pod husk	Ethanol: toluene (1:2 v/v)	Pure	78	6	(Akinjokun et al., 2021)
Oil palm trunk	Ethanol: toluene (1:2 v/v)	Pure	80	6	(Lamaming et al., 2015)
Tomato peels	Ethanol: toluene (1:2 v/v)	Pure	70	20	(F. Jiang et al., 2015)
Waste paper	Hot water	Pure	100	12	(Danial et al., 2015)
Switch grass and cotton	Benzene: ethanol (2:1 v/v)	Pure	N/A	6	(Q. Wu et al., 2013)
Sisal, flax and hemp	Ethanol: toluene (1:2 v/v)	Pure	N/A	N/A	(Mondragon et al., 2014b)
Sugarcane	Ethanol	95	75	2	(S. Lu et al., 2022)
Rice straw	Hexane: ethanol (2:1 v/v)	Pure	70	6	(Rivai et al., 2016)
Rice straw	Ethanol: toluene (1:2 v/v)	Pure	N/A	20	(P. Lu et al., 2012)
Enset fibers	Ethanol: toluene (1:2 v/v)	Pure	120	5	(Beyan et al., 2021)
Various alkali treatments					
Cocoa pod husk	NaOH	4	80	2	(Akinjokun et al., 2021)
Oil palm trunk	KOH	6	20	24	(Lamaming et al., 2015)
Tomato peels	NaOH	1, 3, 5 and 8	RT	24	(F. Jiang et al., 2015)
	NaOH	1, 3, 5 and 8	90	5	
	KOH	5	RT	24	
	KOH	5	90	2	

Sources	Chemicals	Treatment Conditions			References
		Concentration (%)	Temperature (℃)	Time (h)	
Waste paper	NaOH	5	N/A	N/A	(Danial et al., 2015)
Switch grass and cotton	KOH	5	90	4	(Q. Wu et al., 2013)
Sisal, flax and hemp	NaOH	2	40	12	(Mondragon et al., 2014b)
	NaOH	7.5	40	1.5	
Sugarcane	NaOH	10	75	1	(S. Lu et al., 2022)
Rice straw	NaOH	17.5	80	0.5	(Rivai et al., 2016)
	NaOH/Na2SO3	2	50	1	
Rice straw	KOH	5	RT	24	(P. Lu et al., 2012)
	KOH	5	90	2	
Corn Stover	NaOH	2	80	4	(Fonseca et al.)
Corn cob	NaOH/H_2O_2 (1:1v/v)	4/24	50	3.5	(Ditzel et al., 2017)
Enset fibers	NaOH	15	130	6	(Beyan et al., 2021)
Rice and Coffee husk	NaOH	4	80	4	(Collazo-Bigliardi et al., 2018)
Khat waste	NaOH	2.5		1	(Gabriel, Wondu, et al., 2021)
Coconut husk fiber	NaOH	2	80	2	(Rosa et al., 2010)
Kenaf fiber	NaOH	4	80	3	(Shin et al., 2012)
Bamboo fiber	NaOH	2	60	4	(T. Lu et al., 2013)
Cotton	NaOH	2	RT	13	(Pereda et al., 2014)

Various delignification/bleaching treatments

Sources	Chemicals	Treatment Conditions			References
		Concentration (%)	Temperature (℃)	Time (h)	
Kenaf fiber	$NaClO_2$/Acetic acid	2/3	70	3	(Mehdi Jonoobi et al., 2009)
	$NaOH/H_2O_2$	1.5/1	70	1.5	
	$NaClO_2$/Acetic acid	1.25/3	70	1.5	
	NaClO	1.2	RT	1	
Rice husk	$NaClO_2$ and Acetic acid	1.7	100–130	4	(Johar et al., 2012)
Rice straw	Nitric acid	3.5	90	2	(Rivai et al., 2016)
	NaClO	3.5	100	0.16 and 0.08	
Waste paper	NaClO	2	N/A	N/A	(Danial et al., 2015)
Corn cob	$NaClO_2$	1.7	80	6	(Silvério, Neto, et al., 2013a)
Rice straw	$NaClO_2$	1.4	70	5	(P. Lu et al., 2012)
Rice and Coffee husks	Acetate buffer and $NaClO_2$	1.7	80	6	(Collazo-Bigliardi et al., 2018)
Oil palm trunk	$NaClO_2$	1.4	70	3	(Lamaming et al., 2015)
Corn Stover	NaClO/buffer solution	1.7	80	6	(Fonseca et al.)
Corn cob	Acetic/HCl acids	0.3/6.8	115	3	(Ditzel et al., 2017)
	$NaOH/H_2O_2$ (1:1v/v)	4/24	50	3.5	
Khat waste	Formic/Acetic acids	40/40	90	1.5	(Gabriel, Wondu, et al., 2021)
	H_2O_2	10	70	1.5	
Tomato peels	$NaClO_2$	1.4	70	5	(F. Jiang et al., 2015)
	$NaOH/H_2O_2$	5/4	45	6	

Sources	Chemicals	Treatment Conditions			References
		Concentration (%)	Temperature (℃)	Time (h)	
Cocoa pod husk	$NaClO_2$	1.7	80	4	(Akinjokun et al., 2021)
Coconut husk	$NaOH/H_2O_2$	4/5	50	1.5	(Nascimento et al., 2014)
Sisal, flax and hemp	Acetic/nitric acids (6:1 v/v)	Pure	N/A	0.5	(Mondragon et al., 2014b)
Sugarcane	$NaClO_2$	8.5	75	2	(S. Lu et al., 2022)
Enset fibers	Acetic acid/NaClO (4:1 v/v)	6	60	2	(Beyan et al., 2021)
Various acid hydrolysis treatments					
Rice and Coffee husks	H_2SO_4	64	50	0.5	(Collazo-Bigliardi et al., 2018)
Oil palm trunk	H_2SO_4	64	45	1	(Lamaming et al., 2015)
Khat waste	H_2SO_4	64	45	1	(Gabriel, Wondu, et al., 2021)
Cocoa pod husk	H_2SO_4	64	45	1	(Akinjokun et al., 2021)
Cotton	H_2SO_4	47	60	2	(Maiti et al., 2013)
	H_2SO_4	64–65	45	1	(P. Lu et al., 2010)
	HCl	Pure	45	1	(Spagnol et al., 2012)
Kenaf fiber	H_2SO_4	30	80	4	(Shi et al., 2011)
	H_2SO_4	65	50	1	(Zaini et al., 2013)
	HCl	2.5 M	105	0.66	

Sources	Chemicals	Treatment Conditions			References
		Concentration (%)	Temperature (°C)	Time (h)	
Corncob	H_2SO_4	9.17 M	45	1	(Silvério, Neto, et al., 2013a)
Coconut husk fiber	H_2SO_4	64	45	2, 2.5 and 3	(Rosa et al., 2010)
Rice husk	H_2SO_4	10 M	50	0.5	(Johar et al., 2012)
Tomato peels	H_2SO_4	64	45	0.5	(F. Jiang et al., 2015)
Waste paper	H_2SO_4	60	45	1	(Danial et al., 2015)
Switch grass and cotton	H_2SO_4	60	45	0.75	(Q. Wu et al., 2013)
Sisal, flax and hemp	H_2SO_4	32	45	0.75	(Mondragon et al., 2014b)
Sugarcane	H_2SO_4	64	45	1	(S. Lu et al., 2022)
Enset fibers	H_2SO_4	33, 40, 50 and 60	20, 30, 45, 60 and 70	0.38, 0.58, 0.66, 1.08 and 1.5	(Beyan et al., 2021)
Rice straw	HCl	2.5 N	100	0.25, 0.5, 0.75 and 1	(Rivai et al., 2016)
Rice straw	H_2SO_4	64–65	45	0.5 and 0.75	(P. Lu et al., 2012)
Corn cob	H_2SO_4	62	44	1.5	(Ditzel et al., 2017)
Coconut husk	H_2SO_4	30	60	6	(Nascimento et al., 2014)

2.9. Properties of Nanocellulose–Filled Polymer Composites

The specific properties of nanocellulose–reinforced polymer composites are significantly influenced by various factors, including the type of nanocellulose, morphology, loading level, compatibility, dispersion, interfacial bonding, type of polymer and processing conditions (Miao et al., 2022; Azzra et al., 2024) as shown in **Figure 10**. The ultimate performance of these composites is highly dependent on the quality of dispersion and the interaction at the interface, as these factors affect the mechanical strength, thermal stability, morphology, structure and overall material durability (Norrrahim et al., 2022; Paran, 2024). Delving into the specific interactions between nanocellulose and polymers can reveal insights into optimizing these composites for various applications.

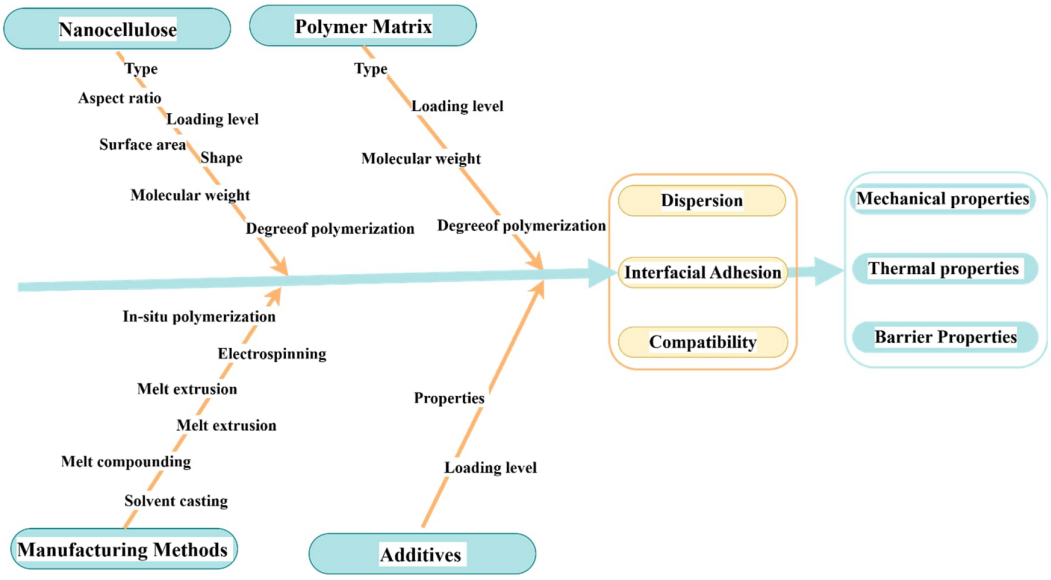

Figure 10. Factors affecting the properties of nanocellulose–reinforced polymer composites (Adapted from (Miao et al., 2022)

2.9.1. Manufacturing methods

The final properties of polymer composites are strongly influenced by the processing method used. Key factors to consider include the characteristics of the nanofillers, the compatibility with the polymer matrix, and the desired product form (Bhaganagar, 2023). Common techniques for incorporating nanomaterials include solvent casting, in situ polymerization, electrospinning, melt processing, and additive manufacturing (Gou et al., 2012; Kargarzadeh, Ahmad, et al., 2017), as shown in **Table 10**.

2.9.1.1. Solvent casting method

Solvent casting is one of the most widely used methods for fabricating nanocomposites, as noted in the literature (F. Deng et al., 2017). This technique involves blending a suitable amount of nanofiller with a polymer matrix dissolved in an appropriate solvent to form a uniform solution. This mixture is agitated using methods such as magnetic stirring, high-shear mixing, refluxing, or ultrasonication to ensure even nanoparticle dispersion. The resulting solution is then poured into a mold, and as the solvent evaporates, a solid nanocomposite film or sheet is formed (Kargarzadeh, Ahmad, et al., 2017). The choice of solvent depends on the solubility of the specific polymer used. This method benefits from the low viscosity of the solution, which aids in effective mixing and nanoparticle dispersion (Gou et al., 2012). For instance, (Ma et al., 2017) used acetone to fabricate CNC/ABS composites; (Selulosa-Polivinilklorida et al., 2015) sed tetrahydrofuran (THF) for CNC/PVC composites; (Kowalczyk et al., 2011) applied dichloromethane (DCM) for CNF/PLA composites; and (Dong et al., 2015) used dimethylformamide (DMF) to develop CNF/PMMA composites.

2.9.1.2. Melt compounding method

Melt compounding is often employed as an alternative technique, especially for processing insoluble thermoplastic polymers (Tanpichai et al., 2012). This method is advantageous because it does not require solvents, making it more environmentally and economically suitable for industrial use. However, a key challenge lies in processing nanocellulose in its dry form (Kowalczyk et al., 2011). Due to their large surface area and strong fiber–fiber interactions, nanocellulose fibers tend to form strong hydrogen bonds, leading to aggregation. Additionally, nanocelluloses particularly those produced through sulfuric acid hydrolysis exhibit limited thermal stability, which can be problematic during high-temperature processing (Martínez-Sanz et al., 2012). Another limitation is their poor compatibility with many polymer matrices (Kargarzadeh, Ahmad, et al., 2017). For example, (Tanpichai et al., 2012) utilized a melt compounding method for mixing MFC/PLA to prepare a polymer composite. Similarly, (Kadry et al., 2015) and (Iwatake et al., 2008) used this method to prepare CNC/PVC and CNF/PLA polymer composites, respectively.

2.9.1.3. Melt extrusion method

Melt extrusion is another melt processing technique used in the manufacturing of nanocellulose–reinforced polymer composites, as it enhances the mechanical properties and

enables the development of advanced materials. This process involves reinforcing nanocellulose with various polymer matrices, resulting in composites with improved performance characteristics. Melt extrusion involves heating and mixing polymers with nanocellulose in a screw extruder, allowing for uniform dispersion and integration of nanofillers into the polymer matrix (Völtz et al., 2022; Bhaganagar et al., 2023). While melt extrusion offers significant advantages in producing high–performance nanocomposites, challenges such as maintaining uniform dispersion and preventing degradation remain critical areas for ongoing research and development (Neena, 2023). This method was utilized and reported by (Dhar et al., 2016), (N. Lin et al., 2013) and (Bhaganagar, 2023) to prepare CNC/PLA, CNC/PS and CNF/PLA polymer composites, respectively.

2.9.1.4. In–situ polymerization method

In the in-situ polymerization method, nanoparticles are initially dispersed within a liquid monomer (Sapkota et al., 2017). Polymerization is then triggered through various means such as heat, radiation, the diffusion of a chemical initiator, or a catalyst attached to the nanoparticle surface (Gou et al., 2012). Once polymerization is complete, the resulting polymer chains either surround the nanoparticles or form covalent bonds with them, depending on the surface properties of the nanoparticles and the nature of the polymer (Nepomuceno et al., 2021). This technique is especially useful for producing nanocomposites from polymers that are insoluble or sensitive to heat, which are unsuitable for conventional melt or solution processing methods (Gou et al., 2012). (Nepomuceno et al., 2021) and (Sapkota et al., 2017) fabricated CNC/PANi and CNC/LDPE polymer composites, respectively, using the in situ polymerization method.

2.9.1.5. Electrospinning methods

Electrospinning is a fiber-forming technique that utilizes electrostatic forces to draw fibers from a charged droplet of liquid polymer (Jalal et al., 2014). This method is widely recognized for its versatility, efficiency, and low cost, offering a continuous process to fabricate nanoscale materials through the influence of electric fields (Kargarzadeh, Ahmad, et al., 2017). This method was used by (Martínez-Sanz et al., 2013) and (Jalal et al., 2014), among others, to produce CNC/EVOH and CNC/PS polymer composites, respectively.

Table 10. Nanocellulose–filled polymer composite processing methods

Filler material	Matrix material	Manufacturing technique	Solvent	Reference
CNC	ABS	Solution casting	Acetone	(Ma et al., 2017)
CNC	PVC	Melt compounding	N/A	(Kadry et al., 2015)
CNC	PMMA	Electro spinning	N/A	(Dong et al., 2012)
CNF	PS	Melt extrusion	N/A	(N. Lin et al., 2013)
CNC	PS	Electro spinning	N/A	(Jalal et al., 2014)
CNC	PMMA	Solution casting	Dimethylacetamide	(F. Deng et al., 2017)
MFC	PLA	Melt compounding	N/A	(Tanpichai et al., 2012)
NC	PVA	Solution casting	Distilled water	(Lani et al., 2014)
CNF	PMMA	Solution casting	Dimethylformamide (DMF)	(Dong et al., 2015)
CNF	PLA	Melt extrusion	N/A	(Bhaganagar, 2023)
CNC	PVC	Solution casting	Tetrahydrofuran (THF)	(Selulosa-Polivinilklorida et al., 2015)
CNF	PS	Solvent casting and melt extrusion	Benzene, acetone and hexane.	(Zimmermann et al., 2018)
CNF	PLA	Solvent casting and melt compounding	Acetone	(Iwatake et al., 2008)
CNF	PLA	Solution casting and melt compounding	Dichloromethane (DCM)	(Kowalczyk et al., 2011)
CNC	PLA	Melt compounding	N/A	(Martínez-Sanz et al., 2012)
CNC	PANi	In situ polymerization	N/A	(Nepomuceno et al., 2021)
CNC	PLA	Melt extrusion	N/A	(Dhar et al., 2016)
CNC	EVOH	Electro spinning and melt compounding	N/A	(Martínez-Sanz et al., 2013)
CNC	LDPE	In situ polymerization	N/A	(Sapkota et al., 2017)

2.9.2. Nanocellulose loading level and dispersion

Increasing the nanocellulose content generally improves the mechanical properties of the composite, such as the tensile strength and modulus, due to enhanced reinforcement. However, there is a limit beyond which additional loading may lead to diminishing returns or even a decrease in performance. This is often due to issues with dispersion and agglomeration (James et al., 2024; Tu et al., 2024). At high loading levels, nanocellulose particles can form aggregates or clusters, leading to poor dispersion and reduced mechanical reinforcement. Therefore, finding the optimal loading is essential to maximize benefits while maintaining processability and composite quality (Issam, 2022; Neciosup-Puican et al., 2023).

Different studies have reported the effects of nanocellulose loading on the properties of polymer composites, as shown in **Table 11.** For instance, (Sanchez-Garcia et al., 2010) produced PLA composites reinforced with CNCs in concentrations ranging from 1 to 5 wt.% using the solvent casting technique. Differential Scanning Calorimetry (DSC) analysis showed that both the melting temperature and crystallinity increased as the CNC content rose, indicating that the fillers promoted crystallization. Thermogravimetric Analysis (TGA) demonstrated that small amounts of CNCs had no significant impact on the thermal degradation of the PLA matrix. Additionally, with just 3 wt.% of CNCs, water permeability was reduced by up to 82%, and oxygen permeability decreased by up to 90%.

(Martínez-Sanz et al., 2012) developed PLA composites reinforced with 1–3 wt.% CNCs using electrospinning. The addition of CNCs achieved good dispersion within the PLA matrix at concentrations up to 3 wt.%, which, due to strong matrix–filler interactions, led to enhanced mechanical performance. Specifically, at CNC loadings of around 2–3 wt.%, the composites exhibited approximately a 17% increase in elastic modulus and a 14% rise in tensile strength compared to pure PLA, without significantly compromising ductility. Regarding barrier performance, water permeability was reduced by 43% at 3 wt.% CNC content. Furthermore, all nanocomposites showed a notable improvement in oxygen barrier properties at 0% relative humidity (RH). However, at 80% RH, only composites with 1 wt.% bacterial cellulose nanowhiskers (BCNW) demonstrated enhanced oxygen barrier performance.

Table 11. Various nanocellulose loading levels in polymer composites

Type of NC	Polymer	NC loading (wt.%)	Research focus	References
CNC	PLA	5	Mechanical property	(Oksman et al., 2006; Bondeson et al., 2007)
		1–5	Oxygen barrier property	(Sanchez-Garcia et al., 2010)
		1–5	Hydrolytic degradation behavior	(De Paula et al., 2011)
		1–3	Oxygen barrier and mechanical properties	(Martínez-Sanz et al., 2012)
		1–5	Mechanical and thermal properties	(Hossain et al., 2012)
		0.5 –7	Crystallization, rheological and mechanical properties	(Kamal et al., 2015)
		0.5 –5	Mechanical and thermal properties	(Ambrosio-Martín et al., 2015)
		1–3	Barrier, mechanical, and thermal properties	(P. Dhar et al., 2015)
		1	Mechanical, thermal, and optical properties	(Herrera et al., 2016)
	PVA	8	Mechanical property	(Wen Li et al., 2012)
		2	Water permeability, morphology, thermal and mechanical properties	(D. Chen et al., 2012)
		3	Water vapor barrier, optical and thermal properties	(Pereira et al., 2014)
		8 –12	Structural and thermal properties	(Voronova et al., 2015)
		7	Thermal, mechanical, leaching test and morphology	(W. Zhang et al., 2014)

Type of NC	Polymer	NC loading (wt.%)	Research focus	References
CNF	PLA	3–20	Mechanical and thermal properties	(Iwatake et al., 2008; Okubo et al., 2009)
		1 and 2	Mechanical property	(Nakagaito et al., 2009)
		10 –90	Mechanical property	(Suryanegara et al., 2009)
		10	Mechanical and thermal properties	(Suryanegara et al., 2010; Suryanegara et al., 2011)
		2	Crystallization, mechanical, and thermal properties	(Kowalczyk et al., 2011)
		8–32	Mechanical and thermal properties	(T. Wang et al., 2012)
		20.5	Micromechanics	(Tanpichai et al., 2012)
		1 –20	Crystallization	(Song et al., 2013)
		0.1 –1	Crystallization	(Ding et al., 2015)
		5 and 10	Rheological and mechanical properties	(Kiziltas et al., 2016)
	PVA	1	Mechanical and thermal properties	(Pereira et al., 2014)
		4	Morphology and mechanical properties	(Wei Li et al., 2013)
		5	Thermal and dynamic mechanical properties	(Baheti et al., 2013)
		2	Morphology, mechanical, thermal and optical properties	(Yuwawech et al., 2015)
		2	Morphology, mechanical and thermal properties	(J. Peng et al., 2015)
		2	Morphology, physical, mechanical, thermo–mechanical and thermal properties	(Kakroodi, 2014)

Another study by (Ambrosio-Martín et al., 2015) investigated PLA composites reinforced with varying CNC contents ranging from 0.5 to 5 wt.%. The study showed that increasing the CNC concentration led to greater aggregation. However, the well-dispersed CNC fraction served as effective nucleation sites, enhancing the crystallization rate and overall crystallinity of the composites. The thermal stability remained largely unchanged, with a slight increase observed in the onset of degradation temperature. Compared to neat PLA, the nanocomposites exhibited improved thermomechanical performance and barrier properties. Interestingly, the film with the lowest CNC loading demonstrated the best mechanical and thermomechanical performance, as well as reduced oxygen permeability under high relative humidity an outcome attributed to the superior dispersion of CNCs at lower concentrations.

2.9.3. Interfacial adhesion

Interfacial adhesion describes the bonding strength between nanocellulose reinforcements and the surrounding polymer matrix in composite materials. This interaction is vital, as it determines how well the reinforcement performs and influences the composite's mechanical behavior. Strong interfacial adhesion allows efficient stress transfer from the polymer to the nanocellulose, resulting in enhanced strength, rigidity, and overall durability of the material (Hayward, 2019; Kawaguchi et al., 2023; G. Wang et al., 2023).

The surface chemistry of nanocellulose significantly influences its interfacial adhesion with polymer matrices, primarily due to the presence of hydroxyl groups that can form hydrogen bonds (Psochia et al., 2024). However, the effectiveness of these interactions is contingent upon the chemical compatibility between the nanocellulose and the polymer. To improve adhesion, surface treatments such as oxidation, grafting, or the application of coupling agents can be used to introduce additional functional groups that enhance bonding. For example, coupling agents such as silanes can chemically bond with both the nanocellulose and the polymer matrix, improving compatibility and adhesion (James et al., 2024; Kamada et al., 2024).

Similarly, the nature of the polymer matrix also influences the interfacial adhesion. Polarity is a key factor; polar polymers generally exhibit better adhesion to polar nanocellulose owing to favorable interactions between their functional groups. Additionally, the molecular weight and chain length of the polymer affect how well it can interact with and encapsulate the nanocellulose. Higher–molecular–weight polymers with longer chains tend to create

stronger bonds through entanglement with nanocellulose fibers, improving overall adhesion (Marcuello et al., 2023; M. Zhang et al., 2024).

Moreover, the characteristics of nanocellulose, including its size, shape, and aspect ratio, impact interfacial adhesion. Nanocellulose with a high aspect ratio provides a larger surface area for interaction with the polymer matrix, leading to better reinforcement and improved adhesion. The size and shape of the nanocellulose also affect its distribution and dispersion within the matrix, which are critical for achieving optimal adhesion (Neelambaram et al., 2023; Qin et al., 2024). Uniform dispersion of nanocellulose within the polymer matrix is essential for achieving strong interfacial adhesion. Poor dispersion or aggregation of nanocellulose can create weak spots in the composite, leading to reduced mechanical performance. To improve dispersion, various methods, such as the use of dispersants or compatibilizers, can be employed. These additives increase the compatibility between the nanocellulose and the polymer, ensuring a more homogeneous distribution and better adhesion (James et al., 2024).

The processing conditions used during the fabrication of nanocellulose–reinforced composites have a substantial effect on interfacial adhesion. Temperature and mixing methods are crucial factors. Higher processing temperatures can enhance the interaction between nanocellulose and the polymer but must be controlled to avoid degradation of either component. The method of incorporating nanocellulose, such as melt blending or solution casting, also affects the quality of the interface and the final properties of the composite (Magunga et al., 2023).

2.10. Overview of Polylactic Acid (PLA)

Polylactic acid (PLA) is a bio-based thermoplastic polyester that has drawn increasing interest as a sustainable alternative to conventional fossil-derived plastics (Ramezani Dana et al., 2023). It is produced from renewable resources such as corn starch, sugarcane, and another carbohydrate-rich biomass (A. Ahmad et al., 2020; Ioannidou et al., 2022). PLA is distinguished by its biodegradability, biocompatibility, and commercial scalability (Ioannidou et al., 2022). As the global production of plastics exceeds 368 million tons annually, the accumulation of plastic waste has become an environmental crisis. In response, PLA offers a promising solution through its capacity to decompose under industrial composting conditions, reducing long-term environmental impact (Ramezani Dana et al., 2023).

The appeal of polylactic acid (PLA) is attributed not solely to its ecological advantages but also to its multifaceted physical and mechanical attributes. It possesses the ability to attain elevated molecular weights, thereby allowing it to rival the strength and rigidity of commonly utilized polymers. Moreover, this polymer can be processed via an array of both conventional methodologies, including extrusion, injection molding, and additive manufacturing techniques such as 3D printing (La Gala et al., 2022). PLA has positioned itself within a variety of industries, spanning from packaging to biomedical applications, primarily due to its adaptable properties and the opportunity for both chemical and physical modifications (Benwood et al., 2018). These characteristics, in conjunction with its cost-effectiveness, render PLA a preeminent biopolymer within the burgeoning bio-economy (Panda et al., 2024).

2.10.1. Types and classifications of PLA

The characteristics of PLA are heavily influenced by the stereochemistry of its monomeric units, specifically, the L- and D-enantiomers of lactic acid. The polymer can be synthesized from pure L-lactic acid to form poly-L-lactic acid (PLLA), which exhibits semi-crystalline behavior, a high melting point, and high tensile strength (Zin et al., 2021).

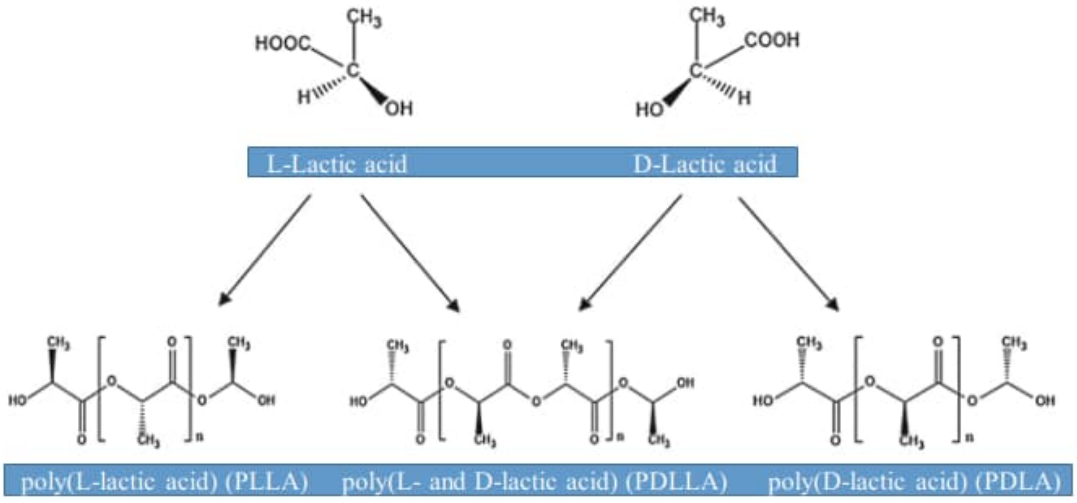

Figure 11. Stereo forms of polylactic acid (PLA) (Y. Chen et al., 2020)

This version is ideal for medical implants and other applications requiring long-term structural integrity. In contrast, when PLA is synthesized using a mixture of L- and D-isomers, the resulting polymer is amorphous and more flexible. These racemic forms, often

referred to as poly-DL-lactic acid (PDLLA), degrade faster and are suitable for short-term applications such as drug delivery (Ramezani Dana et al., 2023).

2.10.2. Synthesis methods of PLA

PLA is synthesized primarily from lactic acid, which is obtained via microbial fermentation of sugars or, less commonly, through chemical synthesis (Singhvi et al., 2019). The conversion of lactic acid to PLA involves three main polymerization methods, each with distinct advantages and limitations (Ramezani Dana et al., 2023). The most basic is direct polycondensation, in which lactic acid molecules react to form PLA through the removal of water. Although this method is economically attractive, it typically produces low molecular weight polymers due to incomplete water removal, making the resulting PLA brittle and unsuitable for many demanding applications (Desai et al., 2023).

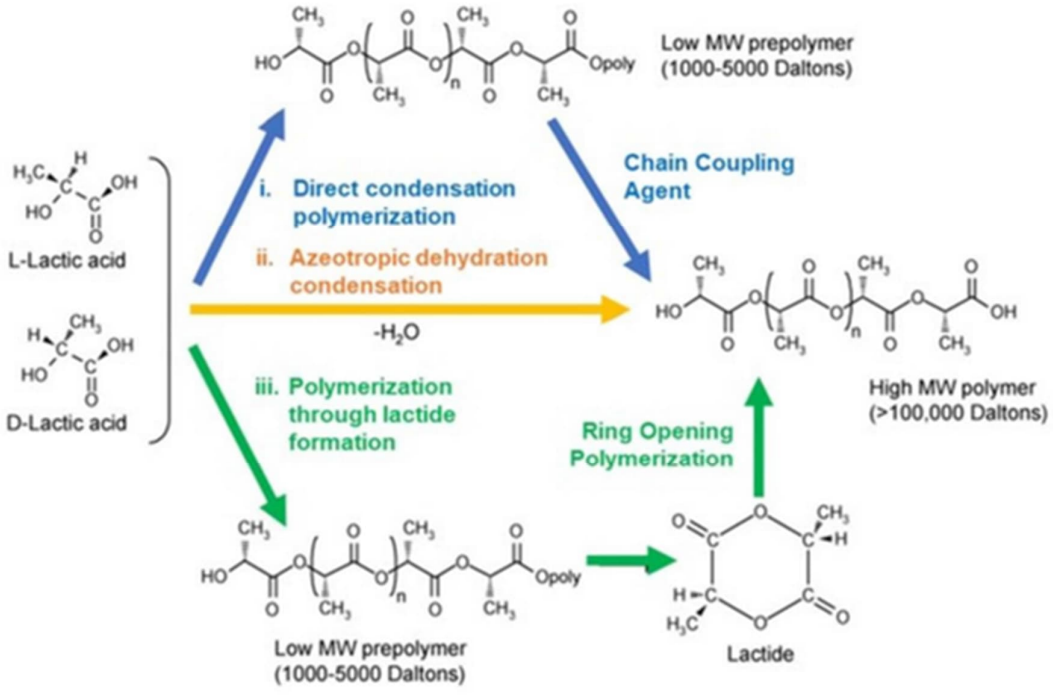

Figure 12. Synthesis methods of polylactic acid (PLA) from L- and D-lactic acids (Yeo et al., 2024).

To overcome the limitations of direct condensation, the azeotropic dehydration method is employed. This process involves refluxing lactic acid in a high-boiling-point aprotic solvent under reduced pressure, effectively removing water and producing PLA with higher molecular weight. Although more complex and resource-intensive, this method yields superior material quality (Desai et al., 2023). The most widely used industrial process is the

ring-opening polymerization (ROP) of lactide—a cyclic dimer of lactic acid. ROP, typically catalyzed by stannous octoate, enables excellent control over polymer molecular weight, chain architecture, and stereochemistry. The purity of the lactide monomer and the absence of moisture and impurities are critical for achieving high-quality PLA suitable for medical and high-performance engineering applications (Tschan et al., 2021).

2.10.3. Properties of PLA

PLA exhibits a diverse set of mechanical, thermal, and rheological properties that can be modified through its formulation or processing conditions. Mechanically, PLA is known for its high tensile strength and modulus, which are comparable to those of traditional polymers such as polystyrene and PET. However, its primary limitations are its brittleness and low elongation at break (<10%), which restricts its use in flexible applications (Barkhad et al., 2020). To improve its toughness, PLA is often modified through blending with other polymers or by incorporating plasticizers and elastomers (Asanda Mtibe et al., 2021).

Thermally, PLA has a glass transition temperature in the range of 50–60°C and a melting point of 160–180°C (Nguyen et al., 2018). These values make PLA suitable for moderate-temperature applications. During melt processing, PLA behaves as a viscoelastic, non-Newtonian fluid with shear-thinning characteristics. This makes it ideal for processes such as extrusion and 3D printing (Rezvani Ghomi et al., 2021). Due to its outstanding mechanical properties, ease of processing, and biodegradability, polylactic acid (PLA) has attracted significant research interest as a biomaterial over the past few decades (J. C. Tan et al., 2020). Nevertheless, its limited heat resistance significantly restricts its range of applications. To overcome this drawback, various strategies have been explored, including the addition of nucleating agents, fiber reinforcement, compounding, blending with other materials, forming stereo complexes, and chemical modification (Jin et al., 2019).

In terms of gas permeability and barrier properties, PLA provides moderate resistance to oxygen and moisture but falls short of high-performance barrier materials. Enhancing its barrier function is possible through crystallinity optimization, blending with other polymers, or adding nanofillers. These improvements are crucial in applications such as food packaging, where gas control is essential (Marano et al., 2022). Furthermore, its biodegradability is one of its most attractive features. Under industrial composting conditions specifically, elevated temperature (>58°C), moisture, oxygen and active microbes, it can degrade into carbon dioxide, water, and biomass within 3–6 months.

However, PLA breaks down much more slowly in soil or aquatic environments, which remains a challenge for broader environmental disposal (Taib et al., 2023).

2.10.4. Applications of polylactic acid (PLA)

Due to its excellent performance and environmental benefits, PLA has found widespread use in various applications. In the realm of additive manufacturing particularly fused deposition modeling (FDM) 3D printing, PLA is one of the most commonly used materials (Rezvani Ghomi et al., 2021). It is biodegradable, compostable, and environmentally friendly, making it an ideal candidate for sustainable 3D printing (J. C. Tan et al., 2020). PLA is especially preferred in both desktop and industrial FDM printers due to its low melting temperature (approximately 180–220 °C), minimal warping, strong layer adhesion, and low emission of toxic fumes. Although a heated bed is not strictly required, moderate heating (around 50–60 °C) can enhance bed adhesion and surface finish attributes (Y. Li et al., 2023). Furthermore, PLA offers excellent dimensional accuracy and a smooth surface appearance, which are highly desirable for prototyping, educational models, artistic creations, and functional end-use parts (Alexandre et al., 2020). The potential applications of polylactic acid (PLA) are shown in **Figure 13**.

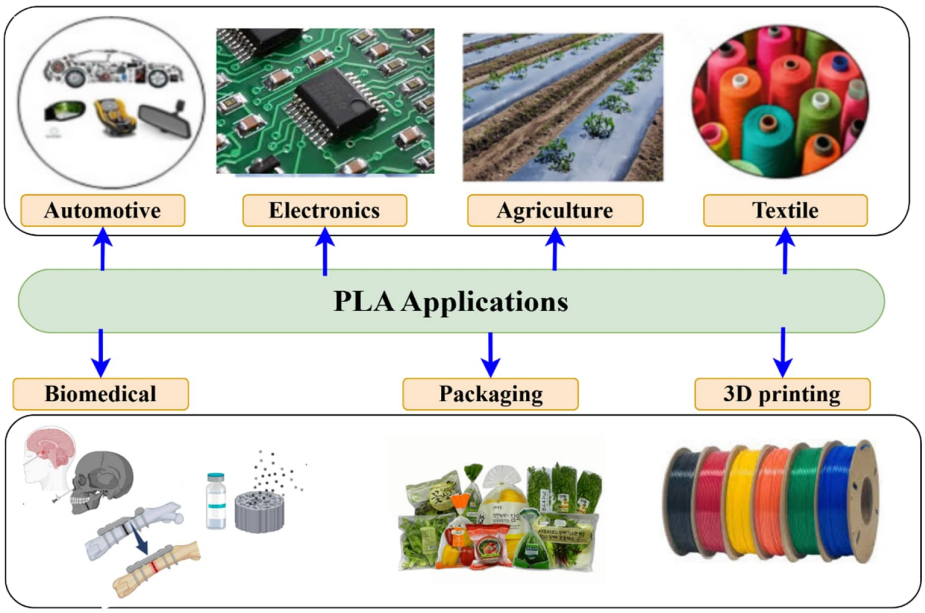

Figure 13. Potential applications of Polylactic acid (PLA) (Adapted from (Rezvani Ghomi et al., 2021)

Despite these advantages, PLA also has certain limitations. It is relatively brittle compared to other engineering thermoplastics, has low impact resistance, and shows poor thermal stability mainly during multiple extrusion cycles, which restricts its use in functional or load-bearing parts, especially in high-temperature environments. Furthermore, its mechanical properties may degrade over time under humid or outdoor conditions. To address these performance limitations, PLA is often reinforced with fillers or blended with other materials to create composites. Incorporation of natural fibers, nanoparticles, or other polymers can significantly enhance its mechanical, thermal, and functional properties while retaining its biodegradability (Trivedi, Gupta, et al., 2023; Khouri et al., 2024).

Overall, Polylactic acid (PLA) is a cornerstone material in Fused Deposition Modeling (FDM) 3D printing, celebrated for its printability, environmental benefits, and accessibility. However, enhancing PLA's mechanical properties while maintaining its biodegradability poses a significant challenge. Recent research has focused on various modification strategies to improve PLA's performance without compromising its eco-friendly attributes (Y. Li et al., 2023). Polylactic Acid (PLA) is increasingly recognized in the biomedical sector for its versatility and safety in applications such as sutures, bone screws, and tissue engineering scaffolds. Its biodegradability and biocompatibility allow it to degrade without toxic byproducts, making it suitable for various medical applications. Recent advancements, particularly in 3D printing, have enabled the creation of customized scaffolds that cater to specific patient needs, enhancing therapeutic outcomes (Hussain et al., 2024).

In packaging, PLA is used to produce containers, films, and trays for food products. Its transparency, rigidity, and compost ability make it suitable for fresh produce and takeaway packaging. However, its relatively poor barrier properties to moisture and gases limit its use for longer shelf-life items unless modified. Solutions include coating PLA with other biopolymers, laminating with barrier layers, or developing PLA-based nanocomposites to improve functionality. PLA is also increasingly used in composite materials for consumer goods and automotive components. These composites, often reinforced with natural fibers or nanofillers, offer lightweight alternatives with reduced environmental footprints. In the automotive sector, PLA composites are being explored for interior panels and trims, where mechanical demands are moderate but sustainability is a priority (Swetha et al., 2023).

Overall, PLA represents a versatile and sustainable alternative to conventional plastics. Despite certain challenges such as brittleness, thermal instability, and slow degradation in natural environments, continuous advancements in synthesis, formulation, and processing

are expanding its applicability. Its favorable environmental profile, combined with an ability to be customized for performance, ensures PLA's growing relevance in modern material science and engineering. A critical consideration in enhancing PLA is balancing performance gains with environmental sustainability and biodegradability (Khouri et al., 2024).

2.11. Overview of Fused Deposition Modeling (FDM)

Additive manufacturing (AM), widely known as 3D printing, has transformed the fabrication of intricate shapes, prototypes, and final parts in numerous industries (Kanishka et al., 2023). Among the various AM technologies, Fused Deposition Modeling (FDM), also referred to as Fused Filament Fabrication (FFF), stands out as one of the most popular and commercially successful techniques due to its ease of use, affordability, and broad range of applications (Behseresht et al., 2024; Romanenko et al., 2024).

FDM operates by melting a thermoplastic filament and extruding it through a nozzle to construct a three-dimensional object layer by layer. Its straightforward process and compatibility with many thermoplastic materials have driven its widespread adoption, especially for rapid prototyping, small-scale manufacturing, and customized product development (Acierno et al., 2023).

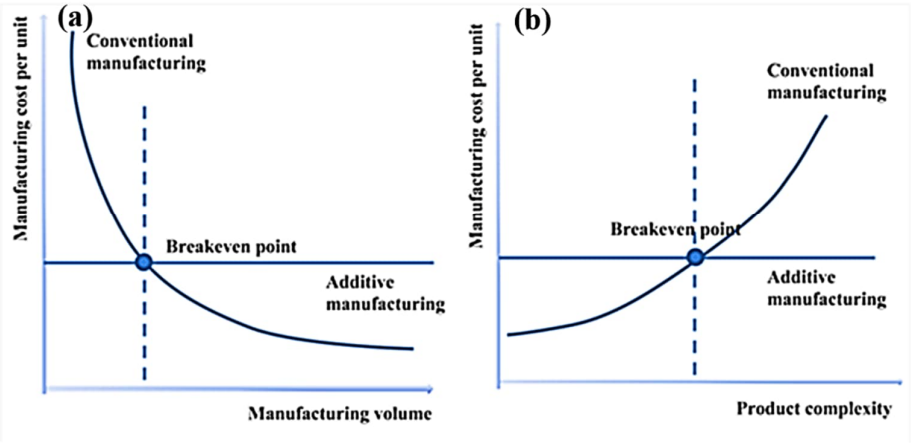

Figure 14. Comparisons of traditional and additive manufacturing techniques in terms of manufacturing cost per unit with (a) quantity and (b) complexity (Shang et al., 2020)

Conventional manufacturing techniques, such as injection molding and extrusion, often involve high energy consumption and complex processing steps. In contrast, 3D printing offers a versatile, energy–efficient, and customizable approach to fabricating bio nanocomposite materials as shown in the comparative Figure 14. This technology enables precise control over the material composition and structure, allowing for the production of

complex geometries and tailored properties that are difficult to achieve with traditional methods (García-Gascón et al., 2022).

FDM is a material extrusion-based process in which a filament material in diameter of 1.75 mm or 2.00 mm is heated and extruded through a nozzle in a thickness typically of 0.25 mm to build a 3D object layer by layer (Behseresht et al., 2024). The Schematic diagram of fused deposition modeling process is shown in **Figure 15.**

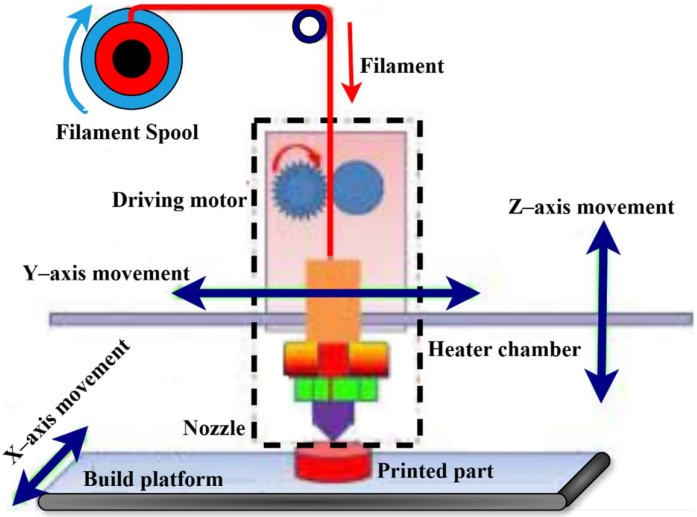

Figure 15. Schematic diagram of fused deposition modeling process (Adapted from (Behseresht et al., 2024).

2.11.1. Filament materials for fused deposition modeling (FDM)

Various types of FDM filament materials have been developed to date, including pure thermoplastics, bioplastics, and their composites. To enhance the performance of FDM printed parts, different reinforcements such as fibers, micro-sized particles, and nanoparticles are added to the pure polymer filaments, as illustrated in **Figure 16** (Dey et al., 2021).

2.11.1.1.Neat polymer filaments

A variety of thermoplastic polymers are available as filaments for the FDM process. These include acrylonitrile butadiene styrene (ABS), polylactic acid (PLA), polycarbonate (PC), polyether ether ketone (PEEK), polyetherimide (PEI), nylon, and high-impact polystyrene (HIPS), among others (Dey et al., 2021). An overview of the FDM filament materials and their classifications that are commercially available or have been studied at the laboratory scale is shown in **Figure 17**.

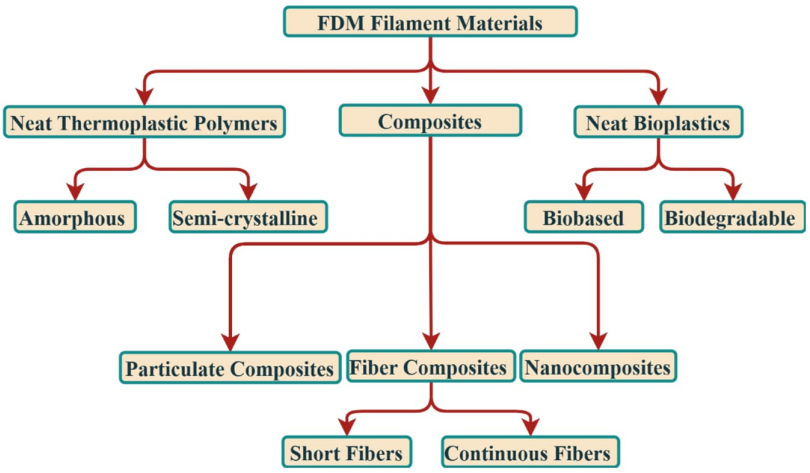

Figure 16. The classification of existing FDM filament materials (Adapted from (Dey et al., 2021).

(C. W. Ziemian et al., 2012) investigated the anisotropic mechanical properties of ABS parts fabricated via FDM. This highlights the significant variation in mechanical properties, such as tensile and compressive strengths, depending on the direction of fabrication. This research emphasizes the importance of understanding the material properties of ABS and the influence of FDM build parameters on these anisotropic characteristics. The study by (Afrose et al., 2016) investigated the fatigue behavior of PLA parts produced through FDM, focusing on how different build orientations affect their performance under cyclic loading conditions. The research highlights that parts built at the 45° orientation exhibit superior tensile fatigue properties compared with those built in the X and Y orientations, indicating a significant influence of the build orientation on the fatigue life.

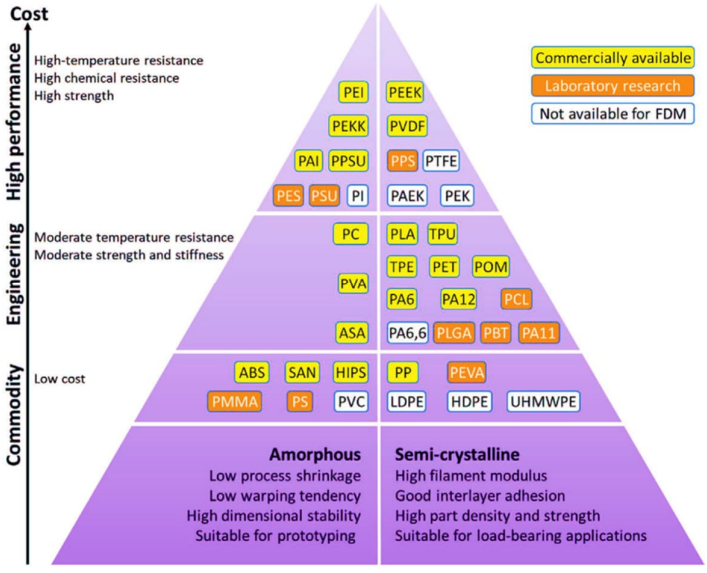

Figure 17. An overview of polymer filaments for FDM (L. J. Tan et al., 2020).

(Gong et al., 2017) examined the strain-controlled fatigue behavior of FDM-printed porous PLA-based scaffolds, which are important for biomedical applications due to their mechanical strength and biocompatibility. Their study emphasized how the scaffolds' mechanical properties, including tensile strength and fatigue resistance, are affected by microstructural features like the connections within the nanofibrous network. (Wittbrodt et al., 2015) investigated how the color of polylactic acid (PLA) affects the material properties of 3D–printed components, particularly the tensile strength and crystallinity. Research has established a strong correlation between tensile strength and percent crystallinity, which is influenced by the extruder temperature during the printing process. As the extruder temperature increased, the percent crystallinity of the PLA also increased, leading to enhanced mechanical properties. This relationship underscores the importance of processing conditions, as variations in color and temperature can significantly alter the structural order of a polymer, thereby affecting its mechanical properties. The findings highlight that the mechanical properties of PLA, including tensile strength, elasticity, and toughness, are dependent not only on the material composition but also on printing parameters such as layer height and fill density. In the study by (Rinaldi et al., 2018), the authors explored additive layer manufacturing (ALM) of poly(ether ketone) (PEEK) via Fused Deposition Modeling (FDM), a prevalent technique in the field of additive manufacturing. This research emphasizes the importance of optimizing FDM parameters, including the printing speed, layer thickness, and temperature, to enhance the mechanical properties of printed PEEK parts. Additionally, this study highlights the necessity of postprocessing techniques, such as hot pressing and surface treatments, to further improve the mechanical characteristics of the final products. Given the unique properties of PEEK, specific processing conditions are crucial for achieving the desired outcomes in FDM applications. **Table 12** shows different pure thermoplastic polymer filaments and the effect of printing parameters on properties of the printed parts were investigated and reported by different studies.

Table 12. Thermoplastic polymer filaments for FDM

Filament materials	Studied printing parameters	Investigated properties of printed parts	References
ABS	Air gap and raster width	Tensile and compressive strengths	(C. W. Ziemian et al., 2012)
	Raster orientation	Tensile strength and fatigue resistance	(S. Ziemian et al., 2015)
	N/A	Fatigue and stiffness degradation	(C. W. Ziemian et al., 2016)
	Build directions	Tensile and compressive strengths	(Ahn et al., 2002)
	Varying temperature	Modulus and damping characteristics	(Dawoud et al., 2016)
	Layer orientation	Tensile strength, modulus of rupture, and impact resistance	(Es-Said et al., 2000)
	Different geometries and print raster patterns	Strength and toughness	(Torrado et al., 2016)
PLA	Raster orientation	Tensile strength and elasticity	(Letcher et al., 2014)
	Build orientations	Tensile fatigue	(Afrose et al., 2016)
	Varying load conditions	Tensile strength, fatigue resistance and microstructure	(Gong et al., 2017)
	Color, extruder temperature, layer height and fill density	Tensile strength, elasticity, toughness and crystallinity	(Wittbrodt et al., 2015)
	Different printing angles and layer thicknesses	Ultimate tensile strength	(Yao et al., 2019)
	Layer thickness, infill orientation and the number of shell perimeters	Ultimate tensile strength and the nominal strain at break	(Lanzotti et al., 2015)

Filament materials	Studied printing parameters	Investigated properties of printed parts	References
	Extrusion temperature and layer height	Mechanical properties and dimensional accuracy	(Qattawi et al., 2017)
	Layer height, infill density, and printing speed	Mechanical properties and surface finish	(Leite et al., 2018)
	Different raster orientations	Tensile strength, rigidity and microstructure	(Fatimatuzahraa et al.)
Nylon12	Feasibility study	Tensile and impact strengths	(Mostafa et al., 2018)
	Complex loading conditions	Fracture Resistance	(Zolfagharian et al., 2020)
PEEK	Printing speed, layer thickness, temperature and post– processing techniques	Mechanical properties	(Rinaldi et al., 2018)
	Ambient temperature and nozzle temperature	Tensile strength, elastic modulus, breaking elongation and crystallinity	(Xiaoyong et al., 2017)
	Layer thickness, printing temperature and interlayer bonding	Tensile, compressive and bending strengths	(X. Deng et al., 2018)
	Feasibility study	Biocompatibility and bioactivity	(Arif et al., 2018)
PET	Comparative study	Elongation at break and Tensile strength	(Grabowik et al., 2017)
PETG	Printing temperature	Tensile strength, microstructure and printability	(Guessasma et al., 2019)

2.11.1.2.Polymer composite filaments

Currently, pure thermoplastic filaments face limitations like low strength and stiffness, which hinder the performance of FDM-produced parts (L. Yang et al., 2023). These thermoplastics tend to soften and lose their shape when exposed to high temperatures. As a result, products made from thermoplastic filaments often fail to satisfy certain specific functional demands (Dul et al., 2018). Compared with the properties of injection–molded parts, the properties of FDM–built parts are often inadequate (Ahn et al., 2002). In application fields, there is a continuous search for FDM filament materials that are lightweight, have high strength, and have good surface quality (Kabir et al., 2020). Composite materials are viewed as viable options to meet these requirements since composite materials have been reported to exhibit superior properties compared with those of pure polymers (Rahim, Abdullah, et al., 2019; Kabir et al., 2020). For this purpose, for the last decade, several studies have aimed to investigate the development of new composite filaments with enhanced or unique properties in comparison with those of parental thermoplastics through the incorporation of various types of functional fillers. Different types of functional fillers have been considered and categorized as carbon, metal, ceramic, cellulose or hybrid–based fillers (Angelopoulos et al., 2021).

Carbon–based fillers

The use of functional fillers in composite filaments can significantly impact the performance and characteristics of the final printed parts. Each type of filler offers distinct advantages and presents specific challenges (Le et al., 2021). Carbon–based fillers are widely recognized for their ability to enhance the mechanical properties of composite filaments. The incorporation of carbon–based fillers such as carbon nanotubes, graphene, MWCNTs, carbon fibers and carbon black can greatly increase the tensile strength and stiffness of the material, making it ideal for applications demanding high performance (B. Wang et al., 2021). Additionally, carbon fillers contribute to a lightweight composite, which is beneficial for applications where weight is a critical factor. They also improve the thermal conductivity, aiding in heat dissipation (Ghislandi et al., 2013). However, these benefits have certain drawbacks. The cost of carbon fillers, particularly high–quality options such as carbon fibers or nanotubes, can be quite high, potentially increasing the cost of the composite filament. Furthermore, the processing of carbon fillers can be challenging due to their abrasiveness, leading to increased wear on extrusion equipment (Sezer et al., 2019). Additionally, not all

polymers effectively bond with carbon fillers, which can affect the overall performance and structural integrity of the composite (Turku et al., 2014; Angelopoulos et al., 2021).

Metal–based fillers

Metal–based fillers, such as aluminum, copper, magnesium, bronze and iron powders, offer significant enhancements in strength and durability. They can also improve the thermal and electrical conductivity of the composite, making them suitable for applications requiring efficient heat dissipation or electrical conduction (Y. Zhu et al., 2016). On the downside, metal fillers add substantial weight to the composite, which may be a disadvantage in applications where maintaining a lightweight structure is crucial. The abrasive nature of metal fillers can lead to increased wear and tear on extrusion equipment, resulting in increased maintenance costs. Moreover, the cost of metal fillers can be substantial, and their incorporation often requires careful adjustment of processing parameters, adding to the complexity of filament production (Nabipour et al., 2020; Angelopoulos et al., 2021).

Ceramic–based fillers

Ceramic–based fillers, such as Fe_3O_4, Al_2O_3, ZrO_2, TiO_2 and SiO_2, are known for their ability to improve the heat resistance and hardness of composite filaments for FDM. They enhance the thermal stability of the composite, making it suitable for high–temperature applications. Additionally, ceramics increase the hardness and wear resistance of the material, which is beneficial in abrasive environments. However, the inclusion of ceramic fillers can also introduce some challenges. Ceramics tend to make the composite more brittle, potentially reducing its impact resistance and flexibility. The extrusion process may become more complex because of the presence of ceramic fillers, requiring adjustments to processing conditions. Furthermore, high–quality ceramic fillers can be expensive, which can increase the cost of the composite filament (Angelopoulos et al., 2021; Hassan et al., 2022).

Cellulose–based fillers

Cellulose–based fillers, such as macro–fibers, micro–cellulose and nanocellulose, offer an environmentally friendly alternative that is biodegradable and derived from renewable resources. Compared with other types of fillers, they are often less costly, which can make the composite filament more affordable. Cellulose fillers also contribute minimal weight to the composite filaments, preserving a good strength–to–weight ratio. Despite these advantages, cellulose–based fillers have several limitations. They may not significantly enhance the mechanical properties of the composite filaments to the same extent as carbon or metal fillers do. Additionally, cellulose can absorb moisture, which can affect the

properties of the composite and pose challenges in storage and processing. Compatibility issues may also arise, as cellulose fillers might not work well with all types of polymers, potentially impacting the performance of the final printed part (Rahim, Abdullah, et al., 2019; Angelopoulos et al., 2021). In summary, selecting the appropriate filler for composite filaments involves balancing the desired performance characteristics with the associated costs and processing challenges. Each type of filler offers unique benefits that can enhance the specific properties of the composite but also presents trade–offs that must be carefully considered on the basis of the application requirements. Different studies have explored the development of nanocomposite filaments for Fused Deposition Modeling (FDM) by incorporating various fillers such as carbon nanotubes (CNTs), nanocellulose, carbon fibers, metal particles, and metal oxides into thermoplastic matrices to enhance their mechanical, electrical, and functional properties.as shown in **Table 13**.

For instance, (Dul et al., 2018) investigated MWCNT–ABS nanocomposites and identified 250°C and 10 wt.% as the optimal printing temperature and filler concentration. They reported that increasing CNT content enhanced nanoparticle polymer interactions but also raised the viscosity, as evidenced by a decrease in the melt flow index. Similarly, (Le et al., 2021) evaluated the mechanical performance of MWCNT–ABS samples with varying filler loadings (0.5–4 wt.%) and found that 2 wt.% CNTs led to a 40% increase in tensile strength, accompanied by morphological changes such as an increase in shear lips at higher concentrations.

Moreover, (B. Wang et al., 2021) showed that CNTs up to 8 wt.% in ABS did not compromise adhesion or porosity but significantly enhanced mechanical properties, with modulus improvements of 10.25% and 40% for 1 wt.% and 8 wt.% loadings, respectively. Further supporting these findings, (Sezer et al., 2019) reported even greater gains a 210% increase in ultimate tensile strength using 10 wt.% MWCNTs, although they noted diminishing returns at higher concentrations due to CNT agglomeration. Consistently, literature suggests that the mechanical benefits peak around 9–10 wt.% CNTs, beyond which issues like poor dispersion, brittleness, and nozzle clogging emerge.

Expanding on this, (Pan et al., 2021) studied PPS–CNT nanocomposites and found 26% and 29% increases in tensile and bending strength, respectively, at 10 wt.% CNTs. However, their findings reaffirmed that high filler content can negatively affect processability and ductility. (B. Han et al., 2022) examined the electromagnetic wave absorption performance of polyamide 12 parts reinforced with 7–12 wt.% MWCNTs produced via FDM. Due to the

inadequate electrical properties at lower CNT loadings, higher concentrations were selected. When comparing 12 wt.% CNT-filled FDM parts with their injection-molded counterparts, the FDM samples retained 94.45% of the tensile strength, 85.51% of the impact resistance, and 92.94% of the flexural modulus. Although the FDM parts exhibited slightly lower mechanical properties due to lower density, they showed comparable wave absorption capability. Notably, the FDM samples demonstrated better reflection loss performance, attributed to the advantageous alignment of nanotubes within the printed matrix.

In an earlier study, (L. Yang et al., 2019) demonstrated that incorporating 6 wt.% CNTs into PLA resulted in significant enhancements in mechanical performance, with tensile strength increasing by 64.12% and flexural strength by 29.29%. The authors also recommended using a greater layer thickness during the printing process to achieve further improvements in electrical properties. In another study, (L. Yang et al., 2023) reported that adding 4 wt.% CNTs to PLA effectively improved the electromagnetic shielding capabilities of 3D printed nanocomposites. They also highlighted that, even at a fixed CNT concentration, the composite properties could be optimized by modifying the FDM processing parameters.

(Ning et al., 2015) investigated the effect of varying carbon fiber content and length on the mechanical performance of ABS-based composite filaments. ABS pellets were blended with carbon fibers at different weight percentages (3%, 5%, 7.5%, 10%, and 15%) using fibers of 100 μm and 150 μm in length (diameter: 7.2 μm). After blending, the materials were re-extruded to enhance bulk density. The study found that the optimal mechanical performance was achieved at 7.5 wt.% fiber content, where the tensile strength increased from 35 MPa to 42 MPa, and the Young's modulus rose from 1.9 to 2.5 GPa. Fiber contents above 7.5 wt.% negatively affected the mechanical properties due to increased porosity. Additionally, longer fibers (150 μm) resulted in better mechanical strength and stiffness compared to shorter ones (100 μm).

(Angel R. Torrado Perez et al., 2014) developed a composite filament by incorporating 5 wt.% titanium dioxide (TiO_2) into an ABS copolymer using a twin-screw extruder operated at 230°C. The addition of TiO_2 led to a 13.2% increase in tensile strength and a 30% enhancement in fracture strength compared to the neat ABS filament. However, the strain at fracture was reduced by 29%, indicating a more brittle behavior. The study primarily aimed to explore how the filler size influences the mechanical properties of polymer composites.

In another study (Hwang et al., 2015)explored the development of metal–polymer composite filaments by incorporating copper and iron particles into ABS to improve thermomechanical

performance for FDM applications. The study demonstrated that increasing the metal content enhanced the thermal conductivity of the filaments; however, it also led to a reduction in tensile strength. This highlighted a trade-off between thermal and mechanical properties depending on the metal loading level.

Beyond carbon, ceramic and metal-based fillers, alternative cellulose-based fillers have also been explored. For instance, (X. Wu et al., 2022) investigated PLA/CNC nanocomposites with an emphasis on achieving uniform dispersion of CNCs using the melt blending method, as opposed to the solution method. To enhance compatibility, CNCs were grafted with polyvinyl acetate (PVAc) before being incorporated into the PLA matrix. The resulting 5 wt.% CNC nanocomposites showed significantly improved dispersion, leading to enhanced melt processability and stronger interlayer bonding. These improvements translated into notable increases in tensile break energy (254%), notched impact toughness (57%), and interlayer adhesion (103%). In a similar investigation, (Wiratma, 2021) explored the influence of crystalline nanocellulose (CNC) on pure PLA. CNC powders were incorporated into the PLA matrix and extruded at 185°C with filler loadings of 1, 3, and 5 wt.%. The results showed that introducing 1 wt.% CNC enhanced the tensile strength by 19.04%. However, increasing the CNC content beyond this level led to a decline in mechanical performance, which was attributed to the agglomeration of nanocellulose particles within the polymer matrix.

Table 13. Polymer composite filaments for FDM

Filler/reinforcement materials	Size of fillers/reinforcements	Matrix materials	Filler loading levels (wt.%)	Enhanced properties of printed parts	References
Carbon Based Fillers/Reinforcements					
MWCNTs	Nano	ABS	10	Morphology, viscosity electrical, and mechanical	(Dul et al., 2018)
MWCNTs	Nano	ABS	2	Morphology and tensile strength	(Le et al., 2021)
CNTs	Nano	ABS	8	Tensile strength and tensile modulus	(B. Wang et al., 2021)
CNTs	Nano	ABS	10	Ultimate tensile strength and electrical properties	(Sezer et al., 2019)
CNTs	Nano	PPS	10	Tensile and bending properties	(Pan et al., 2021)
MWCNTs	Nano	Polyamide 12	12	Tensile strength, impact resistance, and flexural modulus	(B. Han et al., 2022)
CNTs	Nano	PLA	4	Electromagnetic shielding properties	(L. Yang et al., 2023)
CNTs	Nano	PLA	6	Tensile and flexural strength	(L. Yang et al., 2019)
Graphene nanoplatelet	Nano	PP	10	Thermal conductivity	(Shmueli et al., 2020)
Graphene	Micro	PLA	2	Electrical, thermal, and mechanical properties	(García et al., 2020)

Filler/reinforcement materials	Size of fillers/reinforcements	Matrix materials	Filler loading levels (wt.%)	Enhanced properties of printed parts	References
Graphene	Micro	PLA	0.2	Tensile strength and Young's Modulus	(Plymill et al., 2016)
Graphene Oxide	Micro	ABS	0.06	Strain–to–failure and toughness	(Yamamoto et al., 2018)
Graphene	Micro	ABS	5.6	Electrical conductivity	(Wei et al., 2015)
Carbon Fiber	Milli	PLA	41	Flexural strength and modulus	(Vatandaş et al., 2023)
Carbon Fiber	Milli	PEEK	5	Tensile and flexural strength	(P. Wang et al., 2020)
Carbon Fiber	Micro	ABS	7.5	Tensile strength and Young's modulus	(Ning et al., 2015)
Carbon Black	Micro	PLA	53	Thermal and electrical conductivity	(Tirado-Garcia et al., 2021)
Glass based reinforcements					
Glass Fiber	Milli	PEEK	5	Interfacial bonding	(P. Wang et al., 2020)
Glass Fiber	Milli	Epoxy	43	Tensile strength and tensile modulus	(Ming et al., 2020)
Glass Fiber	Milli	ABS	18	Tensile strength	(Zhong et al., 2001)
Glass fiber	Milli	PP	30	Modulus and strength	(Sodeifian et al., 2019)
Cellulose Based Fillers/Reinforcements					
Fiber	Macro	PLA	5	Impact strength and ductility	(Daver et al., 2018a)

Filler/reinforcement materials	Size of fillers/reinforcements	Matrix materials	Filler loading levels (wt.%)	Enhanced properties of printed parts	References
Fiber	Macro	PLA	15	Tensile properties.	(Magalhães da Silva et al., 2020)
Fiber	Macro	PP	30	Ultimate tensile strength and Young's modulus	(Milosevic et al., 2017)
CNCs	Nano	PLA	5	Melt processability, interlayer adhesion, tensile break energy and notched impact toughness	(X. Wu et al., 2022)
CNCs	Nano	PLA	1	Tensile strength	(Wiratma, 2021)
CNCs	Nano	TPU	5	Ductility	(Bardot et al., 2020)
CNFs	Nano	HDPE	10	Young's modulus	(Dalloul et al., 2022)
Ceramic based fillers					
TiO_2	Micro	ABS	5	Tensile and fracture strength	(Angel R. Torrado Perez et al., 2014)
Al_2O_3	Micro	Nylon–6	40	Percentage elongation, Young's modulus, tensile and yield strength	(Singh et al., 2016)
Al_2O_3	Micro	LDPE	50	Printability	(Nötzel et al., 2018)
ZnO	Micro	ABS	14	Stiffness and elasticity property	(Aw et al., 2018)

Filler/reinforcement materials	Size of fillers/reinforcements	Matrix materials	Filler loading levels (wt.%)	Enhanced properties of printed parts	References
Fe_3O_4	Micro	Nylon	76	Stiffness and thermal properties	(Masood et al., 2004)
SiO_2 and $CaCO_3$	Nano	ABS	1	Glass transition temperature, surface quality and accuracy	(Meng et al., 2017)
Metal based fillers					
Iron and Copper	Micro	ABS	40	Stiffness and thermal conductivity	(Nikzad et al., 2011)
Copper	Micro	PLA	12	Compression strength	(Pavan et al., 2020)
Copper	Nano	PLA	14	Compressive and flexural strength	(Balamurugan et al., 2021)
Copper and Iron	Micro	ABS	50	Thermal conductivity	(Hwang et al., 2015)
Tungsten	Micro	PC	3	Radiation shielding	(Shemelya et al., 2015)
Aluminum	Micro	PLA	6.95	Surface quality storage modulus and Glass transition temperature	(X. Zhang et al., 2020)
Aluminum	Micro	PLA	6.95	Storage modulus, elongation at break and Glass transition temperature	(X. Zhang et al., 2019)

2.11.2. FDM–based printing methods of polymer composites

The printing techniques for continuous fiber–reinforced composites (CFRCs) are generally classified into three main types: out-of-nozzle impregnation using a dual extruder system, in-nozzle (or in situ) impregnation, and methods that utilize pre-impregnated fibers (Nejatpour et al., 2024), as shown in **Figure 18**.

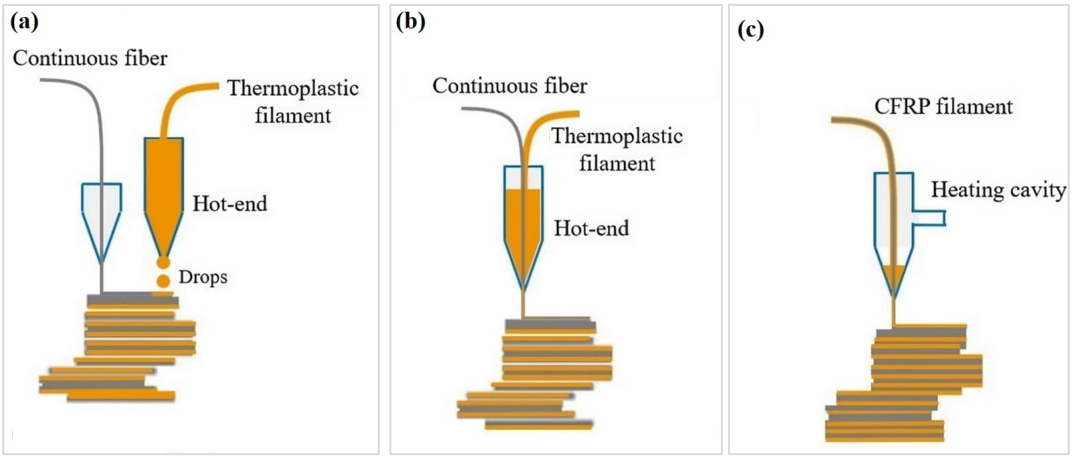

Figure 18. Printing methods for CFRCs (a) out–of–nozzle impregnation, (b) in–nozzle impregnation and (c) pre–impregnated (Nejatpour et al., 2024).

In-nozzle impregnation is the most widely used and straightforward method for printing continuous fiber–reinforced composites. It involves feeding the matrix and continuous fibers separately into the print head, where the matrix is melted and impregnates the fibers during extrusion (Nejatpour et al., 2024). This technique supports various reinforcement forms, including dry fibers and prepregs, and is favored for its simplicity, low cost, and material versatility. However, the quick impregnation process can lead to poor matrix–fiber bonding, which may reduce mechanical performance (Terekhina et al., 2022; Nejatpour et al., 2024). Out of nozzle impregnation uses two separate nozzles (dual extruders), one for the thermoplastic matrix and another for the reinforcement fibers, on the same printing platform (Nejatpour et al., 2024). This setup enables faster printing while maintaining good surface quality and offers better control over fiber content and impregnation. However, it typically requires more time due to the separate operation of the nozzles and demands specialized, costly equipment, which can also restrict the selection of materials (T. Wang et al., 2021; Nejatpour et al., 2024). The preimpregnated fiber method uses filaments that have been impregnated with the matrix material prior to printing (Krajangsawasdi et al., 2021). This ensures consistent impregnation and allows for additional impregnation during the printing

process, which improves the bonding between the matrix and fibers. Although this method can enhance mechanical performance, it requires sophisticated equipment for filament production and offers limited flexibility in material choices, often relying on commercially available filaments (Baumann et al., 2017; Nejatpour et al., 2024). For short fiber, micro, and nano-reinforced polymer composites used in Fused Deposition Modeling (FDM), production typically involves compounding (mixing) and extrusion processes (Krajangsawasdi et al., 2021), as shown in **Figure 19**.

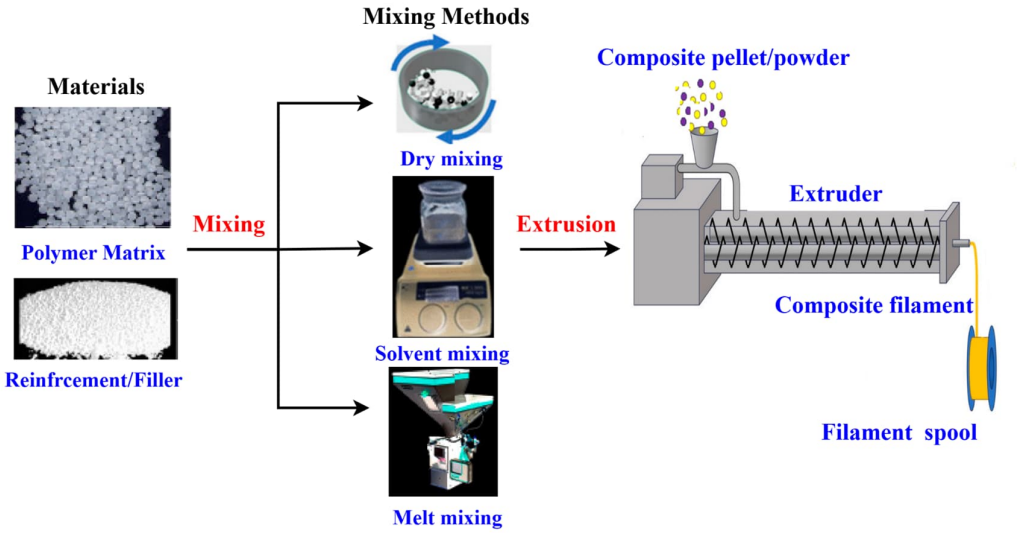

Figure 19. Production methods of polymer composite filament (Adapted from (Sola et al., 2023).

Compounding is a critical step in achieving uniform dispersion of fillers within a thermoplastic matrix before filament extrusion. Different compounding techniques offer unique benefits and challenges (Silviya et al., 2009). Solvent mixing dissolves the polymer in a solvent to enhance filler distribution and bonding, but the choice of solvent affects solubility, evaporation, and final mechanical properties (Zerankeshi et al., 2022). Hot melt mixing uses high temperatures to improve polymer–filler interaction and minimize agglomeration, though it requires precise temperature control to avoid thermal degradation (Albdiry, 2024). Dry mixing is a simpler method involving physical blending of polymer pellets with fillers, but achieving uniform dispersion can be difficult and depends on material characteristics and processing parameters (Aumnate et al., 2018).

After compounding, extrusion plays a key role in determining the filament's diameter and uniformity, which are critical for effective FDM 3D printing. There are two main types of extrusion: single-screw and twin-screw (Fuenmayor et al., 2018; Dhaval et al., 2022). While single-screw extrusion is suitable for basic applications, it offers limited mixing efficiency,

which can lead to poor filler dispersion and weakened mechanical properties. In contrast, twin-screw extrusion provides better mixing and a more controlled environment, reducing thermal degradation and improving filler distribution. This makes it more suitable for high-performance, high-filler content composites, resulting in superior material properties (Fuenmayor et al., 2018; Dhaval et al., 2022).

(B. Wang et al., 2021) reported the preparation of acrylonitrile butadiene styrene (ABS) nanocomposites reinforced with multi–walled carbon nanotubes (MWCNTs) through melt blending and extrusion into filaments using a single–screw extruder for fused deposition modeling. Similarly, (L. Yang et al., 2023) prepared a CNT/PLA composite by properly mixing the components in a blender. The CNT/PLA polymer composite pellet was then extruded via a twin–screw extruder to produce a composite filament. In another study, (Yamamoto et al., 2018) produced a micro graphene oxide (GO)–filled ABS composite filament through solvent mixing with acetone, followed by an extrusion process. Moreover, (Wiratma, 2021) reported that dried NCC powder and PLA pellets were dry–mixed with varying NCC concentrations, and the composite filament was prepared using a single–screw extruder. Another study by (Nötzel et al., 2018) described the production of composite filament from LDPE thermoplastic polymer and Al_2O_3 ceramic powder, prepared by melt compounding and subsequently extruded via a twin extruder. The calculated weight portion of copper nano–powder was dry–mixed with finely ground PLA powder, which was then ball milled and heated to soften. Finally, the paste was transferred to the extruder and extruded to create a composite FDM filament (Balamurugan et al., 2021).

Despite these advancements, thermal degradation remains a significant challenge in the production of polymer composite filaments, particularly due to repeated thermal cycles during processing, which can adversely affect both the polymer matrix and nanofillers, ultimately compromising mechanical performance and longevity of printed parts (Wynn et al., 2023; Kaptan et al., 2024). The degradation mechanisms, including oxidation and cross–linking, are influenced by factors such as melting temperature and processing environment, which can lead to changes in crystallinity and mechanical properties (Lyu et al., 2023; Wynn et al., 2023). Effective temperature control throughout the production process is essential to mitigate these risks, as demonstrated by studies showing that optimized thermal conditions can enhance crystallization and mechanical properties while minimizing degradation (Lyu et al., 2023; Özsin et al., 2023). Furthermore, the integration of protective strategies and

innovative materials can help preserve the integrity of these composites, aligning with sustainability goals in material science (Mokobia et al., 2024).

Additionally, achieving a homogeneous distribution of fillers is vital for obtaining the desired mechanical and thermal properties in the final product. Uneven filler dispersion can lead to weak points in printed parts, undermining their overall performance in practical applications (J. Chen et al., 2023; Y. Zhang et al., 2024).

Recent studies have introduced innovative methods aimed at addressing these challenges and enhancing filament production. (Martinsson et al., 2022) designed and reported a novel 3D–printer which can extrude and print directly from the raw material. It performed both compounding and printing. A novel in–situ reinforcement approach reported by (Ismail et al., 2023), where the filler is deposited in between layers during printing via a special designed filler dozer, instead of using a premixed composite filament. Another researcher studied printing a polymer filament on a woven reinforcement material (Franco-Urquiza et al., 2021).

Several studies have explored different techniques for producing polymer nanocomposite filaments suitable for fused deposition modeling (FDM). For example, (B. Wang et al., 2021) developed ABS nanocomposites reinforced with multiwalled carbon nanotubes (MWCNTs) through melt blending and extrusion using a single screw extruder. Similarly, (L. Yang et al., 2023) prepared a CNT and PLA composite by blending the components, followed by extrusion using a twin screw extruder. (Yamamoto et al., 2018) used solvent mixing with acetone to disperse graphene oxide (GO) into ABS before extrusion. In another study, (Wiratma, 2021) dry mixed nanocrystalline cellulose (NCC) with PLA pellets at various concentrations, and the resulting mixture was extruded using a single screw extruder. (Nötzel et al., 2018) produced a composite filament from LDPE and aluminum oxide through melt compounding followed by twin screw extrusion. (Mokobia et al., 2024) reported the preparation of a copper nanoparticle reinforced PLA filament by dry mixing, ball milling, and extrusion after softening the blend.

Despite these developments, thermal degradation remains a major challenge during filament production. Repeated heating cycles can deteriorate both the polymer matrix and the nanofillers, negatively affecting the mechanical properties and long term performance of printed parts (Wynn et al., 2023; Kaptan et al., 2024). Degradation mechanisms such as oxidation and cross linking are influenced by processing temperature and environment, which in turn affect crystallinity and structural integrity (Lyu et al., 2023; Wynn et al., 2023).

Maintaining precise temperature control during processing has been shown to reduce these effects and improve the crystallization and mechanical behavior of the composites (Lyu et al., 2023; Özsin et al., 2023). Achieving uniform dispersion of fillers is also critical, as poor distribution can result in weak zones within the printed part and reduce overall performance (J. Chen et al., 2023; Y. Zhang et al., 2024). Recent innovations have been introduced to address these issues. (Martinsson et al., 2022) developed a novel 3D printer that combines compounding and printing directly from raw materials. (Ismail et al., 2023) proposed an in-situ reinforcement approach where fillers are deposited between layers during printing using a specially designed filler dispenser, eliminating the need for precompounded filament. (Franco-Urquiza et al., 2021) explored printing onto woven reinforcement materials to enhance structural performance. These advancements reflect ongoing efforts to improve the quality and durability of composite filaments, optimize processing conditions, and support the development of high performance and sustainable FDM technologies.

2.11.3. Composite filament properties and printability

The performance and application potential of composite filaments used in fused deposition modeling (FDM) depend on a range of key properties. These include tensile strength, thermal resistance, viscosity, ductility, flexibility, elastic modulus, crystallization characteristics, consistency in filament diameter, and overall printability (Dey et al., 2021), as illustrated in **Figure 20**. One of the main factors influencing the properties of the filament is the type of filler or reinforcement material used(Sadan, 2023; Vieweger et al., 2024). Fillers such as carbon, ceramic, metal, glass, and cellulose have a significant effect on the overall characteristics of the filament. The mechanical properties are influenced by the type of filler, its weight percentage in the matrix, and the size of its particles (Dey et al., 2021). Moreover, the level of dispersion of these fillers within the matrix is crucial. Good dispersion results in uniform properties, while poor dispersion can lead to inconsistent performance (Sadan, 2023; Vieweger et al., 2024).

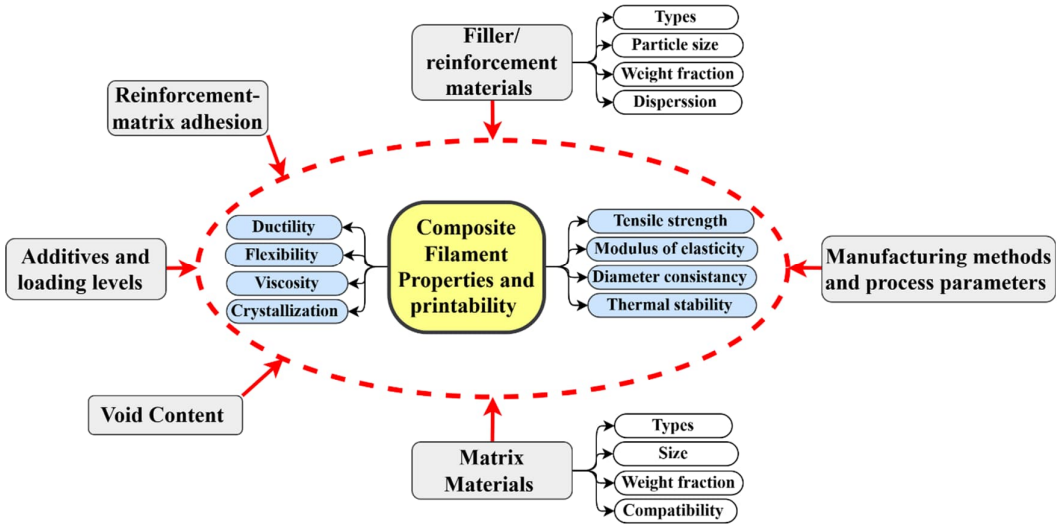

Figure 20. Factors affecting the properties and printability of composite filaments (Adapted from (Dey et al., 2021).

The selection of the matrix material, which forms the foundation of the filament, is also a critical consideration. Materials like PLA, ABS, PETG, PEEK, and PC interact with the fillers and play a key role in determining the overall performance of the filament (Dey et al., 2021). The matrix influences how effectively the fillers are integrated and how they impact the final properties. As a result, choosing an appropriate matrix is essential for achieving specific qualities such as strength, flexibility, and thermal resistance (Niendorf et al., 2021). Additives play a vital role in modifying the properties of composite filaments. These substances are incorporated with the matrix or filler materials to enhance particular features, such as improving thermal stability, adjusting viscosity for easier processing, or increasing impact resistance. The use of additives enables precise tuning of filament characteristics to better suit specific application requirements (Sastri, 2014). Another important factor is the adhesion between the reinforcement and the matrix. Strong bonding ensures that fillers effectively contribute to the filament's strength and durability. Conversely, poor adhesion can result in weak spots within the filament, reducing its overall mechanical performance and reliability (Seyni et al., 2011).

Additionally, the manufacturing methods and parameters, including extrusion techniques, temperature control, and cooling rates, significantly influence the filament's microstructure and performance. Variations in these processes can cause differences in properties such as strength, flexibility, and uniformity (Cojocaru et al., 2022). In summary, the combined effects of filler selection, matrix material, additives, adhesion quality, and manufacturing

conditions collectively determine the printability and functionality of composite filaments. Optimizing these factors is essential for producing high-performance filaments tailored to the demands of specific additive manufacturing applications (Hasanzadeh et al., 2023).

2.11.4. Properties of FDM–printed polymers and composite parts

The quality and performance of parts produced through fused deposition modeling (FDM) depend on a combination of factors, including the choice of filament material, printing parameters, and postprocessing methods (N. Ahmad et al., 2022). Selecting the appropriate filament is essential, as different polymers offer distinct mechanical and thermal properties. For example, PLA is easy to work with and provides a smooth surface finish, making it ideal for general-purpose applications. On the other hand, ABS offers higher impact resistance and can withstand elevated temperatures, which makes it suitable for more demanding conditions (Doshi et al., 2022).

The use of fillers and reinforcements can significantly improve the strength, stiffness, and thermal stability of printed parts (Sztorch et al., 2022). Moreover, maintaining a consistent filament diameter is important for ensuring smooth extrusion and accurate layer deposition. A standard filament diameter of 1.75 millimeters, with a typical tolerance of ± 0.2 millimeters, is widely accepted in FDM printing (Tuan Rahim et al., 2015).

Once the filament material is chosen, various printing process parameters become critical in determining the final quality of the printed parts. The build orientation, for example, affects the mechanical properties due to the layer–by–layer construction method; parts printed in vertical orientations often exhibit greater strength in that direction (Eryıldız, 2021). Layer thickness is another significant factor, while thinner layers can produce smoother surfaces and finer details, they also require more time to print (Shubham et al., 2016). Furthermore, the printing speed and temperature are vital for ensuring optimal material flow and adhesion; excessive speeds can compromise layer bonding, whereas incorrect temperatures can lead to issues such as warping or under–extrusion (Ansari et al., 2021). The infill density also plays a crucial role, as higher infill percentages generally increase the mechanical strength but increase the material usage and print duration (Srinivasan et al., 2020). **Figure 21** shows the summarized causes and effect diagram on properties of FDM printed parts.

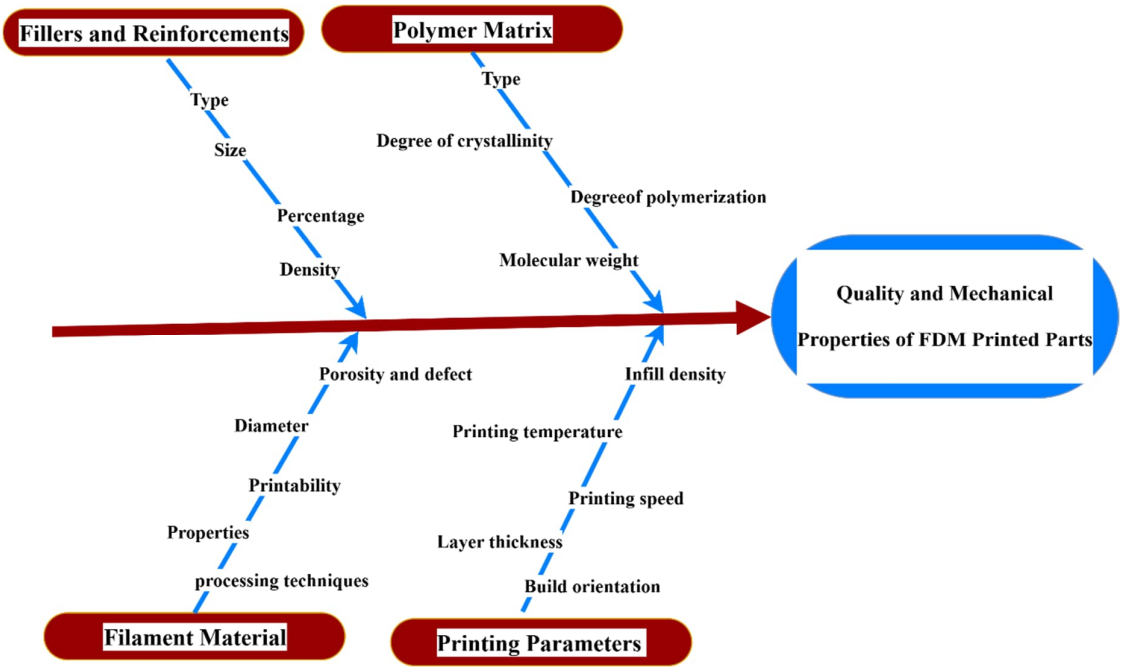

Figure 21. Factors affecting the quality and properties of FDM–printed parts (Adapted from (Rahim, Manaf, et al., 2019)

After the printing process, postprocessing techniques present additional opportunities to improve the properties of FDM–printed parts. Methods such as annealing can relieve internal stresses and enhance thermal stability, making parts more reliable in challenging applications. Sanding improves the surface finish and dimensional accuracy, whereas coatings can provide added protection against environmental factors and enhance the visual appeal of the parts. The choice of postprocessing method should align with the intended application and specific performance requirements of the final product (L. Cao et al., 2023). In conclusion, achieving high–quality FDM–printed parts require a comprehensive understanding of how filament materials, printing parameters, and postprocessing methods interact. By optimizing these factors, researchers and manufacturers can meet a wide range of performance needs across various applications, thereby advancing the capabilities of additive manufacturing (Rahim, Manaf, et al., 2019).

2.11.5. Applications of FDM–Printed Polymers and Composites

Fused Deposition Modeling (FDM) has become a widely used and versatile 3D printing technology that supports the fabrication of components using both pure polymers and high-performance composites. Common thermoplastics such as PLA, ABS, PETG, and nylon are popular due to their ease of processing, affordability, and broad applicability. These

materials are commonly used in prototyping, educational tools, consumer products, and functional mechanical parts including gears and bearings, particularly where moderate mechanical properties are acceptable (Ligon et al., 2017).

Recently, advanced composites reinforced with materials such as carbon, glass, metal, or ceramic micro and nanofillers offer substantial enhancements in mechanical, thermal, and electrical properties. These improvements make them suitable for demanding applications in sectors such as aerospace, automotive, and healthcare. Their benefits include a higher strength to weight ratio, increased rigidity, and excellent impact resistance, which are essential for high-performance and safety-critical environments (Weaver, 2017).

As FDM technology continues to develop, its applications are expanding significantly. In the aerospace industry, composite materials enable the production of lightweight yet strong components that can withstand extreme conditions, which is vital for ensuring safety and efficiency (Pervaiz et al., 2021). In automotive engineering, these materials are used to manufacture components that endure high thermal and mechanical stress, thereby enhancing the performance and durability of various vehicle systems (Salifu et al., 2022). The healthcare sector also benefits from FDM, where biocompatible and mechanically robust materials are used for custom medical devices, prosthetics, and anatomical models, allowing for both precision and reliability (Friedrich et al., 2013).

In electronics, FDM printed composites with conductive fillers support the development of components such as device enclosures, circuit elements, and durable tooling solutions. These applications contribute to improved functionality and extended service life in manufacturing environments (J. Han et al., 2013). Overall, the continued development and application of both pure polymers and advanced composites in FDM 3D printing demonstrate the technology's potential to address a wide range of needs across multiple industries, driving innovation and expanding possibilities for future applications. The ongoing development and application of pure polymers and advanced composites in FDM 3D printing demonstrate the technology's potential to meet a wide range of industrial needs, fostering innovation and expanding future possibilities. **Figure 22** shows the main application areas of FDM printed polymers and composites.

Recent research has demonstrated several innovative biomedical uses, including the creation of polylactide-based scaffolds, hydroxypropyl methylcellulose reinforced structures, and PLA mixed with stainless steel for tissue engineering and medical devices (G. Jiang et al., 2020; D. Wang et al., 2020). Different PLA scaffolds and biocompatible PLA–biphasic

calcium phosphate composites have shown promise for tissue engineering applications (Nevado et al., 2020; P. Kumar et al., 2024). PLA–stainless steel polymeric composites have been fabricated for specific biomedical uses (Shamsudin et al., 2023). Multicolor extrusion techniques have also made it possible to produce cost-effective anatomical models. Furthermore, both ABS and PLA have been used to develop canine tibia models and complete dentures for clinical simulation and training (M. Y. Chen et al., 2020), and FDM has been utilized to create an acrylonitrile butadiene styrene canine tibia model as well as complete dentures (Hsu et al., 2020).

Within the pharmaceutical industry, FDM has emerged as a promising technique for manufacturing tablets and implants with customizable drug release profiles. During the COVID-19 pandemic, the technology was widely adopted for the rapid production of protective gear, including face masks and respirator shields (Tan et al., 2018; Tareq et al., 2021; Agarwal, 2022).

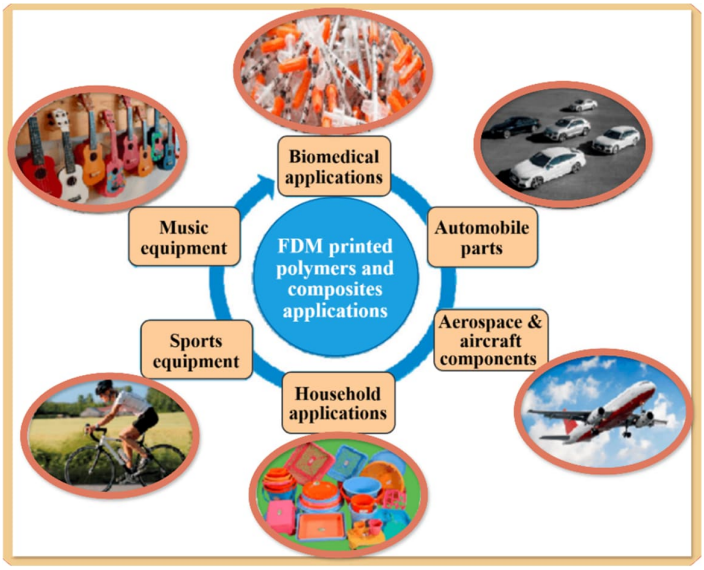

Figure 22. Scope of FDM–based polymers and its composites in various applications (Monfared et al., 2021).

Beyond conventional applications, FDM is being explored in more advanced areas. These include the fabrication of metal and polymer composite filaments for functional automotive parts such as brake pedals (Sargini et al., 2021). (Kading et al., 2015) proposed solutions for extraterrestrial construction, including on Mars and (Helú et al., 2021) used FDM printed parts for the fabrication of microelectrodes and multielectrode probes. The applications also include shock–resistant polypropylene dipping chambers for synthesis and analytical

purposes (Jaxel et al., 2020) and PLA dielectric substrates for microstrip patch antennas (Prakash et al., 2021). A particularly promising development is the integration of FDM with smart materials, commonly referred to as four-dimensional (4D) printing. This approach enables the creation of dynamic structures such as thermally responsive hinges, orthotic devices, and high-performance shape memory polymers used in biomedical technologies (Q. Chen et al., 2020; S. K. Sinha, 2020; Cano-Vicent et al., 2021). In conclusion, the expanding range of materials and continuous advancements in FDM printing technology are driving innovation across various industries. The ability to produce customized, functional, and high-performance components confirms the transformative potential of FDM in shaping the future of additive manufacturing (Nezhad et al., 2021; Mohammadi et al., 2022).

2.12. Characterization and Testing Methods

2.12.1. Characterizations of fiber, micro and nanocellulose

A comprehensive understanding of the structure and properties of fibers, micro cellulose, and nanocellulose is essential when evaluating their potential applications. Therefore, critical structural characteristics such as particle size, morphology, crystallinity, purity, and degree of polymerization should be thoroughly examined(Kaur et al., 2021). The properties of micro cellulose and nanocellulose, as well as their associated characterization methods, largely depend on the production technique used, whether it is mechanical, chemical, or biological. These properties are also influenced by the source material, which may include wood, pulp, recycled paper, bamboo, agricultural waste, cotton, or other forms of biomass, as well as the intended final application (Balea Martín et al., 2021). Characterization protocols provide detailed information on a wide range of parameters including dimensions such as length and diameter, aspect ratio, morphology, surface charge, surface chemistry, crystallinity, mechanical performance, and rheological behavior (Foster et al., 2018b; Balea Martín et al., 2021). Various analytical techniques are utilized to assess these characteristics. These include scanning electron microscopy, transmission electron microscopy, atomic force microscopy, optical microscopy, dynamic light scattering, Fourier transform infrared spectroscopy, X–ray diffraction, solid state nuclear magnetic resonance, X–ray photoelectron spectroscopy, and energy dispersive X–ray spectroscopy. Additionally, properties such as tensile strength, flexural behavior, thermal stability, and surface area are evaluated using tensile, flexural, and compression testing, dynamic mechanical analysis, thermogravimetric analysis, differential scanning calorimetry, differential thermal analysis,

differential thermogravimetry, and the Brunauer–Emmett Teller method (Foster et al., 2018b; Balea Martín et al., 2021).

Microscopic techniques such as scanning electron microscopy, transmission electron microscopy, and atomic force microscopy are frequently used by researchers to determine the size and morphology of nanocellulose. Other methods based on light interactions, electrical behavior, sedimentation, sorting, classification, or surface adsorption, such as dynamic light scattering, can also be employed to estimate particle size (Foster et al., 2018b). However, the values provided by dynamic light scattering do not directly correspond to the actual length or cross section of the particles. Instead, the technique measures the apparent hydrodynamic diameter, which may not accurately reflect the shape of anisotropic particles (Mazloumi et al., 2018). Additionally, the translational diffusion of particles varies depending on their orientation, which means that the resulting distributions cannot reliably represent actual particle size distributions. Although light scattering techniques are typically faster than microscopic methods, their underlying assumptions are often not valid for nanocrystals or nanofibers (Mazloumi et al., 2018). On the other hand, microscopic techniques provide sufficient resolution at the nanometer scale for visualizing nanocellulose and determining specific dimensions based on the particle shape. The accuracy of these techniques is influenced by the particle's geometry and physicochemical characteristics such as chemical composition, heterogeneity, surface topography, surface charge density, and the nature of the dispersion medium (Balea Martín et al., 2021).

Among these microscopic approaches, transmission electron microscopy is the most commonly applied method for nanoparticle characterization due to its higher spatial resolution compared to scanning electron microscopy (Foster et al., 2018b). However, the preparation of samples for transmission electron microscopy can be challenging and requires skilled operation, which may limit its accessibility (Ghomrasni et al., 2020). The ratio of crystalline to amorphous domains, or the degree of crystallinity, is a key property that influences the physical, chemical, and functional behavior of nanocellulose (Kargarzadeh, Ahmad, et al., 2017; Picot-Allain et al., 2023). The crystallinity index of cellulose is frequently used to monitor structural changes following chemical, mechanical, or enzymatic treatments. This index can be determined using techniques such as ^{13}C nuclear magnetic resonance, infrared spectroscopy, and X ray diffraction, with X ray diffraction being the most widely adopted method (Kargarzadeh, Ahmad, et al., 2017; Picot-Allain et al., 2023). Additionally, wide angle X ray scattering is used to examine the positions, intensities, and

widths of diffraction peaks, providing insights into the types and proportions of crystalline structures, interplanar distances, nanocrystal sizes, and lattice distortions (Kargarzadeh, Ahmad, et al., 2017).

Thermogravimetric analysis is an essential technique for evaluating the thermal stability and decomposition behavior of cellulose materials by measuring weight changes as a function of temperature or time. The resulting thermal curves offer important data on onset, peak, and final decomposition temperatures, which are necessary for assessing material performance under various conditions (Martincic et al., 2024). To gain deeper insights into decomposition kinetics, differential thermogravimetry (DTG) is used to calculate the rate of weight loss and to identify the temperature at which the most significant degradation occurs (Blanco et al., 2021). Differential scanning calorimetry (DSC) is another important thermal analysis method that assesses heat flow associated with physical transitions such as glass transition temperature (T_g), melting point (T_m), fusion enthalpy (ΔH_f), and degree of crystallinity (X_c). This technique operates by measuring the energy absorbed or released by the sample in comparison to a reference material during controlled heating or cooling (Gill et al., 2010).

Fourier transform infrared spectroscopy (FT–IR) is especially useful during the extraction of micro cellulose and nanocellulose, as it provides critical information on the removal of non–cellulosic substances and the structural changes that take place during processing (Mehdi Jonoobi et al., 2010). The technique has shown a clear reduction in the presence of lignin and hemicellulose due to chemical treatments such as alkalization, delignification, and bleaching. These changes are confirmed by the weakening or disappearance of spectral peaks related to non–cellulosic components, and the enhancement of peaks associated with cellulose, indicating the successful isolation and purification of the cellulose phase (Mehdi Jonoobi et al., 2010). FT–IR analysis demonstrated that structural changes in the fiber occurred during treatment, particularly a reduction in both intermolecular and intramolecular hydrogen bonding. This disruption, along with the removal of non–cellulosic components and partial degradation of cellulose chains, enhances access to the microfibrillar regions, thereby promoting the selective extraction of cellulose and increasing its crystallinity (Janardhnan et al., 2011).

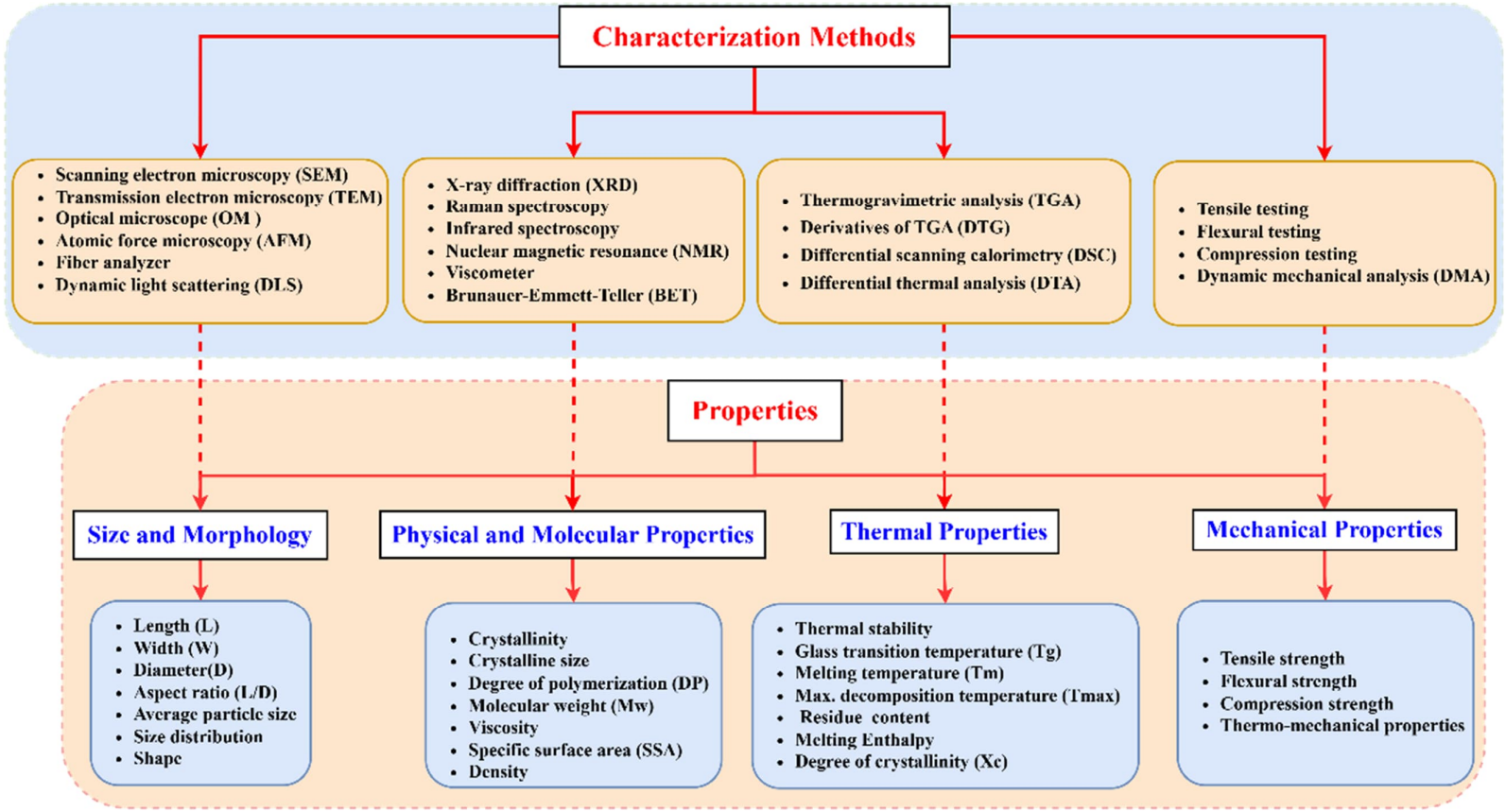

Figure 23. Properties and characterization techniques for fiber, micro/nanocellulose and its polymer composite (Adapted from (Kaur et al., 2021).

When combined with complementary techniques such as X–ray diffraction, FT–IR further confirms the enhanced crystallinity resulting from the elimination of amorphous cellulose regions (Montoya-Escobar et al., 2022). Overall, FT–IR not only reveals important chemical changes but also highlights the effectiveness of the extraction process in purifying and structurally modifying micro cellulose and nanocellulose (Trivedi & Gupta, 2023). In summary, the characterization of fibers, micro cellulose, and nanocellulose involves a broad spectrum of analytical methods aimed at assessing their structural, morphological, thermal, and mechanical properties. The combined application of these techniques provides the necessary foundation for optimizing cellulose materials for advanced functional applications in various industrial and biomedical fields (Kaur et al., 2021). **Figure 23** illustrates the major properties and analytical methods used to characterize fibers, micro cellulose, nanocellulose, and their polymer composites.

2.12.2. Characterizations of cellulose–based polymer composites

Polymer composites reinforced with micro and nanocellulose have gained increasing attention due to their outstanding properties and potential for diverse applications. A thorough characterization of these materials is essential to evaluate their performance in terms of mechanical, thermal, morphological, structural, optical, electrical, and barrier properties (Omran et al., 2021). Mechanical characterization focuses on evaluating strength, stiffness, and ductility using standard methods such as tensile, flexural, and impact tests. These assessments provide critical insights into how the composites respond to stress under real-world conditions (Vasile et al., 2022). Thermal behavior is typically analyzed using differential scanning calorimetry (DSC) and thermogravimetric analysis (TGA), which help determine thermal stability, glass transition temperature, and decomposition pattern, that are the key factors for thermal applications (Priyadarshini, 2021).

Morphological features are examined through techniques such as scanning electron microscopy and transmission electron microscopy. These methods reveal the distribution and interaction of cellulose fibers within the polymer matrix, offering insights into composite homogeneity and interfacial bonding (Chandrasekar et al., 2021). Structural analysis is performed using X–ray diffraction (XRD) and Fourier transform infrared spectroscopy (FT–IR), which identify crystallinity levels and chemical bonding patterns that influence the physical and mechanical behavior of the material (Abhilash et al., 2016).

In applications where visual properties are important, ultraviolet-visible spectroscopy (UV–Vis) is used to evaluate transparency and light transmittance (Venkatachalam, 2016). Electrical characteristics, such as conductivity and dielectric behavior, are examined through impedance spectroscopy, which is especially relevant for developing smart and functional materials (Kalyon et al., 2002). Barrier properties, critical in packaging and coating applications, are assessed by measuring gas permeability and moisture absorption. These tests help determine the material's ability to protect contents from environmental exposure while maintaining structural integrity (Laurindo, 2016). In conclusion, comprehensive characterization of cellulose-reinforced polymer composites across multiple domains is essential for optimizing their performance and expanding their applicability in fields ranging from packaging to electronics (Tingaut et al., 2011).

2.12.3. Composite filament 3D printed part characterization methods

Composite filaments, which are crucial in advanced additive manufacturing, consist of a polymer matrix reinforced with various fillers or fibers (Dickson et al., 2020). These filaments have garnered significant attention because of their enhanced mechanical properties, lightweight nature, and versatility in design. The ability of these materials to combine strength with reduced weight makes them highly desirable for a wide range of applications that require both performance and efficiency (Dickson et al., 2020; Angelopoulos et al., 2021). To fully understand and optimize the performance of these composite filaments and their corresponding printed parts, comprehensive characterization is essential. This process involves assessing multiple aspects of the filaments and printed parts, including their morphological, physical, thermal, and mechanical properties (Çanti et al., 2018; Oviedo et al., 2020).

Starting with morphological properties, the analysis of fracture surfaces provides insights into how the filament and printed parts behave under stress (Oviedo et al., 2020). Techniques such as scanning electron microscopy (SEM) are used to examine fracture patterns and surface defects. This examination helps identify failure mechanisms such as fiber pull–out or matrix cracking, which are crucial for understanding the durability of a material and for refining its formulation (Angel R Torrado Perez et al., 2014). Additionally, surface analysis is important for evaluating the uniformity and quality of the surface of a filament. Optical microscopy or profilometry can reveal surface roughness and the presence of defects, which

influence the printing process and the final part's quality (Angel R Torrado Perez et al., 2014).

With respect to physical properties, diameter, density and porosity measurements are fundamental for evaluating the integrity and uniformity of filaments (Angelopoulos et al., 2021). High–density filaments with minimal porosity are typically preferred, as they offer better strength and reliability. Techniques such as Archimedes' principle for density measurement and optical microscopy can be used to obtain the diameter of the filament (Angelopoulos et al., 2021).

Thermal properties are another critical aspect of filament characterization. Differential scanning calorimetry (DSC) and thermogravimetric analysis (TGA) provide valuable information about thermal transitions and stability (Trhlíková et al., 2016). DSC helps determine important thermal properties, such as the glass transition temperature (Tg) and melting temperature (Tm), which influence processing conditions and the performance of the filament under heat. TGA assesses the thermal stability and degradation temperatures, offering insights into how the filament will behave under various thermal stresses (Trhlíková et al., 2016).

Finally, the mechanical properties of the composite filaments and printed parts are evaluated through various tests. Tensile strength and elongation measurements provide information on how the filaments and printed parts withstand applied forces and deform before breaking (Oviedo et al., 2020). These properties are essential for predicting the performance of printed parts under loading (Grabowik et al., 2017). Flexural strength and modulus tests assess the resistance of printed parts to bending, which is crucial for applications involving flexural stresses. Additionally, impact resistance testing evaluates the ability of printed parts to absorb and dissipate energy during sudden impacts, which is important for ensuring durability and shock resistance (Grabowik et al., 2017; Oviedo et al., 2020).

Overall, the characterization of composite filaments and printed parts is a multifaceted process that provides critical insights into their suitability for different applications (Çanti et al., 2018). The performance of these materials can vary significantly on the basis of the type of polymer matrix and reinforcement used, process parameters used for filament production and 3D printing, making detailed characterization indispensable for optimizing their use in various technological and industrial applications (Çanti et al., 2018).

2.13. Challenges and Future Prospects

The integration of agricultural wastes for nanocellulose extraction holds significant promise, yet it also faces several challenges that need to be addressed for broader adoption. Challenges include variability in the composition of agricultural residues, which can affect the consistency, yield, property and quality of the extracted nanocellulose, impacting its effectiveness as a filler. Additionally, extraction processes, which often involve chemical treatments, can be costly and environmentally taxing, necessitating the development of more sustainable and efficient methods. Similarly, the extraction processes may require optimization to ensure efficiency and cost effectiveness (C. H. Lee et al., 2021).

Moreover, ensuring the compatibility and interlayer bonding of nanocellulose with various polymers used in FDM 3D printing is crucial for optimizing performance. Researchers must also address issues related to dispersion within the polymer matrix, as uneven distribution and agglomerations can affect the properties of the composites. In addition, the future challenge in 3D printing is the quantification of the interface properties of the composite. Currently, most interface properties are characterized qualitatively by scanning electron microscopy (SEM) images. More detailed research is therefore needed to evaluate the interfacial strength of composites and optimize the printing parameters (C. H. Lee et al., 2021; Scaffaro et al., 2021).

In the future, advancements in extraction technologies, such as enzymatic or green chemical methods, could mitigate some of these challenges. Furthermore, enhanced nanocellulose isolation, drying and modification methods may lead to innovative solutions for optimizing the use of nanocellulose in polymer composites and in 3D printing applications (Dey et al., 2021; Scaffaro et al., 2021).Despite these hurdles, future perspectives are promising. As the focus on sustainability intensifies, leveraging agricultural wastes for nanocellulose not only provides a valuable resource for enhancing polymer composites but also promotes waste reduction and environmental stewardship. Ultimately, this approach could pave the way for the development of high–performance, eco–friendly materials that align with global sustainability goals in manufacturing and product design (Dey et al., 2021).

2.14. Summary of Literature Review

Cellulose, the most abundant natural polymer, is composed of long chains of β–1,4–linked glucose units. These chains bundle together to form microfibrils and macrofibril, which contribute to the structural integrity of plant cell walls. Cellulose can be processed into various forms such as microcrystalline cellulose (MCC), cellulose nanofibrils (CNFs), and cellulose nanocrystals (CNCs), each offering unique physical properties depending on their morphology and scale. Among the most promising sources of cellulose are natural plant fibers derived from wood, non-wood plants, and agricultural residues. Agricultural by-products such as corncobs, teff straw, coffee husk, sugarcane bagasse, and rice straw are especially attractive due to their low cost, renewability, and favorable cellulose content. The chemical composition of these residues varies significantly, with cellulose contents ranging from 25% to 75%, hemicellulose from 5% to 50%, and lignin from 6% to 40%.

This variability highlights the importance of feedstock selection based on purity, abundance, and ease of processing. Linseed stalks, which are plentiful in Ethiopia and other regions, represent a particularly underutilized resource with great potential for cellulose extraction.

Nanocellulose has gained attention across various industries for its exceptional mechanical, thermal, and barrier properties. It is increasingly being explored for use in packaging, biomedical applications, electronics, and filtration systems. To obtain nanocellulose from plant biomass, the fibers must first be isolated using techniques such as mechanical decortication or biological and chemical retting. These methods differ in processing time, cost, environmental impact, and the quality of the fibers they produce. After initial fiber separation, pretreatment steps such as dewaxing, delignification, alkalization, and bleaching are used to purify the material. The production of nanocellulose typically involves acid hydrolysis using sulfuric acid under controlled conditions, followed by steps like centrifugation, dialysis, sonication, and drying to stabilize the nanoscale features. Various agricultural residues can be tailored to yield nanocellulose with specific dimensions and surface characteristics by adjusting the type and concentration of chemicals, temperature, and processing duration. The resulting nanocellulose often exhibits diameters ranging from 3 to 100 nanometers, and lengths spanning from 50 to over 500 nanometers, creating high aspect ratios ideal for composite reinforcement. These particles also demonstrate high crystallinity and good thermal stability, with decomposition starting above 100°C and peaking well above 200°C.

Polylactic acid (PLA) is a leading biopolymer used as a matrix in cellulose-based composites due to its biodegradability, printability, and compatibility with reinforcement materials. It is synthesized from lactic acid monomers through ring-opening polymerization and can be tailored through its stereochemical forms for different performance characteristics. PLA is widely adopted in fused deposition modeling (FDM) 3D printing.

The materials used for filaments vary from neat thermoplastics to polymer composites; however, commercially available options are still limited, especially for bio-based and reinforced composite filaments, which restricts material selection for sustainable and high-performance applications in additive manufacturing. These reinforcement (filler) sizes used in polymer composites include millimeter-scale fibers, microscale, and nanoscale particles. Composite filaments can be fabricated through dry mixing and melt extrusion, using single- or twin-screw extruders, and can be enhanced further using continuous fiber impregnation during or prior to printing. The performance and printability of composite filaments are influenced by multiple factors. These include the type, size, and loading of the filler; the compatibility between filler and matrix; the use of plasticizers or coupling agents; and processing conditions such as extrusion temperature and cooling rate.

Successful printing also requires filaments with uniform diameter, appropriate melt flow properties, and good filler dispersion. The final properties of 3D-printed parts depend not only on the quality of the filament but also on printing parameters such as nozzle temperature, layer thickness, build orientation, infill density, and printing speed. Post-processing treatments, including annealing, surface sanding, or coatings, can significantly improve dimensional stability, mechanical strength, surface smoothness, and thermal resistance. A wide range of fillers has been used to enhance the mechanical, thermal, and functional performance of FDM filaments. Nanocellulose and carbon-based nanomaterials like carbon nanotubes and graphene have been shown to increase tensile strength, stiffness, and thermal stability, even at low loading levels. Microscale fillers such as micro cellulose or ceramic powders improve impact resistance and modulus, while millimeter-scale reinforcements like carbon or glass fibers substantially increase load-bearing capacity. However, higher filler content can lead to increased melt viscosity, extrusion difficulties, and nozzle clogging, highlighting the importance of optimal filler loading and processing conditions. To ensure quality and performance, comprehensive characterization techniques are employed throughout the material development process. Morphological tools like scanning and transmission electron microscopy reveal structural details and dispersion of

reinforcements. Structural characterization using X-ray diffraction and infrared spectroscopy provides information on crystallinity and chemical functionality. Thermal analysis methods assess degradation and melting behavior, while mechanical tests evaluate strength, stiffness, and durability. Other techniques such as dynamic light scattering, BET surface area analysis, and rheological measurements further help link material structure to performance.

2.14.1. Literature Review Gaps

Despite the growing research interest in sustainable Bio nanocomposites and fused deposition modeling (FDM) based 3D printing, several critical gaps remain across material development, processing techniques, and application readiness. Biopolymer matrices continue to face limitations due to brittleness, insufficient thermal resistance, and weak interfacial bonding with fillers. These limitations restrict their mechanical performance and reduce their suitability for demanding or load-bearing applications. On the other hand, synthetic fiber reinforcements, although mechanically strong, are non-renewable, difficult to recycle, and often incompatible with biodegradable matrices. This undermines the environmental advantages typically associated with Bio nanocomposites.

Natural reinforcements offer the benefits of renewability and biodegradability; however, they are hindered by moisture sensitivity, variability in properties, and low thermal stability. These characteristics make processing difficult and result in inconsistent final product performance. In addition, both synthetic and organic micro- and nano-fillers often suffer from issues such as agglomeration, hydrophilic behavior, and thermal degradation. These challenges lead to poor dispersion, weak matrix interaction, and limited commercial scalability.

Compounding and processing methods further exacerbate these problems due to inadequate filler dispersion, incompatibility between fillers and matrices, and degradation of natural components during thermal processing. These challenges are particularly evident in FDM 3D printing, where fixed processing conditions, such as high nozzle temperatures and limited adaptability, constrain the use of bio-based materials. Issues such as nozzle clogging, poor interlayer adhesion, and dimensional inaccuracies reduce the quality and reliability of printed components.

Moreover, while agricultural crop residues represent a promising and underutilized resource, they present difficulties due to their variable composition, high content of non-cellulosic

materials, and seasonal availability. These factors lower the consistency and yield of extracted cellulose and necessitate intensive preprocessing. The limited availability of high-performance Bio nanocomposite filaments and the restricted compatibility with existing FDM machines further hinder the adoption of sustainable materials in additive manufacturing. Collectively, these gaps point to the need for comprehensive research focused on material innovation, improved processing strategies, and enhanced equipment adaptability to fully realize the potential of Bio nanocomposites in advanced manufacturing applications. **Table 14** illustrates the summary of literature review gaps and their implications.

Table 14. Summary of literature review gaps and their implications

Key focus areas	Gaps / Limitations	Implications
Bio polymer matrices	o Limited range of biodegradable polymers o Brittleness o Poor thermal resistance o Weak interfacial bonding	o Restricted performance for flexibility o Poor durability o Limited use in high-demand applications
Synthetic fiber reinforcements	• Poor compatibility • Non-renewable • Difficult to recycle • Processing challenges	• Compromises environmental benefits of Bio nanocomposites • Increases carbon footprint
Natural fiber reinforcements	o Moisture sensitivity o Inconsistent properties o Low thermal stability o High fiber volume fraction	o Degrades during processing o Unpredictable properties o Requires additional treatments
Synthetic micro/nanofillers	• Agglomeration issues • Poor dispersion • Melt viscosity • Potential toxicity	• Reduced material performance • Health/environmental risks • Increases processing complexity
Organic micro/nano fillers	o Hydrophilicity o Poor dispersion o Thermal degradation o Complex postprocessing	o Weak matrix bonding o Processing challenges o Limited scalability and commercialization
Bio nanocomposite compounding methods	• Inadequate filler dispersion • Filler/matrix incompatibility • Thermal degradation of fillers • Limited solvents to dissolve biopolymers	• Low composites performances • Restricted biopolymer selection • Increased operational costs

Key focus areas	Gaps / Limitations	Implications
Bio nanocomposite manufacturing methods	o High processing temperatures o Difficulty producing complex geometries o Nozzle clogging o Poor interlayer adhesion	o Limits the use of thermally sensitive natural fillers o Limits design freedom o Leads to defective prints and material waste o Poor dimensional accuracy and performance
Polymer Bio nanocomposites	• Poor fiber–matrix adhesion • Heterogeneity and variability • Dimensional instability • Moisture absorption and sensitivity	• Mechanical performance limitations • Durability and weathering resistance limitations • Makes precise applications challenging
Agricultural crop residues	o Variable fiber properties o Presence of high amount of non-cellulosic components o Seasonal availability o Improper waste disposal o Underutilized resources	o Inconsistent mechanical properties o Lowers yield and purity of cellulose o Intensive preprocessing required o Supply chain complexity o Environmental pollutions o Wasted resource value
Filament materials	• Limited commercially available bio nanocomposite filaments • Poor filler–matrix compatibility in composite filaments • Moisture sensitivity of bio-based filaments	• Restricts material choices for sustainable applications • Weak mechanical properties • Nozzle clogging and inconsistent print quality
FDM 3D printer machines	o Fixed processing temperature range in single head nozzle o Limited nozzle diameter o Limited adaptability to emerging filament types	o Restricts fiber size and content in bio nanocomposite filaments o Fiber degradation or incomplete melting o Difficulty in optimizing print parameters for new filaments

Therefore, together, these gaps underscore the need for integrated solutions to address the integrated challenges in the field by synergizing different strategies as shown in **Figure 24.** Optimized material selection, advanced processing, and advanced compounding methods to enhance the performance. Nanotechnology elevates performance further through nano-scale fillers, improving performance using low and optimized concentration of nanofiller loading. Concurrently, additive manufacturing (3D printing) enables precise, low-waste production of complex geometries, supported by advancements in 3D printers, filament preparation, optimized extrusion parameters and printing process parameters to ensure printability and functional integrity. Environmentally, selection of all bio-based materials, eco-friendly extraction methods and renewable feedstocks minimize waste. Together, these strategies reduce the challenges and align with circular economy principles.

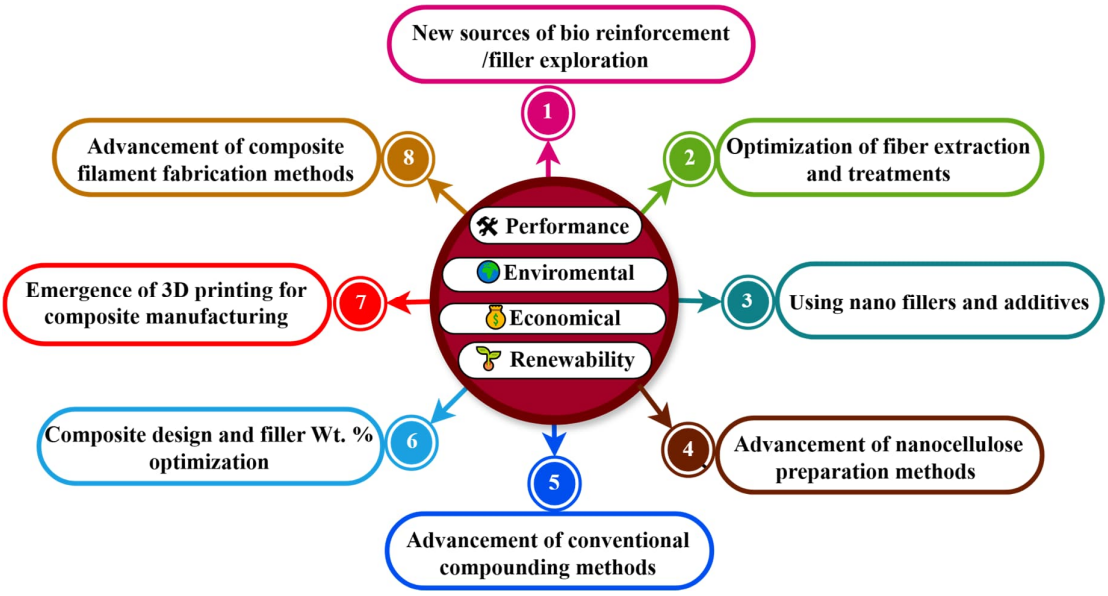

Figure 24. A holistic framework strategies for addressing integrated challenges in the bio nanocomposite field.

CHAPTER 3

MATERIALS AND METHODS

This chapter outlines the materials, methodologies, experimental procedures and data collection methods employed in this study. It provides a comprehensive overview of the list of chemicals, raw materials, laboratory equipment, and analytical instruments used for extraction, processing, characterization, and testing. Detailed descriptions of the samples and sampling techniques, experimental design and procedures, and data collection and analysis methods are also included. Furthermore, the software tools utilized for data analysis, experimental design, and visualization are discussed to highlight their role in supporting the research.

3.1. Materials

This section outlines the raw materials and chemicals used throughout the study. It includes the details of each material, including their grades and specific roles in the experiment as shown in **Table 15**.

3.2. Research Methodology and Approaches

In this study, an experimental research methodology alongside quantitative and qualitative research approaches were used. This research methodology and research approaches were applied at various stages of the research. The experimental methodology played a main role, particularly in the controlled laboratory experiments where various samples preparation processes such as fiber retting, chemical treatments, micro-cellulose extraction, CNC isolation, composite preparation, and 3D printing were systematically conducted. The experimental design involved the manipulation of variables including retting durations, chemical treatment conditions, micro-cellulose and nanocellulose extraction processes and composite processing conditions and parameters.

A mixed-methods approach integrating both quantitative and qualitative data collection strategies were utilized. The quantitative data collection approach included the measurement of physical parameters, as well as the structural, thermal, and mechanical properties of the samples. It also encompassed the statistical analysis of the data. Meanwhile, the qualitative data collection approach was applied in interpreting visual data from morphological and structural analyses such as SEM/TEM images and spectra or graphs from XRD, FT-IR, TGA, DTA, and DSC characterization techniques.

3.3. Samples and Sampling Techniques

Initially, linseed stalk residue was collected from a single farm using convenience sampling, based on the availability and accessibility of the raw material. To ensure consistency, uniform stalks of consistent length were selected from the middle section using purposive sampling. A total of eight sample groups (RT_1 to RT_8) were designed according to the maximum retting duration and predefined withdrawal intervals using systematic sampling.

After the retting process, and based on the assessment of end-retting indicators, the fibers were categorized into four groups: under-retted (R_1), optimally retted (R_2), over-retted (R_3), and a control group of non-retted fibers (R_0). This categorization was performed using purposive sampling. From each group, stratified random sampling was employed to select ten individual fibers for subsequent testing and analysis.

During the multistep optimization of chemical treatments, the extraction factors including solvent concentration, reaction temperature, and reaction time, with levels defined as low, medium, and high, were determined using purposive sampling based on relevant literature. The Taguchi L_9 Orthogonal Array was also selected purposively. The combinations of factor levels were arranged using the standard L_9 layout to evaluate their effects on the removal of extractives, hemicellulose, and lignin. Among the nine experimental runs, the optimal condition was selected using the larger is better performance criterion. Following this, purposive sampling was used to collect three representative samples from each treatment stage, specifically dewaxed fiber, alkalized fiber, and bleached fiber, along with one non-retted fiber as a control. These samples were used for thermal and FT–IR analyses to assess the effect of the treatments on fiber properties.

Throughout the CNC isolation process including pretreatments, acid hydrolysis, and post-treatments, all process parameters such as chemical and solvent types, concentrations, reaction times, temperatures, replication, and mixing ratios were selected using purposive methods. These decisions were based on literature reviews and preliminary trials aimed at ensuring process efficiency. The CNC, micro cellulose (MC), and raw fiber (RF) samples were also purposively selected as they represented key stages in the material transformation from raw fiber to micro cellulose and then to nanocellulose. These representative materials were analyzed using advanced characterization techniques to evaluate the effectiveness of each treatment step.

In the preparation of the bio nanocomposite, purposive sampling was applied to select CNC weight percentages from the literature. Three PLA/CNC composite samples were prepared using CNC contents of 1%, 3%, and 5% by weight, in addition to a control sample consisting of neat PLA. These concentrations were strategically chosen to represent low, moderate, and relatively

high CNC loading, allowing for a comparative evaluation of the influence of nanocellulose content on composite properties. All four samples were systematically selected for further characterization and testing, ensuring a comprehensive assessment of morphological, thermal, structural, and chemical properties. The composite sample demonstrating the most favorable combination of properties was identified as the optimal formulation, which was subsequently used for filament preparation.

Finally, the printing parameters for the FDM 3D printing process were established based on the material properties of the composite and standard parameters used for PLA. The build plate temperature and printing temperature were customized based on the glass transition temperature (Tg) and melting temperature (Tm), as determined through differential scanning calorimetry (DSC), to ensure proper adhesion and extrusion. Parameters such as printing speed, initial layer thickness, and layer thickness were set following standard guidelines for PLA. The nozzle size was chosen according to the specifications and performance capabilities of the 3D printer. Additionally, the infill density and printing orientation angle were selected based on literature recommendations and best practices for PLA composites to enhance the mechanical strength of the printed parts.

Table 15. List of materials used in the study

Material	Manufacturer/Supplier	Function
Toluene (AR, 99.9%)	Blulux Laboratories Pvt. Ltd., Faridabad, India	Used for extractives removal and dewaxing during cellulose extraction and composition analysis
Ethanol (LR, 97%)	Fine Chemical GTP PLC, Addis Ababa, Ethiopia	Used for dewaxing, washing, and purification steps to eliminate residual chemicals
Sodium Hydroxide (NaOH, LR, 98%)	Blulux Laboratories Pvt. Ltd., Faridabad, India	Used in alkali treatment to remove hemicellulose and impurities from fibers
Sulfuric Acid (H_2SO_4, AR, 98%)	Loba Chemie Pvt. Ltd., Mumbai, India	Used for hydrolysis treatment of MC to isolate CNC and quantify lignin in chemical analysis
Acetone (AR, 99.5%)	Alpha Chemika, Maharashtra, India	Used as a solvent for cleaning and intermediate drying steps of nanocellulose
Hydrogen Peroxide (H_2O_2, LR, 30%)	Fine Chemical GTP PLC, Addis Ababa, Ethiopia	Used as an oxidizing agent during the bleaching process to purify fibers
Deionized Water (LR, >50 MS)	Fine Chemical GTP PLC, Addis Ababa, Ethiopia	Used throughout chemical treatments for washing and dilution to prevent ionic contamination

Material	Manufacturer/Supplier	Function
Urea (AR, 99%)	GHTEC (JHD), Vietnam	Used with NaOH as a solvent during micro cellulose and CNC viscosity testing
Dichloromethane (DCM, AR/ACS, 99.5%)	Loba Chemie Pvt. Ltd., Mumbai, India	Used for polymer dissolution during Bio nanocomposite preparation
Ethylene Glycol (EG, 99%)	Alpha Chemika, Mumbai, India	Used as a plasticizer/solvent aid to enhance CNC dispersion in PLA matrix
Linseed stalks (length of 50–70 cm and 2–4 mm diameter)	Collected from Dima, Arsi, Eastern Oromia, Ethiopia	Used as raw material for fiber extraction, micro cellulose production, and CNC isolation
Poly (Lactic Acid) (PLA) pellets (Grade 2003D, Mw: 180,477 g/mol, ρ: 1.24 g/cm³)	Nature Works LLC, Minnetonka, Minnesota, USA; purchased via Natur Tec Pvt. Ltd., Chennai, India	Used as the biodegradable matrix material for bio ocomposite fabrication
PLA filament (1.75± 0.03mm diameter, 1.25 g/cm³ density)	FlashForge (Zhejiang Flashforge 3D Technology Co., Ltd., China)	used as a base substrate for coating with the PLA/CNC solution and as a control for comparison with the coated filament and 3D-printed samples.

Table 16. List equipment, instruments and machines used in the study

Instruments/Machines	Manufacturer/Supplier	Purpose
Soxhlet extraction apparatus (500 mL flask, Soxhlet tube, 300 mm condenser, cellulose thimbles, heating mantle, chiller)		The set up is used for removal of extractives from raw fiber in the dewaxing process
AD8000 pH Meter	Adwa Instruments, Szeged, Hungary	For pH measurement of solutions and solvents
JF-2004 Electronic Balance	Tsingtao Unicom-Optics Instruments Co., Ltd., Laixi, China	For precise weight measurements
NE9-56S Drying Oven	Nickel-Electro Ltd., Weston-Super-Mare, UK	For drying of samples
SX-2.5-12 Box-Type Resistance Furnace	Taisite Lab Science Inc., New York, NY, USA	For determination of ash content in chemical composition analysis
CeVI-558 Centrifuge machine	Avishkar International Pvt. Ltd., Mumbai, India	For the separation, purification, and washing of CNC from solution after acid hydrolysis
GFL 1083 Shaking Water Bath	GFL Water Baths, Hamburg, Germany	For hydrolyzing MC in controlled temperature with shaking to isolate nanocellulose
Ultrasonic bath Sonicator	Analab Scientific Instruments Pvt. Ltd, Gujarat, INDIA	Breaks up agglomerates and ensures uniform dispersion of CNC in water after isolation

Instruments/Machines	Manufacturer/Supplier	Purpose
IKA RH Basic Magnetic Stirrer	Labortechnik, Staufen, Germany	For nanocellulose dispersion in dissolved polymer matrix during composite fabrication
AVI-017B Vertical Autoclave	Avishkar International Pvt. Ltd., Mumbai, India	Hydrothermal treatment of acid hydrolyzed fiber for lignin extraction in chemical composition analysis
FT-IR-6600 Spectrometer	JASCO Inc., Easton, Maryland, USA	FT-IR analysis of functional groups of chemical treated fiber samples and composite samples
Spectrum 65 FT-IR Spectrometer	PerkinElmer, USA	FT-IR analysis of functional groups of RF, MC, and CNC samples during CNC isolation
HRM–300 Optical Microscope	Huvitz Co., Ltd., Anyang-si, South Korea	Observation and diameter measurement of extracted fibers from different retting time
Gemini SUPRA 35VP FEG-SEM	Carl Zeiss, Jena, Germany	Imaging of surface morphology and size of MC
JCM–6000 Plus SEM	JEOL Ltd., Tokyo, Japan	Surface and morphological analysis of composites, filaments, and 3D printed samples
JEM–F200 FE-TEM	JEOL Ltd., Tokyo, Japan	Nanoscale imaging of CNC for size, shape and structural analysis

Instruments/Machines	Manufacturer/Supplier	Purpose
XRD 7000S X-ray Diffractometer	Shimadzu Corporation, Kyoto, Japan	To determine crystalline structure parameters of RF, MC, CNC and composites samples
HCT–3 TGA-DTA/DSC Instrument	Beijing Henven Instruments, Beijing, China	Thermal analysis (TGA, DTA, DSC) of treated fiber samples and CNC-based composite samples
DTG–60H TGA/DTG Instrument	Shimadzu Corporation, Kyoto, Japan	Thermal property analysis of RF, MC, and CNC samples during CNC isolation.
Ubbelohde Viscometer 50101 (Cap.–no.0a)	Schott Instruments, Mainz, Germany	Intrinsic viscosity measurement of MC and CNC samples
Fiber Tenso-Lab-331A Strength Tester	Mesdan-Lab, Raffa, Italy	Single-fiber tensile testing of fibers from different degree of retting
Universal Tensile Testing Machine (DSCK)		Tensile testing of filaments and 3D printed of PLA and PLA/CNC composite specimens
Ender–3 Pro 3D Printer (220×220×250 mm)	Creality 3D Technology Co., Ltd., Shenzhen, China	For 3D printing of PLA and PLA/CNC composite specimens

Table 17. List of software tools used in the study

Software	Developer	Purpose
OriginPro (V9.5.0)	Origin Lab Corporation	Statistical analysis, data processing, and graphical representation of experimental results
Minitab (V17)	Minitab LLC	Design of Experiments (DoE) and statistical calculations and results
Diagrams.net (Web app)	JGraph Ltd.	Creation of schematic diagrams and flowcharts
Tinker cad (Web app)	Autodesk, Inc.	Designing 3D models of specimens for 3D printing
Ulti Maker Cura (V5.9.0)	Ulti Maker B.V.	3D model slicing, print parameter setting, and print simulation visualization
ImageJ (V1.8.0)	National Institutes of Health (NIH), USA	Image processing, particle size measurement and analysis from microscopy images

3.4. Equipment, Instruments and Machines

This section presents a comprehensive list of the equipment, instruments, and machines utilized throughout the experimental work in this study. It encompasses a wide range of tools, from basic laboratory apparatus to advanced analytical and characterization instruments and machines. Each item is described along with its key specifications and the specific role it played in the experimental procedures as shown in **Table 16**.

3.5. Software Tools

A range of software tools was employed throughout this study to support data analysis, modeling, visualization, and documentation. The selected software packages were chosen based on their suitability for statistical analysis, process modeling, image analysis, and technical diagramming. **Table 17** provides a list of the software tools utilized in this study.

3.6. Experimental Design and Procedures

The experimental procedure outlines how the experiment was conducted, detailing the design of experiments, procedures and methods used for each step of the process as shown in **Figure 25.**

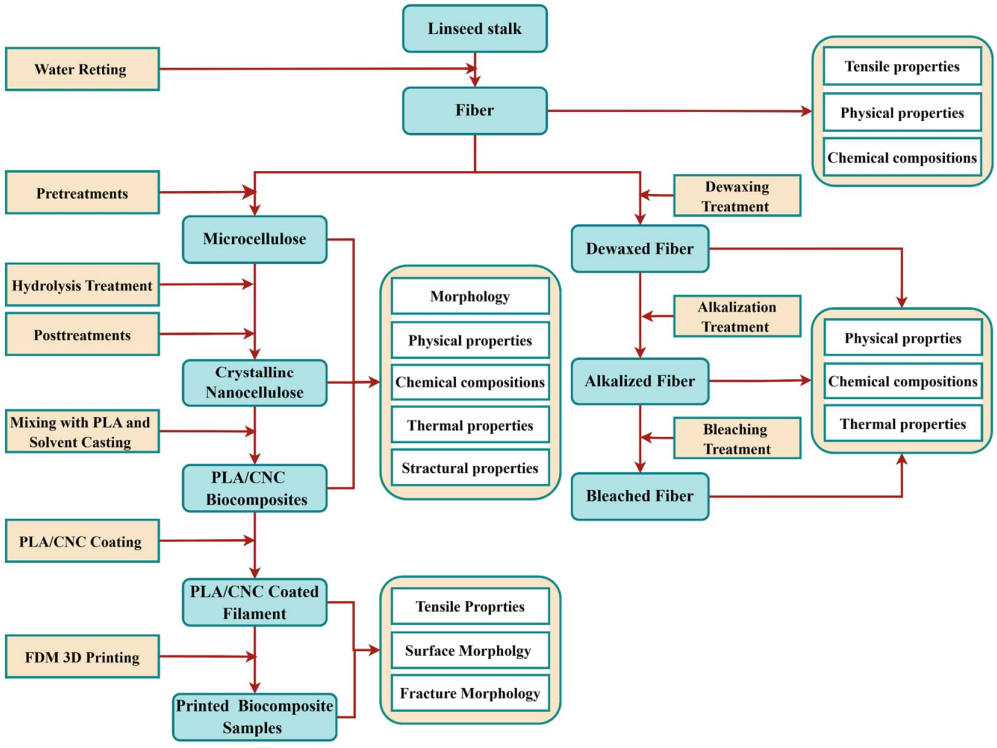

Figure 25. Flow diagram of experimental procedures, samples and data collection methods

3.6.1. Fiber extraction

The linseed stalks were first washed, and the middle portions were trimmed into uniform lengths of 20 cm in preparation for the water retting process (H. Yu et al., 2010; Ruan et al., 2015). Transparent plastic water bottles were used as containers for the retting treatment. Each bottle was filled with a consistent volume of 1650 mL of water. Then, 50 grams of linseed stems, measuring 20 cm in length and 2 to 4 mm in diameter, were placed into the bottles without caps and left at room temperature (Ruan et al., 2015) maintaining a solid-to-liquid ratio of 1:33 to ensure effective stalk water absorption (Pandey, 2016).

Table 18. Sample names and their retting durations used for retting extraction

Sample	**RT_0**	**RT_1**	**RT_2**	**RT_3**	**RT_4**	**RT_5**	**RT_6**	**RT_7**	**RT_8**
Retting Time (h)	0	48	96	144	168	192	216	240	264
Retting Duration (days)	0	2	4	6	7	8	9	10	11

The retting process was carried out over a total duration of 264 hours (11 days), in alignment with existing studies that suggest a typical retting period ranges between 7 and 14 days (C. H. Lee et al., 2020). To assess the influence of retting time, individual samples were prepared and labeled RT_1 through RT_8, representing retting durations of 48, 96, 144, 168, 192, 216, 240, and 264 hours, as summarized in **Table 18**. At the end of each specified duration, the linseed stalks were removed from the bottles, rinsed with clean water, and the wet stalks were weighed. They were then left to air-dry at room temperature for 4 hours. Following this, the fibers were manually separated from the stalks, dried, weighed again, and stored in zip-lock plastic bags for subsequent analysis.

3.6.2. Chemical composition determination

The experimental procedures for determination of chemical compositions are aimed to quantify the percentage amount of cellulose, hemicelluloses, lignin and extractives of the linseed fiber by isolating them using different solvents, following TAPPI standards and related literatures as shown in **Figure 26**.

3.6.2.1. Extractives Content

3.6.2.2. The fibers were first oven-dried at 105 °C to facilitate grinding. They were then cut into smaller pieces using scissors and further milled in a laboratory grinder until they could pass through a 5 mm mesh screen (Morán et al., 2008). The ground fibers were subsequently

dried again at 105 °C until a constant weight was achieved prior to extraction. For the extraction process, three grams of the dried fiber were placed into a pre-dried extraction thimble, and the combined weight of the fiber and thimble was recorded. An extraction solvent composed of ethanol (96%) and toluene (99%) mixed in a 1:2 ratio was prepared for use (Borchani et al., 2015; Teli et al., 2017; D'Auria et al., 2021). A volume of 250 mL of this solvent mixture was added to a 500 mL round-bottom flask, and Soxhlet extraction was carried out for 6 hours at 98 °C, allowing for approximately 18 to 24 solvent cycles (Morán et al., 2008; H. Chen et al., 2016). Following extraction, any excess solvent was removed via suction, and the samples were thoroughly rinsed with ethanol and distilled water to eliminate residual solvents. Finally, the fibers were dried at 105 °C to a constant weight, and the extractive-free fiber mass was recorded for determining the extractives content (D'Auria et al., 2021).

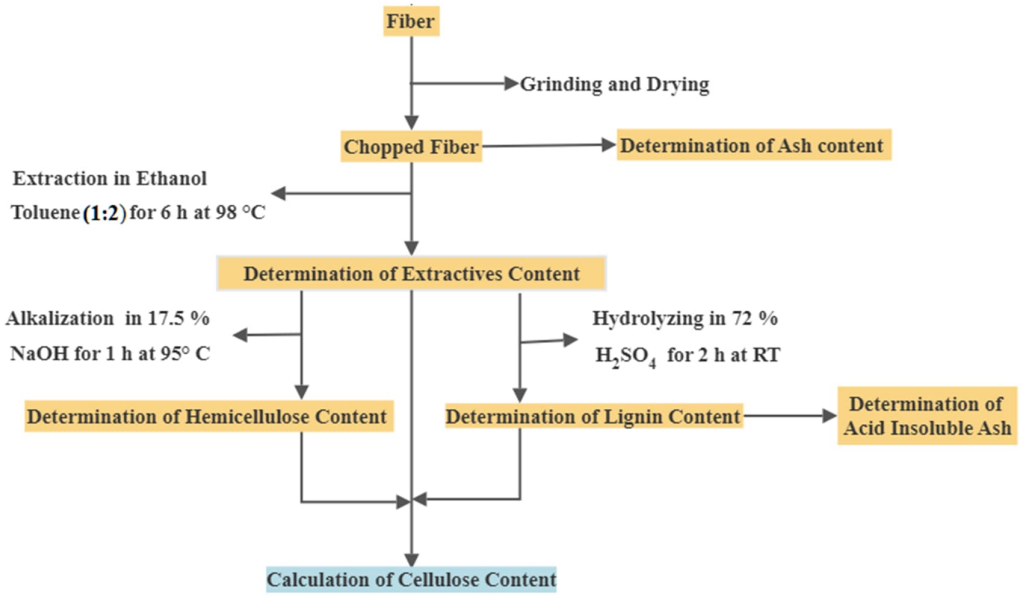

Figure 26. Flow chart of chemical compositions determination

3.6.2.3. Hemicellulose Content

One gram of extractive-free, oven-dried sample was accurately weighed and mixed with 10 mL per gram of a 17.5% sodium hydroxide (NaOH) solution (w/v) in a 50 mL glass tube, following the procedures described by (Zhihua Zhu et al., 2018; Kang et al., 2019). The mixture was thoroughly agitated for 10 minutes and then subjected to boiling at 95 °C for 60 minutes in a reciprocating water bath (Mahjoub et al., 2014; Teli et al., 2017). After heating, the mixture was allowed to cool to room temperature before undergoing filtration. The resulting alkalized residue was repeatedly washed and centrifuged at 5,000 rpm for 15

minutes using distilled water and ethanol to ensure complete neutralization (Azanaw et al., 2019; Banerjee et al., 2019). Finally, the samples were dried in an oven at 105 °C until a constant weight was achieved and then weighed to determine the hemicellulose content (Azanaw et al., 2019).

3.6.2.4. Lignin Content

The extractive-free fibers were first dried in an oven at 105 °C until a constant weight was achieved, then allowed to cool in a desiccator. From these, 0.5 g of sample was accurately weighed and transferred into a 50 mL glass test tube. To each tube, 15 mL of 72% sulfuric acid (H_2SO_4) was added to ensure complete wetting of the fiber, and the mixture was manually stirred with a glass rod every 15 minutes over a 2-hour period at room temperature to promote uniform hydrolysis (Kale et al., 2019). Following this, the hydrolyzed samples were transferred into a 1000 mL Erlenmeyer flask and diluted with 560 mL of distilled water to reduce the acid concentration to approximately 3%, (adapted from TAPPI T–222 om–02) (Kale et al., 2019). The diluted solution was autoclaved for 1 hour at 121 °C, then cooled to room temperature for about 20 minutes. The suspension was centrifuged at 5000 rpm for 15 minutes and subsequently vacuum filtered. The solid residues were collected in pre-dried and pre-weighed crucibles (adapted from TAPPI T–211).

The crucibles containing the residues were oven-dried at 105 °C until a constant weight was reached, and the mass was recorded. The total mass of residue, which includes acid-insoluble lignin and ash, was determined by subtracting the weight of the empty crucible from the total. To quantify the ash content, the crucibles were placed in a muffle furnace at 550 °C for 3 hours (adapted from TAPPI T–211). After cooling in a desiccator, the crucibles were reweighed. The ash content was calculated by subtracting the crucible weight from the total weight. Finally, the Klason lignin content (acid-insoluble lignin) was determined by subtracting the ash content from the weight of the original acid-insoluble residue (Ranganagowda et al., 2019).

3.6.2.5. Ash content

3.6.2.6. A 3-gram sample of chopped fiber was first dried in an oven at 105 °C until a constant weight was achieved. Prior to use, crucibles with lids were thoroughly cleaned and preheated in a furnace at 525 °C for 30 to 60 minutes to ensure a stable baseline weight. After ignition, the crucibles were cooled to room temperature in a desiccator and then weighed. The dried fiber samples were placed into the crucibles and ashed in a muffle

furnace at 550 °C for 4 hours, following the procedure described by (Kale et al., 2019). Once the heating was complete, the crucibles were removed, cooled in a desiccator, and weighed again. The ash content was calculated based on the weight difference, in accordance with TAPPI standard T 211 om–02.

3.6.3. Design of experiment for extraction process optimization

The removal of non-cellulosic constituents namely extractives, hemicellulose and lignin from the fiber was conducted through optimization of sequential chemical treatments as shown in **Figure 27**.

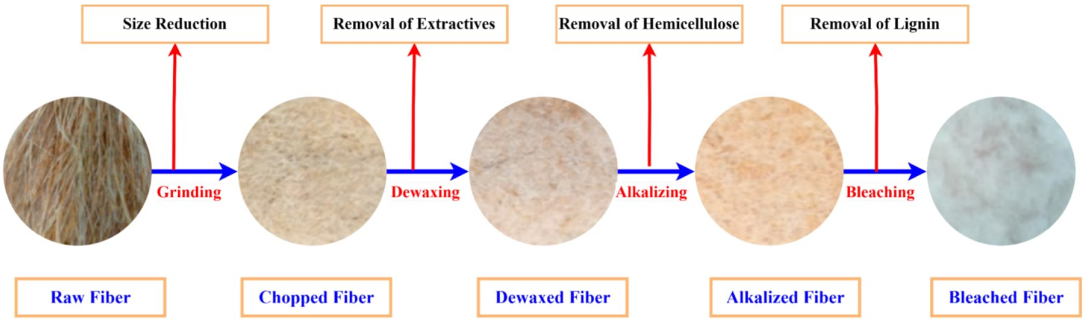

Figure 27. Flow chart of extraction process for non-cellulosic components removal

A Taguchi L_9 Orthogonal Array (OA) design of experiments (DoE) was employed to investigate the contribution of selected extraction conditions (independent variables) namely concentration of solvents, reaction temperature and reaction time on the yield removal of dependent variables (responses) namely extractives, hemicellulose and lignin as shown as shown in **Table 19**.

Table 19. Taguchi L9 orthogonal array for design of experiments

Experimental Run	Concentration (%)	Temperature (°C)	Time (min)
1	-1	-1	-1
2	-1	0	0
3	-1	+1	+1
4	0	-1	0
5	0	0	+1
6	0	+1	-1
7	+1	-1	+1
8	+1	0	-1
9	+1	+1	0

3.6.3.1. Dewaxing process

To facilitate grinding, linseed fibers were first oven-dried at 105 °C. The dried fibers were then cut into small pieces using scissors and further ground with a laboratory mill until they could pass through a 5 mm mesh screen. The resulting ground fiber was again dried at 105 °C

until a constant weight was reached prior to extraction. A 3-gram portion of the dry fiber was placed in a clean, dry extraction thimble, and the combined weight of the fiber and thimble was recorded. Three types of extraction solvents were prepared: a pure ethanol (96%) and toluene (99%) mixture in a 1:2 ratio, and two diluted versions of this mixture at 75% and 50% ethanol-to-toluene concentration using water as the diluent (Borchani et al., 2015; Teli et al., 2017; D'Auria et al., 2021).

A volume of 250 mL of the selected solvent was added to a 500 mL round-bottom flask (H. Chen et al., 2016), and Soxhlet extraction was performed for durations of 4, 6, and 8 hours at temperatures of 78 °C, 88 °C, and 98 °C, respectively. This process allowed for approximately 16 to 32 cycles of solvent exchange. After extraction, any remaining solvent was removed using suction. The fiber samples were then rinsed with ethanol to eliminate residual toluene, followed by washing with distilled water to remove ethanol. Finally, the fibers were dried at 105 °C until a constant weight was achieved. The weight of the extractive-free fiber was determined by subtracting the weight of the empty thimble, allowing for the calculation of extractives removed during the dewaxing process (H. Chen et al., 2016).

3.6.3.2. Alkalization process

For the alkalization process, one gram of extractive-free, oven-dried fiber was accurately weighed and mixed with 10 mL per gram of sodium hydroxide (NaOH) solutions at concentrations of 2%, 6%, and 10% (w/v), as described by (Zhihua Zhu et al., 2018; Kang et al., 2019). The mixture was placed in 50 mL glass tubes and vigorously shaken for 10 minutes. Subsequently, the samples were subjected to heating in a reciprocating water bath at temperatures of 50 °C, 62.5 °C, and 75 °C for durations of 30, 60, and 90 minutes, respectively (Mahjoub et al., 2014; Teli et al., 2017). After treatment, the samples were cooled to room temperature and then filtered. To neutralize the alkalized fibers, the residues were repeatedly washed with distilled water and ethanol, followed by centrifugation at 5,000 rpm for 15 minutes (Azanaw et al., 2019; Banerjee et al., 2019). The treated fibers were finally dried in an oven at 105 °C until a constant weight was achieved, and then weighed to determine the extent of hemicellulose removal (Azanaw et al., 2019).

3.6.3.3. Bleaching process

3.6.3.4. For the bleaching process, 0.5 g of fiber sample was placed into 50 mL of hydrogen peroxide (H_2O_2) solution at concentrations of 2%, 6%, and 10%, and mixed manually to

ensure uniform wetting. The treated samples were then placed in a reciprocating water bath shaker and maintained at controlled temperatures of 80 °C, 90 °C, and 100 °C for durations of 60, 90, and 120 minutes, respectively, as described (Kamali Moghaddam et al., 2020; Mamaye et al., 2020). Following the treatment, the fiber suspensions were transferred to petri dishes and thoroughly rinsed with distilled water until a neutral pH was achieved. The cleaned fibers were subsequently oven-dried at 105 °C until they reached a constant weight. The final dried weight was recorded to calculate the extent of lignin removal (Mamaye et al., 2020). The factors and levels of solvents utilized for the extraction processes are shown in **Table 20**.

Table 20. Factors and levels of solvents for the extraction processes

Solvents	Factors								
	Concentration (%)			Temperature (℃)			Time (min)		
	Levels			Levels			Levels		
	–1	0	+1	–1	0	+1	–1	0	+1
Ethanol: Toluene	50	75	100	78	88	98	240	360	480
Sodium Hydroxide	2	6	10	50	62.5	75	30	60	90
Hydrogen Peroxide	2	6	10	80	90	100	60	90	120

$^{-1}$ Low, ^{0} Medium and $^{+1}$ High levels of the factors

3.6.4. Extraction of crystalline nanocellulose (CNC)

The procedures used for CNC isolation were pre–treatment, acid hydrolysis treatment and post–treatments (Kargarzadeh, Ioelovich, et al., 2017b) as shown in **Figure 28**. The extraction of crystalline nanocellulose (CNC) from linseed stalk fibers began with a pre-treatment phase designed to purify the raw material. Initially, the chopped raw fibers were thoroughly washed and boiled in hot distilled water for one hour to remove dust and water-soluble impurities. After drying, the fibers underwent a dewaxing step using Soxhlet extraction with a toluene: ethanol mixture (2:1) at 98 °C for four hours to eliminate waxes, fats, and resins (Gapsari et al., 2022).

The dewaxed fibers were then delignified by treating them with an alkaline hydrogen peroxide (AHP) solution composed of 5% NaOH and 10% H_2O_2, adjusted to pH 11. This mixture was stirred at 90 °C for two hours to break down and remove lignin (Qu et al., 2005). Under alkaline conditions, hydrogen peroxide generates hydroperoxide anions (HOO^-) that attack phenolic and non-phenolic lignin structures through nucleophilic mechanisms,

effectively degrading the lignin matrix (De Morais Teixeira et al., 2011; Ovalle-Serrano et al., 2018).

To further purify the cellulose, the delignified material was treated with 17.5% NaOH at 80 °C for three hours under constant stirring to remove hemicellulose and any remaining lignin. This alkalization caused fiber swelling and hydrolyzed the ester linkages binding hemicellulose (mainly xylan) to lignin (Owonubi et al., 2021). During the alkalization mechanism, NaOH reacts with the ester linkages in hemicellulose, where the hydroxide ions (OH^-) from NaOH act as nucleophiles. These ions attack the intermolecular ester bond, which crosslinks Xylan (hemicellulose) and lignin, breaking them down. This process leads to the solubilization and removal of hemicellulose and residual lignin from the fiber matrix (H. V. Lee et al., 2014). The final pre-treatment step involved bleaching the fibers in a 3% H_2O_2 solution at pH 11 for two hours at 90 °C in a water bath (Y. Wu et al., 2019). This oxidative bleaching removed color-inducing compounds and residual lignin, resulting in purified micro cellulose, which was then oven-dried at 60 °C (Sarno, 2020).

The main treatment phase, acid hydrolysis, was performed to convert the purified cellulose into CNC. In this process, the dried micro cellulose was mixed with 64% sulfuric acid at a ratio of 1 gram of cellulose to 15 milliliters of acid(L. Chen et al., 2015; Vanderfleet et al., 2021). The mixture was stirred continuously in a water bath at 45 °C for 60 minutes. This step selectively degraded the amorphous regions of the cellulose, reducing the fiber to nanoscale dimensions and increasing its crystalline content (Michael Ioelovich, 2012; Naduparambath et al., 2018).

After hydrolysis, the post-treatment phase was conducted to recover and purify the CNC. The acidic suspension was diluted tenfold with distilled water to reduce the acid concentration to 4%, then centrifuged at 10,000 rpm for 15 minutes to remove excess acid (Zirui Zhu et al., 2021). The resulting CNC suspension was sonicated in an ice bath for 10 minutes to prevent agglomeration and ensure uniform dispersion of the nanocrystals (A. Kumar et al., 2014a). To facilitate drying and further reduce particle aggregation, a solvent exchange method was applied. The CNC gel was first dispersed in acetone, centrifuged, then re-dispersed in toluene and centrifuged again. Finally, the CNC–toluene mixture was dried in an oven at 60 °C to yield CNC in fine powder form (Araki et al., 2017; Zirui Zhu et al., 2021).

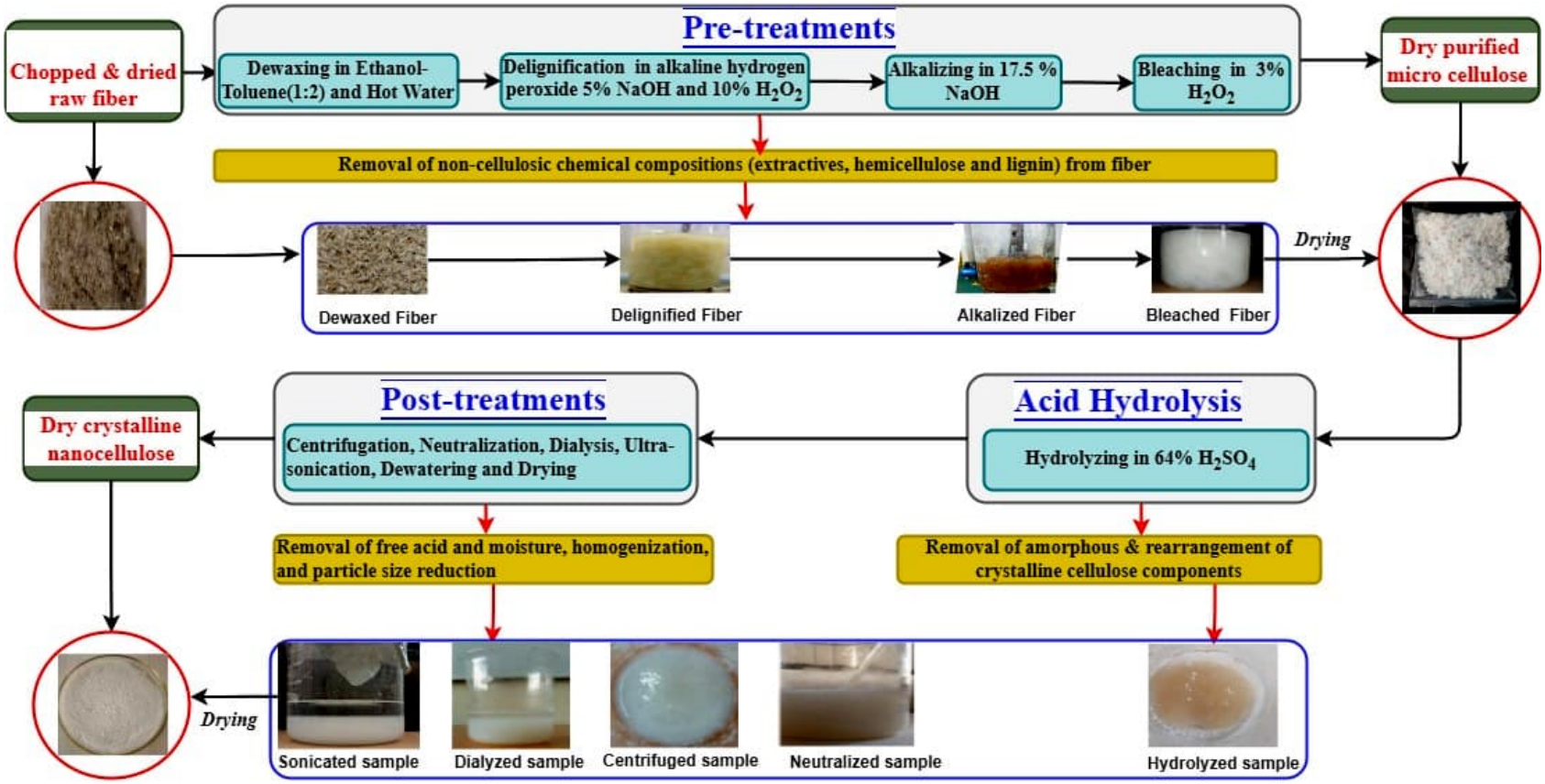

Figure 28. Crystalline nanocellulose isolation methods and procedure

3.6.5. Bio nanocomposite manufacturing

The composite fabrication process began by drying PLA pellets and CNC powder at 60°C for 4 hours to remove residual moisture (Zirui Zhu et al., 2021). Following the formulations outlined in **Table 21**, pre-weighed PLA pellets were dissolved in dichloromethane (DCM) at a concentration of 5% (w/v) for 24 h at room temperature (H. Li et al., 2018). Similarly, a pre weighed CNC powders based on the formulation were dispersed in DCM (5% w/v) using a magnetic stirrer for 15 minutes at room temperature to ensure uniform suspension. Then, the PLA/DCM solutions and CNC/DCM suspensions were mixed and stirred continuously for 2 hours at room temperature (Duygulu et al., 2020). During blending, 10 wt.% ethylene glycol (EG) was gradually incorporated into the mixture as a plasticizer (Zuo et al., 2015; Ibrahim et al., 2019; Fernández-Santos et al., 2021). The resulting composite solutions were cast onto a glass Petri dish and air-dried at room temperature for 24 h to produce films and labeled as PLA/CNC1%, PLA/CNC3%, and PLA/CNC5%. Finally, the composite films were ground for further characterization and experiments. The basic procedures for preparation of the PLA/CNC bio–nanocomposite is shown in **Figure 29.**

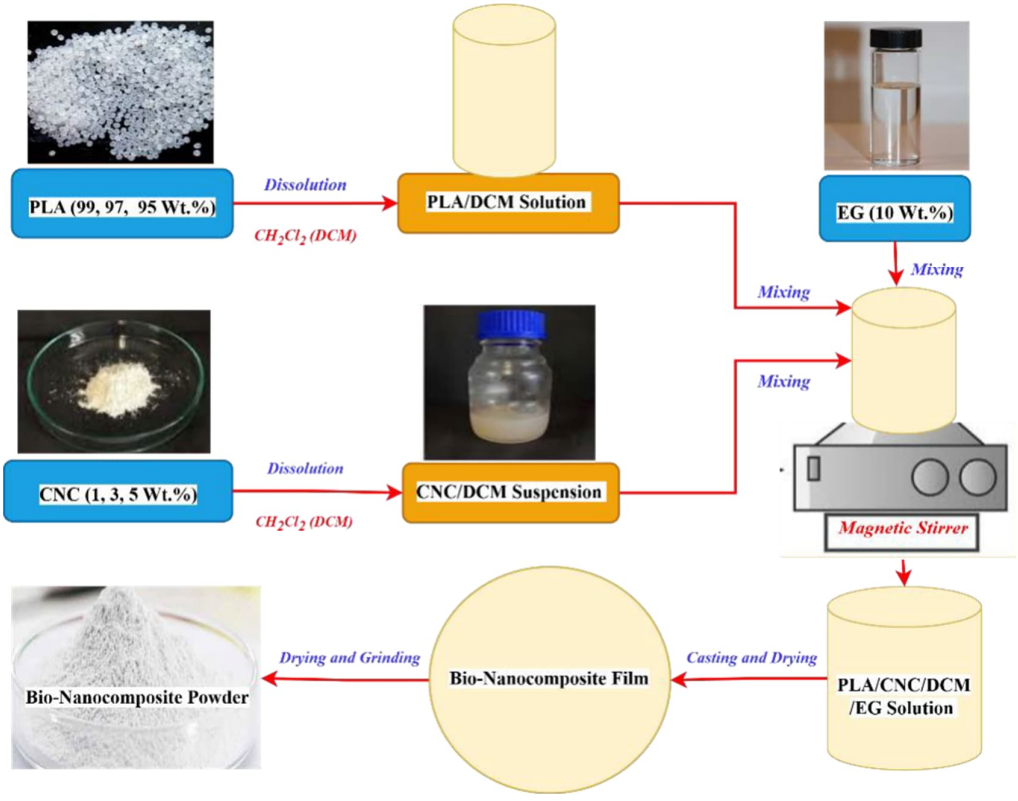

Figure 29. The scheme for preparation of the PLA/CNC bio–nanocomposite

Table 21. PLA/CNC bio–nanocomposite formulation

Samples	Weight (%)		Weight (g)	
	PLA	CNC	PLA	CNC
Neat PLA	100	0	15	0
PLA/CNC1%	99	1	14.85	0.15
PLA/CNC3%	97	3	14.55	0.45
PLA/CNC5%	95	5	14.25	0.75

3.6.6. Polylactic-acid (PLA) filament preparation

The optimized PLA/CNC3 % Bio nanocomposite powder was dissolved in dichloromethane (DCM) at a concentration of 5% (w/v) for 24 h at room temperature (H. Li et al., 2018). Commercial PLA filament was slightly socked in a DCM solvent at room temperature and dried at room temperature for 24 h to create some micro porous surface on the filament due to evaporation of the solvent (Phaechamud et al., 2016). Then, dry filament was deep coated in to the prepared solution of PLA/CNC3%/DCM at room temperature. Finaly, the coated filament was allowed to dry at room temperature for 24 h and polishing with a DCM for diameter consistency and smoothing purpose. This step was repeated three times followed by drying of the coated filament at room temperature for 24 h to ensure the uniform coating on the surface of the filament (K. M. Z. Hossain et al., 2014).

3.6.7. Fused deposition modeling (FDM) 3D printing

Tensile specimens were designed according to ASTM 3039/3039M with a length of 165 mm, width of 20 mm and thickness of 3 mm (Faidallah et al., 2023) by Autodesk Tinker cad web app. The 3D model was exported as .STL file to Ulti maker Cura 5.9.0 slicing software to generate the G–codes. The basic steps and procedures of FDM 3D printing process are shown in **Figure 30**. The specimens were printed using a commercial 3D printer (Ender–3 Pro, 220×220×250 mm) from CREALITY. The parameters used for printing the specimens are described in **Table 22**.

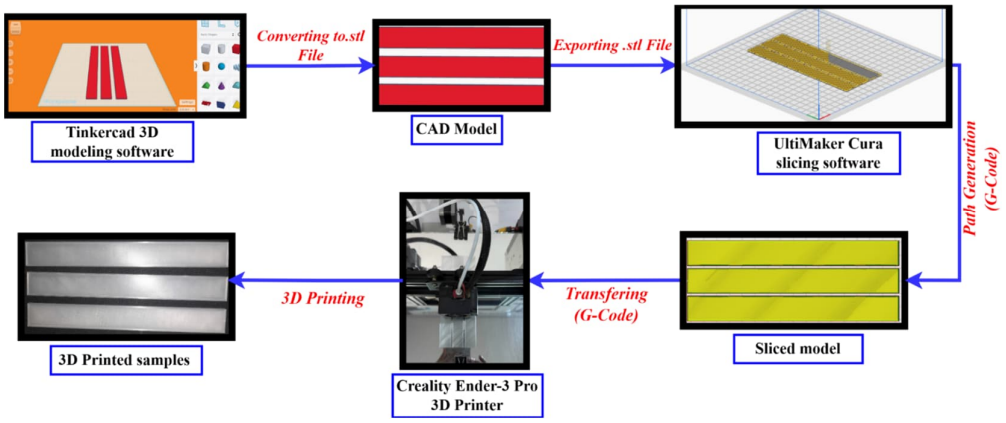

Figure 30. Basic steps of the FDM 3D printing process

Table 22. The fixed 3D printing process parameters used for manufacturing the specimens

Parameters	Values
Initial layer thickness	0.3 mm
Layer thickness	0.2 mm
Printing temperature	200 ℃
Build plate temperature	60 ℃
Infill density	100 %
Print speed	45 mm/s
Nozzle size	0.4 mm
Orientation angle	Crossed ±45°

3.7. Data Collection and Analysis Methods

Data were collected and analyzed at multiple stages throughout the experimental workflow to comprehensively evaluate the effects of each processing step on properties of the samples using different characterization, testing, statistical and numerical analyses methods as generally shown in **Figure 25**.

3.7.1. Physical properties

The density of the samples was measured with distilled water using the liquid pycnometer technique. Two grams of non–retted, under–retted, optimum, and over–retted linseed fiber bundle samples were oven dried at 105°C for 24 h to a constant weight (Rude et al., 2000; Baley et al., 2005; Truong et al., 2009). The mass of the empty pycnometer (m_1), pycnometer filled with chopped fibers (m_2), pycnometer filled with water (m_3), pycnometer filled with water and chopped fibers (m_4) were measured and calculated. The density of fibers (ρ_f) was estimated based on **Eq.(1)** (Truong et al., 2009; Manimaran et al., 2018).

$$\rho_f = \left(\frac{m_2 - m_1}{(m_3 - m_1) - (m_4 - m_2)} \right) \rho_w \quad \text{Eq. (1)}$$

The obtained output mass (m_o) of the fiber, MC and CNC was measured and the percentage yield (Y%) of the extracted fibers obtained by varied retting time durations, micro–cellulose (MC) and crystalline nanocellulose (CNC) from the weighed initial mass (m_i) of linseed stalk, fiber and MC, respectively, was determined using **Eq. (2)** (Pandey, 2016; Dhanani et al., 2017) (Gabriel, Belete, et al., 2021b).

$$Y\,(\%) = \frac{m_o}{m_i} \times 100 \quad \text{Eq. (2)}$$

Huvitz HRM–300 series optical microscope (Huvitz Co., Ltd, Anyang–si, South Korea) was used to measure the diameter of the extracted fibers. Three equidistant points were marked on a single fiber and the diameters of these points were measured with four replications. The average diameter was then calculated, which could be considered as the mean diameter (Widnyana et al., 2020).

The water absorption test of the extracted fibers (non–retted, under, optimum and over–retted), micro–cellulose, neat PLA, nanocomposite samples prepared with different CNC loadings (PLA/CNC1%, PLA/CNC3%, and PLA/CNC5%) was conducted. An oven dried at 105 °C to a constant weight of the fiber and the MC with a dry weight (m_d) was taken from each sample. Then, the dried samples were soaked in 1 L of distilled water at room temperature. The weight of the wet fiber and MC (m_w) samples was measured every 24 h till the saturation point.

Similarly, the water absorption behavior of the neat PLA and the composite samples was measured according to the ASTM D570–03 standard at room temperature. Before the water absorption test, the PLA and composite films with dimensions of 10 mm × 10 mm × 2 mm were dried in an oven at 60 °C overnight and then weighed. Three samples were immersed in distilled water, removed every 12 h, wiped with a soft cotton cloth, and weighed at ambient temperature and repeating this step till the saturation point. Finally, The water absorption percentage (W_a%) of the samples was estimated based on **Eq.(3)** (Baley et al., 2005; Mittal et al., 2018).

$$W_a\,(\%) = \frac{m_w - m_d}{m_d} \times 100 \quad \text{Eq. (3)}$$

3.7.2. Numerical and statistical analysis of extraction process

The removal percentages of extractives, hemicellulose, and lignin from linseed fibers were quantified using dry-based gravimetric analysis, which involves measuring the dry weight of the samples before (W_1) and after (W_2) each treatment steps. All measurements were performed in triplicate to ensure accuracy and reproducibility. The percentage removals of non-cellulosic constituents were determined using **Eq. (4)** (S. Li et al., 2004).

$$\mathrm{R}\,(\%) = \frac{W_1 - W_2}{W_1} \times 100 \qquad \text{Eq. (4)}$$

where, R is the removal percentage the non-cellulosic constituents,

- W_1 is the weight of raw fiber and W_2 is the weight of dewaxed fiber for extractives removal,
- W_1 is the weight of dewaxed fiber and W_2 is the weight of alkalized fiber for hemicellulose removal, and
- W_1 is the weight of alkalized fiber and W_2 is the weight of bleached fiber for lignin removal.

The type signal–to–noise ratio (S/N) analysis using Taguchi method for optimization was selected based on the requirements of response (non-cellulosic constituents removal). Therefore, the larger–the–better signal–to–noise ratio (S/N) was used and computed using **Eq. (5)** (Sivaiah et al., 2019; Qazi et al., 2020).

$$S/N \text{ ratio} = (-10) \times \log_{10}\left(\frac{1}{n}\right)\sum_{i=1}^{n}\frac{1}{R_{ij}^2} \qquad \text{Eq. (5)}$$

where, S/N is signal to noise ratio, n is number of observations and R_i is response values each response

3.7.3. Chemical composition analysis

The chemical composition of the natural fiber was quantified using gravimetric methods on a dry weight basis. This analytical approach enabled the determination of key components, namely extractives, hemicellulose, lignin, and ash based on mass differences before and after sequential chemical treatments. Extractives and hemicellulose contents were calculated from the weight loss between the initial and final mass, with the hemicellulose calculation using extractive-free samples as a baseline using **Eq. (6)** and **(7)**.

$$\text{Extractives}\,(\%) = \frac{W_1 - W_2}{W_1} \times 100 \qquad \text{Eq. (6)}$$

where, W_1 is the weight of raw fiber and W_2 is the weight of dewaxed fiber

$$\text{Hemicellulose}\,(\%) = \frac{W_1 - W_2}{W_1} \times 100 \qquad \text{Eq. (7)}$$

where, W_1 is the weight of dewaxed fiber and W_2 is the weight of alkalized fiber

The acid insoluble lignin (Kalson) and ash contents were assessed from the mass of the residual solids remaining after specific treatments. The percentage content of each component was determined using **Eq. (8)** and **(9)**.

$$\text{Lignin}\,(\%) = \frac{W_2}{W_1} \times 100 \qquad \text{Eq. (8)}$$

where, W_1 is the weight of raw fiber and W_2 is the weight of lignin

$$\text{Ash}\,(\%) = \frac{W_2}{W_1} \times 100 \qquad \text{Eq. (9)}$$

where, W_1 is the weight of raw fiber and W_2 is the weight of ash

Finally, to calculate the cellulose content by assuming that extractives, hemicellulose, lignin, ash, and cellulose were the main components (S. Li et al., 2004; L. Lin et al., 2010; Adeeyo et al., 2015). The cellulose content in percent was calculated using **Eq. (10)**.

$$\text{Cellulose}\,(\%) = 100\,\% - \text{Non-cellulosic constituents}\,(\%) \qquad \text{Eq. (10)}$$

3.7.4. Morphology analysis

A field emission gun scanning electron microscope (FEG–SEM, Gemini SUPRA 35VP (ZEISS) (Carl Zeiss, Jena, Germany)) was utilized to investigate the morphology and size of the MC sample obtained from the SEM images. Measurements of the MC sizes and distribution were performed using ImageJ (*V*1.8.0) and Origin (*V*9.95) software, respectively. The surface morphology of the composite films (PLA/CNC1%, PLA/CNC3%, and PLA/CNC5%) and the surface and fracture morphology of the coated, neat PLA filaments and 3D printed samples was studied using scanning electron microscopy (SEM) (JOEL, JCM–6000 plus (JOEL Ltd., Tokyo, Japan)). A field emission transmission electron microscope (FE–TEM, JEOL JEM–F200, Tokyo, Japan) was used to examine the length, diameter, aspect ratio and size and distribution of the CNCs, which were measured using ImageJ (*V*1.8.0) and Origin (*V*9.95) software, respectively.

3.7.5. Fourier transform infrared spectroscopy (FT–IR) analysis

FT–IR spectra of the fibers (non–retted, retted, extracted, alkalized and bleached), the composite samples (PLA/CNC1%, PLA/CNC3%, and PLA/CNC5%) and neat PLA and were recorded using FT/IR–6600 spectrometer with a 2 mm/sec scanning speed and 4 cm^{-1} resolution in a range of 400–4000 cm^{-1} wavenumbers (S. Alix et al., 2009; Kale et al., 2019; Suaniti et al., 2019; Prabhu et al., 2021). Additionally, Fourier transform infrared (FT–IR) spectroscopy was performed using a PerkinElmer Spectrum 65 FT–IR spectrometer (USA) to analyze the RF, MC and CNC samples. Prior to this analysis, all the samples were ground and subsequently mixed with KBr to prepare homogeneous suspensions, pressed into transparent pellets and analyzed in transmittance mode within the range of 4000–400 cm^{-1} at room temperature.

3.7.6. X–ray diffraction (XRD) analysis

Structural and phase analyses of the samples (RF, MC, CNC, neat PLA, PLA/CNC1%, PLA/CNC3%, and PLA/CNC5%) were implemented using an X–ray diffractometer (XRD 7000S, Shimadzu, Japan) with Cu–Kα radiation (wavelength of 1.5405 Å) and step–scan mode (2θ range: 5°– 80°, at a scan speed of 3°/min). The crystallinity index (C_rI) of the RF, MC and CNC samples was calculated according to the Segal method and for the neat PLA, PLA/CNC1%, PLA/CNC3%, and PLA/CNC5% samples peak deconvolution method was used, as shown in **Eq. (11 & 12)**, respectively (Segal et al., 1959; Elazzouzi-Hafraoui et al., 2008).

$$C_rI(\%) = \frac{(I_{200} - I_{Am})}{I_{200}} \times 100 \qquad \text{Eq. (11)}$$

where, C_rI is the crystallinity index, I_{200} is the maximum peak intensity corresponding to the crystalline region at the (200) lattice plane around 2θ = 22° and I_{Am} is the peak intensity of the amorphous region at approximately 2θ = 18° between planar reflections (110) and (200).

$$C_rI(\%) = \left(\frac{A_{cry}}{A_{total}}\right) \times 100 \qquad \text{Eq. (12)}$$

where C_rI is the crystallinity index, A_{cry} is the crystalline peak area, and A_{total} is the total area (crystalline and amorphous).

The mean crystalline size of all the samples was estimated using the Debye–Scherer equation, as shown in **Eq. (13)**.

$$D = \frac{k\lambda}{\beta\cos\theta} \quad \text{Eq. (13)}$$

where D is the average crystallite size, β is the line broadening in radians, θ is the Bragg angle, λ is the X–ray wavelength and k is the Scherrer constant.

The Z–discriminant function(Z) developed by Wada and Okano for the determination of the cellulose crystalline structure (monoclinic and triclinic) in natural fibers was used. By employing discriminant analysis, it is possible to categorize cellulose as type I_α or I_β. The Z value indicates whether cellulose is dominant in the I_α or I_β type. When Z>0 that indicates I_α–rich, while Z<0 indicates I_β–dominant. The function that discriminates between I_α or I_β is given by **Eq. (14)** (Wada et al., 2001).

$$Z = 1693d_1 - 902d_2 - 549 \quad \text{Eq. (14)}$$

where d_1 and d_2 are the d–spacings of the peaks at the (1–10) and (110) lattice planes, respectively.

The contents of C_{I} and C_{II} were calculated by using **Eq. (15 & 16)**, respectively (Xing et al., 2018)

$$C_{\text{I}}(\%) = \frac{\sum A_{\text{CI}}}{\sum(A_{\text{CI}} + A_{\text{CII}})} \times 100 \quad \text{Eq. (15)}$$

$$C_{\text{II}}(\%) = \frac{\sum A_{\text{CII}}}{\sum(A_{\text{CI}} + A_{\text{CII}})} \times 100 \quad \text{Eq. (16)}$$

where $\sum A_{\text{CI}}$ and $\sum A_{\text{CII}}$ are the sums of peak areas corresponding to C_{I} and C_{II}, respectively.

According to the hypothetical nanocellulose cylinder model, the specific surface area was calculated by **Eq. (17)** (Q. He, Y. Yang, et al., 2022).

$$SSA = \frac{4}{\rho \times d} \quad \text{Eq. (17)}$$

where SSA is the specific surface area (m^2/g), d is the CNC particle size (nm) and ρ is the CNC density (g/cm^3).

3.7.7. Thermal characterization

The thermal characteristics of the fibers (non–retted, retted, extracted, alkalized and bleached), neat PLA and its composite samples (PLA/CNC1%, PLA/CNC3% and

PLA/CNC5%) were evaluated via a simultaneous TGA–DTA/DSC instrument (TGA–DTA/DSC, HCT–3; Beijing Henven Instruments, Beijing, China). The samples (10 mg) were heated from room temperature to 600 °C at a heating rate of 20 °C/min in a nitrogen atmosphere at a flow rate of 50 ml/min (Karthik et al., 2013; George et al., 2014; M. K. Hossain et al., 2014; Syafri et al., 2018). The degree of crystallinity (X_c) values of the neat PLA and its composite samples (PLA/CNC1%, PLA/CNC3% and PLA/CNC5%) of were determined from the DSC heating curve via **Eq.(18)** (Kong et al., 2002; Doumeng et al., 2021).

$$X_c(\%) = \frac{\Delta H_m}{W_{PLA} \times \Delta H_m^0} \times 100\% \qquad \text{Eq. (18)}$$

where W_{PLA} is the weight fraction of PLA in the PLA/CNC composites, ΔH_m is the heat of melting (J/g), and ΔH_m^0 is the heat of melting for 100% crystallized PLA (93.6 J/g) (X. Gao et al., 2020).

Additionally, thermogravimetric analysis (TGA) was used to analyze the thermal decomposition properties of RF, MC and CNC using TGA/DTG (Differential Thermo Gravimetry) (DTG–60H, Shimadzu, Japan). The samples were heated from room temperature to 800 °C with heating rate of 15 °C/min in a nitrogen atmosphere flow rate of 50 ml/min.

3.7.8. Rheological characterization

The viscosity, molecular weight and degree of polymerization of the MC and CNC samples were measured and calculated. The solvent used for measuring viscosity was made by mixing 6 wt.% NaOH and 4 wt.% urea with 100 mL of distilled water. MC and CNC, weighing $4x10^{-3}$ gmL^{-1}, were dispersed in this solvent, stirred for 15 minutes, and then refrigerated at –4 °C for 12 h. The frozen solid was dissolved and vigorously stirred at room temperature to produce a solution. The viscosity of the MC and CNC solutions was then measured at room temperature using an Ubbelohde viscometer 50101, Cap.–no.0a, Schott instruments, Mainz, Germany (L. Zhang et al., 2001; Jinping Zhou et al., 2004). The intrinsic viscosity (η), was estimated in mLg^{-1} using **Eq. (19)** (Hamad et al., 2010; Xiong et al., 2012b).

$$\log\left[\left(\eta_r - 1\right)/C\right] = \log\left[\eta\right] + 0.13\left[\eta\right]C \qquad \text{Eq. (19)}$$

Where, η is the intrinsic viscosity, η_r is the relative viscosity ($\eta/\eta_0 = t/t_0$), t is the time flow of solution, t_0 is the time flow of solvent and *C* is the concentration.

The average molecular weight (M_w) was estimated using Mark–Houwink Equation shown in **Eq. (20)** (Bu et al., 2019; B. He et al., 2022).

$$[\eta] = K(M_w)^{\alpha} \quad \text{Eq. (20)}$$

Where, η is the intrinsic viscosity, M_w is the average molecular weight, *K* is the Mark–Houwink constant (2.45×10^{-2}), and α is the Mark–Houwink exponent (0.815) for NaOH/urea solvent (Jinping Zhou et al., 2004).

The average degree of polymerization was calculated using **Eq. (21)** (Ono et al., 2018).

$$DP = \frac{M_w}{162} \quad \text{Eq. (21)}$$

Where, *DP* is the average degree of polymerization, 162 (g/mol) is the molecular weight of glucose unit.

3.7.9. Mechanical testing

3.7.9.1. Single fiber tensile testing

The tensile test was performed according to an ASTM D 3822–07 using a single fiber electronic strength tester (Fiber Tenso–Lab–331A), Mesdan–Lab, Italy. The test was carried out at a room temperature, with a gauge length of 100 mm, a load range of 5 N, and a test speed of 100 mm/min. The maximum breaking force (cN), elongation at break (%), and tenacity (cN/tex) of the fibers were measured for every single fiber and the mean values of ten singe fibers were reported (Sreenivasan et al., 2011; Lomelí-Ramírez et al., 2018)

3.7.9.2. Filament and 3D printed sample tensile testing

The 3D-printed tensile specimens were designed and tested according to the ASTM D3039/D3039M standard, with a flat shape measuring 165 mm in length, 20 mm in width, and 3 mm in thickness. The printed samples were tested at room temperature using a universal testing machine (DSCK) equipped with a 50 kN load cell, with a gauge length of 50 mm and a crosshead speed of 5 mm/min. For filament testing, specimens were prepared and evaluated according to the ASTM D638 standard, using a gauge length of 30 mm and a test speed of 3 mm/min. Three specimens from each group were tested, and the average values were reported. During the tests, force and elongation data were continuously recorded to determine the tensile properties of the samples.

CHAPTER 4

RESULTS AND DISCUSSIONS

4.1. Retting Process Analysis

This study aims to optimize the retting process by systematically evaluating key factors, including the pH of the retted water, the weight loss of the stalks, and the water absorption capacity during fiber extraction. By analyzing these parameters, this research intends to identify optimal retting conditions that enhance both fiber quality and yield, thereby contributing to more efficient fiber extraction methods (Sow et al., 2021).

4.1.1. Retted water pH analysis

Figure 31(a, b) illustrates the relationship among the water retting duration, pH of retting water, stalk water absorption, and stalk weight loss. Different bacteria namely *Clostridium sp.*, *Clostridium butiricum*, *Granulobacter pectinovorum*, *Clostridium felsineum*, *Clostridium guerfelli* and *Bacillus amylobacter* are known to promote the retting process by producing pectinolytic enzymes that break down the α-1,4 linkages in pectin, which is rich in galacturonic acid (Kozłowski et al., 2020). A critical phase of this process is the hydrolysis of pectic matter, which surrounds and cements the fibers, thereby loosening them from the stem and facilitating their extraction (Datta et al., 2024) .The results indicate that the pH value of the retting water decreased from approximately 7.00 to 4.86 over a period of 192 h, remaining steady for an additional 24 h. Then, the pH value began to increase again. This increase can be attributed to the depletion of pectic matter available for hydrolysis and the utilization of D-galacturonic acid (GA) by bacteria, leading to a reduced concentration of GA. This condition suggests the end of bacterial hydrolysis and marks the completion of the retting process. Therefore, 216 h is considered the optimal duration for effective fiber extraction (Lisha Zhang, 2013; Datta et al., 2024).

4.1.2. Investigation of stalk equilibrium water absorption

Fiber extraction through water retting occurs when water penetrates the center–stalk section of the bast, causing the interior cells to swell and breaking down the outermost layer. This process enhances water absorption and promotes the growth of bacteria that facilitate retting (D. P. Ray et al., 2015; Ramesh, 2016). Thus, achieving equilibrium in water absorption is essential for the effective removal of pectin and successful fiber extraction during water

retting. **Figure 31(b)** illustrates the relationship between retting time and stalk water absorption. The percentage of water absorption increased rapidly to 172.47% within the first 48 h, followed by a gradual rise to an equilibrium water absorption percentage of 187.21% at 168 h. After this period, the water absorption percentage stabilized, with variations of less than 1% observed, indicating that no further weight gain of the wetted linseed stalk occurred during subsequent retting time increments. Following saturation of water absorption, an additional 48 h was allowed for microbial processes to complete the degradation of pectin. In total, a retting duration of 216 h is considered optimal for successful fiber extraction.

4.1.3. Stalk weight loss analysis

Retting involves the hydrolysis of pectic substances that bind the fibers to one another and to the stem. As pectin is removed, the overall mass of the stalk decreases (P. M. Tahir et al., 2011; Datta et al., 2024). The reduction in stalk weight after retting serves as an indicator of the effective retting process. **Figure 31(a)** illustrates the increase in weight loss percentage, which ranges from 5.74% to 12.3% at 168 hours, attributed to the removal of impurities and pectic components from the stalk. Following this period, the variations in weight loss percentage stabilized at less than 1%, indicating effective degumming; this duration is thus considered optimal for retting. However, extending the retting time beyond this point may result in the removal of other non–cellulosic constituents (Duchemin et al., 2012; Nair et al., 2013). As a result, the retting water pH, stalk water absorption, and stalk weight loss values help to predict the optimal retting time for effective fiber extraction.

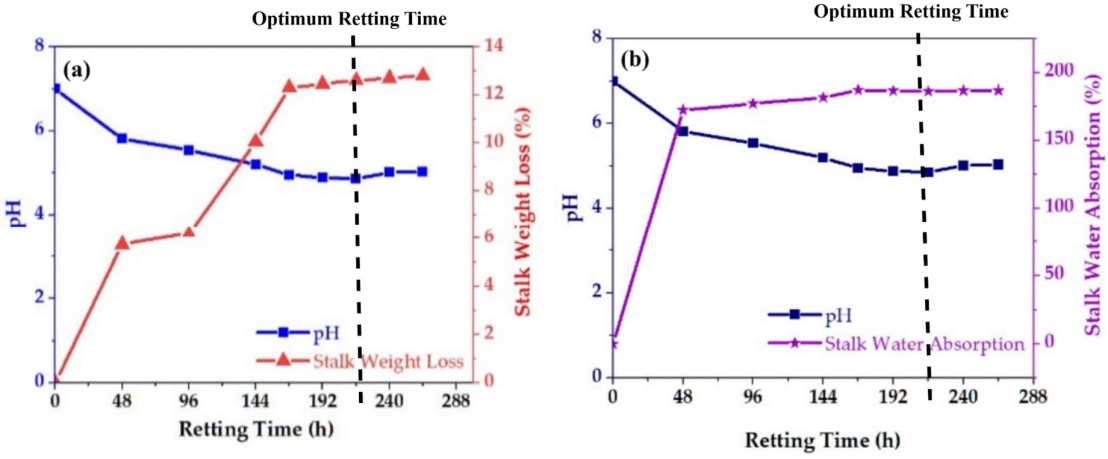

Figure 31. Effect of retting time on (a) retted water pH and stalk weight loss (b) retted water pH and stalk water absorption

4.2. Chemical Composition Analysis

Following the successful extraction of fiber from linseed stalks, a chemical composition analysis was performed to determine the percentage of key chemical constituents, specifically cellulose, hemicellulose, lignin, extractives, and ash. The findings indicated that the fiber comprises 68% cellulose, 20% hemicellulose, 5% lignin, 4% extractives, and 3% ash as illustrated in **Figure 32**. Notably, the cellulose content is significantly higher compared to various lignocellulosic biomasses derived from agricultural residues, including teff straw (37%), corncob (45%), wheat straw (38%), rice straw (35%), barley straw (38%) coffee hull (36%) and enset fiber (60%) (Kallel et al., 2016). Thus, linseed stalk straw is identified as a promising source of cellulose.

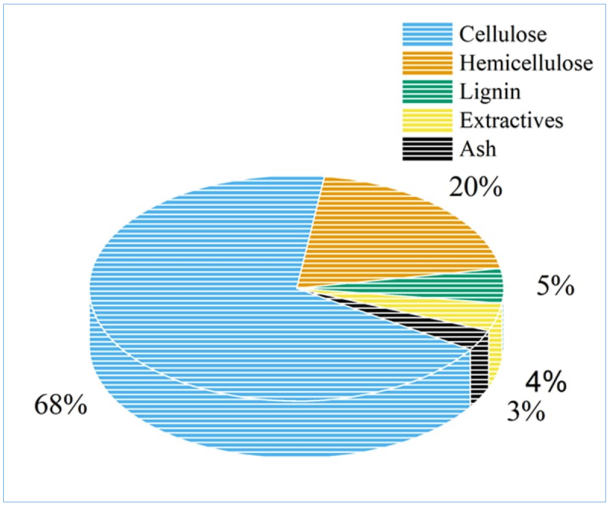

Figure 32. Chemical composition of linseed fiber

The literatures reveal notable variations in the chemical compositions of various agricultural crop residues. The composition of these constituents can differ even within the same species, influenced by factors such as the geographical region of cultivation and the specific genotype. While all fibers share the same fundamental constituents, they are present in varying proportions, leading to distinct characteristics and behaviors (Komuraiah et al., 2014).

4.3. Physical Properties Analysis

4.3.1. Effect of retting duration on fiber physical properties

The analysis of retting duration's impact on the physical properties of fiber specifically density, moisture absorption, diameter, and yield provide valuable insights into fiber

characteristics. Based on the retting process, the extracted fibers were categorized into three groups: under–retted (R_1), optimally retted (R_2), and over–retted (R_3), as illustrated in **Figure 33**.

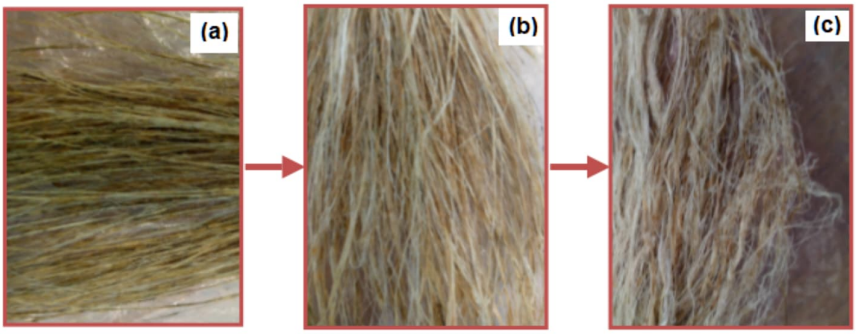

Figure 33. Images of (a) under–, (b) optimally, and (c) over–retted fibers

The results from **Table 23**, indicate that as the degree of retting increases, the average diameter of the fiber decreases due to the removal of surface components during the retting process (Sain et al., 2006; Mazian et al., 2018). Initially, an increase in density values was observed with higher retting degrees, attributed to the elimination of less–dense constituents and impurities, such as pectin (Abbass et al., 2021; S. Y. Nayak et al., 2021). However, fibers that were over–retted exhibited a relative reduction in density, which can be explained by cell–wall decompression (Amel et al., 2013; Kandemir et al., 2020). The mean density of optimally retted fiber was measured at 1.52 g/cm³, aligning with previously reported values for flax fiber, which range from 1.40 to 1.55 g/cm³ (Stamboulis et al., 2001; Le Gall et al., 2018), These values were derived from various measurement methods, including helium pycnometer (1.54 g/cm³) (Sawsen et al., 2014), gas pycnometer (1.49 to 1.52 g/cm³) (Amiri et al., 2017), and water immersion (1.54 g/cm³) (Kharine et al., 2003).

Table 23. Summary of the average physical parameters and properties of fibers at different retting durations

Samples	Diameter (µm)	Density (g/cm^3)	Moisture (%)	Yield (%)
R_0	–	1.33 ±0.03	9.34 ± 0.21	15.65
R_1	128.22 ±31	1.43 ±0.05	8.57 ±0.11	14.25
R_2	104.65 ±17	1.52 +0.04	8.32 ±0.03	12.67
R_3	90.36 ±7	1.41 ±0.03	7.72 ±0.10	12.00

^{R0} is non-retted fiber, ^{R1} is under-retted fiber, ^{R2} is optimum-retted fiber a2nd ^{R3} is over-retted fiber

Moreover, the moisture content of the fibers decreases with increasing retting duration. This reduction is attributed to the high levels of cortical parenchyma components remaining on the surfaces of non–retted and under–retted fibers, which tend to have greater water interaction (S Alix et al., 2014).

The yield of fibers is significantly affected by the retting process as well. Under–retted fibers yield a high percentage (14.25%) due to insufficient separation and elevated impurity levels, which correspond to residual pectin and other contaminants, negatively impacting both the quality and weight of the fibers. This phenomenon aligns with the observed increase in fiber diameter. In contrast, optimally retted fibers yield a moderate percentage (12.65%) while maintaining relatively good quality, comparable to a reported yield of 15% (Praczyk et al., 2021). Conversely, over–retted fibers exhibit a decreased yield (12%) and compromised quality, as prolonged exposure can lead to cellulose breakdown, resulting in weaker fibers. Understanding these relationships is essential for optimizing the retting process to achieve the desired yield and quality of fiber.

4.3.2. Analysis of MC and CNC physical properties

Crystalline nanocellulose (CNC) has several remarkable physical properties that make it a highly versatile material, such as its high surface area, low density and high aspect ratio, compared to a micro cellulose (MC). The physical properties of MC and CNC such as diameter, length, aspect ratio, density, surface area and yield were analyzed. The size of the extracted MC and CNC were calculated from SEM and TEM images shown in **Figure 35** and **36**, respectively. Micro sized MC fibers with a mean diameter of 14.61 ± 6.77 µm were extracted. However, the MC length is several micro meters, as the fibril ends are not apparent in the SEM micrographs. The extracted size of the MC was compared with the acceptable diameter range (10–15 µm) according to standardized terms for cellulose nanomaterials (TAPPI WI3021).

Similarly, Nanosized CNC fibers with an average diameter of 7.06 ± 1.95 nm, length of 66.14 ± 28.58 nm, and aspect ratio of 10.02 ± 4.87 were successfully isolated. The results obtained in this study were compared to established industry standards and relevant literature to assess their conformity to expected ranges. According to standardized terms for cellulose nanomaterials (*TAPPI WI3021*), the acceptable ranges for the CNC diameter and aspect ratio are 3–10 nm and 5–50, respectively. Additionally, it was compared with the reported studies of CNC sizes (diameter, length and aspect ratio) extracted from different sources, such as

from sisal (10 ± 5 nm, 403 ± 159 nm and 40),(Mondragon et al., 2014a) white coir (8 ± 3 nm, 172 ± 88 nm and 22 ± 8),(Nascimento et al., 2014) corncob (4.15 ± 1.08 nm, 210.8 ± 44.2 nm 53.4 ± 15),(Silvério, Neto, et al., 2013c) soy hulls (2.77 ± 0.67 nm, 122.66 ± 9.4 nm and 44),(Neto et al., 2013) rice straw (11.2 nm, 117 nm and 10.5) (P. Lu et al., 2012) and kenaf (12 ± 3.4 nm, 158.4 ± 63.6 nm and 13.2) (Kargarzadeh et al., 2012).

Figure 34 presents the size distributions (diameter, length, and aspect ratio) of the extracted MCs and CNCs, illustrated through a histogram. The results of the normality test indicate that both the diameter and aspect ratio were significantly derived from a normally distributed population at the 0.05 level. In contrast, the length distribution of the CNCs did not conform to a normal distribution at this significance level. Overall, the majority of the distributions appeared to be adequately fitted to a normal function.

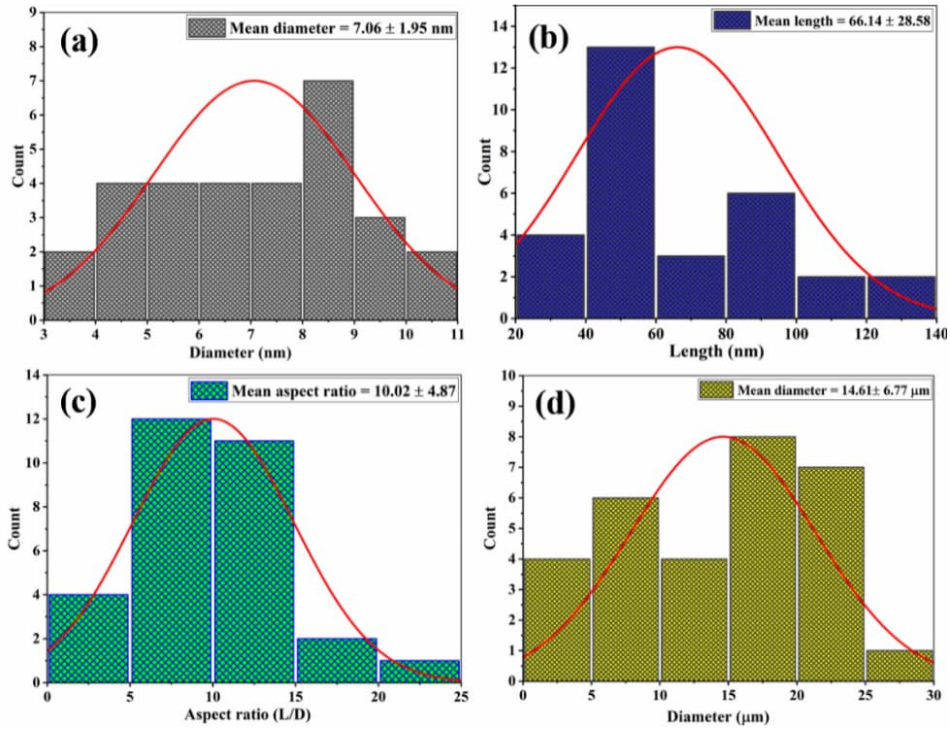

Figure 34. Histograms with skew normal fits of the size distributions of (a) diameter, (b) length and (c) aspect ratio for CNCs and (d) diameter for MCs

Another measure of high importance, which is directly linked to the nanoscale dimensions, is the specific surface area (SSA). It is defined as surface area per unit mass of a material (m^2/g) (Andreas Mautner et al., 2018). The calculated specific surface areas of RF, MC and CNC were found to be 0.02 m^2/g, 0.18 m^2/g and 377m^2/g, respectively. This data suggests that specific surface area tends to increase as the fibril diameter decreases, as it is often

calculated based on measured fibril diameters (Brinkmann et al., 2016). Various studies have reported SSA values obtained through different methodologies. For example, theoretical calculations indicated SSA values of 250 m^2/g for CNC and 50–70 m^2/g for CNF. Other studies employing the BET method found CNC values ranging from 216 to 605 m^2/g and CNF at 304 m^2/g, while AFM calculations showed CNF values between 146 and 219 m^2/g and CNC values from 138 to 226 m^2/g (Andreas Mautner et al., 2018). These values can vary significantly depending on factors such as the cellulose source, the extraction and SSA determination techniques employed. Additionally, the yield of isolated CNCs from MC was determined to be 79.87 ± 1.35%. Yields of CNCs isolated from various other sources also differ, with reported values of 50.0 ± 3.32% from teff straw, 70.0 ± 1.49% from enset fiber, 64.0 ± 2.79% from sugarcane bagasse, and 25.0 ± 2.11% from coffee hulls (Gabriel, Belete, et al., 2021b).

4.3.3. Water absorption property of Bio nanocomposite samples

From the experimental results, the water absorption percentage of pure PLA and PLA/CNC composites with 1, 3 and 5% CNC concentration are 5.16% in 24 h, 58.55% in 24 h, 34.86% in 72 h and 56.75% in 24 h, respectively. The water absorption behavior of PLA/CNC composite films is significantly influenced by incorporation of CNCs and its concentration. This can be attributed to the higher surface area and the presence of hydroxyl groups on the CNC, which enhance the hydrophilicity of the polymer (Bai et al., 2017; Pakdel et al., 2021). In addition, PLA/CNC composites had water absorption ability due to its porous structure and foamability property, results from incorporation of a plasticizer and evaporation of DCM solvent (Bualuang et al., 2020). The composite film with 3% CNC loading showed low water absorption percentage with slower rate due enhanced compatibility, low agglomeration and porosity (Sucinda et al., 2021).

4.4. Morphology Analysis

4.4.1. Morphology analysis of MC and CNC samples

The morphological study conducted using Scanning Electron Microscopy (SEM) and Transmission Electron Microscopy (TEM) yielded significant insights into the structural characteristics of micro–cellulose (MC), crystalline nanocellulose (CNC), and CNC/PLA composites. This analysis focused on several critical aspects, including the size and shape of both MC and CNC, which are fundamental to understanding their reinforcement capabilities

in composite materials. The morphological structure of MC consists of separated individual fibers during chemical treatment, resulting in the formation of cellulose fibrils. Furthermore, the removal of non–cellulosic constituents by pre–treatment cleaved the fibers into smaller sizes. **Figure 35** presents SEM images of micro–cellulose (MC), illustrating the effective removal of amorphous materials from the raw fiber following chemical pretreatments. These observations corroborate the findings obtained from FT–IR and XRD analyses.

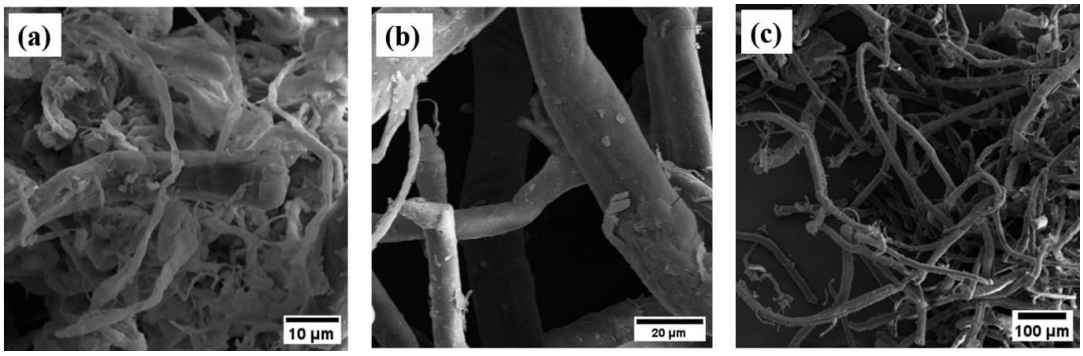

Figure 35. SEM images of MC at different resolutions: (a) 10 µm (2130X), (b) 20 µm (1030X) and (c) 100 µm (200X)

Transmission Electron Microscopy (TEM) is conducted to characterize the morphological and structural features of crystalline nanocellulose (CNC). It enables detailed visualization shape and provides precise measurements of dimensions like diameter, length, and aspect ratio of CNCs. TEM also helps assess the degree of dispersion or agglomeration of CNC particles. When combined with High-Resolution TEM (HRTEM), it further reveals the crystalline structure at the nanoscale, offering critical insights into CNC quality and its suitability (Kaushik et al., 2015).

Figure 36 indicates that the rod-like crystalline nanocellulose (CNC) maintains good dispersion in ethanol, with minimal clumping or aggregation. This suggests that the CNC has stable colloidal behavior in ethanol, which is important for ensuring uniform distribution when incorporated into composite materials. The observed rod-like structure also confirms the expected morphology of well-isolated CNC particles, which is favorable for reinforcing polymers (Hirase et al., 2022).

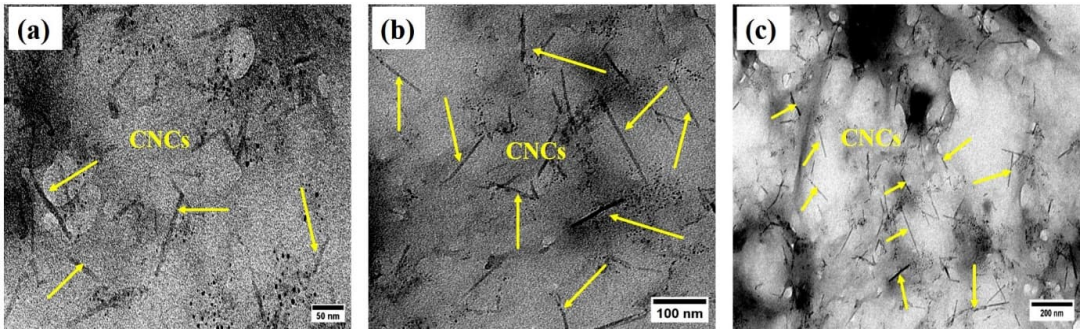

Figure 36. TEM images of CNC at different resolutions: (a) 50 nm (40000X), (b) 100 nm (20000X) and (c) 200 nm (10000X)

Figure 37 illustrates the measurement steps for d–spacing from the HRTEM image. To analyze this structure at the nanoscale, a fast Fourier transform (FFT) technique was used on the HRTEM image, isolating key crystallographic features. Then, an inverse FFT (IFFT) was applied to reconstruct the real-space image of the crystalline lattice (Imamov et al., 2011). The analysis reveals a lattice spacing, the distance between repeating units in the crystal structure of approximately 0.35 nanometers (3.54 Å). This spacing corresponds to the typical (200) plane of cellulose Iβ, which is the dominant crystalline form of CNC (A. Sinha et al., 2015). Notably, this result is in good agreement with X-ray diffraction (XRD) data, which reported a mean lattice spacing of 0.36 nm. The close match between the two techniques (HRTEM and XRD) confirms the high crystallinity and consistent internal structure of the CNCs.

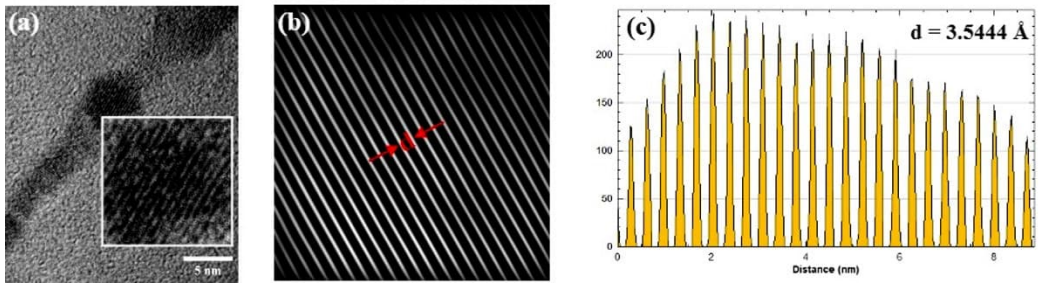

Figure 37. Measurement steps for d–spacing from the (a) HRTEM image (600000X), (b) d–spacing, and (c) profile plot

4.4.2. Morphology analysis of bio–nanocomposite samples

One of the key findings was the assessment of the effectiveness of CNC dispersion and distribution within polymer matrices. SEM imaging allowed for the visualization the Bio nanocomposite samples, revealing how well the CNC with different contents was integrated

into the polymer matrix. This integration is crucial, as uniform dispersion enhances the mechanical properties of the composites. Additionally, the study identified instances of agglomeration, which can compromise the performance of the material by reducing the effective surface area available for bonding with the matrix. Such insights are vital for optimizing composite formulations to achieve desired properties.

The morphology of the neat PLA and PLA/CNC composites with varying CNC weight percentages (1%, 3%, and 5%) was investigated through scanning electron microscopy (SEM) analysis, as shown in the **Figure 38**. The SEM images revealed an almost uniform and smooth surface of the neat PLA sample, except for the small air bubbles indicated by yellow arrows, which formed during drying. The PLA/CNC1% image shown in **Figure 38 (A)** showed good dispersion, with some empty space in the matrix material, as shown in **Figure 38 (B)**, as indicated by the yellow arrow.

Compared with the other samples, the PLA/CNC3% shown in **Figure 38 (C)** sample revealed better homogenous dispersion, with some closed pores formed due to the addition of the plasticizer and evaporation of the solvent during drying. However, at higher CNC contents (PLA/CNC5%) shown in **Figure 38 (D)** , some agglomeration was observed, likely because the increased filler loading exceeded the dispersibility limit within the polymer matrix (Z. Wang et al., 2019; Bualuang et al., 2020; Sucinda et al., 2021).

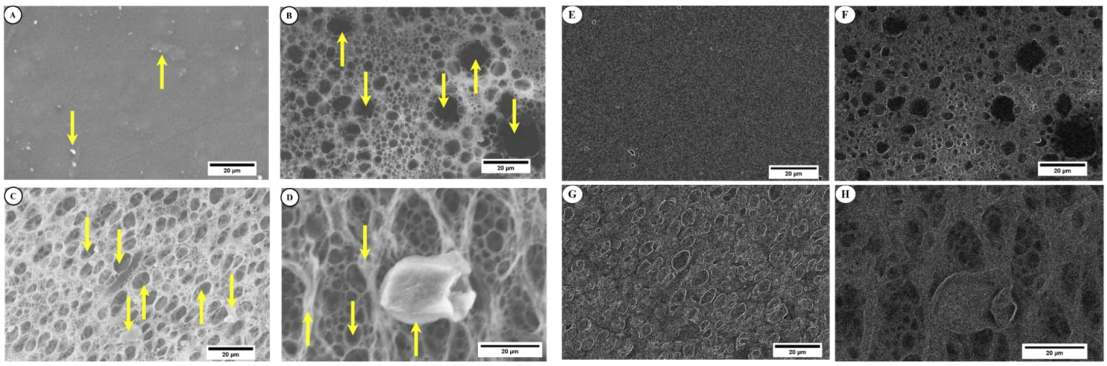

Figure 38. SEM images of (A, E) neat PLA (1000X) (B, F) PLA/CNC1% (1000X) (C, G) PLA/CNC3% (1000X) and (D, H) PLA/CNC5% (×1000X)

4.4.3. Morphology analysis of filaments and 3D printed samples

The surface and tensile fracture morphologies of PLA and PLA/CNC3% filaments and 3D printed samples provide valuable insights into the effects of CNC and processing condition. By examining these aspects, we can better understand the structural and mechanical performance of these materials in both filament form and as 3D printed samples. The neat

PLA filament exhibits smooth and uniform surfaces, reflecting the homogeneity of the pure PLA matrix, as shown in **Figure 39 (a)**. For PLA/CNC3% coated filaments, the coating of on to PLA filament results in surface roughness and visible textural features. Uniform coating ensures consistent surface features, while uneven coating create irregularities or protrusions, as shown and indicated in **Figure 39 (b).**

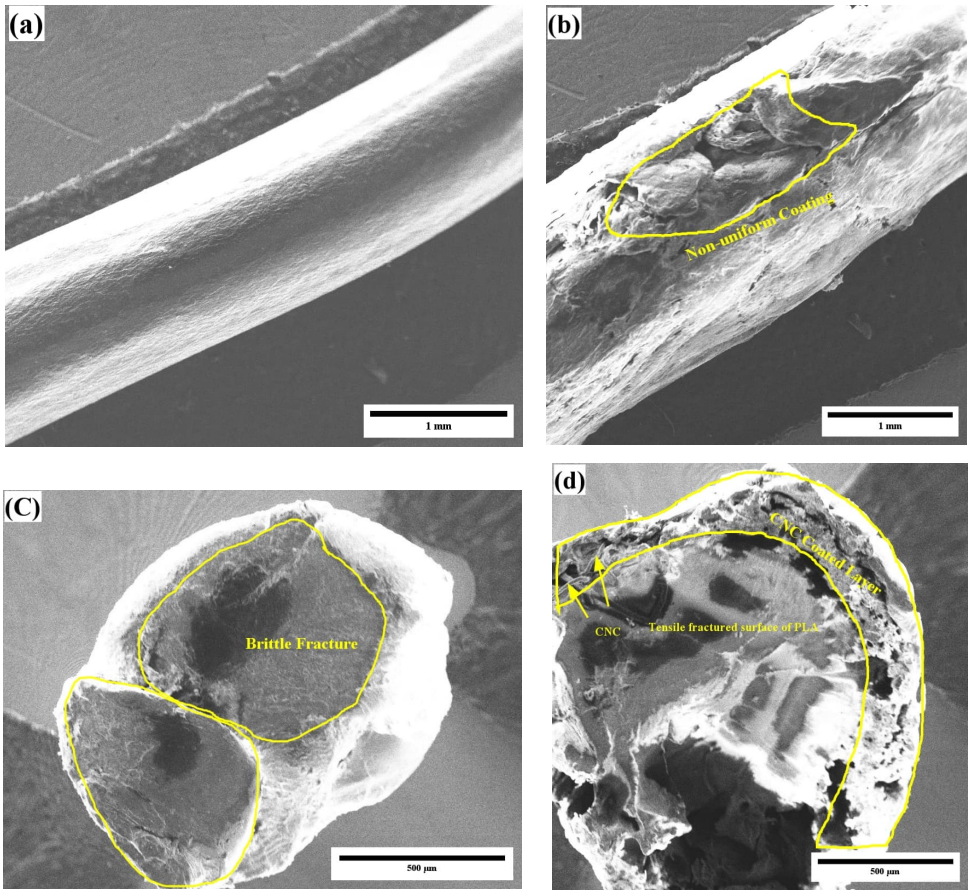

Figure 39. SEM images of filaments (a) neat PLA filament (22X) (b) PLA/CNC (22X) (c) fractured neat PLA (45X) and (d) fractured PLA/CNC (45X)

The tensile fracture morphology of filaments provides insights into their mechanical behavior under stress and the effects of coating. Neat PLA filaments typically showed brittle failure with smooth and planar fracture surfaces, consistent with PLA's inherent brittleness as shown **Figure 39 (c)** (Daver et al., 2018b; Fernández-Santos et al., 2021). In contrast, PLA/CNC3% coated filaments exhibited modified fracture behavior due to the influence of the surface coating on the PLA filament. Effective bonding between the PLA filament and the coating enhances energy absorption during fracture, resulting in rougher surfaces with evidence of ductile tearing.

For 3D-printed samples, the pure PLA sample exhibited smooth surfaces with clearly defined layers, reflecting the consistent flow properties of neat PLA. In PLA/CNC3% samples, the CNC influenced the printed surface morphology, increasing roughness and creating some visible air pores and CNC aggregations, as shown **Figure 40 (a** and **b),** respectively.

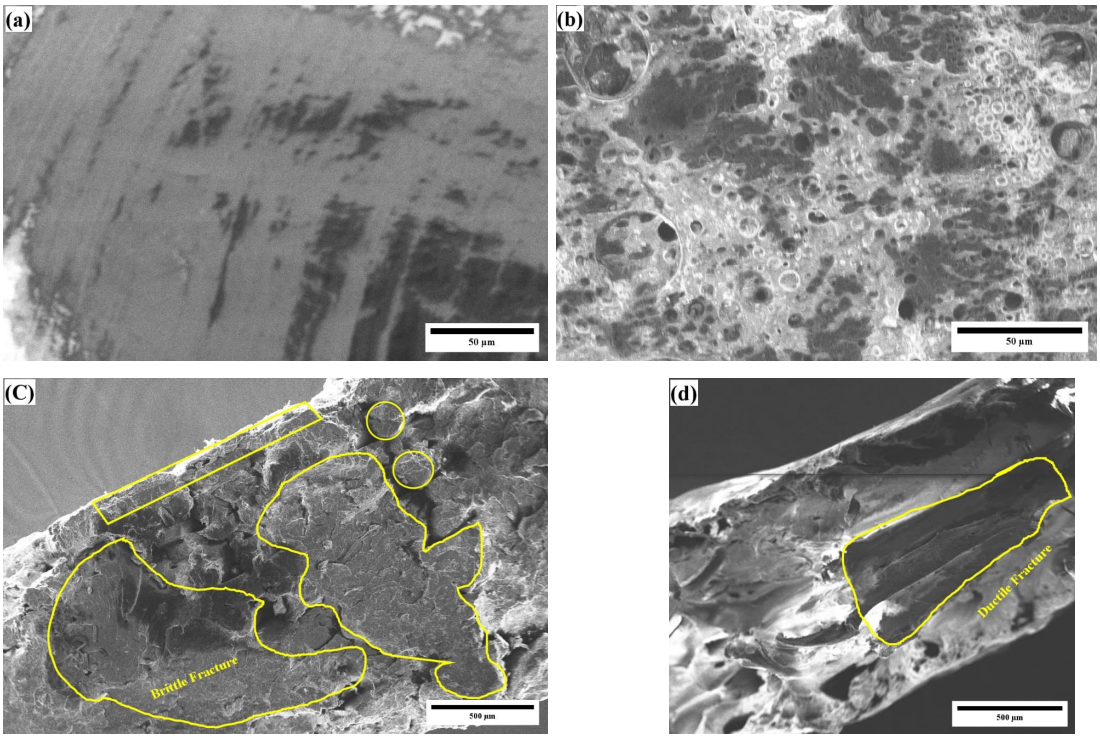

Figure 40. SEM images of 3D printed samples (a) neat PLA (450X) (b) PLA/CNC (450X) (c) fractured neat PLA (45X) and (d) fractured PLA/CNC (45X)

The tensile fracture morphology of 3D-printed samples is heavily influenced by the layer-by-layer printing process and the presence of CNCs. Neat PLA samples generally failed in a brittle manner, with smooth fracture planes and good interlayer bonding. PLA/CNC3% samples, however, display improved fracture behavior due to the incorporation of the CNC. It resulted in rougher fracture surfaces, ductile failure and good interlayer bonding, with some air pores as shown in **Figure 40 (c** and **d),** respectively.

4.5. X–ray diffraction (XRD) Analysis

4.5.1. X–ray diffraction (XRD) analysis of MC and CNC Samples

X–ray diffraction is a widely used technique to analyze the crystal structure of cellulosic samples. The structural properties of micro–cellulose (MC) and crystalline nanocellulose

(CNC), including crystallinity index, crystalline size, d–spacing, and cellulose polymorphs (Iβ, Iα, CI, and CII), were determined from the X–ray diffraction (XRD) patterns. **Figure 41** shows the XRD patterns of the RF, MC and CNC samples Generally, all the samples exhibited similar patterns of four characteristic peaks with different peak intensities. The samples showed main diffraction signals at 2θ values of approximately 14°, 16°, 22° and 34° with assigned crystallographic planes of 1–10, 110, 200 and 004, respectively.

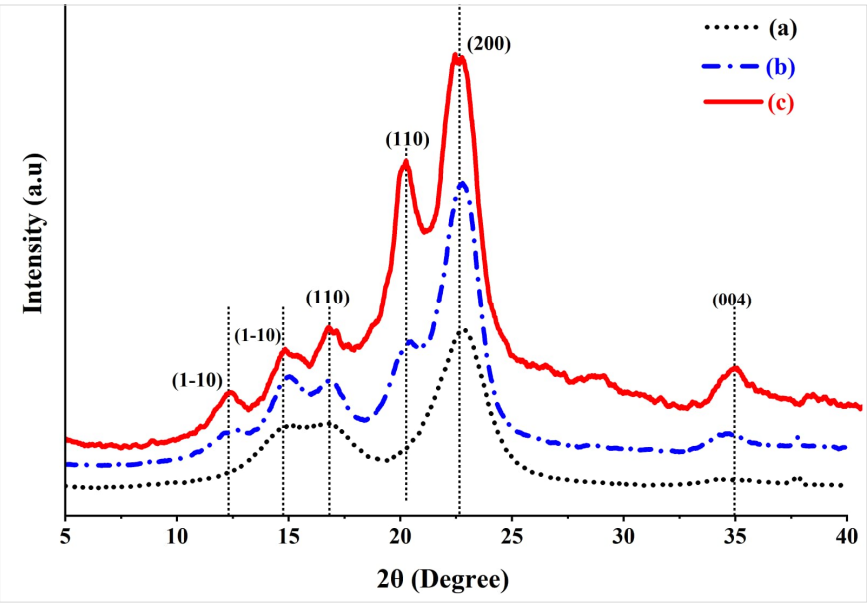

Figure 41. XRD patterns of (a) RF, (b) MC and (c) CNC samples

Table 24 shows the calculated values of C_rI (%), mean crystallite size (nm), mean d–spacing (nm), Z values and cellulose polymorph (I_α, I_β, C_I and C_{II}) contents of all the samples obtained from XRD analysis. The calculated CrI (%) for the RF, MC and CNC samples were 76.71, 80.78 and 73.29%, respectively.

These results are comparable to those of other sources of MC and CNC, such as MC and CNC from teff straw (78.00 and 76.61%), enset fiber (85.56 and 83.41%), sugarcane bagasse (80.92 and 82.60%), coffee hull (77.59 and 80.86%) and commercial cellulose (87.23 and 74.91%) (Gabriel, Belete, et al., 2021b). A slight reduction in the crystallinity of CNCs may occur upon strong acid hydrolysis of highly pure and crystalline micro cellulose, indicating that the amorphous regions were already degraded during the pre–treatment processes and that the acid started to partially attack the crystalline portions (Korolovych et al., 2018; Gabriel, Belete, et al., 2021b).

The d–spacings d_1 and d_2 of RF (0.58 and 0.52 nm), MC (0.59 and 0.52 nm) and CNC (0.60 and 0.530 nm) for the planes 1–10 and 110, respectively, were used for Z value calculations. The Z values for the RF, MC and CNC samples were –26.19, –23.19 and –8.84, respectively. The results indicated that the monoclinic structure (I_β–type cellulose) is dominant in both samples, which is supported by the negative numbers since the I_β type is the dominant polymorph for plant fibers and the I_α polymorph can be converted into I_β by treatments (French, 2014; Gabriel, Belete, et al., 2021b).

Table 24. Parameters obtained from the XRD analysis of the RF, MC and CNC samples

Sample	C_rI (%)	crystallite size (nm)	d–spacing (nm)	Z–Value	Cellulose polymorphs		
					Type	C_I (%)	C_{II} (%)
RF	76.71	3.78	0.39	–26.19	I_β	64.08	35.91
MC	80.78	4.61	0.38	–23.19	I_β	52.68	47.31
CNC	73.29	5.61	0.36	–8.84	I_β	50.55	49.44

The polymorph of native cellulose is rich in the C_I type. After treatment, cellulose crystallizes into various polymorphs (C_I, C_{II}, C_{III}, and C_{IV}) with different packing arrangements (Cui et al., 2014). For the MC and CNC samples, a significant conversion to higher C_{II} contents of 47.31 and 49.44%, respectively, was observed compared to that of the RF sample, which had a lower C_{II} content of 35.91%. Furthermore, the XRD pattern of the MC sample reveals the appearance of doublet peaks at 2θ values of 20.6° and 12.6°, corresponding to the (110) and (1–10) planes, respectively. Similarly, these peaks, with increased intensity, were observed in the CNC sample at 2θ values of 19.98° and 12.16°, corresponding to the (110) and (1–10) planes, respectively, which are indicative of C_{II} (Cui et al., 2014; Xing et al., 2018). This polymorphic transformation may lead to improved properties of composites reinforced with micro/nano crystals extracted from a mixture C_I and C_{II} due to the enhanced hydrogen bonding (P. K. Gupta et al., 2013).

The calculated mean crystallite sizes and d–spacings of RF (3.78 and 0.39) nm, MC (4.61 and 0.38) nm, and CNC (5.61 and 0.36) nm were obtained. After the pre–treatment and acid hydrolysis processes, the mean crystallite size increased, but the d–spacing decreased. This indicates that the treatment processes can reclose the distance between cellulose fibers to produce a more compact fiber structure. Generally, the shorter the distance between cellulose chains is, the greater the size of the crystallite formed. An increase in crystallite size led to recrystallization of the cellulose chains through hydrogen bonding (I. W. F. Arnata, Farah Richana, Nur Sunarti, Titi Candra, 2019).

4.5.2. X–ray diffraction (XRD) analysis of bio–nanocomposites samples

The XRD patterns of neat PLA and PLA/CNC composites with different CNC loadings are shown in **Figure 42**. A sharp peaks were observed at 16° and 19°, which correspond to the (101) and (110/200) planes of α–crystals in neat PLA (Segura Gonzalez et al., 2015; Borkotoky et al., 2018). In the case of the PLA/CNC–based composite samples, these peaks are found at 16° and 22°. The doublet peak observed at 19° with a CNC loading of 5% is related to the presence of cellulose–II CNCs (Xing et al., 2018). The peak at 22° represents the presence of CNCs in the composite samples and indicates the existence of hydrogen bonds between PLA and CNCs in the nanocomposites (Prodyut Dhar et al., 2015; Borkotoky et al., 2018).

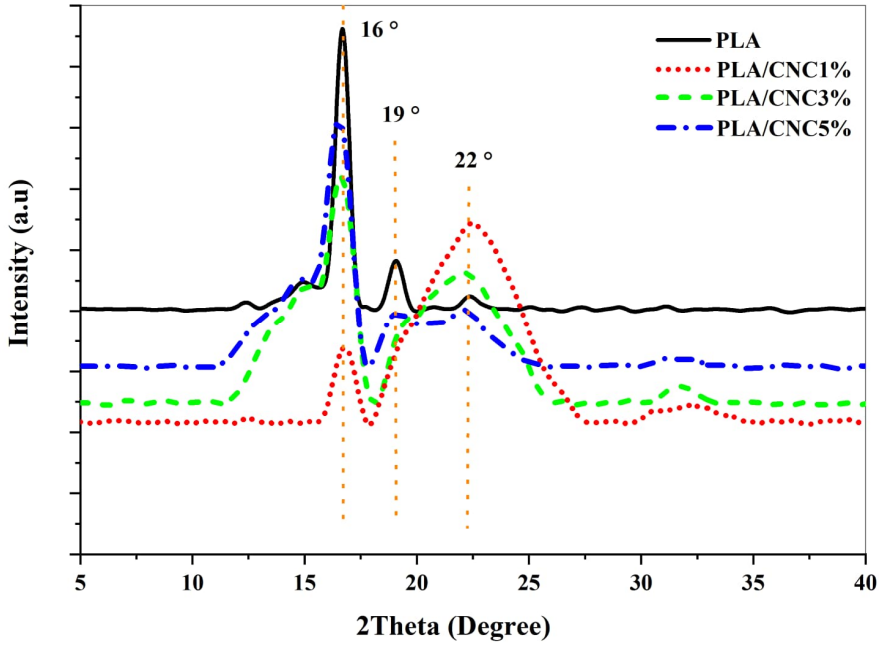

Figure 42. XRD patterns of neat PLA and composite samples

From the XRD pattern analysis, the C_rI (%), crystalline size (nm) and d–spacing were calculated, as shown in **Table 25**. The crystallinities of the semi–crystalline neat PLA, PLA/CNC1%, PLA/CNC3% and PLA/CNC5% samples were calculated as 85.17, 86.94, 77.03 and 70.75%, respectively. The sharp peak of neat PLA found at 16° corresponds to the dominant α–crystals and is reduced for the PLA/CNC composites due to the addition of the plasticizer (Xiao et al., 2009; X. Gao et al., 2020). However, it increases again while incorporating CNCs since the presence of CNCs in the matrix promotes nucleating sites, which causes an increase in peak intensity and the existence of a peak at 22° (Chai et al.,

2020). A further increase in the CNC content affects the crystallinity of the composite, which was also observed via DSC analysis because poor dispersion and agglomeration can lead to reduced effectiveness of CNCs as nucleating agents and poor interactions between PLA and CNCs (Ambrosio-Martín et al., 2015). Similarly, the presence of agglomeration with increasing CNC content was also observed in the morphology study.

Moreover, the presence of CNCs affects the crystallization behavior of PLA. The calculated crystallite sizes of neat PLA, PLA/CNC1%, PLA/CNC3% and PLA/CNC5% are 11.46, 3.95, 3.17 and 3.75 (nm), respectively. The incorporation of CNCs into PLA can lead to smaller crystallite sizes due to the increased number of nucleation sites and potentially faster crystallization kinetics (Clarkson et al., 2020).

Table 25. Parameters obtained from the XRD analysis of neat PLA and composite samples

Sample	Sum of A_{cry}	Sum of A_{total}	CrI (%)	Crystallite size (nm)	d–spacing (nm)
PLA	1723.54	2023.58	85.17	11.46	0.463
PLA/CNC1%	849.58	977.12	86.94	3.95	0.397
PLA/CNC3%	1053.12	1366.98	77.03	3.17	0.406
PLA/CNC5%	1312.34	1854.67	70.75	3.75	0.408

4.6. Fourier Transform Infrared Spectroscopy (FT–IR) Analysis

4.6.1. FT–IR analysis of cellulose fibers at different treatment stages

The effects of retting and different chemical treatments during extraction of cellulose fibers on chemical composition were analyzed using FT–IR. The spectra of the non–retted, retted, extracted, alkalized and bleached fibers shown in **Figure 43**. For every stage of the extraction procedure, FT–IR analysis was done to identify the presence of chemical functional group changes (I. W. Arnata et al., 2020). All samples presented two main absorbance regions, the fingerprint region (700–1,800 cm^{-1}) and the functional group region (2,700–3,500 cm^{-1}). However specific absorption peaks could be identified for each particular component (Morán et al., 2008). The presence of nearly similar functional groups at 3425, 2917, 1636, 1114 and 617 cm^{-1} in all fibers justified the preservation of the basic chemical structure of cellulose fiber and water even after all treatments during the extraction processes. It is expected that during the extraction process, the non–cellulosic components of the fiber hemicellulose, lignin, and extractives (pectin, wax) contents can be completely or partially removed. Therefore, the corresponding absorption peaks of these components disappeared

or diminished their intensity values. The treatments, on the other hand, increased the intensity of the bands corresponding to cellulose (Herlina Sari et al., 2017).

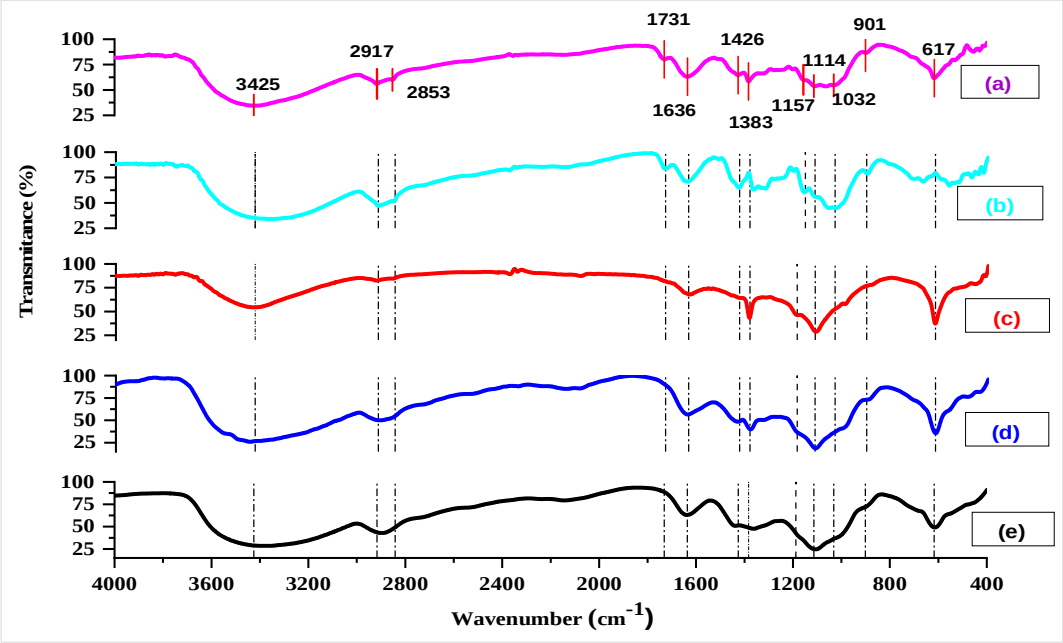

Figure 43. The FT–IR spectra of (a) non–retted, (b) retted, (c) dewaxed, (d) alkalized and (e) bleached fibers.

Absorption peaks corresponding to extractives are 2917, 2853, 1114 and 1032 cm^{-1}. The absorbance peak at 2853 cm^{-1} disappeared and others reduced after retting and extraction due to the removal or reduction of pectin and waxes. The absorption peaks at 3425, 2917, 1732, 1426, 1383, 1114, 1032 and 901 cm^{-1} are related to hemicellulose. The absorption peak at 1731 cm^{-1} disappeared and the others were diminished in their peak intensities because of hemicellulose removal during the alkalization process. Absorption peaks observed at 3425, 2917, 1731 and 1426 cm^{-1} are associated with lignin. The absorption peak at 1731 cm^{-1} disappeared and the others diminished in their peak intensities because of lignin removal during the bleaching process.

4.6.2. FT–IR analysis of MC and CNC samples

The effect of chemical pretreatments and hydrolysis treatment during isolation of crystalline nanocellulose on chemical compositions of the fiber were analyzed using FT–IR. The FT–IR spectra of RF, MC and CNCs are shown in **Figure 44**. The general profiles of all the spectra of the samples are comparable and similar due to the consistent chemical structure of cellulose, which is the main component of plant cell walls. This uniform structure leads

to similar vibrational modes and characteristic peaks in the FT–IR spectra (J. Han et al., 2013). However, subtle differences can still exist, such as shifts in peak positions, changes in peak intensities, variations in peak shapes, and the appearance and/or disappearance of peaks in the FT–IR spectra. The observed broad absorption bands at approximately 3408 cm^{-1}, 3411 cm^{-1} and 3443 cm^{-1} for the RF, MC and CNC samples, respectively, were attributed to O–H stretching vibrations in cellulose and hemicellulose (Apaydın Varol et al., 2023). The absorption bands were observed in all the spectra, revealing the principal functional groups found in the lignocellulosic materials (J. Han et al., 2013).

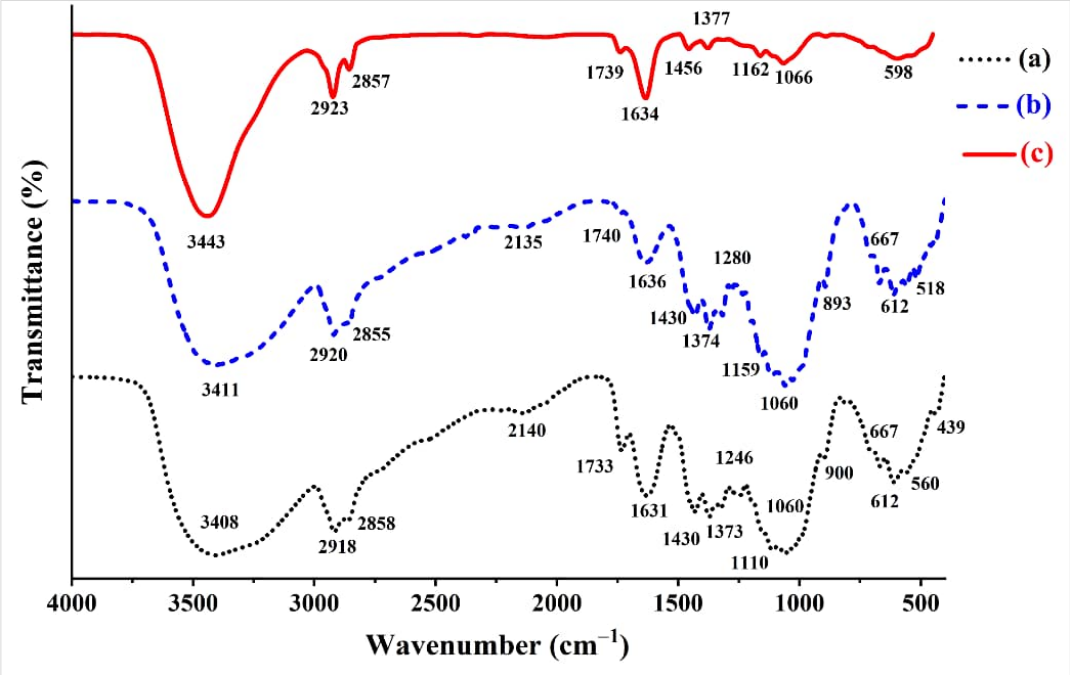

Figure 44. FT–IR spectra of (a) RF, (b) MC and (c) CNC samples

However, an intense peak was observed for CNCs due to hydrolysis, which reflects hydrophilic properties (S. Mishra et al., 2022; Rovera et al., 2023). The other peaks shown at 2918 cm^{-1}, 2920 cm^{-1}, and 2923 cm^{-1} indicate asymmetric C–H stretching vibrations in cellulose and hemicellulose. The sharper band and increase in peak intensity shown in the CNC sample at 2923 cm^{-1} are due to the removal of amorphous cellulose and an alteration of crystalline cellulose by acid hydrolysis (Ciolacu et al., 2011). Similarly, the small peaks observed at 2858 cm^{-1}, 2855 cm^{-1} and 2857 cm^{-1} are attributed to the aliphatic chains of suberin and are attributed to symmetric C–H stretching vibrations (Md Salim et al., 2021). The absorbance band within 1733 cm^{-1} is attributed to the C=O stretching of methyl ester and carboxylate groups in pectin, the acetyl and uronic ester groups of the hemicelluloses or

to the ester linkage of the carboxylic group of the ferulic and p–coumaric acids of lignin and hemicelluloses (B. Wang et al., 2007). This peak strongly decreased for the MCs and CNCs due to the removal of these constituents during the pre–treatment process.

In all the sample spectra, the peaks at 1631 cm^{-1}, 1634 cm^{-1}, and 1636 cm^{-1} correspond to the O–H bending of adsorbed water due to the strong interactions between cellulose and water molecules and difficulty in removing the adsorbed water, even after an appropriate drying process (J. Han et al., 2013; Abu-Thabit et al., 2020). The absorbance peak observed at 1430 cm^{-1} was associated with CH_2 and O–CH in–plane bending vibrations in cellulose (Q. He, Y. Bai, et al., 2022a). The decrease in peak intensity and shift to 1456 cm^{-1} may be due to the alteration of the cellulose structure after hydrolysis. The absorption peaks at 1246 cm^{-1} and 1280 cm^{-1} are attributed to the C–O stretching vibration of the aryl group in lignin (Santos et al., 2022). The peaks are diminished and disappear from the MC and CNC spectra, respectively, due to the removal of lignin.

The absorbance peak at 1060 cm^{-1} was attributed to the C–O–C pyranose ring vibration in cellulose (S. Mishra et al., 2022). The intensity of this peak is very sensitive to the amount of crystalline versus amorphous structure of cellulose, and the broadening of this band reflects more disordered structures (Proniewicz et al., 2001), as shown in the RF and MC samples. The peak corresponding to the CNCs was significantly lower than that corresponding to the other samples, possibly due to the removal of amorphous cellulose after hydrolysis. The subtle peaks at 893 cm^{-1} and 900 cm^{-1} were attributed to the β–1,4 glycosidic bond vibrations in amorphous cellulose. These linkages give cellulose a very long, straight chain conformation, and the disappearance of these peaks after hydrolysis may be related to the destruction of the bond and removal of amorphous cellulose (Proniewicz et al., 2001; Poletto et al., 2014). The absorbance peak at 612 cm^{-1} reveals O–H out of plane bending in native cellulose I_β and I_α. However, due to the different hydrogen bonding strengths of native cellulose I_β and I_α, their O–H out–of–plane bending bands differ (P. Lu et al., 2010).

4.6.3. FT–IR analysis of bio nanocomposite samples

The effect of CNC with varying wt. percentage and plasticizer on the functional group of polymer matrix was studied using FT–IR analysis. The FT–IR spectra of pure PLA, pure CNC, and CNC/PLA composites with different CNC loadings (1%, 3% and 5%) were recorded and analyzed, as shown in **Figure 45**. A broad absorption band at approximately 3400 cm^{-1} was observed for all the samples because of the hydroxyl (O–H) stretching

vibrations (dos Santos et al., 2017). The slight shift to a lower wavenumber and broadening of the O–H stretching band in the composites suggest hydrogen bonding between the hydroxyl groups of CNCs and the ester groups of PLA (de Souza et al., 2020).

This interaction can enhance the compatibility and dispersion of CNCs within the PLA matrix. As the CNC content increases, the intensity of the O–H stretching band becomes more pronounced, reflecting the higher concentration of hydroxyl groups. The absorption bands at approximately 2920 and 2850 cm^{-1} are related to asymmetric and symmetric C–H stretching vibrations in PLA and CNCs (Seraji et al., 2022). The overlap of the PLA and CNC C–H stretching bands can lead to changes in the composite band intensities.

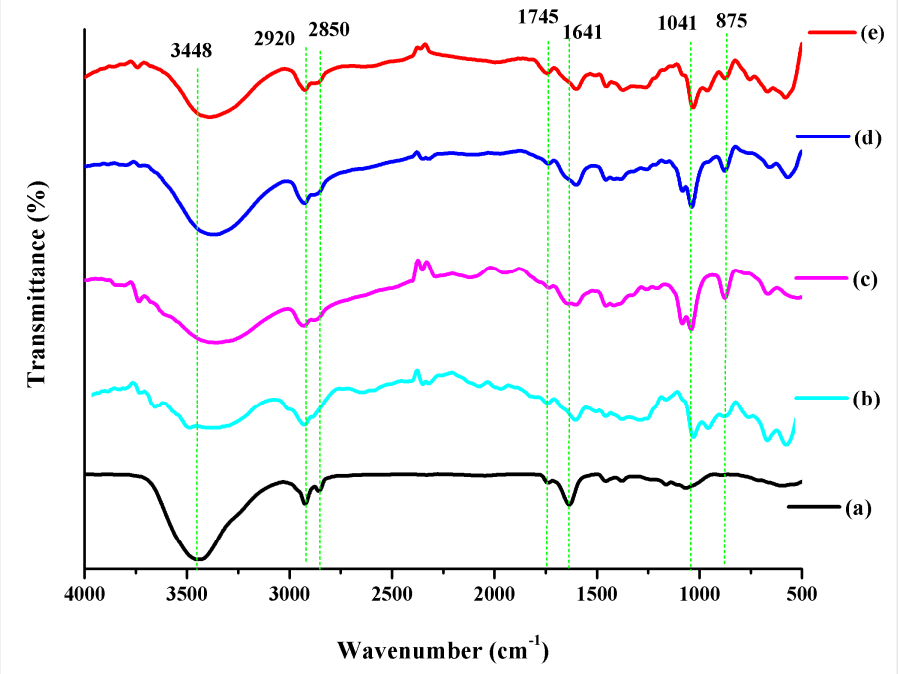

Figure 45. FT–IR spectra of (a) CNCs (b) neat PLA (c) PLA/CNC1% (d) PLA/CNC3% and (e) PLA/CNC5%

The absorption bands at 1640–1740 cm^{-1} is often associated with the presence of carbonyl and amide groups in PLA and CNC, respectively. This absorption typically arises from the stretching vibrations of C=O bonds. Slight shifts and broadening of this band were observed in the composites and with increasing CNC content, which may suggest changes in the hydrogen bonding or molecular interactions between PLA and CNCs (El-Hadi, 2017). The broad absorption band at approximately 1040 cm^{-1} is attributed to the stretching vibrations of the C–O–C and C–O linkages in PLA and CNC, respectively. The composite spectra show

overlapping bands of C–O–C and C–O stretching vibrations from both PLA and CNCs, which lead to an increase in the absorption bands of the composites (Vilarinho et al., 2021). The absorption band at 875 cm^{-1} is related to the C–H out–of–plane bending vibrations in PLA and is indicative of its crystalline nature. An increase in the intensity of this band in the FT–IR spectra of the PLA/CNC composites could indicate changes in the crystalline structure of PLA due to the presence of CNCs. CNCs can act as nucleating agents, potentially enhancing the crystallinity of PLA (Vilarinho et al., 2021).

FT–IR analysis of the PLA/CNC composites revealed significant interactions between CNCs and PLA, primarily through hydrogen bonding and carbonyl group interactions (Marina Patricia Arrieta et al., 2015). These interactions enhance the compatibility and dispersion of CNCs within the PLA matrix, contributing to the improved mechanical properties of the composites (Chakrabarty et al., 2018). The changes in the FT–IR spectra with varying CNC loadings provide a detailed understanding of the molecular–level interactions and the structural integrity of the composites.

4.7. Thermal Property Analysis

4.7.1. Thermal analysis of cellulose fibers at different treatment stages

The decomposition of lignocellulosic materials typically occurs in three distinct stages due to the differing chemical structures of their components: extractives, hemicellulose, cellulose, and lignin. These components decompose at varying temperatures, resulting in a multi–phase degradation process. For linseed straw fiber, the degradation can be categorized into three phases, as illustrated in **Figure 46** and **Figure 47**. The first stage involves drying and evaporation, during which moisture and volatile components are removed. Following this, the second phase is characterized by the decomposition of hemicellulose and the more disordered regions of cellulose. The final stage of degradation involves the thermal breakdown of crystalline cellulose and lignin. This phase occurs at higher temperatures due to the more stable structures of these components (Martin et al., 2013; Draman et al., 2014). The thermal properties of fibers are greatly affected by different chemical treatment processes. Each fiber showed dissimilar weight losses, temperature ranges and peak temperatures in all degradation stages. **Table 26** and **Table 27** summarizes the weight loss percentages, decomposition temperature ranges, peak decomposition temperatures, and residue contents for the fibers at each stage of degradation.

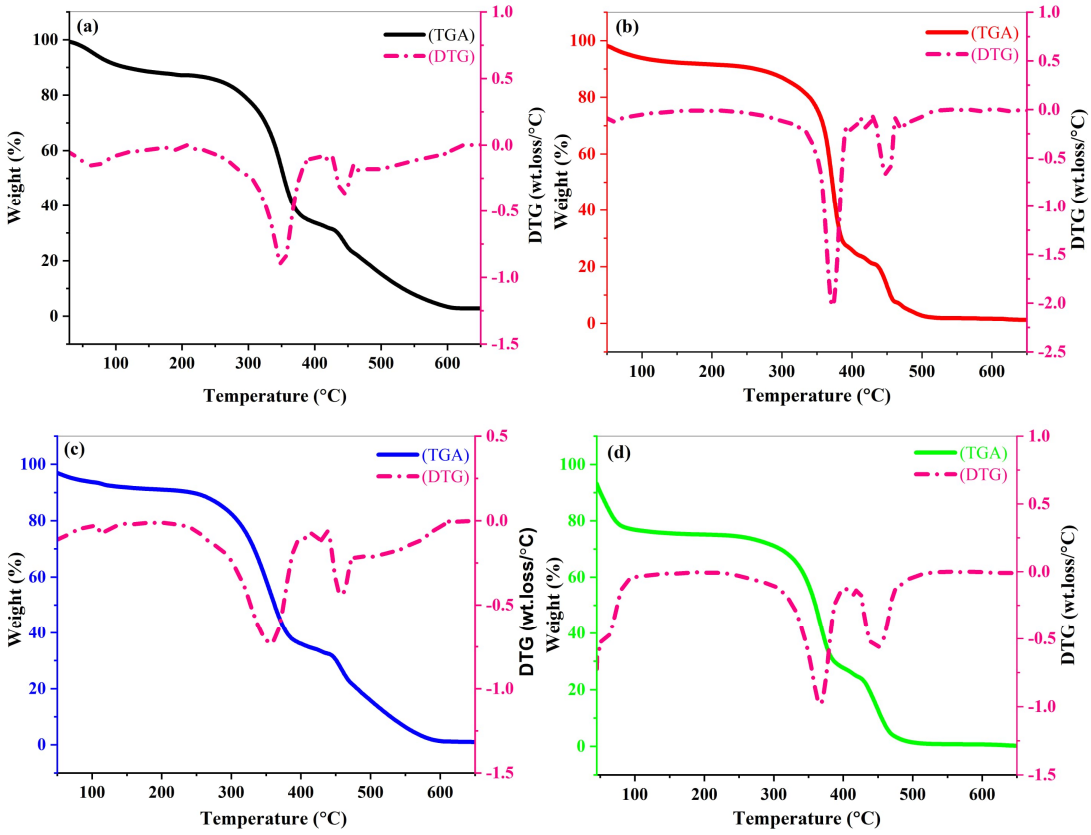

Figure 46. TGA and DTG graphs of (a) raw, (b) dewaxed, (c) alkalized and (d) bleached fibers

The moisture absorption of the fibers varied depending on the treatment applied. The weight loss due to moisture evaporation was 11.36% for raw fibers, 7.51% for dewaxed fibers, 7.44% for alkalized fibers, and 23.5% for bleached fibers. In the first stage, raw fibers exhibited higher weight loss compared to dewaxed and alkalized fibers, which can be attributed to the presence of extractives and higher moisture content. After the removal of extractives and hemicellulose—components responsible for moisture absorption—the weight loss was reduced. Conversely, bleached fibers demonstrated the highest weight loss percentage due to their enhanced moisture absorption properties following the removal of lignin, which is naturally hydrophobic (Begum et al., 2021).

The thermal stability of the fibers varied with different treatments, measuring 179 °C for raw fibers, 205 °C for dewaxed fibers, 250 °C for alkalized fibers, and 269 °C for bleached fibers. Each extraction step contributed to an enhancement in thermal stability, attributed to the retention and improvement of structural order and a reduction in amorphous content (Saravanakumar et al., 2014).

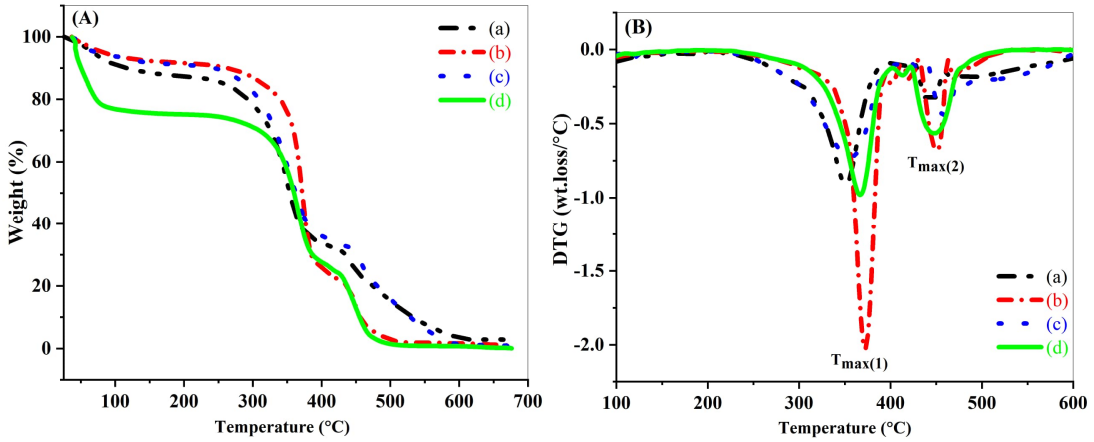

Figure 47. (A) TGA and (B) DTG merged graphs of (a) raw, (b) dewaxed, (c) alkalized and (d) bleached fibers

The weight loss percentages observed during the second step of degradation in thermogravimetric analysis (TGA) highlight the significant impact of various chemical treatments on the thermal stability of fibers. The results indicate that dewaxed fibers exhibited the highest weight loss of 70.45%, followed by raw fibers weight loss of 56.26%. In contrast, alkalized fibers showed a weight loss of 57.20%, while bleached fibers had the lowest weight loss of 49.89%.

Table 26. Thermo–gravimetric analysis of fibers at different extraction steps

Sample	1st Stage		2nd Stage		3rd Stage		Ash (%)
	T (°C)	wt. loss (%)	T (°C)	wt. loss (%)	T (°C)	wt. loss (%)	
Raw fiber	26–145	11.36	179–426	56.26	426–609	28.46	3.00
Dewaxed fiber	37–139	7.51	205–438	70.45	430–510	18.79	2.25
Alkalized fiber	38–121	7.44	250–440	57.20	440–591	30.69	1.72
Bleached fiber	37–110	23.50	269–427	49.89	427–510	22.55	1.13

The elevated weight loss in dewaxed fibers can be attributed to the removal of waxes and other hydrophobic components, which may initially contribute to moisture retention. Once these materials are eliminated, the fibers become more susceptible to thermal degradation. The significant reduction in thermal stability in dewaxed fibers suggests that the treatment enhances the exposure of more thermally labile components, such as hemicellulose and amorphous regions of cellulose, leading to increased degradation (Martin et al., 2013). This is also reflected in a higher weight loss rate observed in the DTG graph. However, it decreased after alkalization and bleaching processes due to the removal of hemicellulose,

lignin and improved the structural order of disordered regions of cellulose (Poletto et al., 2015).

Table 27. TGA and DTG analysis of fibers at different extraction steps

Sample	2nd Stage			3rd Stage		
	T_{onset} (°C)	T_{max} (°C)	T_{endset} (°C)	T_{onset} (°C)	T_{max} (°C)	T_{endset} (°C)
Raw fiber	179	351	426	426	444	609
Dewaxed fiber	205	371	438	430	450	510
Alkalized fiber	250	356	440	440	458	591
Bleached fiber	269	367	427	427	447	510

The thermal degradation characteristics among raw, dewaxed, alkalized, and bleached fibers can be effectively analyzed through the peak temperatures observed in the DTG (Derivative Thermogravimetric) graph show in **Figure 47 (B)**. The data reveals distinct patterns highlighting how various treatments impact the peak thermal degradation temperature. Dewaxed and alkalized fibers exhibit high peak decomposition temperatures 450 °C and 458 °C, respectively. Attributed to their ordered cellulose structure and the presence of thermally stable lignin. However, after bleaching, there is a reduction in peak decomposition temperature due to the removal of lignin. Finally, the residues correspond to the ash content decreased during the extraction steps as a result of non–cellulosic matter removal which is responsible for ash content (Angelini et al., 2015; Jankauskienė et al., 2015).

4.7.2. Thermal analysis of MC and CNC samples

The thermal properties of the RF, MC and CNC samples were investigated via thermogravimetric methods. The TGA/DTG/DTA patterns of all the samples are shown in **Figure 48**–**Figure 50** and the analyzed TGA data are summarized in **Table 28**. For the raw fibers, thermal decomposition occurred in three main steps. This phenomenon can be found in other reports related to lignocellulosic materials (NM Nurazzi et al., 2021). The first weight loss, recorded below 200 °C, corresponds to the evaporation of absorbed moisture. The second weight loss, which occurs above 180 °C until approximately 375 °C, resulted mainly from the thermal decomposition of hemicelluloses and some portion of lignin.

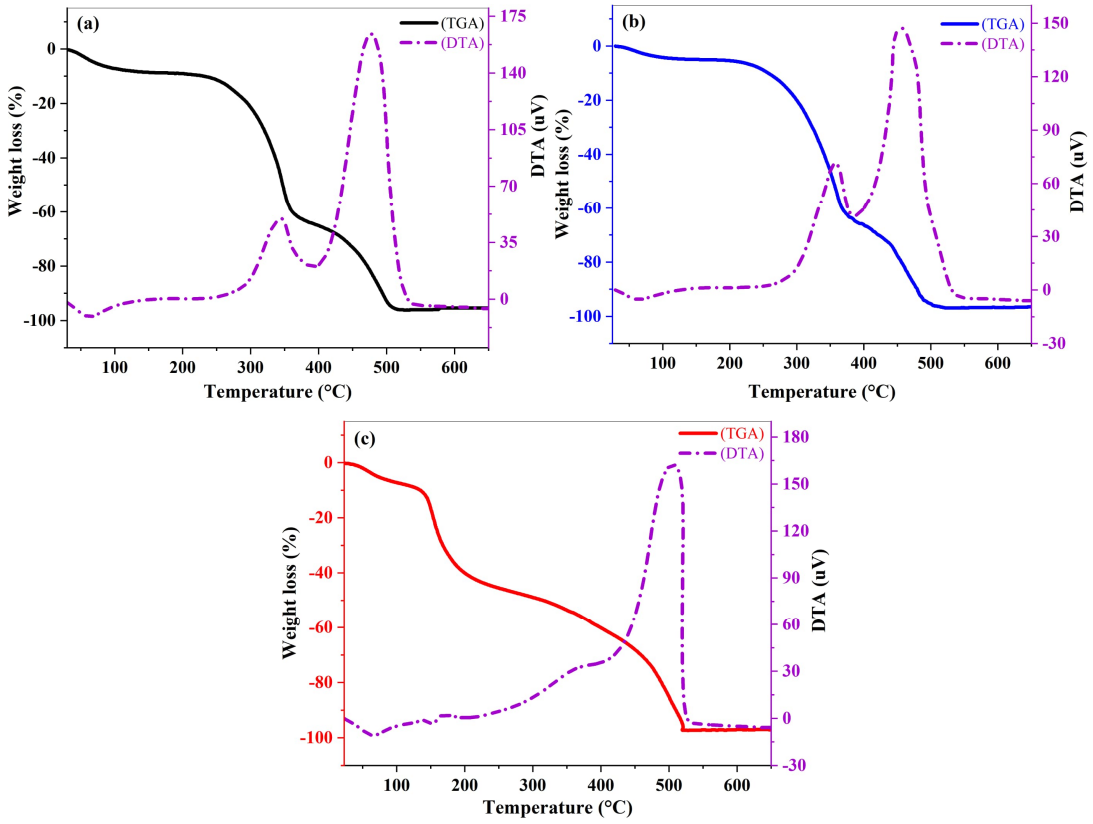

Figure 48. TGA and DTA curves of the (a) RF (b) MC and (c) CNC samples

The last stage in the high–temperature range (375 °C –517 °C) is associated with the degradation of cellulose and lignin. In this temperature range, almost all the cellulose components decomposed. However, lignin is the most difficult to decompose because of the presence of phenyl groups, and its decomposition extends to the whole temperature range, starting below 200 °C and continuing to increase to 700 °C (NM Nurazzi et al., 2021).

Table 28. TGA analysis results of RF, MC and CNC samples

Samples	1st Sage		2nd Stage		3rd Stage		Residual
	Temp (°C)	Wt. loss (%)	Temp (°C)	Wt. loss (%)	Temp (°C)	Wt. loss (%)	Wt. (%)
RF	30–180	8.40	180–375	54.08	375–517	33.02	4.50
MC	30–200	4.94	200–370	55.52	370–520	35.65	3.65
CNC	30–124	8.20	124–256	37.43	256–520	50.44	3.98

Similarly, the degradation of MC was a three–step process. A minor weight loss at approximately 200 °C corresponds to moisture loss by evaporation. The second decomposition stage at a temperature of 200–370 °C is related to amorphous cellulose, and

the third decomposition stage at a temperature of 370–520 °C corresponds to crystalline cellulose. Typically, the CNC sample exhibited three main degradation stages. The first stage involves the loss of moisture content below 124 °C. The second stage involves the degradation of the amorphous regions of cellulose at a temperature of 124–256 °C, which can be attributed to the breaking of glycosidic bonds of amorphous cellulose, sulfate half ester groups and large specific surface area of CNC chains. The third stage involves the thermal degradation of the interior non–sulfated and large crystallite size nano cellulose crystals at a temperature of 256–520 °C (Borsoi et al., 2016b).

Table 29. TGA/DTG analysis results of RF, MC and CNC samples

Samples	2nd Stage			3rd Stage		
	T_{onset} (°C)	T_{peak} (°C)	T_{endset} (°C)	T_{onset} (°C)	T_{peak} (°C)	T_{endset}(°C)
RF	180	344	375	375	494	517
MC	200	355	370	370	481	520
CNC	124	155	256	256	515	520

From the summarized results shown in **Table 29,** the onset degradation temperature, decomposition temperature range, weight loss (%) and peak decomposition temperature of the samples are different due to the difference in type, structure, size and content of chemical compositions present in the samples. The onset degradation temperatures of the RF, MC and CNC samples are at 180 °C, 200 °C and 124 °C, respectively. The results showed that the onset degradation temperature of the MC sample was higher than that of the RF and CNC samples due to the removal of non–cellulosic components. However, the lowest onset decomposition temperature of the CNCs sample exhibited might be associated with the introduction of the negatively charged sulfate half ester groups, larger number of free ends of chains, smaller size and larger specific surface area of CNCs. These factors lead to faster heat transfer and lower activation energy (Roman et al., 2004; W. Chen et al., 2011). This condition was also observed in MCs and CNCs extracted from different sources, such as teff straw (207 °C and 134 °C), enset fiber (210 °C and 133 °C), sugarcane bagasse (199 °C and 139 °C), coffee hull (282 °C and 134 °C), and commercial cellulose (268 °C and 142 °C), respectively.

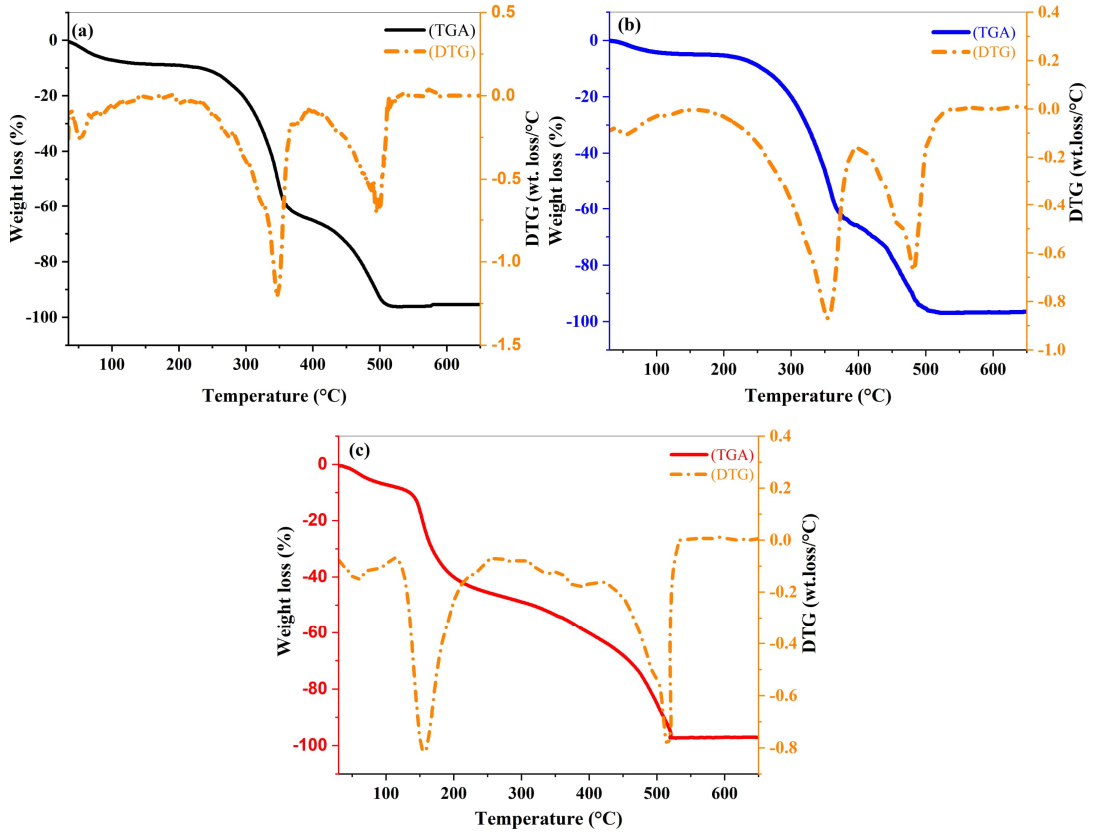

Figure 49. TGA and DTG curves of the (a) RF (b) MC and (c) CNC samples

The maximum weight loss more than 50% of the weight of the RF and MC samples decomposed during the second stage of degradation at 180 °C –375 °C and 200 °C –370 °C, respectively. However, for the CNC sample a maximum weight loss more than half of its weight was observed during the third stage decomposition at a wider range of temperature from 256 °C –520 °C. The peak decomposition temperatures at the second degradation step were 344°C, 355 °C and155 °C, similarly at the third degradation step were 494 °C, 481°C and 515 °C, for the RF, MC and CNC samples respectively.

The results indicated that the peak decomposition temperature at the third stage for CNCs was higher than that for RF and MC samples due to the greater crystallite size (Poletto et al., 2012). However, it was lowest at the second step of degradation, due to the negatively charged sulfate half ester groups, larger number of free ends of chains, smaller size and larger specific surface area of CNCs. These factors lead to faster heat transfer and lower activation energy (W. Chen et al., 2011). The reported peak decomposition temperatures for raw fibers, micro cellulose and nanocellulose extracted from different sources were coconut husk fiber (368 °C, 389 °C and 322 °C), Nypa fruticans trunk (361°C, 400 °C and 207 °C) and rice

husk (375 °C, 370 °C and 286 °C), respectively (Nang An et al., 2020). At the end of the pyrolysis process, the residue remaining at 600 °C–800 °C depends on the lignocellulosic resources and their forms (raw fiber, micro cellulose and nanocellulose) (Nang An et al., 2020).

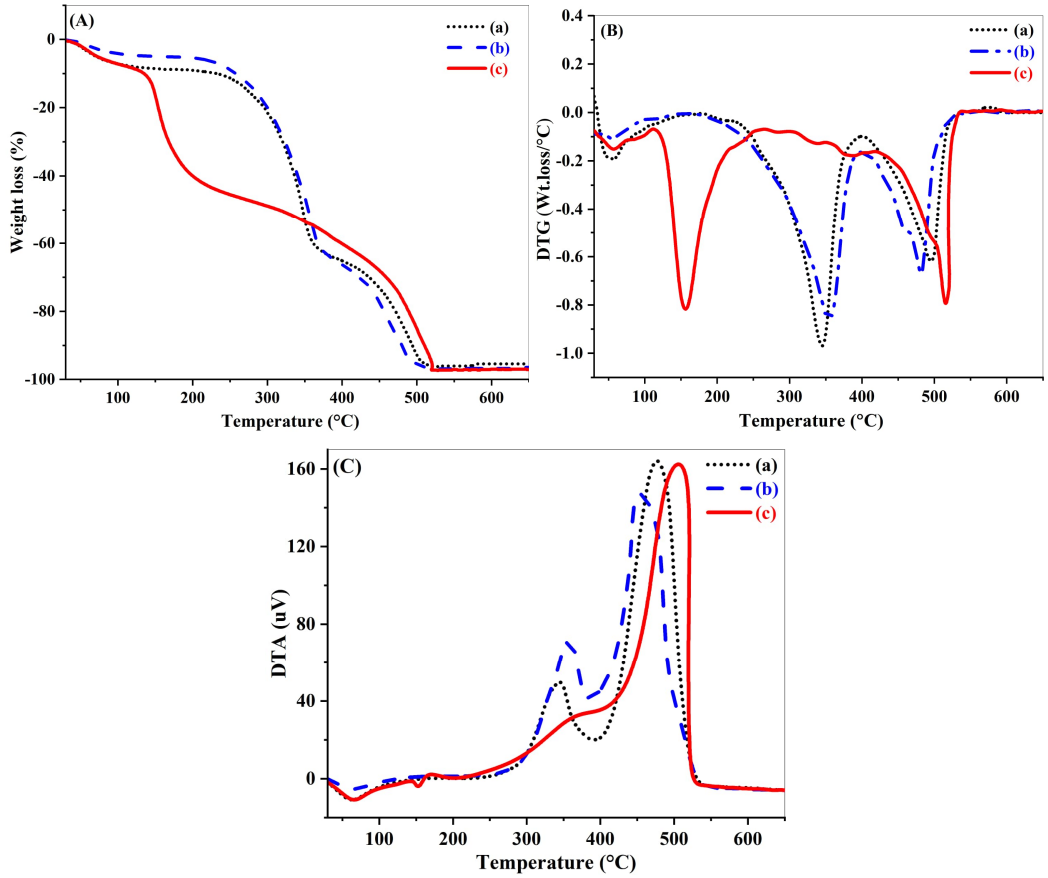

Figure 50. (A)TGA (B) DTG and (C) DTA curves of the (a) RF (b) MC and (c) CNC samples

The final residue weights (%) at 600°C–800 °C for the RF, MC and CNC samples were 4.50%, 3.65% and 3.98%, respectively. The relatively greater residue of RF compared to that of MC and CNC is due to the presence of more ash in the raw fibers (Maheswari et al., 2012). However, the slight increase in residue (%) for the CNC sample compared to the MC sample is due to a dehydration effect of the sulfate group as flame retardants (Gabriel, Shibeshi, et al., 2022). In general, the residue weights of all the samples were relatively small compared to those in the reported studies of raw fibers, micro cellulose and nanocellulose extracted from different sources, namely, nypa fruticans trunks (30.9%, 11.9% and 25.9%), rice husks (29.2%, 17.7% and 21.1%) and coconut husk fibers (23.7%, 11.9% and 13.9%), respectively (Maheswari et al., 2012; Nang An et al., 2020). The low residue indicates the

effective removal of the non–cellulosic components, as well as a low percentage of these constituents present in the raw fiber (Romruen et al., 2022).

4.7.3. Thermal analysis of Bio nanocomposites samples

The thermal decomposition of neat PLA and the derived nanocomposites (PLA/CNC1%, PLA/CNC3% and PLA/CNC5%) was examined via thermogravimetric analysis (TGA) and derivative thermogravimetry (DTG) curves, as shown in **Figure 51** and **Figure 52**.

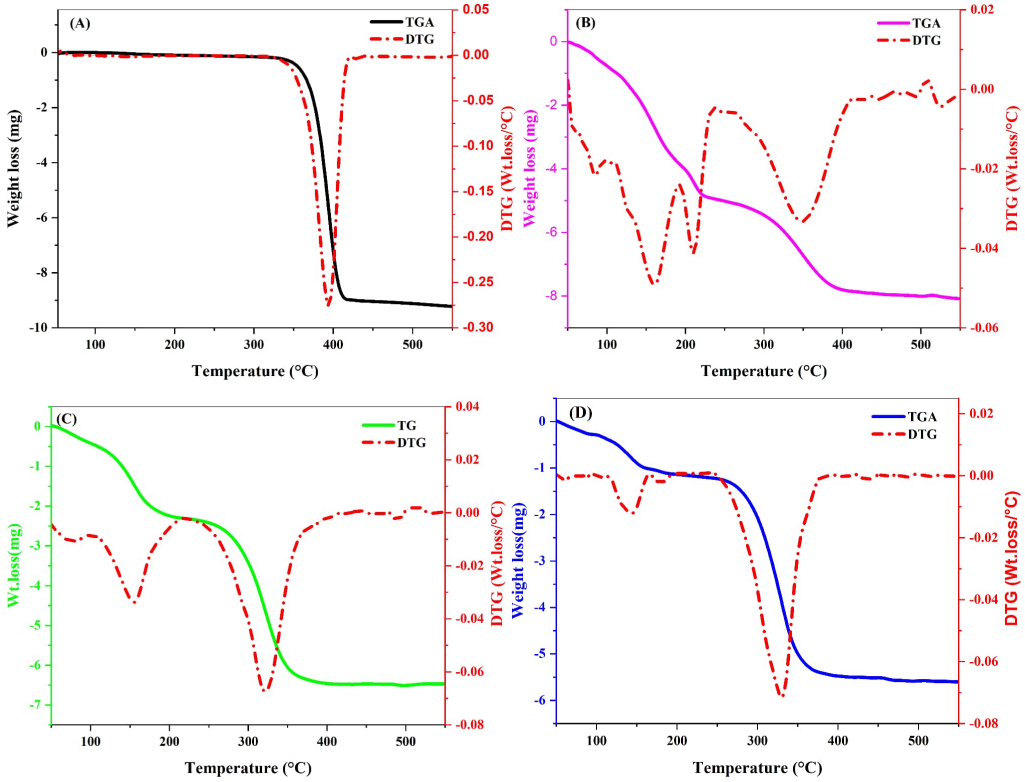

Figure 51. TGA and DTG graphs of (A) neat PLA (B) PLA/CNC1% (C) PLA/CNC3% and (D) PLA/CNC5%

The results obtained from the TGA and DTG graphs are summarized in **Table 30**. The neat PLA showed a single–step degradation peak, and this degradation behavior was similar to previously reported values (Faraj et al., 2021). However, the composite samples, with the exception of PLA/CNC1%, exhibited two–step degradation (Faraj et al., 2021). The PLA/CNC1% sample presented one extra small degradation peak at approximately 200 °C, which contributed to a 9.3% weight loss. This may be due to phase separation resulting from poor compatibility. This means that regions with higher CNC contents might decompose at a different rate than regions with higher PLA contents (Bhiogade et al., 2021).

The small peak shown in the composite samples below 100 °C is related to evaporation of the absorbed moisture. A slight weight loss is observed between 100 and 200 °C in all the composite samples due to the dehydration of ethylene glycol and the breaking of the glycosidic bonds of the amorphous CNCs (X. Jiang et al., 2004; D'Acierno et al., 2020). Compared with PLA, the composites exhibit greater weight loss during the first step of degradation due to the hygroscopic nature of the composites after incorporation of the plasticizer and hydrophilic CNCs. In addition, strong weight loss occurred during the third step of degradation for all the samples from 248–424 °C, which was probably related to the degradation of the PLA and CNCs. The onset decomposition temperatures of PLA, PLA/CNC1%, PLA/CNC3% and PLA/CNC5% are 320, 257, 248 and 248 °C, respectively.

Table 30. TGA and DTG analysis results of neat PLA and its nanocomposites

Sample	T_{onset} (°C)	T_{peak} (°C)	T_{endset} (°C)	Wt. Loss (%)			Residue (%)
				1st Step	2nd Step	3rd Step	
PLA	320	394	424	89.6	–	--	10.40
PLA/CNC1%	257	341	408	38.5	9.3	30.3	21.9
PLA/CNC3%	248	321	381	24.9	–	39.4	35.7
PLA/CNC5%	248	329	382	12.4	–	42	45.6

Moreover, the DTG curves show a decrease in the maximum degradation temperature of the composites compared with that of pure PLA. The maximum degradation temperatures for PLA, PLA/CNC1%, PLA/CNC3% and PLA/CNC5% occurred at 394, 341, 321 and 329 °C, respectively. The thermal analysis results confirmed that CNCs do not significantly improve the thermal stability of PLA. The inferior thermal properties of the PLA–based composites have also been reported in different studies. This might be associated with the poor thermal stability of the plasticizer, which was added to improve the flexibility of the PLA and for better dispersion of the PLA matrix and CNC reinforcement (Bhiogade et al., 2021; Faraj et al., 2021). In addition, the introduction of negatively charged sulfate half ester groups resulted in a larger number of free ends of the chains, a smaller size and a larger specific surface area of the CNCs. These factors lead to faster heat transfer and lower activation energy (Roman et al., 2004; Bhiogade et al., 2021). Compared with those of the other composite samples, the relatively wide degradation temperature with a smooth transition curve is shown for PLA/CNC3%, which can be attributed to better hybridization of the composite reflected by a better interaction between 3% CNCs and PLA (N'gatta et al., 2022a). Compared with that of the PLA sample, the residue weight (%) of the composite

samples significantly increased. In addition, the TGA results clearly revealed that the residue weight (%) increased with increasing CNC content. This is due to the formation of carbonaceous residue (char) and the dehydration effect of the sulfate group as a flame retardant derived from the CNCs (Faraj et al., 2021; Gabriel, Belete, et al., 2022).

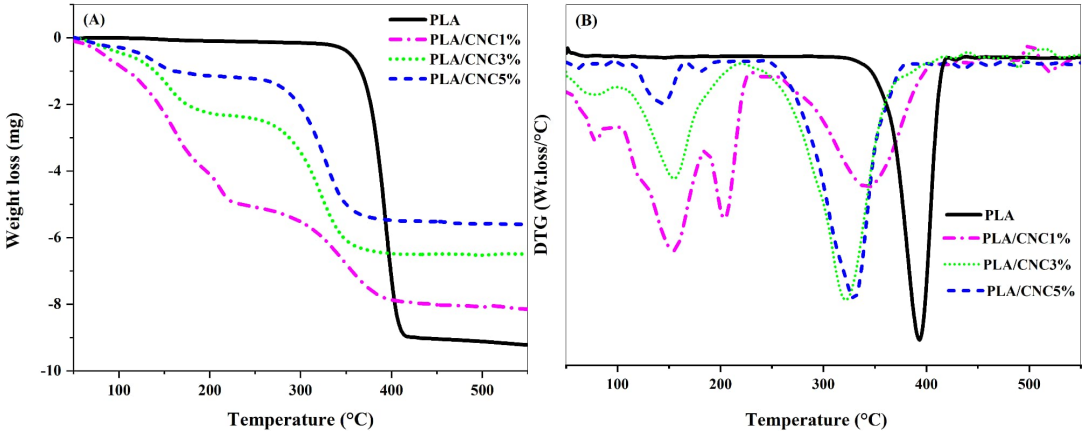

Figure 52. (A) TGA and (B) DTG curves of neat PLA and nanocomposite samples

Differential scanning calorimetry (DSC) analysis was performed to examine the thermal behavior of the PLA and PLA/CNC composite samples. In DSC thermograms, changes in the size and shape of the T_g and T_m curves indicate changes in the content of amorphous/crystalline components. Similarly, a peak shift to a lower temperature indicates easy movement of particles, and a peak shift to higher temperatures is related to difficulty in the movement of particles to plasticize and melt (Nurazzi et al., 2022). As shown in the DSC curves in **Figure 53**, all the samples revealed endothermic stage changes related to the glass transition, followed by melting.

The DSC analysis results of the neat PLA and nanocomposite samples are summarized in **Table 31**. Compared with those of neat PLA, the glass transition and melting peaks of the composite samples shift toward the lowest onset temperatures, as shown**.** This suggests that the addition of CNCs and plasticizers tends to decrease the change–of–state temperatures of PLA (N'gatta et al., 2022a). However, the peak T_g values of the composite samples were higher than those of the PLA sample. Furthermore, the glass transition and melting peak temperature ranges widened with increasing CNC loading. This suggests the nucleating effects of CNCs on the PLA matrix.

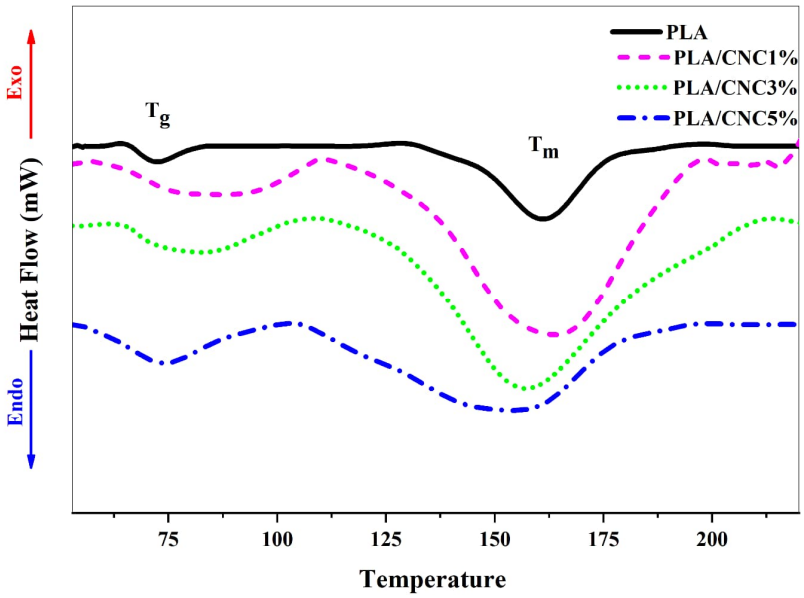

Figure 53. DSC curves of neat PLA and nanocomposite samples

However, at higher CNC contents, a reduction in the peak melting temperature was noted, possibly due to the presence of CNC agglomerates hindering polymer chain mobility (Murphy et al., 2018). Compared with PLA, the incorporation of 3% CNCs into the PLA matrix caused a wider glass transition and melting temperature and a high peak T_g temperature with a relatively close onset Tg temperature. This indicates a better interaction between CNCs and PLA and therefore could reflect good dispersion and good interfacial adhesion (Murphy et al., 2018; N'gatta et al., 2022a).

Table 31. DSC analysis results of neat PLA and nanocomposite samples

Sample	Glass transition temperature (T_g) (°C)			Melting temperature (T_m) (°C)			Heat of melting (ΔH_m) (J/g)	X_C (%)
	Onset	Peak	Endset	Onset	Peak	Endset		
PLA	64	72	82	130	161	190	36.03	38.49
PLA/CNC1%	57	84	110	110	163	199	49.32	59.20
PLA/CNC3%	61	82	108	108	157	200	58.33	71.63
PLA/CNC5%	54	74	104	104	154	214	40.59	51.01

Differential scanning calorimetry (DSC) analysis reveals significant insights into the crystallinity of pure polylactic acid (PLA) and its composites with varying concentrations of cellulose nanocrystals (CNCs). Pure PLA has a low degree of crystallinity at 38.49%, which aligns with its typically semi–crystalline nature and low degree of crystallization. However, the introduction of CNCs dramatically altered this behavior. For example, the crystallinity

of the PLA/CNC1% composite increases to 59.20%, highlighting the effective nucleating role of CNCs. This enhancement is indicative of the CNCs facilitating the organization of the PLA chains during the crystallization process, thereby improving the thermal and mechanical properties of the material. A further increase in the CNC content to 3% results in an even greater crystallinity of 71.63%, suggesting a saturation point where the presence of CNCs continues to promote crystallization. This higher degree of crystallinity could lead to significant improvements in tensile strength.

However, the trend shifts at 5% CNC, where the crystallinity decreases to 51.01%. This unexpected decrease may be attributed to the oversaturation of CNCs, leading to agglomeration and a decrease in the number of effective nucleation sites. Consequently, while CNCs enhance PLA crystallization up to a certain concentration, excessive amounts can hinder the mobility of PLA chains, impeding effective crystallization. These findings underscore the importance of optimizing the CNC content in PLA composites to achieve the desired structural, thermal and mechanical properties.

4.8. Rheological Property Analysis of MC and CNC Samples

The average intrinsic viscosity (η), molecular weight (M_W), and degree of polymerization (*DP*) of the obtained MC and CNC were investigated to determine the influence of the hydrolysis process on the cellulose chains. The measured and calculated values of η, M_W, and *DP* of the MC sample were 134 mL/g, 3.85×10^4 g/mol and 238, respectively. Similarly, the values for the CNC were 90 mL/g, 2.36×10^4 g/mol and 146, respectively.

These results show a significant decrease in viscosity, molecular weight and degree of polymerization during the preparation of CNC due to full or partial depolymerization of the cellulose chains by hydrolysis. Another study reported the average intrinsic viscosity and molecular weight of cellulose extracted from cotton linters and dissolved in 6 wt.% NaOH/4 wt.% urea aqueous solution with different concentrations, in the ranges of 112–332 mL/g and $3.22–12.86 \times 10^4$ g/mol, respectively (Jinping Zhou et al., 2004). Similarly, different reports investigated a decrease in *DP* from 219 to 144 and from 750 to 67.5 during the preparation of spherical nanocellulose from waste cotton fabrics (Xiong et al., 2012b) and cellulose nanofibers from curaua fibers (Corrêa et al., 2010), respectively.

4.9. Mechanical Property Analysis

4.9.1. Analysis of single fiber tensile properties

The effect of retting duration on tensile properties specifically the breaking force, breaking elongation and tenacity of the under retted, optimal retted and over retted fibers were tested as shown in **Table 32** and **Figure 54.**

Table 32. Summary of the average tensile properties of fibers at different retting durations

Samples	Breaking force (cN)	Elongation at Break (%)	Tenacity (cN/tex)
R_1	219.9 ±87	2.17 ±0.41	41.7 ± 5
R_2	278.4 ±67	2.06 ±0.39	59.1 ± 13
R_3	193.4 ±41	1.73 ±0.14	54.6 ± 2

The tensile properties of the fibers varied with degree of retting, measuring breaking force of 219.9 cN for under retted, 278.4 cN for optimal retted and 193.4 cN for over retted fibers. Similarly, tenacity of 41.7 cN/tex, 59.1 cN/tex and 54.6 cN/tex for under, optimal and over retted fibers, respectively.

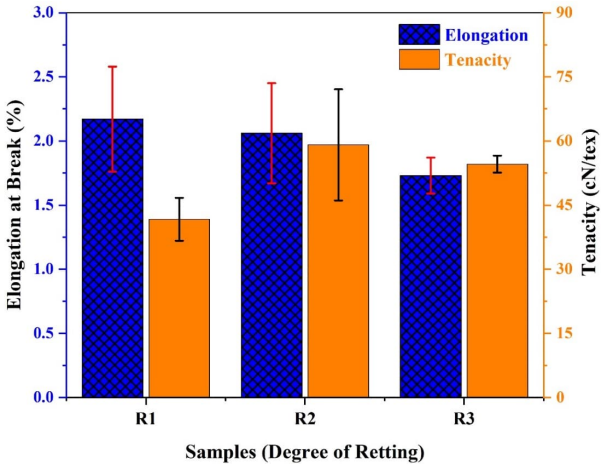

Figure 54. Effect of retting duration on fiber tensile properties

Initially, the mean breaking force and tenacity of a single fiber were enhanced due to the removal of a larger amount of weak substances such as pectin and other impurities, then the results were reduced with further increments of retting duration due to the cellulose component degradation results in the presence of more weak spots and reduction in diameter of the fibers (Sain et al., 2006; Marrot et al., 2013; Martin et al., 2013). Moreover, the mean elongation results of 2.17% for under, 2.06% for optimal and 1.73% for over retted fibers

were measured. The results showed that the mean elongation at break values decreased with an increasing degree of retting due to the removal of non–cellulosic components and this tends to fiber brittleness (N. Reddy et al., 2005; H. Yu et al., 2010).

4.9.2. Tensile property analysis of filament and 3D printed samples

The experimental results from **Figure 55** and **Figure 56** as summarized in **Table 33** highlight the mechanical properties and performance characteristics of different samples, including filament-based (F–PLA and F–PLA/CNC) and 3D printed (3DP–PLA and 3DP–PLA/CNC) samples.

Table 33. Tensile properties of PLA and PLA/CNC filaments and 3D printed samples

Samples	Tensile Strength (MPa)	Elongation (%)	Maximum Force (N)	Modulus (MPa)	Toughness (MJ/m^3)
F–PLA	20.76	4.85	40 ±	693.28	0.73
	±1.39	±0.70	3.53	± 20.59	±0.18
F–PLA/CNC3%	24.70	6.83	50	664.16	1.26
	±2.79	±1.40	± 7.07	±10.29	±0.37
3DP–PLA	23.75	4.09	1448	579.67	0.4
	±3.49	±0.85	± 128	± 129	±0.07
3DP–PLA/CNC3%	26.72	28.87	1605	287.55	7.28
	±3.41	±1.94	±207	±72	±0.15

[F] Filament and [3DP] 3D Printed sample

The coating of PLA/CNC3% to PLA filament resulted in improved tensile strength and elongation, while slightly decreasing modulus. F–PLA/CNC3% exhibited a higher tensile strength of 24.70 ± 2.79 MPa, representing an increase of approximately 18.96% compared to F–PLA (20.76 ± 1.39 MPa), indicating that PLA/CNC3% composite coating reinforces the filament by providing additional structural support at the microscopic level. This enhancement is accompanied by a significant increase in elongation, with F–PLA/CNC reaching 6.83 ± 1.40%, which is approximately 40.82% higher than F–PLA (4.85 ± 0.70%). This suggests better flexibility and reduced brittleness due to the presence of optimized CNC and EG. However, the modulus of F–PLA/CNC3% (664.16 ± 10.29 MPa) was slightly lower than that of F–PLA (693.28 ± 20.59 MPa), reflecting a trade-off between increased flexibility and reduced stiffness. It can be also observed that, the higher modulus was exhibited by the filaments compared to the 3D printed samples. This was probably related to the liquid filaments adhering to the solid layer surface, leading to poor entanglement of polymer molecules, due to the presence of interface voids in printed samples that acted as stress-concentrating sites, initiating cracks during the tensile test and the thermal degradation

of both PLA and CNC during printing. similar findings were also demonstrated by (Weng et al., 2016; N. D. Ahmad et al., 2023).

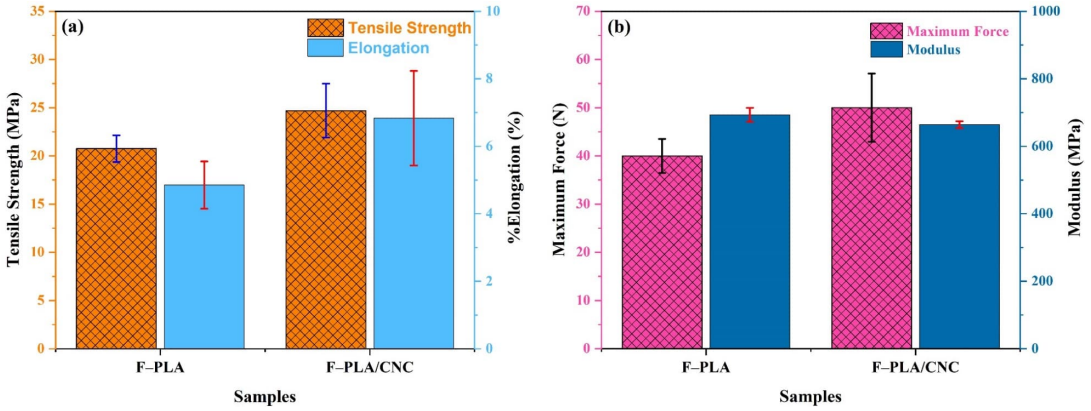

Figure 55. (a) Tensile strength and elongation (b) maximum force and modulus of F–PLA and F–PLA/CNC samples

The 3DP–PLA/CNC sample exhibits a tensile strength of 26.72 ± 3.41 MPa, which is approximately 12.50% higher than the 23.75 ± 3.49 MPa observed for the pure 3DP–PLA sample. This increase in tensile strength can be attributed to the reinforcing effect of CNC in the PLA matrix. The crystalline structure of CNC particles, along with their high aspect ratio, contributes to better interfacial bonding between the polymer chains, enhancing the overall strength of the composite. These results are consistent with previous research that indicates CNC can improve the tensile strength of PLA–based composites due to its reinforcing role (S. D. Kumar et al., 2020; N'gatta et al., 2022b; N. D. Ahmad et al., 2023). Furthermore, the maximum breaking force values corroborate the superior mechanical performance of 3DP–PLA/CNC. The maximum force for 3DP–PLA/CNC (1605 ± 207 N) exceeds that of the 3DP–PLA sample (1448 ± 128 N), further confirming that the CNC content enhances the material's ability to withstand applied loads. The addition of CNC likely leads to a more uniform distribution of forces across the material, preventing premature localized failure. In addition to tensile strength and maximum breaking force, the percentage elongation at break shows a significant improvement. The 3DP–PLA/CNC sample demonstrates an elongation of 28.87 ± 1.94%, which is a significant increase of compared to the 4.09 ± 0.85% seen in pure 3DP–PLA. This significant improvement in elongation suggests that the addition of optimized CNC3% contributes to the material's flexibility and ductility by reducing the inherent brittleness and rigidity of PLA (Daver et al., 2018b; Fernández-Santos et al., 2021).

While previous study has reported enhanced ductility by 20% increase in elongation at break at 1 wt.% CNC without improvement in tensile strength due to CNC agglomeration, the current study demonstrates simultaneous enhancement in both tensile strength and ductility. Similarly, the toughness results provide further evidence of the positive impact of CNC on the PLA matrix. The toughness of the 3DP–PLA/CNC sample (7.28 ± 0.15 J/m³) is significantly higher than that of 3DP–PLA (0.4 ± 0.07 J/m³).

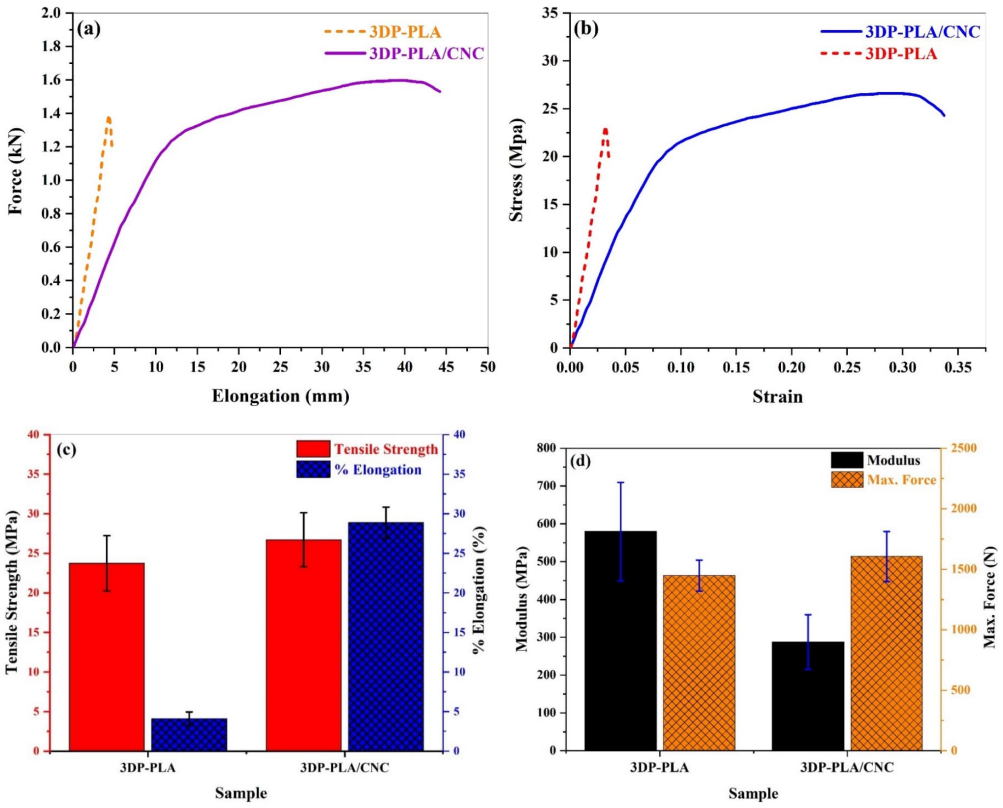

Figure 56. (a) force–elongation (b) stress–strain (c) tensile strength and elongation (d) modulus and maximum force of 3DP–PLA and 3DP–PLA/CNC samples

This significant increase indicates that the composite material is much more resistant to fracture and crack propagation. The enhanced toughness is attributed to the ability of CNC to improve the energy absorption capacity of the material. However, the addition of CNC3% decreased the modulus of 3DP–PLA (579.67 ± 129 MPa) to 3DP–PLA/CNC (287.55 ± 72 MPa), which is expected given the increased ductility and flexibility observed in the elongation data. Generally, when using nanocellulose in PLA-based composites, most studies reported improved tensile strength and elastic modulus but at the cost of elasticity. These results are consistent with other studies reported by (C. Gao et al., 2017; Daver et al., 2018b; Fernández-Santos et al., 2021).

In conclusion, the 3DP–PLA/CNC3% composite significantly improves mechanical properties, including tensile strength, percentage elongation, maximum breaking force, and toughness. While the modulus is reduced, the overall performance of the 3DP–PLA/CNC3% composite is enhanced, making it a promising material for applications that require a combination of strength, flexibility, and impact resistance with sustainability and biodegradability. This makes suitable for industries such as flexible protective packaging, flexible electronic devices, and biomedical devices.

4.10. Statistical Analysis and Optimization of Extraction process

4.10.1. Effect of process parameters on non-cellulosic components removal

The objective of the Taguchi design analysis was to optimize the treatment process by evaluating the effects of three key process parameters: chemical concentration (%), temperature (°C), and time (min), on the performance of dewaxing, alkalizing, and bleaching steps. Optimization was conducted using two key performance metrics, namely the signal-to-noise (S/N) ratio, which reflects the robustness of the process, and the mean, which indicates its overall effectiveness. The main effect plots and for S/N ratios and means are shown in **Figure 57** and **Figure 58**. The summarized results in **Table 34** and Table 35 indicate the ranks of each factor and the corresponding best levels for all treatment processes. From both the S/N ratio and means response tables, concentration (%) consistently emerged as the most significant factor, ranked first in both cases for all treatment processes.

The main effect plots and the response tables illustrate that concentration at level two for both cases and for the dewaxing and alkalizing processes shows best performance. However, it shows best performance at the third level for the bleaching process. Similarly, temperature (℃) ranked second at the third level in both cases for dewaxing and alkalizing processes. However, it ranked third and level two was found to be optimal for bleaching process. Moreover, time (min) ranked third in both cases for dewaxing and alkalizing processes at its highest level with small variations in mean values. However, it ranked as the second important factor for bleaching process.

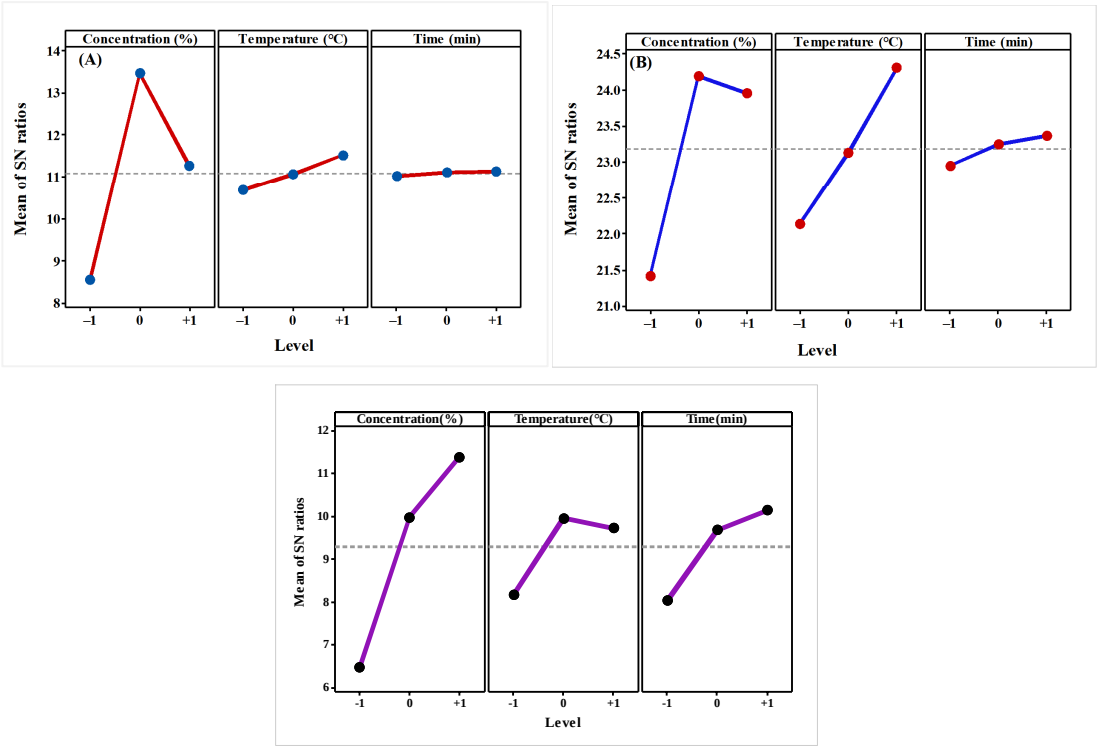

Figure 57. Main effect plots for S/N ratios of (A) dewaxing (B) alkalizing and (C) bleaching processes

Table 34. Response tables for S/N ratios

Level	Concentration (%)	Temperature (°C)	Time (min)
Dewaxing process			
1	8.552	10.683	11.026
2	13.456	11.067	11.112
3	11.264	11.522	11.134
Delta	4.904	0.838	0.108
Rank	1	2	3
Alkalization process			
1	21.42	22.13	22.95
2	24.19	23.13	23.25
3	23.96	24.30	23.36
Delta	2.78	2.17	0.41
Rank	1	2	3
Bleaching process			
1	6.482	8.166	8.029
2	9.980	9.961	9.681
3	11.387	9.722	10.139
Delta	4.906	1.795	2.110
Rank	1	3	2

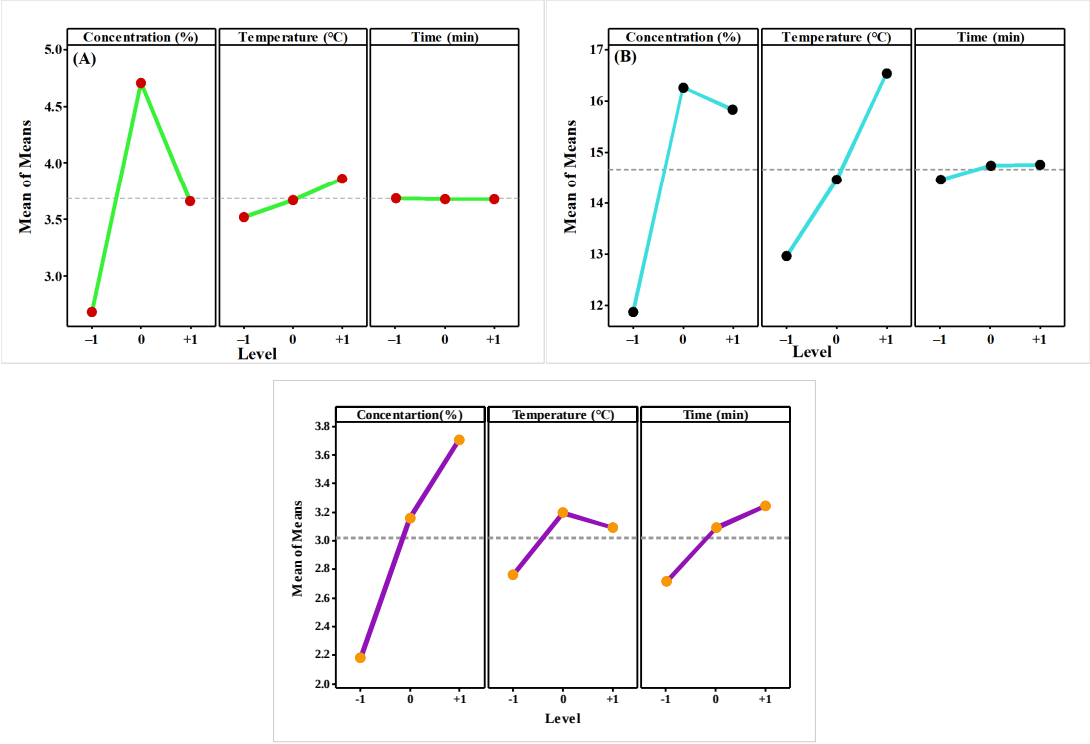

Figure 58. Main effect plots for means of (A) dewaxing (B) alkalizing and (C) bleaching processes

Table 35. Response tables for means

Level	Concentration (%)	Temperature (°C)	Time (min)
Dewaxing process			
1	2.680	3.520	3.690
2	4.710	3.670	3.680
3	3.660	3.860	3.680
Delta	2.030	0.340	0.010
Rank	1	2	3
Alkalization process			
1	11.87	12.97	14.47
2	16.27	14.47	14.73
3	15.83	16.53	14.77
Delta	4.40	3.57	0.30
Rank	1	2	3
Bleaching process			
1	2.180	2.760	2.713
2	3.160	3.197	3.090
3	3.710	3.093	3.247
Delta	1.530	0.437	0.533
Rank	1	3	2

4.10.2. Selection of optimum treatment conditions

From the main effect plots and the response table for S/N ratios and means it was observed that the predicted highest mean S/N ratio and mean for the dewaxing process is achieved

with concentration, temperature, and time set at medium (0), high (+1), and high (+1) levels, respectively. Therefore, the optimal process parameters for maximizing extractives removal in the dewaxing process using the Taguchi method are 75% concentration, 98°C temperature, and 480 minutes of time. Similarly, the predicted factor levels for the alkalization process are a medium concentration level (0), high temperature (+1), and high time (+1), corresponding to 6% concentration, 75°C temperature, and 90 minutes of time. Additionally, for the bleaching process, the predicted optimal combination is at high (+1) concentration, medium (0) temperature, and high (+1) time, represented by 10% concentration, 90°C temperature, and 120 minutes of time.

4.10.3. Regression analysis and modeling

To determine the influence of key process parameters on the removal of extractives, hemicellulose, and lignin from fibers, analysis of variance (ANOVA) was performed for each extraction stage. The effects of chemical concentration, temperature, and time were evaluated based on their statistical significance (p-values), contribution percentages, and model fit metrics (R^2, adjusted R^2, predicted R^2) as shown in Table

For the dewaxing process, the results indicate that concentration is by far the most influential factor in the dewaxing process, with a contribution of 97.25% and a highly significant p-value ($p = 0.000$). Temperature also had a statistically significant effect ($p = 0.001$), although with a much smaller contribution of 2.74%. Time, however, had no measurable impact ($p = 0.500$, 0% contribution). The model explains virtually all of the variation in the response, as reflected by an R^2 of 100%, adjusted R^2 of 99.99%, and predicted R^2 of 99.94%, confirming an excellent model fit and predictive capability. In the alkalization stage, concentration and temperature were again the two dominant factors, contributing 64.36% and 35.10% respectively, both with significant p-values ($p = 0.004$ and $p = 0.007$). Time was statistically insignificant ($p = 0.455$, 0.30% contribution), similar to the dewaxing process. The model demonstrated a strong fit with $R^2 = 99.75\%$, adjusted $R^2 = 99.01\%$, and predicted $R^2 = 94.99\%$, indicating robust predictability and reliability. These findings emphasize that hemicellulose removal is highly dependent on both concentration and temperature, with minimal effect from process duration.

Table 36. Analysis of variance (ANOVA)

Source	DF	Seq SS	Adj SS	Adj MS	F	P	Contribution (%)
Removal of extractive by dewaxing process							
Concentration(%)	2	6.18380	6.18380	3.09190	30919.00	0.000	97.25
Temperature (℃)	2	0.17420	0.17420	0.08710	871.00	0.001	2.74
Time (min)	2	0.00020	0.00020	0.00010	1.00	0.500	0.00
Residual Error	2	0.00020	0.00020	0.00010			0.00
Total	8	6.35840					100
		R^2	R^2 (adj)	R^2 (pred)			
Model Summary		100.00%	99.99%	99.94%			
Removal of hemicellulose by alkalization process							
Concentration(%)	2	35.2822	35.2822	17.6411	260.28	0.004	64.36
Temperature (℃)	2	19.2422	19.2422	9.6211	141.95	0.007	35.10
Time (min)	2	0.1622	0.1622	0.0811	1.20	0.455	0.30
Residual Error	2	0.1356	0.1356	0.0678			0.25
Total	8	54.8222					100
		R^2	R^2 (adj)	R^2 (pred)			
Model Summary		99.75%	99.01%	94.99%			
Removal of lignin by bleaching process							
Concentration (%)	2	3.6038	3.6038	1.80190	23.95	0.040	79.77
Temperature (℃)	2	0.3125	0.3125	0.15623	2.08	0.325	6.92
Time (min)	2	0.4509	0.4509	0.22543	3.00	0.250	9.98
Residual Error	2	0.1505	0.1505	0.07523			3.33
Total	8	4.5176					100
		R^2	R^2 (adj)	R^2 (pred)			
Model Summary		96.67%	86.68%	32.55%			

For the bleaching process, concentration remained the most significant parameter, contributing 79.77% to the total variance and a p-value just below the significance threshold ($p = 0.040$). Temperature and time, while showing moderate contributions (6.92% and 9.98%, respectively), were not statistically significant at the 95% confidence level ($p = 0.325$ and $p = 0.250$). The model's fit was acceptable with an R^2 of 96.67%, but the adjusted R^2 (86.68%) and especially the predicted R^2 (32.55%) suggest a reduced ability to generalize predictions for unseen data. This may indicate potential variability or noise in the bleaching process not captured by the current model. The significant p–values and high contributions indicate that the independent variables effectively explain the variability in the dependent variables, supporting the model's validity in the study (Gould et al., 2020).

Based on the multiple linear regression model chosen to fit the data, the relations between the non–cellulosic components percentage removal specifically, hemicellulose removal (HR), extractives removal (ER) and lignin removal (LR), and the three selected independent

variables; concentration, temperature and time (X_1, X_2 and X_3), respectively at their low (l), medium (m) and high (h) levels with the regression coefficients (β_0, β_1, β_2 and β_3) are indicated in **Eq. (22–24).**

$$\begin{aligned}\text{ER}(\%) = {} & 3.683 - 1.003X_1(\text{l}) + 1.026X_1(\text{m}) - 0.023X_1(\text{h}) - 0.163X_2(\text{l}) - 0.013X_2(\text{m}) \\ & + 0.176X_2(\text{h}) + 0.006X_3(\text{l}) - 0.003X_3(\text{m}) - 0.003X_3(\text{h})\end{aligned} \quad \text{Eq. (22)}$$

$$\begin{aligned}\text{HR}(\%) = {} & 14.655 - 2.789X_1(\text{l}) + 1.611X_1(\text{m}) + 1.178X_1(\text{h}) - 1.689X_2(\text{l}) - 0.189X_2(\text{m}) \\ & + 1.878X_2(\text{h}) - 0.189X_3(\text{l}) + 0.078X_3(\text{m}) + 0.111X_3(\text{h})\end{aligned} \quad \text{Eq. (l3)}$$

$$\begin{aligned}\text{LR}(\%) = {} & 3.0167 - 0.837X_1(\text{l}) + 0.143X_1(\text{m}) + 0.693X_1(\text{h}) - 0.257X_2(\text{l}) + 0.180X_2(\text{m}) \\ & + 0.077X_2(\text{h}) - 0.303X_3(\text{l}) + 0.073X_3(\text{m}) + 0.230X_3(\text{h})\end{aligned} \quad \text{Eq. (24)}$$

To assess the accuracy and predictive performance of the Taguchi-based models, experimental responses were compared against predicted values across all nine experimental runs for extractive, hemicellulose, and lignin removal as shown in **Table 37**. Each test condition was defined by varying levels of chemical concentration, temperature, and time, coded as –1 (low), 0 (medium), and +1 (high). The corresponding predicted values were calculated using regression models derived from the Taguchi design, with associated 95% confidence intervals (CI) and prediction intervals (PI) to account for variability and model uncertainty.

For the extractives removal, predicted values closely matched the experimental results for all nine runs, with all experimental values falling within their respective 95% confidence and prediction intervals, demonstrating a strong fit between the model and observed data. This close agreement is further supported by a very low standard error (SE = 0.008), indicating minimal variability and high precision in the model's predictions. The model's accuracy across a wide range of parameter combinations confirms its reliability for predicting extractive removal under varying conditions.

For hemicellulose removal, the predicted and experimental values also showed strong alignment across all conditions. All experimental values lay comfortably within their associated confidence and prediction intervals, suggesting that the model captured both central tendency and variability effectively. The standard error remained relatively low (SE = 0.229), and no significant deviation was observed between actual and predicted responses. These findings validate the model’s robustness in forecasting hemicellulose removal performance under different parameter levels.

Although the predicted values for lignin removal generally followed the experimental trends, slightly greater variation was observed compared to the other responses. The standard error

was higher (SE = 0.241), and the confidence and prediction intervals were wider, reflecting increased variability in lignin removal outcomes. Nonetheless, all experimental results remained within the prediction intervals, indicating acceptable model performance despite the broader uncertainty. This suggests that while the model provides a reasonable approximation, lignin removal is likely more sensitive to uncontrolled or unmodeled factors. A confirmation test was conducted to validate the optimal process parameters identified through Taguchi analysis for extractive removal (ER), hemicellulose removal (HR), and lignin removal (LR). The optimal combinations of factor levels were not part of the original L_9 experimental runs and were therefore tested separately to assess the accuracy and predictive capability of the model (Rudrapati et al., 2023). As summarized in **Table 38**, the experimental results were compared against the predicted mean values using both 95% confidence intervals (CI) and 95% prediction intervals (PI). The results for all three responses (ER%, HR% and LR%), fell within both their respective confidence and prediction intervals. This confirms that the experimental outcomes are statistically consistent with the predicted values and fall within the range of expected variability, validating the robustness and reliability of the optimization model (Francis et al., 2024). The statistical agreement between predicted and experimental values highlights the effectiveness of the selected optimal process parameters. Moreover, the narrow confidence and prediction bounds, particularly for extractive and hemicellulose removal, indicate strong model precision and low process variability. These findings confirm that the optimized conditions can be confidently applied to achieve consistent and efficient non-cellulosic constituents removal (Murray-Smith, 2015).

Table 37. Comparison of experimental and predicted responses

Run	Variables			Responses				
	Concentration (%)	**Temperature (°C)**	**Time (min)**	**EXP**	**PRED**	**95% CI**	**95% PI**	**SE**
Extractives Removal (%)								
1	–1	–1	–1	2.52	2.523	(2.485, 2.561)	(2.465, 2.580)	
2	–1	0	0	2.67	2.663	(2.625, 2.701)	(2.605, 2.720)	
3	–1	+1	+1	2.85	2.853	(2.815, 2.891)	(2.795, 2.910)	
4	0	–1	0	4.54	4.543	(4.505, 4.581)	(4.485, 4.600)	
5	0	0	+1	4.69	4.693	(4.655, 4.731)	(4.635, 4.750)	0.008
6	0	+1	–1	4.90	4.893	(4.855, 4.931)	(4.835, 4.950)	
7	+1	–1	+1	3.50	3.493	(3.455, 3.531)	(3.435, 3.550)	
8	+1	0	–1	3.65	3.653	(3.615, 3.691)	(3.595, 3.710)	
9	+1	+1	0	3.83	3.833	(3.795, 3.871)	(3.775, 3.890)	
Hemicellulose Removal (%)								
1	–1	–1	–1	10.0	9.988	(9.001, 10.976)	(8.4953, 11.482)	
2	–1	0	0	11.9	11.755	(10.767, 12.743)	(10.262, 13.249)	
3	–1	+1	+1	13.7	13.855	(12.867, 14.843)	(12.362, 15.349)	
4	0	–1	0	14.5	14.6556	(13.667, 15.643)	(13.162, 16.149)	0.229
5	0	0	+1	16.2	16.1889	(15.201, 17.176)	(14.695, 17.682)	
6	0	+1	–1	18.1	17.9556	(16.967, 18.94)	(16.462, 19.449)	
7	+1	–1	+1	14.4	14.2556	(13.267, 15.243)	(12.762, 15.749)	
8	+1	0	–1	15.3	15.4556	(14.467, 16.443)	(13.962, 16.949)	

9	+1	+1	0	17.8	17.7889	(16.801, 18.776)	(16.295, 19.282)	
Lignin Removal (%)								
1	–1	–1	–1	1.45	1.622	(0.579, 2.660)	(0.04, 3.193)	
2	–1	0	0	2.46	2.433	(1.392, 3.474)	(0.859, 4.006)	
3	–1	+1	+1	2.63	2.486	(1.445, 3.527)	(0.913, 4.060)	
4	0	–1	0	3.12	2.976	(1.935, 4.017)	(1.403, 4.550)	
5	0	0	+1	3.40	3.570	(2.529, 4.610)	(1.996, 5.143)	0.241
6	0	+1	–1	2.96	2.933	(1.892, 3.974)	(1.359, 4.506)	
7	+1	–1	+1	3.71	3.683	(2.642, 4.724)	(2.109, 5.256)	
8	+1	0	–1	3.73	3.586	(2.545, 4.627)	(2.013, 5.160)	
9	+1	+1	0	3.69	3.860	(2.819, 4.900)	(2.286, 5.433)	

$^{-1}$low level, ^{0}medium level, $^{+1}$high level, ^{EXP}experimental, ^{PRED}predicted, ^{SE}standard error, ^{CI}confidence interval and ^{PI}prediction interval

Table 38. Conformation test results for optimal extraction process parameters

Extraction Process	**Factors and levels**			**Mean responses**				**SE**
	Concentration (%)	**Temperature (℃)**	**Time (min)**	**PRD**	**EXP**	**95% CI**	**95% PI**	
ER (%)	0	+1	+1	4.88	4.90	(4.845, 4.921)	(4.825, 4.940)	0.008
HR (%)	0	+1	+1	18.22	19.41	(17.267, 19.243)	(16.762, 19.749)	0.229
LR (%)	+1	0	+1	4.12	4.63	(3.079, 5.160)	(2.546, 5.693)	0.241

4.11.Statistical Analysis of Significant Difference in Means

4.11.1. Significant difference in mean tensile properties of fibers

The retting duration is categorized into three groups: under–retted, optimally–retted, and over–retted. The tensile and physical properties of the fibers from these categories were analyzed. One–way ANOVA and Welch's tests, complemented by Games–Howell post hoc tests and box plots, effectively assessed mean differences across multiple sample groups (Hess et al., 2018), as illustrated in **Figure 59** and **Figure 60**.

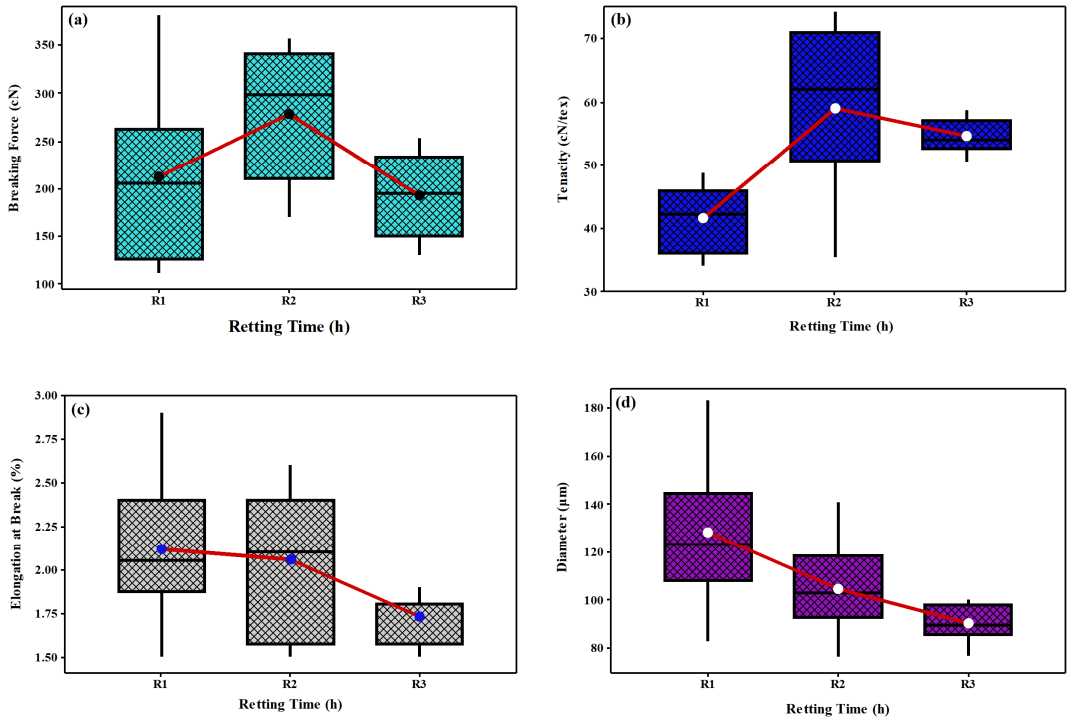

Figure 59. Box chart of fiber properties for different retting durations

Welch's test is a statistical method used to determine whether there are significant differences between the means of two groups, particularly when the groups have unequal variances (Ahad et al., 2014). It serves as an alternative to the traditional T–test and is part of the broader category of T–tests (West, 2021). The p–values obtained from Welch's tests for breaking force (0.014), tenacity (0.000), elongation at break (0.013), and diameter (0.001) indicate significant differences in the means across the different sample groups. A p–value less than 0.05 provides strong evidence against the null hypothesis, suggesting that at least one group mean differs from the others (Andrade, 2019).

The Games–Howell simultaneous tests offered further insights into specific group differences. The plots revealed intervals that do not contain zero, indicating significant differences between the means of certain pairs (Agbangba et al., 2024). **Figure 60 (a–d)** illustrates the presence of mean differences between the optimal and over–retted pairs in the breaking force test. Similarly, mean differences were observed for tenacity between the optimal and under–retted pairs, as well as between the over–retted and under–retted pairs. Additionally, significant differences in means were found for elongation at break between the over–retted and under–retted pairs, and between the over–retted and optimally–retted pairs. Finally, almost all selected sample groups for diameter measurement exhibited significant differences in means at 95% confidence intervals.

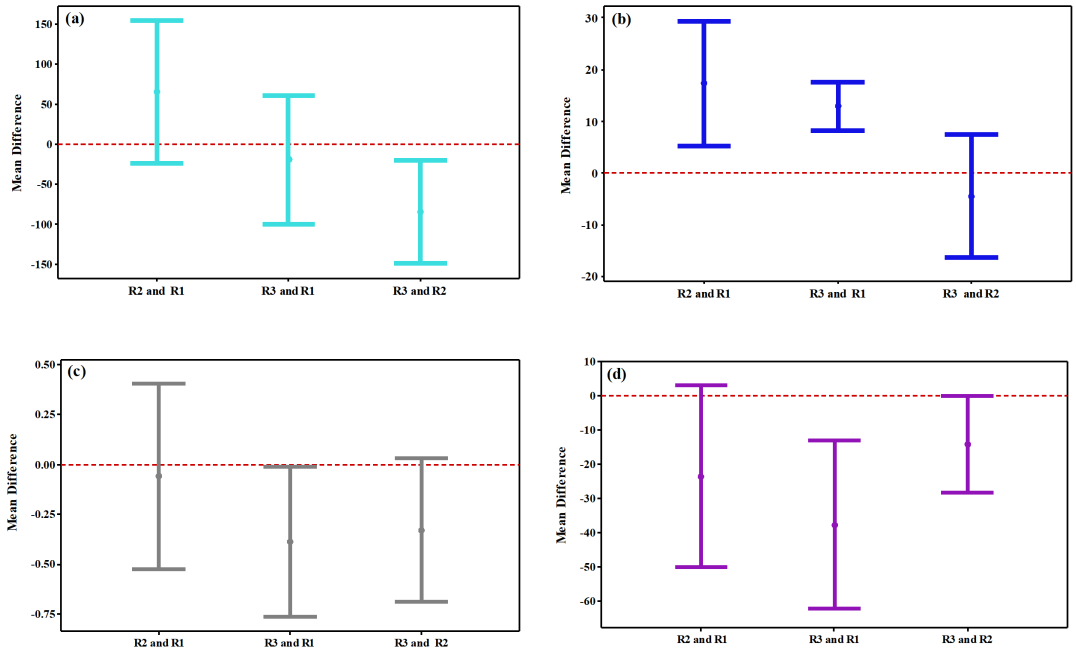

Figure 60. Mean difference plots of (a) breaking force, (b) tenacity, (c) elongation at beark and (d) diameter for different retting durations

The box plots corresponding to each measurement provide a visual representation of the data distribution and the significant differences identified through statistical testing, as shown in **Figure 59 (a–d)**. These plots illustrate the median values, interquartile ranges, and mean values for each group, facilitating a clearer understanding of the data spread (Morales et al., 2021). The box plots visually confirm the significant differences suggested by the p–values and Games–Howell test results, with certain groups displaying distinctly higher or lower performance metrics.

4.11.2. Significant difference in mean tensile properties of samples

The significance of the differences in the tensile properties (tensile strength, elongation at break, and modulus) between pure PLA filament and PLA/CNC filament was analyzed, comparing both the filament materials and their corresponding 3D printed samples. The statistical comparison was conducted using one-way ANOVA, specifically employing Box plots and Hsu's Multiple Comparisons (MCB) plot, as shown in **Figure 61** and **62 (a-f)**, respectively (Bogunovic et al., 2020; Nanda et al., 2021).

The box plot revealed that PLA/CNC filament and 3D printed samples have higher median tensile strength and elongation at break than pure PLA. This improvement is expected due to the inclusion of CNCs and the plasticizer. However, the interquartile range (IQR) for PLA/CNC showed more variation compared to pure PLA, suggesting that the addition of CNCs and plasticizer led to less uniform material properties. On the other hand, both pure PLA and PLA/CNC filaments exhibited higher median tensile modulus than the 3D printed samples. This decrease in modulus is attributed to the addition of the plasticizer, but a significant difference in modulus was observed in the 3D printed samples. This difference can be attributed to the effects of the printing process, in addition to the plasticizer.

Hsu's MCB plot is a statistical tool used for pairwise comparisons, providing insights into which specific groups differ significantly from each other. The significance levels between the different groups (pure PLA, PLA/CNC filaments, and their corresponding 3D printed samples) can be visualized in the Hsu MCB plot, along with the corresponding p-values.

According to Hsu, if an interval has zero as an endpoint, the corresponding means are significantly different. Therefore, all the samples showed a significant difference between means, except for the tensile strength values of the 3D printed samples ($p = 0.17$). The tensile strength of PLA and PLA/CNC filaments is significantly different, with an adjusted p-value of 0.04. Similarly, the mean values of elongation at break for filaments and 3D printed samples are significantly different, with adjusted p-values of 0.04 and 0.00, respectively. Although significant differences in tensile modulus were observed for both filaments and 3D printed samples, with adjusted p-values of 0.04 and 0.01, respectively, a reduction in modulus properties was noted

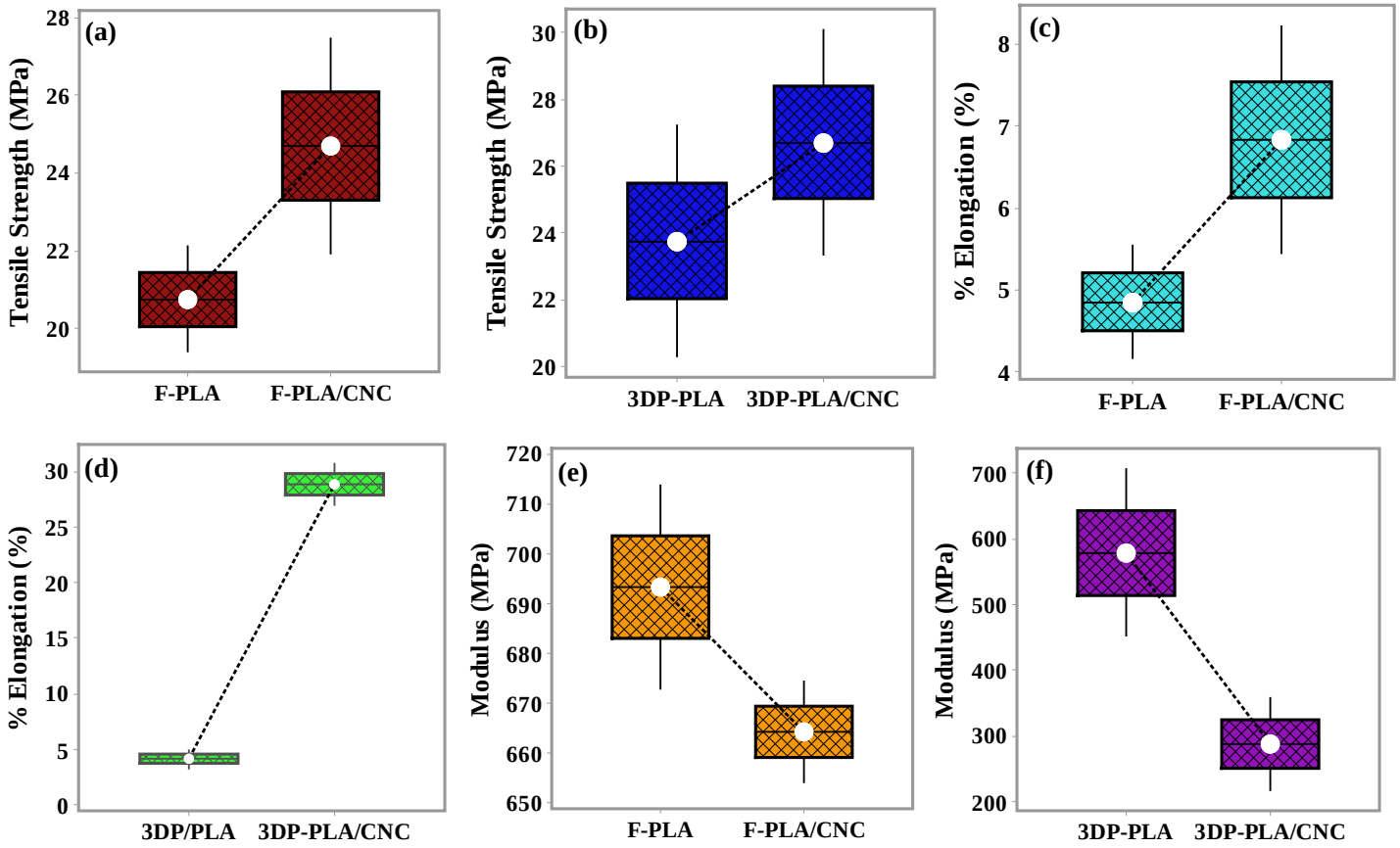

Figure 61. Box chart of (a-b) tensile strength (c-d) elongation (e-f) modulus for filament and 3D printed samples

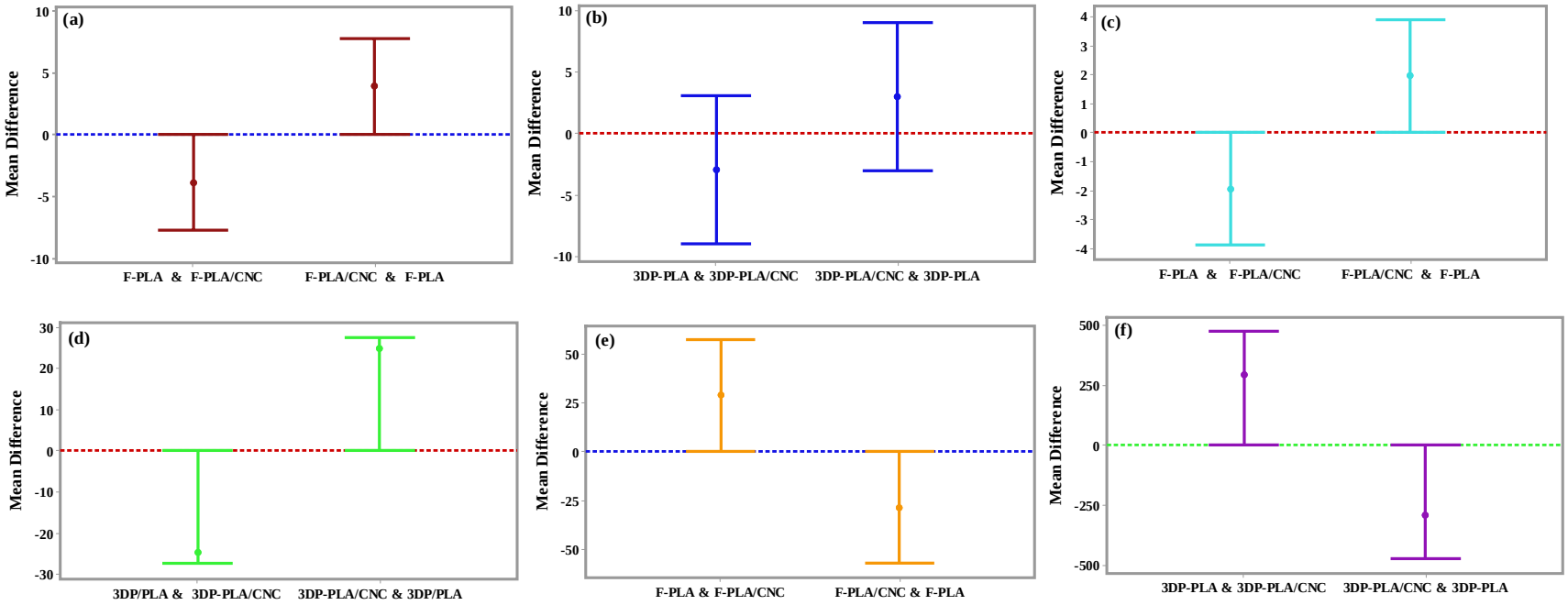

Figure 62. Mean difference plots of (a-b) tensile strength (c-d) elongation (e-f) modulus for filament and 3D printed samples

CONCLUSION, RECOMMENDATION AND FUTURE OUTLOOKS

Conclusion

This study explored the transformation of linseed stalk residue into high-value crystalline nanocellulose (CNC) and its application as a nanofiller in PLA-based Bio nanocomposites for FDM 3D printing. The investigation began with optimization of the water retting process, where an optimum retting duration of 216 h was identified. This duration was determined based on key indicators namely pH stabilization of retting water, stalk weight loss, and equilibrium water absorption, which collectively predicted the end of the retting process. These parameters serve as effective indicators to ensure timely fiber extraction, preventing both under- and over-retting conditions.

The degree of retting significantly influenced the physical and mechanical properties of the extracted fibers. Optimally retted fibers demonstrated the best performance, exhibiting a higher density of 1.52 g/cm³, a moderate yield of 12.67%, and superior tensile strength, with a breaking force of 278.4 cN and a tenacity of 59.1 cN/tex, compared to both under-retted and over-retted fibers. The findings highlight that optimal retting significantly improves fiber extraction by facilitating the effective removal of pectin and other binding materials, thereby enabling easier separation of fibers. It also preserves the structural integrity of cellulose, resulting in fibers with enhanced physical and mechanical properties.

The chemical composition analysis revealed that linseed stalk fibers consist of 68% cellulose, significantly higher than many commonly studied agricultural residues. In contrast, lower contents of hemicellulose (20%), lignin (5%), extractives (4%), and ash (3%) were observed. This favorable composition implies that linseed stalks are a potential source of cellulose with minimal non-cellulosic impurities, especially lignin and ash making them ideal for further refinement into micro cellulose (MC) and CNC with reduced pretreatment requirements and higher yield.

Through sequential chemical pretreatments, MC was successfully extracted and further hydrolyzed into CNC with a yield of 79.87%, meeting the dimensional standards of crystalline nanocellulose with diameter of 7.06 nm, length of 66.14 nm, and aspect ratio of 10.02. Additionally, the specific surface area of 377 m²/g and crystallinity of 73.29%. These results affirm the potential MC as an effective precursor for CNC, and CNC as a promising nanofiller in polymer composites due to its smaller size, moderate aspect ratio, and high surface area.

At 3% CNC loading, the composite achieves optimal dispersion and interfacial adhesion, as evidenced by SEM imaging, resulting in enhanced crystallinity (71.63% via DSC) and reduced water absorption (34.86% in 72 h) due to minimized porosity and agglomeration. XRD and FTIR analyses confirm hydrogen bonding between CNC hydroxyl groups and PLA ester linkages, crucial for stress transfer. However, at 1%, enhancements were minimal, and at 5%, performance declined due to CNC agglomeration, which impaired interfacial adhesion and thermal transitions. The excessive CNC (5%) disrupts polymer chain mobility, lowering crystallinity and thermal performance. These findings underline the importance of optimizing CNC loading to prevent agglomeration while maximizing reinforcement effects. PLA/CNC3% composite coated filament was successfully used in FDM 3D printing, and the printed specimens improved mechanical properties compared to the pure PLA, including tensile strength (26.72 ±3.41MPa) percentage elongation (28.87 ±1.94 %) and toughness (7.28 ±0.15 J/m^3). While the modulus (287.55 ±72 Mpa) is reduced, the overall performance of the 3DP–PLA/CNC3% composite is enhanced, making it a promising material for applications that require a combination of strength, flexibility, and impact resistance with sustainability and biodegradability. This makes suitable for industries such as flexible protective packaging, flexible electronic devices, and biomedical devices.

Recommendations

The findings of this study open promising pathways for the valorization of linseed stalk residues into a range of high-value bio-based materials with diverse potential applications. The high cellulose content (68%) of the linseed stalks suggests that they could serve as a dependable and sustainable feedstock for various cellulose-based industries. This abundant source of cellulose may be harnessed in future for applications such as biodegradable packaging, eco-friendly paper products, and films, supporting global initiatives toward sustainable and circular material economies.

The optimally retted fibers, which demonstrated superior mechanical and physical properties, may hold potential for applications in the industrial textiles and their structure and strength also position them well for use in natural fiber-reinforced composites in automotive parts, construction panels, and insulation materials, where lightweight yet strong reinforcements are required.

Micro cellulose (MC), extracted as an intermediate product in this study, also presents a wide future application possibilities. Owing to its moderate particle size, high surface area, and biodegradability, MC can be used in different fields, it may serve as a rheology modifier in

cosmetics and pharmaceuticals. In the material sciences, MC could find future roles in coatings, biodegradable films, and as an absorbent in hygiene products and filtration systems.

Crystalline nanocellulose (CNC), with its nanoscale dimensions, high crystallinity, and excellent surface functionality, holds promise as a reinforcing agent in polymer nanocomposites, as demonstrated in this study. Beyond this, CNC could independently be applied in numerous high-value sectors. It may be used as a reinforcing filler in sustainable packaging materials as a functional material in biomedical applications such as wound dressings, drug delivery systems, or tissue scaffolds.

The 3D printed PLA/CNC Bio nanocomposites developed in this study, showed improvements in tensile strength, elongation, and toughness. This could make it a promising material for future applications in biodegradable and flexible 3D-printed products, that require a combination of strength and flexibility. This makes suitable for industries such as flexible protective packaging, flexible electronic casings, and biomedical devices.

In conclusion, the study demonstrates the multi-stage conversion of agricultural waste into high-value added products with wide-ranging potential applications. By extracting nanocellulose from linseed stalks and incorporating it into PLA for FDM 3D printing, this research not only enhances material performance but also supports sustainable development goals. The renewable and biodegradable nature of the developed material makes it particularly attractive for future eco-friendly product innovations across different industries.

Future Outlooks

Building on the findings of this study, future research should first address the variability of linseed stalk feedstocks sourced from different geographical regions. Since factors such as soil type, climate, and farming practices influence fiber composition, comparative studies are essential to understand these variations. Additionally, investigation into the environmental performance of PLA/CNC composites is necessary. Standardized biodegradation tests under industrial composting and natural conditions should be conducted to evaluate how the incorporation of CNC affects PLA's degradation behavior. Furthermore, analyzing degradation byproducts will help determine the ecological safety of these materials, ensuring they align with circular economy principles.

Automating the filament coating process and optimizing 3D printing parameters is another crucial area for enhancing the performance of bio nanocomposites applications. To support industrial applications, future studies should also expand performance evaluation beyond

standard mechanical testing. Long-term durability assessments will provide insights into real-world reliability. Incorporating additional functionalities, such as electrical conductivity through conductive fillers or flame retardancy, could further broaden the application potential of these Bio nanocomposites.

Lastly, it is essential to evaluate the economic and environmental feasibility of scaling up the production processes for fiber, cellulose, nanocellulose and filament. Techno-economic analysis and lifecycle assessment (LCA) can help to compare the overall cost and environmental impact to that of petroleum-based alternatives. Collaborative efforts with industry partners will be key to piloting large-scale fiber, CNC and filament production.

PUBLICATIONS

The list of publications both original and review articles produced form the dissertation study are:

1. Feleke, K., Thothadri, G., Beri Tufa, H., Rajhi, A. A., & Ahmed, G. M. S. (2023). Extraction and characterization of fiber and cellulose from Ethiopian linseed straw: Determination of retting period and optimization of multi-step alkaline peroxide process. Polymers, 15(2), 469. https://doi.org/10.3390/polym15020469 .
2. Feleke, K., Ganesh, T., Beri, H., & Murtaza, A. (2024). Preparation and characterization of crystalline nanocellulose (CNC) from linseed straw fibers: As a potential alternative source of nanofillers in polymer composites. Journal of Engineered Fibers and Fabrics, 19, 15589250241265709. https://doi.org/10.1177/15589250241265709 .
3. Processing and characterization of crystalline nanocellulose–based bionanocomposites via solvent casting: a study on the effects of the CNC percentage on the morphology, thermal and structural properties. *(Submitted original article)*
4. Agricultural Waste as a Sustainable Source of Nanocellulose: A Concise Insight into Isolation, Characterization, Specific Characteristics and Applications. *(Submitted review article)*
5. Recent advancements of filament materials for fused deposition modeling (FDM)–based 3D printing. *(Submitted review article)*

REFERENCES

Abbass, A., Paiva, M. C., Oliveira, D. V., Lourenço, P. B., & Fangueiro, R. (2021). Insight into the effects of solvent treatment of natural fibers prior to structural composite casting: chemical, physical and mechanical evaluation. *Fibers, 9*(9), 54.

Abdel-Hakim, A., & Mouradb, R. M. (2023). Nanocellulose and its polymer composites: preparation, characterization, and applications. *Russ. Chem. Rev, 92*(4).

Abdul Rahman, N. H., Chieng, B. W., Ibrahim, N. A., & Abdul Rahman, N. (2017). Extraction and characterization of cellulose nanocrystals from tea leaf waste fibers. *Polymers, 9*(11), 588.

Abhilash, V., Rajender, N., & Suresh, K. (2016). X-ray diffraction spectroscopy of polymer nanocomposites. In *Spectroscopy of Polymer Nanocomposites* (pp. 410-451): Elsevier.

Abu-Thabit, N. Y., Judeh, A. A., Hakeem, A. S., Ul-Hamid, A., Umar, Y., et al. (2020). Isolation and characterization of microcrystalline cellulose from date seeds (Phoenix dactylifera L.). *International Journal of Biological Macromolecules, 155*, 730-739.

Abubakar, I. R., Maniruzzaman, K. M., Dano, U. L., AlShihri, F. S., AlShammari, M. S., et al. (2022). Environmental sustainability impacts of solid waste management practices in the global South. *International journal of environmental research public health, 19*(19), 12717.

Acierno, D., & Patti, A. (2023). Fused deposition modelling (FDM) of thermoplastic-based filaments: process and rheological properties—an overview. *Materials, 16*(24), 7664.

Adeeyo, O., Oresegun, O. M., & Oladimeji, T. E. (2015). Compositional analysis of lignocellulosic materials: Evaluation of an economically viable method suitable for woody and non-woody biomass. *American Journal of Engineering Research (AJER), 4*(4), 14-19.

Afrose, M. F., Masood, S., Iovenitti, P., Nikzad, M., & Sbarski, I. (2016). Effects of part build orientations on fatigue behaviour of FDM-processed PLA material. *Prog Addit Manuf 1*, 21-28.

Agarwal, R. (2022). The personal protective equipment fabricated via 3D printing technology during COVID-19. *Annals of 3D Printed Medicine, 5*, 100042.

Agbakoba, V. C., Hlangothi, P., Andrew, J., & John, M. J. (2023). Preparation of cellulose nanocrystal (CNCs) reinforced polylactic acid (PLA) bionanocomposites filaments using biobased additives for 3D printing applications††Electronic supplementary information (ESI) available. *Nanoscale Advances, 5*(17), 4447-4463.

Agbangba, C. E., Aide, E. S., Honfo, H., & Kakai, R. G. (2024). On the use of post-hoc tests in environmental and biological sciences: A critical review. *Heliyon*.

Ahad, N. A., & Yahaya, S. S. S. (2014). *Sensitivity analysis of Welch'st-test.* Paper presented at the AIP Conference proceedings.

Ahmad, A., Banat, F., Taher, H., & Innovation. (2020). A review on the lactic acid fermentation from low-cost renewable materials: Recent developments and challenges. *Environmental Technology, 20*, 101138.

Ahmad, N., Wong, Y. H., & Ghazali, N. N. N. (2022). A systematic review of fused deposition modeling process parameters. *Soft Science, 2*(3), 11.

Ahmad, N. D., & Wildan, M. W. (2023). Preparation and properties of cellulose nanocrystals-reinforced Poly (lactic acid) composite filaments for 3D printing applications. *Results in Engineering, 17*, 100842.

Ahn, S. H., Montero, M., Odell, D., Roundy, S., & Wright, P. K. (2002). Anisotropic material properties of fused deposition modeling ABS. *Rapid prototyping journal, 8*(4), 248-257.

Akin, D. E., Henriksson, G., Evans, J. D., Adamsen, A. P. S., Foulk, J. A., et al. (2004). Progress in enzyme-retting of flax. *Journal of Natural Fibers, 1*(1), 21-47.

Akinjokun, A. I., Petrik, L. F., Ogunfowokan, A. O., Ajao, J., & Ojumu, T. V. (2021). Isolation and characterization of nanocrystalline cellulose from cocoa pod husk (CPH) biomass wastes. *Heliyon, 7*(4).

Albdiry, M. (2024). Effect of melt blending processing on mechanical properties of polymer nanocomposites: a review. *Polymer Bulletin, 81*(7), 5793-5821.

Alexandre, A., Cruz Sanchez, F. A., Boudaoud, H., Camargo, M., & Pearce, J. M. (2020). Mechanical properties of direct waste printing of polylactic acid with universal pellets extruder: comparison to fused filament fabrication on open-source desktop three-dimensional printers. *3D Printing and Additive Manufacturing, 7*(5), 237-247.

Ali, M. F., Mekbib, F., & Wakjira, A. (2014). Morphological diversity of Ethiopian linseed (Linum usitatissimum L.) landrace accessions and non-native cultivars. *Journal of Plant Breeding Genetics, 2*(3), 115-124.

Alix, S., Colasse, L., Morvan, C., Lebrun, L., & Marais, S. (2014). Pressure impact of autoclave treatment on water sorption and pectin composition of flax cellulosic-fibres. *Carbohydrate polymers, 102*, 21-29.

Alix, S., Philippe, E., Bessadok, A., Lebrun, L., Morvan, C., et al. (2009). Effect of chemical treatments on water sorption and mechanical properties of flax fibres. *Bioresour Technol, 100*(20), 4742-4749.

Ambrosio-Martín, J., Lopez-Rubio, A., Fabra, M. J., Gorrasi, G., Pantani, R., et al. (2015). Assessment of ball milling methodology to develop polylactide-bacterial cellulose nanocrystals nanocomposites. *Journal of Applied Polymer Science, 132*(10).

Amel, B. A., Paridah, M. T., Sudin, R., Anwar, U., & Hussein, A. S. (2013). Effect of fiber extraction methods on some properties of kenaf bast fiber. *Industrial Crops and Products, 46*, 117-123.

Amin, K. N. M., Hosseinmardi, A., Martin, D. J., & Annamalai, P. K. (2022). A mixed acid methodology to produce thermally stable cellulose nanocrystal at high yield using phosphoric acid. *Journal of Bioresources and Bioproducts, 7*(2), 99-108.

Amiralian, N., Annamalai, P. K., Garvey, C. J., Jiang, E., Memmott, P., et al. (2017). High aspect ratio nanocellulose from an extremophile spinifex grass by controlled acid hydrolysis. *Cellulose, 24*, 3753-3766.

Amiri, A., Triplett, Z., Moreira, A., Brezinka, N., Alcock, M., et al. (2017). Standard density measurement method development for flax fiber. *Industrial crops and products, 96*, 196-202.

Andrade, C. (2019). The P value and statistical significance: misunderstandings, explanations, challenges, and alternatives. *Indian journal of psychological medicine, 41*(3), 210-215.

Andreas Mautner, M. H., Ville Rissanen , & and Tekla Tammelin. (2018). Nanocellulose and sustainability: production, properties, applications, and case studies. In K.-Y. Lee (Ed.), *Nanocellulose and Sustainability: Production, Properties, Applications, and Case Studies* (1st Edition ed., pp. 314). Boca Raton: CRC Press.

Angelini, L. G., Scalabrelli, M., Tavarini, S., Cinelli, P., Anguillesi, I., et al. (2015). Ramie fibers in a comparison between chemical and microbiological retting proposed for application in biocomposites. *Industrial Crops and Products, 75*, 178-184.

Angelopoulos, P. M., Samouhos, M., & Taxiarchou, M. (2021). Functional fillers in composite filaments for fused filament fabrication; a review. *Materials Today: Proceedings, 37*, 4031-4043.

Ansari, A. A., & Kamil, M. (2021). Effect of print speed and extrusion temperature on properties of 3D printed PLA using fused deposition modeling process. *Materials Today: Proceedings, 45*, 5462-5468.

Apaydın Varol, E., & Mutlu, Ü. (2023). TGA-FTIR Analysis of Biomass Samples Based on the Thermal Decomposition Behavior of Hemicellulose, Cellulose, and Lignin. *Energies, 16*(9), 3674.

Araki, J., & Arita, T. (2017). Production of ultrafine dry powders of surface-intact and unmodified cellulose nanowhiskers via homogenization in nonpolar organic solvents. *Chem. Lett., 46*(9), 1438-1441.

Arantes, V., Dias, I. K. R., Berto, G. L., Pereira, B., Marotti, B. S., et al. (2020). The current status of the enzyme-mediated isolation and functionalization of nanocelluloses: production, properties, techno-economics, and opportunities. *Cellulose, 27*(18), 10571-10630.

Arif, M., Kumar, S., Varadarajan, K., & Cantwell, W. (2018). Performance of biocompatible PEEK processed by fused deposition additive manufacturing. *Materials Design, 146*, 249-259.

Arnata, I. W., Suprihatin, S., Fahma, F., Richana, N., & Sunarti, T. C. (2020). Cationic modification of nanocrystalline cellulose from sago fronds. *Cellulose, 27*(6), 3121-3141.

Arnata, I. W. F., Farah Richana, Nur Sunarti, Titi Candra. (2019). Cellulose production from sago frond with alkaline delignification and bleaching on various types of bleach agents. *Orient. J. Chem., 35*, 8.

Arrieta, M. P., Fortunati, E., Dominici, F., López, J., & Kenny, J. M. (2015). Bionanocomposite films based on plasticized PLA–PHB/cellulose nanocrystal blends. *Carbohydrate polymers, 121*, 265-275.

Arrieta, M. P., Peltzer, M. A., López, J., & Peponi, L. (2017). PLA-Based Nanocomposites Reinforced with CNC for Food Packaging Applications: From Synthesis to Biodegradation. In S. N. Goyanes & N. B. D'Accorso (Eds.), *Industrial Applications of Renewable Biomass Products: Past, Present and Future* (pp. 265-300). Cham: Springer International Publishing.

Ashori, A., Rafieyan, F., Kian, F., Jonoobi, M., & Rezaei Tavabe, K. (2019). Effect of cellulose nanocrystals on performance of polyethersulfone nanocomposite membranes using electrospinning technique. *Polymer Composites, 40*(S1), E835-E841.

Assefa, E. G., Kiflie, Z., & Demsash, H. D. (2023). Valorization of abundantly available Ethiopian teff (Eragrostis tef) straw for the isolation of cellulose fibrils by alkaline hydrogen peroxide treatment method. *Journal of Polymers and the Environment, 31*(3), 900-912.

Asyraf, M., Rafidah, M., Ishak, M., Sapuan, S., Yidris, N., et al. (2020). Integration of TRIZ, Morphological Chart and ANP method for development of FRP composite portable fire extinguisher. *Polymer Composites, 41*(7), 2917-2932.

Aumnate, C., Pongwisuthiruchte, A., Pattananuwat, P., & Potiyaraj, P. (2018). Fabrication of ABS/graphene oxide composite filament for fused filament fabrication (FFF) 3D printing. *Advances in Materials Science engineering, 2018*(1), 2830437.

Aw, Y. Y., Yeoh, C. K., Idris, M. A., Teh, P. L., Hamzah, K. A., et al. (2018). Effect of printing parameters on tensile, dynamic mechanical, and thermoelectric properties of FDM 3D printed CABS/ZnO composites. *Materials, 11*(4), 466.

Azanaw, A., Haile, A., & Gideon, R. K. (2019). Extraction and characterization of fibers from Yucca Elephantine plant. *Cellulose, 26*(2), 795-804.

Azzra, N., Atiqah, A., Fadhlina, H., Jalar, A., Bakar, M., et al. (2024). Effect of nanofibril cellulose empty fruit bunch-reinforced thermoplastic polyurethane nanocomposites on tensile and dynamic mechanical properties for flexible substrates. *Polymer Composites*.

Baheti, V., & Militky, J. (2013). Reinforcement of wet milled jute nano/micro particles in polyvinyl alcohol films. *Fibers and Polymers, 14*(1), 133-137.

Bai, L., Bossa, N., Qu, F., Winglee, J., Li, G., et al. (2017). Comparison of hydrophilicity and mechanical properties of nanocomposite membranes with cellulose nanocrystals and carbon nanotubes. *Environmental sciencetechnology, 51*(1), 253-262.

Balamurugan, K., Venkata Pavan, M., Ahamad Ali, S. K., & Kalusuraman, G. (2021). Compression and flexural study on PLA-Cu composite filament using FDM. *Materials Today: Proceedings, 44*, 1687-1691.

Balea Martín, A., Blanco Suárez, M. Á., Delgado-Aguilar, M., Monte Lara, M. C., Tarrés, Q., et al. (2021). Nanocellulose characterization challenges. *BioResources, 16*(2), 4382-4410.

Baley, C., Morvan, C., & Grohens, Y. (2005). Influence of the Absorbed Water on the Tensile Strength of Flax Fibers. *Macromolecular Symposia, 222*(1), 195-202.

Banerjee, S., Misra, A., Chaudhury, S., & Dam, B. (2019). A Bacillus strain TCL isolated from Jharia coalmine with remarkable stress responses, chromium reduction capability and bioremediation potential. *Journal of hazardous materials, 367*, 215-223.

Bangar, S. P., Harussani, M., Ilyas, R., Ashogbon, A. O., Singh, A., et al. (2022). Surface modifications of cellulose nanocrystals: Processes, properties, and applications. *Food Hydrocolloids, 130*, 107689.

Bangar, S. P., Whiteside, W. S., Kajla, P., & Tavassoli, M. (2023). Value addition of rice straw cellulose fibers as a reinforcer in packaging applications. *International Journal of Biological Macromolecules, 243*, 125320.

Barbash, V., & Yashchenko, O. (2020). Preparation and application of nanocellulose from non-wood plants to improve the quality of paper and cardboard. *Applied Nanoscience, 10*(8), 2705-2716.

Bardot, M., & Schulz, M. D. (2020). Biodegradable poly (Lactic acid) nanocomposites for fused deposition modeling 3d printing. *Nanomaterials, 10*(12), 2567.

Barkhad, M. S., Abu-Jdayil, B., Mourad, A. H. I., & Iqbal, M. Z. (2020). Thermal insulation and mechanical properties of polylactic acid (PLA) at different processing conditions. *Polymers, 12*(9), 2091.

Baumann, F., Scholz, J., & Fleischer, J. (2017). Investigation of a New Approach for Additively Manufactured Continuous Fiber-reinforced Polymers. *Procedia CIRP, 66*, 323-328.

Begum, H. A., Tanni, T. R., & Shahid, M. A. (2021). Analysis of Water Absorption of Different Natural Fibers. *Journal of Textile Science and Technology, 7*(4), 152-160.

Behseresht, S., Park, Y. H., Love, A., & Pastrana, O. A. V. (2024). Application of Numerical Modeling and Finite Element Analysis in Fused Filament Fabrication: A Review. *Materials, 17*(17), 4185.

Benwood, C., Anstey, A., Andrzejewski, J., Misra, M., & Mohanty, A. K. (2018). Improving the impact strength and heat resistance of 3D printed models: structure, property, and processing correlationships during fused deposition modeling (FDM) of poly (lactic acid). *ACS Omega, 3*(4), 4400-4411.

Beroual, M., Boumaza, L., Mehelli, O., Trache, D., Tarchoun, A. F., et al. (2021). Physicochemical properties and thermal stability of microcrystalline cellulose isolated from esparto grass using different delignification approaches. *Journal of Polymers and the Environment, 29*(1), 130-142.

Besbes, I., Alila, S., & Boufi, S. (2011). Nanofibrillated cellulose from TEMPO-oxidized eucalyptus fibres: effect of the carboxyl content. *Carbohydrate Polymers, 84*(3), 975-983.

Beyan, S. M., Amibo, T. A., Prabhu, S. V., & Ayalew, A. G. (2021). Production of nanocellulose crystal derived from enset fiber using acid hydrolysis coupled with ultrasonication, isolation, statistical modeling, optimization, and characterizations. *Journal of Nanomaterials, 2021*, 1-12.

Beyene, D., Chae, M., Vasanthan, T., & Bressler, D. C. (2020). A biorefinery strategy that introduces hydrothermal treatment prior to acid hydrolysis for co-generation of furfural and cellulose nanocrystals. *Front. Chem.. 8*, 323.

Bhaganagar, S. (2023). *Cellulose Nano Fibers Infused Polylactic Acid Using the Process of Twin Screw Melt Extrusion for 3d Printing Applications.* (Master of Enginnering Master), Purdue, Indianpolis, Indiana.

Bhaganagar, S., Biswas, P. K., Agarwal, M., & Dalir, H. (2023). *Enhancing Polylactic Acid (PLA) for 3D Printing with Cellulose Nanofibers via Twin Screw Melt Extrusion.*

Paper presented at the Proceedings of the American society for composites-thirty-eighth technical conference.

Bhiogade, A., & Kannan, M. (2021). Studies on thermal and degradation kinetics of cellulose micro/nanoparticle filled polylactic acid (PLA) based nanocomposites. *Polymer Composites, 29*(9_suppl), S85-S98.

Bingxin, F., & Linghao, Z. (2015). Hydrogen-Bonding Network and OH Stretch Vibration of Cellulose: Comparison of Computational Modeling with Polarized IR and SFG Spectra. *The Journal of Physical Chemistry B, 149*(19), 15138–15149.

Blanco, I., & Siracusa, V. (2021). The use of thermal techniques in the characterization of bio-sourced polymers. *Materials, 14*(7), 1686.

Bogunovic, I., Viduka, A., Magdic, I., Telak, L. J., Francos, M., et al. (2020). Agricultural and forest land-use impact on soil properties in Zagreb periurban area (Croatia). *Agronomy, 10*(9), 1331.

Bondeson, D., & Oksman, K. (2007). Polylactic acid/cellulose whisker nanocomposites modified by polyvinyl alcohol. *Composites Part A: Applied Science and Manufacturing, 38*(12), 2486-2492.

Borchani, K. E., Carrot, C., & Jaziri, M. (2015). Untreated and alkali treated fibers from Alfa stem: effect of alkali treatment on structural, morphological and thermal features. *Cellulose, 22*(3), 1577-1589.

Borkotoky, S. S., Dhar, P., & Katiyar, V. (2018). Biodegradable poly (lactic acid)/Cellulose nanocrystals (CNCs) composite microcellular foam: Effect of nanofillers on foam cellular morphology, thermal and wettability behavior. *International journal of biological macromolecules, 106*, 433-446.

Borsoi, C., Zimmernnam, M. V., Zattera, A. J., Santana, R. M., & Ferreira, C. A. (2016a). Thermal degradation behavior of cellulose nanofibers and nanowhiskers. *Journal of Thermal Analysis Calorimetry, 126*, 1867-1878.

Borsoi, C., Zimmernnam, M. V. G., Zattera, A. J., Santana, R. M. C., & Ferreira, C. A. (2016b). Thermal degradation behavior of cellulose nanofibers and nanowhiskers. *J. Therm. Anal. Calorim, 126*, 1867-1878.

Bos, H. (2004). *The potential of flax fibres as reinforcement for composite materials.* Wageningen University and Research, Eindhoven, the Netherlands.

Brinkmann, A., Chen, M., Couillard, M., Jakubek, Z. J., Leng, T., et al. (2016). Correlating cellulose nanocrystal particle size and surface area. *Langmuir, 32*(24), 6105-6114.

Bu, D., Hu, X., Yang, Z., Yang, X., Wei, W., et al. (2019). Elucidation of the relationship between intrinsic viscosity and molecular weight of cellulose dissolved in tetra-n-butyl ammonium hydroxide/dimethyl sulfoxide. *Polym, 11*(10), 1605.

Bualuang, W., Threepopnatkul, P., & Sittattrakul, A. (2020). *Mechanical properties and foaming behavior of Poly (lactic acid) blend Polybutylene Succinate.* Paper presented at the IOP Conference Series: Materials Science and Engineering.

Businesswaste. (2024). Agricultural waste facts. Retrieved from https://www.businesswaste.co.uk/sectors/agricultural-waste-management/agricultural-waste-facts/

Cano-Vicent, A., Tambuwala, M. M., Hassan, S. S., Barh, D., Aljabali, A. A., et al. (2021). Fused deposition modelling: Current status, methodology, applications and future prospects. *Additive manufacturing, 47*, 102378.

Çanti, E., Aydın, M., & Yıldırım, F. (2018). Production and characterization of composite filaments for 3D printing. *Politeknik Dergisi, 21*(2), 397-402.

Cao, L., Xiao, J., Kim, J. K., & Zhang, X. (2023). Effect of post-process treatments on mechanical properties and surface characteristics of 3D printed short glass fiber reinforced PLA/TPU using the FDM process. *CIRP Journal of Manufacturing Science Technology, 41*, 135-143.

Cao, Y., Wang, W., Wang, Q., & Wang, H. (2013). Application of Mechanical Models to Flax Fiber/Wood Fiber/Plastic Composites. *BioResources, 8*(3).

Chai, H., Chang, Y., Zhang, Y., Chen, Z., Zhong, Y., et al. (2020). The fabrication of polylactide/cellulose nanocomposites with enhanced crystallization and mechanical properties. *International journal of biological macromolecules, 155*, 1578-1588.

Chaka, K. T. (2022). Extraction of cellulose nanocrystals from agricultural by-products: a review. *Green Chemistry Letters and Reviews, 15*(3), 582-597.

Chakrabarty, A., & Teramoto, Y. (2018). Recent advances in nanocellulose composites with polymers: a guide for choosing partners and how to incorporate them. *Polymers, 10*(5), 517.

Chandrasekar, M., Senthilkumar, K., Senthil Muthu Kumar, T., Sabarish, R., & Siengchin, S. (2021). Morphological characterization of the wood polymer composites. *Wood Polymer Composites: Recent Advancements Applications*, 93-112.

Chen, C., Li, D., Hu, Q., & Wang, R. (2014). Properties of polymethyl methacrylate-based nanocomposites: Reinforced with ultra-long chitin nanofiber extracted from crab shells. *Materials Design, 56*, 1049-1056.

Chen, D., Lawton, D., Thompson, M. R., & Liu, Q. (2012). Biocomposites reinforced with cellulose nanocrystals derived from potato peel waste. *Carbohydrate Polymers, 90*(1), 709-716.

Chen, H., Yu, Y., Zhong, T., Wu, Y., Li, Y., et al. (2016). Effect of alkali treatment on microstructure and mechanical properties of individual bamboo fibers. *Cellulose, 24*(1), 333-347.

Chen, J., An, R., Tey, W. S., Zeng, Q., Zhao, L., et al. (2023). In Situ Filler Addition for Homogeneous Dispersion of Carbon Nanotubes in Multi Jet Fusion–Printed Elastomer Composites. *Advanced Science, 10*(25), 2300593.

Chen, L., Wang, Q., Hirth, K., Baez, C., Agarwal, U. P., et al. (2015). Tailoring the yield and characteristics of wood cellulose nanocrystals (CNC) using concentrated acid hydrolysis. *Cellulose, 22*, 1753-1762.

Chen, M. Y., Skewes, J., Woodruff, M. A., Dasgupta, P., & Rukin, N. J. (2020). Multi-colour extrusion fused deposition modelling: a low-cost 3D printing method for anatomical prostate cancer models. *Scientific Reports, 10*(1), 10004.

Chen, Q., Han, L., Ren, J., Rong, L., Cao, P., et al. (2020). 4D printing via an unconventional fused deposition modeling route to high-performance thermosets. *ACS applied materials interfaces, 12*(44), 50052-50060.

Chen, W., Yu, H., Liu, Y., Hai, Y., Zhang, M., et al. (2011). Isolation and characterization of cellulose nanofibers from four plant cellulose fibers using a chemical-ultrasonic process. *Cellulose, 18*, 433-442.

Chen, Y., Zhao, L., Pan, H., Jia, S., Han, L., et al. (2020). Impact of d-isomer content on the microstructure and mechanical properties of uniaxially pre-stretched poly (lactic acid). *Polymer, 186*, 122022.

Chen, Y. W., Lee, H. V., & Abd Hamid, S. B. (2017). Investigation of optimal conditions for production of highly crystalline nanocellulose with increased yield via novel Cr(III)-catalyzed hydrolysis: Response surface methodology. *Carbohydrate Polymers, 178*, 57-68.

Chime, C. C., Ogbobe, O., Udeozo, P. I., Orie, K. J., & Nsude, O. P. (2022). Isolation, physicochemical and BET analysis of cellulose from pentaclethra macrophylla benth (Oil Bean) pod biomass wastes. *Int. Res. J. Pure Appl. Chem., 23*, 9-22.

Chopra, L. (2022). Extraction of cellulosic fibers from the natural resources: A short review. *Materials Today: Proceedings, 48*, 1265-1270.

Chopra, L. (2022). Extraction of cellulosic fibers from the natural resources: a short review. *Materials Today: Proceedings, 48*, 1265-1270.

Chu, Y., Sun, Y., Wu, W., & Xiao, H. (2020). Dispersion properties of nanocellulose: a review. *Carbohydrate polymers, 250*, 116892.

Ciolacu, D., Ciolacu, F., & Popa, V. I. (2011). Amorphous cellulose—structure and characterization. *Cellulose Chemistry and Technology, 45*(1), 13.

Clarkson, C. M., Azrak, S. M. E. A., Schueneman, G. T., Snyder, J. F., & Youngblood, J. P. (2020). Crystallization kinetics and morphology of small concentrations of cellulose nanofibrils (CNFs) and cellulose nanocrystals (CNCs) melt-compounded into poly (lactic acid)(PLA) with plasticizer. *Polymer, 187*, 122101.

Cojocaru, V., Frunzaverde, D., Miclosina, C.-O., & Marginean, G. (2022). The influence of the process parameters on the mechanical properties of PLA specimens produced by fused filament fabrication—A review. *Polymers, 14*(5), 886.

Collazo-Bigliardi, S., Ortega-Toro, R., & Chiralt Boix, A. (2018). Isolation and characterisation of microcrystalline cellulose and cellulose nanocrystals from coffee husk and comparative study with rice husk. *Carbohydrate Polymers, 191*, 205-215.

Corrêa, A. C., de Morais Teixeira, E., Pessan, L. A., & Mattoso, L. H. C. (2010). Cellulose nanofibers from curaua fibers. *Cellulose, 17*, 1183-1192.

Cui, T., Li, J., Yan, Z., Yu, M., & Li, S. (2014). The correlation between the enzymatic saccharification and the multidimensional structure of cellulose changed by different pretreatments. *Biotechnol. Biofuels, 7*(1), 1-10.

D'Acierno, F., Hamad, W. Y., Michal, C. A., & MacLachlan, M. J. (2020). Thermal degradation of cellulose filaments and nanocrystals. *Biomacromolecules, 21*(8), 3374-3386.

D'Auria, M., Mecca, M., Bruno, M. R., & Todaro, L. (2021). Extraction Methods and Their Influence on Yield When Extracting Thermo-Vacuum-Modified Chestnut Wood. *Forests, 12*(1), 73.

Dalloul, F., Mietner, J. B., & Navarro, J. R. (2022). Production and 3D printing of a nanocellulose-based composite filament composed of polymer-modified cellulose nanofibrils and high-density polyethylene (HDPE) for the fabrication of 3D complex shapes. *Fibers, 10*(10), 91.

Danial, W. H., Abdul Majid, Z., Mohd Muhid, M. N., Triwahyono, S., Bakar, M. B., et al. (2015). The reuse of wastepaper for the extraction of cellulose nanocrystals. *Carbohydrate Polymers, 118*, 165-169.

Datta, S., Chattopadhyay, L., Barai, S., Mandal, K., Kar, G., et al. (2024). The sequential microbial breakdown of pectin is the principal incident during water retting of jute (Corchorus spp.) bast fibres. *BMC Plant Biology, 24*(1), 295.

Daver, F., Lee, K. P. M., Brandt, M., & Shanks, R. (2018a). Cork–PLA composite filaments for fused deposition modelling. *Composites Science and Technology, 168*, 230-237.

Daver, F., Lee, K. P. M., Brandt, M., & Shanks, R. (2018b). Cork–PLA composite filaments for fused deposition modelling. *Composites Science Technology, 168*, 230-237.

Dawoud, M., Taha, I., & Ebeid, S. J. (2016). Mechanical behaviour of ABS: An experimental study using FDM and injection moulding techniques. *Journal of manufacturing Processes, 21*, 39-45.

de Avila Delucis, R., de Cademartori, P. H. G., Fajardo, A. R., Amico, S. C. J. P. P., & Applications. (2021). Cellulose and its derivatives: properties and applications. 221-252.

De Morais Teixeira, E., Bondancia, T. J., Teodoro, K. B. R., Corrêa, A. C., Marconcini, J. M., et al. (2011). Sugarcane bagasse whiskers: Extraction and characterizations. *Ind. Crops Prod., 33*(1), 63-66.

De Paula, E. L., Mano, V., Pereira, F. V. D., & Stability. (2011). Influence of cellulose nanowhiskers on the hydrolytic degradation behavior of poly (d, l-lactide). *Polymer Composites, 96*(9), 1631-1638.

de Souza, A. G., Barbosa, R. F., & Rosa, D. S. (2020). Nanocellulose from industrial and agricultural waste for further use in PLA composites. *Journal of Polymers the Environment, 28*, 1851-1868.

Deng, F., Li, M.-C., Ge, X., Zhang, Y., & Cho, U. R. (2017). Cellulose nanocrystals/poly(methyl methacrylate) nanocomposite films: Effect of preparation method and loading on the optical, thermal, mechanical, and gas barrier properties. *Polymer Composites, 38*(S1), E137-E146.

Deng, X., Zeng, Z., Peng, B., Yan, S., & Ke, W. (2018). Mechanical properties optimization of poly-ether-ether-ketone via fused deposition modeling. *Materials, 11*(2), 216.

Desai, H., Mehta, T., & Shah, N. (2023). Azeotropic dehydrative (solution) polycondensation of lactic acid to polylactic acid (PLA): A in-depth review of an overlooked method for manufacturing PLA. *Polymer-Plastics Technology Materials, 62*(11), 1394-1402.

Dey, A., Roan Eagle, I. N., & Yodo, N. (2021). A review on filament materials for fused filament fabrication. *Journal of manufacturing materials processing, 5*(3), 69.

Dhanani, T., Shah, S., Gajbhiye, N., & Kumar, S. (2017). Effect of extraction methods on yield, phytochemical constituents and antioxidant activity of Withania somnifera. *Arabian Journal of Chemistry, 10*, S1193-S1199.

Dhar, P., Tarafder, D., Kumar, A., & Katiyar, V. (2015). Effect of cellulose nanocrystal polymorphs on mechanical, barrier and thermal properties of poly (lactic acid) based bionanocomposites. *Rsc Advances, 5*(74), 60426-60440.

Dhar, P., Tarafder, D., Kumar, A., & Katiyar, V. (2015). Effect of cellulose nanocrystal polymorphs on mechanical, barrier and thermal properties of poly(lactic acid) based bionanocomposites. *RSC Advances, 5*(74), 60426-60440.

Dhar, P., Tarafder, D., Kumar, A., & Katiyar, V. (2016). Thermally recyclable polylactic acid/cellulose nanocrystal films through reactive extrusion process. *Polymer, 87*, 268-282.

Dhaval, M., Sharma, S., Dudhat, K., & Chavda, J. (2022). Twin-screw extruder in pharmaceutical industry: history, working principle, applications, and marketed products: an in-depth review. *Journal of Pharmaceutical Innovation, 17*(2), 294-318.

Dickson, A. N., Abourayana, H. M., & Dowling, D. P. (2020). 3D printing of fibre-reinforced thermoplastic composites using fused filament fabrication—A review. *Polymers, 12*(10), 2188.

Ding, W., Chu, R. K. M., Mark, L. H., Park, C. B., & Sain, M. (2015). Non-isothermal crystallization behaviors of poly(lactic acid)/cellulose nanofiber composites in the presence of CO2. *European Polymer Journal, 71*, 231-247.

Ditzel, F. I., Prestes, E., Carvalho, B. M., Demiate, I. M., & Pinheiro, L. A. (2017). Nanocrystalline cellulose extracted from pine wood and corncob. *Carbohydrate Polymers, 157*, 1577-1585.

Dong, H., Sliozberg, Y. R., Snyder, J. F., Steele, J., Chantawansri, T. L., et al. (2015). Highly Transparent and Toughened Poly(methyl methacrylate) Nanocomposite Films Containing Networks of Cellulose Nanofibrils. *ACS Applied Materials & Interfaces, 7*(45), 25464-25472.

Dong, H., Strawhecker, K. E., Snyder, J. F., Orlicki, J. A., Reiner, R. S., et al. (2012). Cellulose nanocrystals as a reinforcing material for electrospun poly(methyl methacrylate) fibers: Formation, properties and nanomechanical characterization. *Carbohydrate Polymers, 87*(4), 2488-2495.

Dos Santos, F. A., Iulianelli, G. C., & Tavares, M. I. (2017). Effect of microcrystalline and nanocrystals cellulose fillers in materials based on PLA matrix. *Polymer Testing, 61*, 280-288.

Doshi, M., Mahale, A., Singh, S. K., & Deshmukh, S. (2022). Printing parameters and materials affecting mechanical properties of FDM-3D printed Parts: Perspective and prospects. *Materials Today: Proceedings, 50*, 2269-2275.

Doumeng, M., Makhlouf, L., Berthet, F., Marsan, O., Delbé, K., et al. (2021). A comparative study of the crystallinity of polyetheretherketone by using density, DSC, XRD, and Raman spectroscopy techniques. *Polymer Testing, 93*, 106878.

Draman, S. F. S., Daik, R., Latif, F. A., & El-Sheikh, S. M. (2014). Characterization and thermal decomposition kinetics of kapok (Ceiba pentandra L.)–based cellulose. *BioResources, 9*(1), 8-23.

Duchemin, B., Thuault, A., Vicente, A., Rigaud, B., Fernandez, C., et al. (2012). Ultrastructure of cellulose crystallites in flax textile fibres. *Cellulose, 19*(6), 1837-1854.

Dul, S., Fambri, L., & Pegoretti, A. (2018). Filaments production and fused deposition modelling of ABS/carbon nanotubes composites. *Nanomaterials, 8*(1), 49.

Duque-Acevedo, M., Belmonte-Ureña, L. J., Cortés-García, F. J., & Camacho-Ferre, F. (2020). Agricultural waste: Review of the evolution, approaches and perspectives on alternative uses. *Global Ecology Conservation, 22*, e00902.

Duygulu, N. E., Ciftci, F., & Ustundag, C. B. (2020). Electrospun drug blended poly (lactic acid)(PLA) nanofibers and their antimicrobial activities. *Journal of Polymer Research, 27*, 1-11.

El-Hadi, A. M. (2017). Increase the elongation at break of poly (lactic acid) composites for use in food packaging films. *Scientific Reports, 7*(1), 46767.

El-Wakil, N. A., Kassem, N. F., & Hassan, M. L. (2016). Hydroxypropyl cellulose/rice straw oxidized cellulose nanocrystals nanocomposites and their use in paper coating. *Industrial crops and products, 93*, 186-192.

Elazzouzi-Hafraoui, S., Nishiyama, Y., Putaux, J.-L., Heux, L., Dubreuil, F., et al. (2008). The shape and size distribution of crystalline nanoparticles prepared by acid hydrolysis of native cellulose. *Biomacromolecules, 9*(1), 57-65.

Elbasiouny, H., Elbanna, B. A., Al-Najoli, E., Alsherief, A., Negm, S., et al. (2019). Agricultural waste management for climate change mitigation: Some implications to Egypt. In N. S. Abdelazim M Negm (Ed.), *Waste Management in MENA Regions* (pp. 149): Springer.

Elfaleh, I., Abbassi, F., Habibi, M., Ahmad, F., Guedri, M., et al. (2023). A comprehensive review of natural fibers and their composites: an eco-friendly alternative to conventional materials. *Results in Engineering*, 101271.

Eryıldız, M. (2021). Effect of build orientation on mechanical behaviour and build time of FDM 3D-printed PLA parts: an experimental investigation. *European Mechanical Science, 5*(3), 116-120.

Es-Said, O. S., Foyos, J., Noorani, R., Mendelson, M., Marloth, R., et al. (2000). Effect of layer orientation on mechanical properties of rapid prototyped samples. *Materials and Manufacturing Processes, 15*(1), 107-122.

Faidallah, R. F., Hanon, M. M., Vashist, V., Habib, A., Szakál, Z., et al. (2023). Effect of Different Standard Geometry Shapes on the Tensile Properties of 3D-Printed Polymer. *Polymers, 15*(14), 3029.

FAOSTAT. (2024). Linseed production in 2022; Crops/Regions/World List/Production Quantity (pick lists). Retrieved from http://www.fao.org/faostat/en/#data/QC

Faraj, H., Sollogoub, C., Guinault, A., Gervais, M., Bras, J., et al. (2021). A comparative study of the thermo-mechanical properties of polylactide/cellulose nanocrystal

nanocomposites obtained by two surface compatibilization strategies. *Materials Today Communications, 29*, 102907.

Fatimatuzahraa, A. W., Farahaina, B., & Yusoff, W. A. Y. (2011, 2011). *The effect of employing different raster orientations on the mechanical properties and microstructure of Fused Deposition Modeling parts.* Paper presented at the 2011 IEEE Symposium on Business, Engineering and Industrial Applications (ISBEIA), Langkawi, Malaysia.

Fernández-Santos, J., Valls, C., Cusola, O., & Roncero, M. B. (2021). Improving filmogenic and barrier properties of nanocellulose films by addition of biodegradable plasticizers. *ACS Sustainable Chemistry Engineering, 9*(29), 9647-9660.

Flauzino Neto, W. P., Silvério, H. A., Dantas, N. O., & Pasquini, D. (2013). Extraction and characterization of cellulose nanocrystals from agro-industrial residue – Soy hulls. *Industrial Crops and Products, 42*, 480-488.

Fonseca, A. F., Pereira, F. V., & Druzian, J. I. (2015). Extraction and characterization of cellulose nanocrystals from corn stover. *Cell Chem Technol, 49*(2), 127-133.

Foster, E. J., Moon, R. J., Agarwal, U. P., Bortner, M. J., Bras, J., et al. (2018a). Current characterization methods for cellulose nanomaterials. *Chem Soc Rev, 47*(8), 2609-2679.

Foster, E. J., Moon, R. J., Agarwal, U. P., Bortner, M. J., Bras, J., et al. (2018b). Current characterization methods for cellulose nanomaterials. *Chemical Society Reviews, 47*(8), 2609-2679.

Francis, D. V., Subhan, A., I. Mourad, A.-H., K. Abdalla, A., & FR Ahmed, Z. (2024). Optimizing germination conditions of Ghaf seed using ZnO nanoparticle priming through Taguchi method analysis. *Scientific Reports, 14*(1), 15946.

Franco-Urquiza, E. A., Escamilla, Y. R., & Alcántara Llanas, P. I. (2021). Characterization of 3D Printing on Jute Fabrics. *Polymers, 13*(19), 3202.

French, A. D. (2014). Idealized powder diffraction patterns for cellulose polymorphs. *Cellulose, 21*(2), 885-896.

Friedrich, K., & Almajid, A. A. (2013). Manufacturing aspects of advanced polymer composites for automotive applications. *Applied Composite Materials, 20*, 107-128.

Fuenmayor, E., Forde, M., Healy, A. V., Devine, D. M., Lyons, J. G., et al. (2018). Material considerations for fused-filament fabrication of solid dosage forms. *Pharmaceutics, 10*(2), 44.

Fukuzumi, H., Saito, T., & Isogai, A. (2013). Influence of TEMPO-oxidized cellulose nanofibril length on film properties. *Carbohydrate Polymers, 93*(1), 172-177.

Gabriel, T., Belete, A., Hause, G., Neubert, R. H., & Gebre-Mariam, T. (2021a). Isolation and characterization of cellulose nanocrystals from different lignocellulosic residues: a comparative study. *Journal of Polymers the Environment, 29*, 2964-2977.

Gabriel, T., Belete, A., Hause, G., Neubert, R. H. H., & Gebre-Mariam, T. (2022). Is mercerization the only factor for (Partial) polymorphic transition of cellulose I to cellulose II in cellulose nanocrystals? *Cellulose Chemistry and Technology, 56*(5-6), 495-507.

Gabriel, T., Belete, A., Hause, G., Neubert, R. H. H., & Gebre-Mariam, T. (2021b). Isolation and characterization of cellulose nanocrystals from different lignocellulosic residues: a comparative study. *Journal of Polymers and the Environment, 29*, 2964-2977.

Gabriel, T., Shibeshi, A., Hause, G., Neubert, R., & Gebre-Mariam, T. (2022). Is mercerization the only factor for (partial) polymorphic transition of cellulose I to cellulose II in cellulose nanocrystals? *Cellulose Chemistry and Technology, 56*, 495-507.

Gabriel, T., Wondu, K., & Dilebo, J. (2021). Valorization of khat (Catha edulis) waste for the production of cellulose fibers and nanocrystals. *PLoS One, 16*(2), e0246794.

Gao, C., Pollet, E., & Avérous, L. (2017). Properties of glycerol-plasticized alginate films obtained by thermo-mechanical mixing. *Food Hydrocolloids, 63*, 414-420.

Gao, S., Su, C., Rong, H., Yuan, G., Caisheng, Q., et al. (2023). Bibliometric Analysis of Research History, Hotspots, and Emerging Trends on Flax with CiteSpace (2000-2022). *Journal of natural fibers, 20*(1), 2194700.

Gao, X., Qi, S., Zhang, D., Su, Y., & Wang, D. (2020). The role of poly (ethylene glycol) on crystallization, interlayer bond and mechanical performance of polylactide parts fabricated by fused filament fabrication. *Additive Manufacturing, 35*, 101414.

Gapsari, F., Andoko, A., Diharjo, K., Sanjay, M., & Siengchin, S. (2022). The effectiveness of isolation and characterization nanocelullose from timoho fiber for sustainable materials. *Biomass Convers. Biorefin., 12*, 1-11.

García-Gascón, C., Castelló-Pedrero, P., & García-Manrique, J. A. J. D. (2022). Minimal surfaces as an innovative solution for the design of an additive manufactured solar-powered unmanned aerial vehicle (UAV). *6*(10), 285.

García, E., Núñez, P., Chacón, J., Caminero, M., & Kamarthi, S. (2020). Comparative study of geometric properties of unreinforced PLA and PLA-Graphene composite materials applied to additive manufacturing using FFF technology. *Polymer Testing, 91*, 106860.

George, M., Mussone, P. G., & Bressler, D. C. (2014). Surface and thermal characterization of natural fibres treated with enzymes. *Industrial Crops and Products, 53*, 365-373.

Ghafari, R., Jonoobi, M., Amirabad, L. M., Oksman, K., & Taheri, A. R. (2019). Fabrication and characterization of novel bilayer scaffold from nanocellulose based aerogel for skin tissue engineering applications. *International journal of biological macromolecules, 136*, 796-803.

Ghislandi, M., de A. Prado, L. A., Schulte, K., & Barros-Timmons, A. (2013). Effect of filler functionalization on thermo-mechanical properties of polyamide-12/carbon nanofibers composites: a study of filler–matrix molecular interactions. *Journal of Materials Science, 48*, 8427-8437.

Ghomrasni, N. B., Chivas-Joly, C., Devoille, L., Hochepied, J.-F., & Feltin, N. (2020). Challenges in sample preparation for measuring nanoparticles size by scanning electron microscopy from suspensions, powder form and complex media. *Powder Technology, 359*, 226-237.

Gill, P., Moghadam, T. T., & Ranjbar, B. (2010). Differential scanning calorimetry techniques: applications in biology and nanoscience. *Journal of biomolecular techniques: JBT, 21*(4), 167.

Gong, B., Cui, S., Zhao, Y., Sun, Y., & Ding, Q. (2017). Strain-controlled fatigue behaviors of porous PLA-based scaffolds by 3D-printing technology. *Journal of Biomaterials Science, Polymer Edition, 28*(18), 2196-2204.

Gou, J., Zhuge, J., & Liang, F. (2012). Processing of polymer nanocomposites. In *Manufacturing Techniques for Polymer Matrix Composites (PMCs)* (pp. 95-119).

Gould, E. D., Simhon, A., & Weinberg, B. A. (2020). Does parental quality matter? Evidence on the transmission of human capital using variation in parental influence from death, divorce, and family size. *Journal of Labor Economics, 38*(2), 569-610.

Grabowik, C., Kalinowski, K., Ćwikła, G., Paprocka, I., & Kogut, P. (2017). *Tensile tests of specimens made of selected group of the filament materials manufactured with FDM method.* Paper presented at the MATEC Web of Conferences.

Guessasma, S., Belhabib, S., & Nouri, H. (2019). Printability and tensile performance of 3D printed polyethylene terephthalate glycol using fused deposition modelling. *Polymers, 11*(7), 1220.

Guo, J., Huang, K., Cao, R., Zhang, J., & Xu, Y. (2021). Aliphatic extractive effects on acetic acid catalysis of typical agricultural residues to xylo-oligosaccharide and enzymatic hydrolyzability of cellulose. *Biotechnol. Biofuels, 14*(1), 1-14.

Gupta, A. P., Upadhyay, P., Sen, T., & Dutta, J. (2023). Agricultural Waste as a Resource: The Lesser Travelled Road to Sustainability. *Agriculture Waste Management and Bioresource: The Circular Economy Perspective*, 1-20.

Gupta, P. K., Uniyal, V., & Naithani, S. (2013). Polymorphic transformation of cellulose I to cellulose II by alkali pretreatment and urea as an additive. *Carbohydrate Polymers, 94*(2), 843-849.

Hamad, W. Y., & Hu, T. Q. (2010). Structure–process–yield interrelations in nanocrystalline cellulose extraction. *CJCE, 88*(3), 392-402.

Han, B., Wang, Y., Zheng, Y., Tao, Y., & Liu, X. (2022). Influence of multi-walled carbon nanotube content on electromagnetic wave absorption and mechanical properties of carbon nanotube/polyamide 12 composite. *Polymer Composites, 43*(11), 7739-7750.

Han, J., Lu, K., Yue, Y., Mei, C., Huang, C., et al. (2019). Nanocellulose-templated assembly of polyaniline in natural rubber-based hybrid elastomers toward flexible electronic conductors. *Industrial Crops Products, 128*, 94-107.

Han, J., Zhou, C., Wu, Y., Liu, F., & Wu, Q. (2013). Self-assembling behavior of cellulose nanoparticles during freeze-drying: effect of suspension concentration, particle size, crystal structure, and surface charge. *Biomacromolecules, 14*(5), 1529-1540.

Harini, K., & Mohan, C. C. (2020). Isolation and characterization of micro and nanocrystalline cellulose fibers from the walnut shell, corncob and sugarcane bagasse. *International Journal of Biological Macromolecules, 163*, 1375-1383.

Hasanzadeh, R., Mihankhah, P., Azdast, T., Aghaiee, S., & Park, C. B. (2023). Optimization of process parameters of fused filament fabrication of polylactic acid composites reinforced by aluminum using Taguchi approach. *Metals, 13*(6), 1013.

Hassan, A. D., Naeem, U. J., & Bachi, I. O. (2022). *Processing and Evaluation of Ceramic Filler Reinforced Polymer Matrix Composites.* Paper presented at the Journal of physics: Conference series.

Hayes, D. J. M. (2013). Biomass Composition and Its Relevance to Biorefining. In K. S. Triantafyllidis, A. A. Lappas, & M. Stöcker (Eds.), *The Role of Catalysis for the Sustainable Production of Bio-fuels and Bio-chemicals* (pp. 27-65). Amsterdam: Elsevier.

Hayward, M. (2019). *Interfacial Adhesion in Fibre-Polymer Composites.* (PhD Doctoral), Victoria University of Wellington, Victoria.

He, B., Ai, J., Ren, J., Zhao, L., Zhao, H., et al. (2022). Alkyl ketene dimer grafted cationic cellulose stabilizing nano magnesium oxide for efficient protection of acidic paper. *Cellulose, 29*(16), 8863-8877.

He, Q., Bai, Y., Lu, Y., Cui, B., Huang, Z., et al. (2022a). Isolation and characterization of cellulose nanocrystals from Chinese medicine residues. *Biomass Convers. Biorefin., 12*, 1-10.

He, Q., Bai, Y., Lu, Y., Cui, B., Huang, Z., et al. (2022b). Isolation and characterization of cellulose nanocrystals from Chinese medicine residues. *Biomass Conversion Biorefinery*, 1-10.

He, Q., Yang, Y., Liu, Z., Shao, D., Jiang, D., et al. (2022). Preparation and characterization of cellulose nanocrystals from spent edible fungus substrate. *Journal of the Science of Food and Agriculture, 102*(7), 2761-2772.

Heidarbeigi, J., Afshari, H., & Borghei, A. (2021). Study of physical and mechanical properties of PE/CNC nanocomposite for food packaging applications. *Journal of Thermoplastic Composite Materials, 34*(3), 396-408.

Helú, M. A. B., & Liu, L. (2021). Fused deposition modeling (FDM) based 3D printing of microelectrodes and multi-electrode probes. *Electrochimica Acta, 365*, 137279.

Henriksson, M., Berglund, L. A., Isaksson, P., Lindström, T., & Nishino, T. (2008). Cellulose nanopaper structures of high toughness. *Biomacromolecules, 9*(6), 1579-1585.

Herlina Sari, N., Wardana, I. N. G., Irawan, Y. S., & Siswanto, E. (2017). Characterization of the Chemical, Physical, and Mechanical Properties of NaOH-treated Natural Cellulosic Fibers from Corn Husks. *Journal of Natural Fibers, 15*(4), 545-558.

Herrera, N., Salaberria, A. M., Mathew, A. P., & Oksman, K. (2016). Plasticized polylactic acid nanocomposite films with cellulose and chitin nanocrystals prepared using extrusion and compression molding with two cooling rates: Effects on mechanical, thermal and optical properties. *Composites Part A: Applied Science and Manufacturing, 83*, 89-97.

Hess, A. S., & Hess, J. R. (2018). Principal component analysis. *Transfusion, 58*(7), 1580-1582.

Hirase, R., & Yuguchi, Y. (2022). Dispersion Characteristics of Cellulose Nanocrystals in Water and Ethanol Using Small-Angle X-Ray Scattering and Scanning Probe Microscopy. *Journal of Fiber Science and Technology, 78*, 89-95.

Holden, N. M., Neill, A. M., Stout, J. C., O'Brien, D., & Morris, M. A. (2023). Biocircularity: a Framework to Define Sustainable, Circular Bioeconomy. *Circular Economy and Sustainability, 3*(1), 77-91.

Hosakun, W., Tsalagkas, D., & Csóka, L. (2022). Nanocellulose-based composites for environmental applications: a review. *Innovation in Nano-Polysaccharides for Eco-sustainability*, 343-351.

Hossain, K. M. Z., Ahmed, I., Parsons, A. J., Scotchford, C. A., Walker, G. S., et al. (2012). Physico-chemical and mechanical properties of nanocomposites prepared using cellulose nanowhiskers and poly(lactic acid). *Journal of Materials Science, 47*(6), 2675-2686.

Hossain, K. M. Z., Hasan, M. S., Boyd, D., Rudd, C. D., Ahmed, I., et al. (2014). Effect of Cellulose Nanowhiskers on Surface Morphology, Mechanical Properties, and Cell Adhesion of Melt-Drawn Polylactic Acid Fibers. *Biomacromolecules, 15*(4), 1498-1506.

Hossain, M. K., Karim, M. R., Chowdhury, M. R., Imam, M. A., Hosur, M., et al. (2014). Comparative mechanical and thermal study of chemically treated and untreated single sugarcane fiber bundle. *Industrial Crops and Products, 58*, 78-90.

Hsu, C.-P., Lin, C.-S., Fan, C.-H., Chiang, N.-Y., Tsai, C.-W., et al. (2020). Geometric accuracy of an acrylonitrile butadiene styrene canine tibia model fabricated using fused deposition modelling and the effects of hydrogen peroxide gas plasma sterilisation. *BMC veterinary research, 16*, 1-8.

Hussain, M., Khan, S. M., Shafiq, M., & Abbas, N. (2024). A review on PLA-based biodegradable materials for biomedical applications. *Giant*, 100261.

Hwang, S., Reyes, E. I., Moon, K.-s., Rumpf, R. C., & Kim, N. S. (2015). Thermo-mechanical characterization of metal/polymer composite filaments and printing parameter study for fused deposition modeling in the 3D printing process. *Journal of Electronic Materials, 44*, 771-777.

Ibrahim, M., Sapuan, S., Zainudin, E., & Zuhri, M. (2019). Physical, thermal, morphological, and tensile properties of cornstarch-based films as affected by different plasticizers. *International journal of food properties, 22*(1), 925-941.

Idumah, C. I., & Obele, C. M. (2021). Understanding interfacial influence on properties of polymer nanocomposites. *Surfaces Interfaces, 22*, 100879.

Ilyas, R., Sapuan, S., Asyraf, M., Atikah, M., Ibrahim, R., et al. (2020). Introduction to biofiller-reinforced degradable polymer composites. In *Biofiller-reinforced biodegradable polymer composites* (pp. 1-23): CRC press.

Ilyas, R., Sapuan, S., Ishak, M., & Zainudin, E. (2017). Effect of delignification on the physical, thermal, chemical, and structural properties of sugar palm fibre. *BioResources, 12*(4), 8734-8754.

Ilyas, R., Sapuan, S., Nurazzi, N. M., Norrrahim, M. N. F., Ibrahim, R., et al. (2021). Macro to nanoscale natural fiber composites for automotive components: Research, development, and application. *Biocomposite synthetic composites for automotive applications*, 51-105.

Imamov, R. M., Klechkovskaya, V. V., & Suvorova, E. I. (2011). High-resolution transmission electron microscopy for crystallographic study of nanomaterials. *Crystallography Reports, 56*(4), 650-661.

Ioannidou, S. M., Ladakis, D., Moutousidi, E., Dheskali, E., Kookos, I. K., et al. (2022). Techno-economic risk assessment, life cycle analysis and life cycle costing for poly (butylene succinate) and poly (lactic acid) production using renewable resources. *Science of The Total Environment, 806*, 150594.

Ioelovich, M. (2017). Characterization of various kinds of nanocellulose. In *Handbook of nanocellulose cellulose nanocomposites* (Vol. 1, pp. 51-100).

Ioelovich, M. (2012). Study of cellulose interaction with concentrated solutions of sulfuric acid. *Int. Scholarly Res. Not., 2012*, 428974.

Islam, M., Saini, P., Das, R., Shekhar, S., Sinha, A., et al. (2023). Rice straw as a source of nanocellulose for sustainable food packaging materials: a review. *BioResources, 18*(1), 2351.

Islam, M. T., Alam, M. M., & Zoccola, M. (2013). Review on modification of nanocellulose for application in composites. *Int. J. Innov. Res. Sci. Eng. Technol, 2*(10), 5444-5451.

Ismail, K. I., Ramarad, S., & Yap, T. C. (2023). Design and fabrication of an in situ short-fiber doser for fused filament fabrication 3D printer: A novel method to manufacture fiber–polymer composite. *Inventions, 8*(1), 10.

Issam, T. (2022). Study the Ideal Proportions of Matrix, Reinforcing Materials and Additives to Obtain a Composite Material with High Tensile Strength. *Revue des Composites et des Materiaux Avances, 32*(5), 243.

Iwatake, A., Nogi, M., & Yano, H. (2008). Cellulose nanofiber-reinforced polylactic acid. *Composites Science and Technology, 68*(9), 2103-2106.

Jaffar, S. S., Saallah, S., Misson, M., Siddiquee, S., Roslan, J., et al. (2022). Recent development and environmental applications of nanocellulose-based membranes. *Membranes, 12*(3), 287.

Jalal, R., Wirjosentono, B., & Gea, S. (2014). Mechanical properties of nanocrystal cellulose reinforced polystyrene with glycerol monostearic as antistatic agent. *International Journal of ChemTech Research, 6*(4), 2421-2426.

James, A., Rahman, M. R., Mohamad Said, K. A., Kanakaraju, D., Sueraya, A. Z., et al. (2024). A review of nanocellulose modification and compatibility barrier for various applications. *Journal of Thermoplastic Composite Materials, 37*(6), 2149-2199.

Jampílek, J., & Kráľová, K. (2020). Preparation of nanocomposites from agricultural waste and their versatile applications. In *Multifunctional hybrid nanomaterials for sustainable agri-food and ecosystems* (pp. 51-98): Elsevier.

Janardhnan, S., & Sain, M. (2011). Targeted disruption of hydroxyl chemistry and crystallinity in natural fibers for the isolation of cellulose nano-fibers via enzymatic treatment. *BioResources, 6*(2), 1242-1250.

Jankauskienė, Z., Butkutė, B., Gruzdevienė, E., Cesevičienė, J., & Fernando, A. L. (2015). Chemical composition and physical properties of dew-and water-retted hemp fibers. *Industrial Crops and Products, 75*, 206-211.

Jarvis, M. C. (2023). Hydrogen bonding and other non-covalent interactions at the surfaces of cellulose microfibrils. *Cellulose, 30*(2), 667-687.

Jaxel, J., Guggenberger, M., Rosenau, T., & Böhmdorfer, S. (2020). Unbreakable and customizable dipping chambers for TLC and HPTLC manufactured by fused deposition modelling. *Talanta, 217*, 121072.

Jhala, A. J., & Hall, L. M. (2010). Flax (Linum usitatissimum L.): current uses and future applications. *Aust. J. Basic Appl. Sci, 4*(9), 4304-4312.

Jiang, F., & Hsieh, Y.-L. (2015). Cellulose nanocrystal isolation from tomato peels and assembled nanofibers. *Carbohydrate Polymers, 122*, 60-68.

Jiang, G., Yang, T., Xu, J., Tao, D., Luo, C., et al. (2020). Investigation into hydroxypropyl-methylcellulose-reinforced polylactide composites for fused deposition modelling. *Industrial Crops Products, 146*, 112174.

Jiang, J., Zhu, Y., & Jiang, F. (2021). Sustainable isolation of nanocellulose from cellulose and lignocellulosic feedstocks: Recent progress and perspectives. *Carbohydrate polymers, 267*, 118188.

Jiang, X., Wang, Y., Herricks, T., & Xia, Y. (2004). Ethylene glycol-mediated synthesis of metal oxide nanowires. *Journal of Materials Chemistry, 14*(4), 695-703.

Jin, F.-L., Hu, R.-R., & Park, S.-J. (2019). Improvement of thermal behaviors of biodegradable poly (lactic acid) polymer: A review. *Composites Part B: Engineering, 164*, 287-296.

Johansson, C., Bras, J., Mondragon, I., Nechita, P., Plackett, D., et al. (2012). Renewable fibers and bio-based materials for packaging applications-a review of recent developments. *BioResources, 7*(2), 2506-2552.

Johar, N., Ahmad, I., & Dufresne, A. (2012). Extraction, preparation and characterization of cellulose fibres and nanocrystals from rice husk. *Industrial Crops and Products, 37*(1), 93-99.

Jordan, J. H., Easson, M. W., Dien, B., Thompson, S., & Condon, B. D. (2019). Extraction and characterization of nanocellulose crystals from cotton gin motes and cotton gin waste. *Cellulose, 26*(10), 5959-5979.

Kabir, S. M. F., Mathur, K., & Seyam, A.-F. M. (2020). A critical review on 3D printed continuous fiber-reinforced composites: History, mechanism, materials and properties. *Composite Structures, 232*, 111476.

Kading, B., & Straub, J. (2015). Utilizing in-situ resources and 3D printing structures for a manned Mars mission. *Acta Astronautica, 107*, 317-326.

Kadry, G., & Abd El-Hakim, A. E. F. (2015). Effect of nanocellulose on the biodegradation, morphology and mechanical properties of polyvinylchloride/nanocellulose nanocomposites. *Research journal of pharmaceutical biological and chemical sciences, 6*(6), 659-666.

Kafy, A., Sadasivuni, K. K., Akther, A., Min, S.-K., & Kim, J. (2015). Cellulose/graphene nanocomposite as multifunctional electronic and solvent sensor material. *Materials Letters, 159*, 20-23.

Kakroodi, A. R. (2014). Shuna Cheng, Mohini Sain, Abdullah Asiri,"Mechanical, Thermal, and Morphological Properties of Nanocomposites Based on Polyvinyl Alcohol and Cellulose Nanofiber from Aloe vera Rind". *Journal of Nano Materials, 2014*, 1-7.

Kale, R. D., Taye, M., & Chaudhary, B. (2019). Extraction and characterization of cellulose single fiber from native Ethiopian Serte (Dracaena steudneri Egler) plant leaf. *Journal of Macromolecular Science, Part A, 56*(9), 837-844.

Kalia, S., Dufresne, A., Cherian, B. M., Kaith, B. S., Avérous, L., et al. (2011). Cellulose-based bio-and nanocomposites: a review. *International journal of polymer science, 2011*(1), 837875.

Kallel, F., Bettaieb, F., Khiari, R., García, A., Bras, J., et al. (2016). Isolation and structural characterization of cellulose nanocrystals extracted from garlic straw residues. *Industrial crops and products, 87*, 287-296.

Kalyon, D. M., Birinci, E., Yazici, R., Karuv, B., & Walsh, S. (2002). Electrical properties of composites as affected by the degree of mixedness of the conductive filler in the polymer matrix. *Polymer Engineering Science, 42*(7), 1609-1617.

Kamada, H., Hata, Y., Sugiura, K., Sawada, T., & Serizawa, T. (2024). Interfacial jamming of surface-alkylated synthetic nanocelluloses for structuring liquids. *Carbohydrate Polymers, 331*, 121896.

Kamal, M. R., & Khoshkava, V. (2015). Effect of cellulose nanocrystals (CNC) on rheological and mechanical properties and crystallization behavior of PLA/CNC nanocomposites. *Carbohydrate Polymers, 123*, 105-114.

Kamali Moghaddam, M., & Karimi, E. (2020). The effect of oxidative bleaching treatment on Yucca fiber for potential composite application. *Cellulose, 27*(16), 9383-9396.

Kandemir, A., Pozegic, T. R., Hamerton, I., Eichhorn, S. J., & Longana, M. L. (2020). Characterisation of natural fibres for sustainable discontinuous fibre composite materials. *Materials, 13*(9), 2129.

Kang, L. Y., & Haslija, A. A. (2019). *Optimization of Alkaline Pulp Extraction from Napier Grass Using Response Surface Methodology.* Paper presented at the IOP Conference Series: Earth and Environmental Science.

Kanishka, K., & Acherjee, B. (2023). Revolutionizing manufacturing: A comprehensive overview of additive manufacturing processes, materials, developments, and challenges. *Journal of Manufacturing Processes, 107*, 574-619.

Kaptan, A., & Kartal, F. S. (2024). A critical review of composite filaments for fused deposition modeling: Material properties, applications, and future directions. *European Mechanical, 8*(3), 199-209.

Kargarzadeh, H., Ahmad, I., Abdullah, I., Dufresne, A., Zainudin, S. Y., et al. (2012). Effects of hydrolysis conditions on the morphology, crystallinity, and thermal stability of cellulose nanocrystals extracted from kenaf bast fibers. *Cellulose, 19*(3), 855-866.

Kargarzadeh, H., Ahmad, I., Thomas, S., & Dufresne, A. (2017). *Handbook of Nanocellulose and Cellulose Nanocomposites*.

Kargarzadeh, H., Ioelovich, M., Ahmad, I., Thomas, S., & Dufresne, A. (2017a). Methods for Extraction of Nanocellulose from Various Sources. In *Handbook of*

Nanocellulose and Cellulose Nanocomposites (Vol. 1, pp. 1-49). Hoboken, New Jersey, U.S.: Wiley online library.

Kargarzadeh, H., Ioelovich, M., Ahmad, I., Thomas, S., & Dufresne, A. (2017b). Methods for extraction of nanocellulose from various sources. In I. A. Hanieh Kargarzadeh, Sabu Thomas, Alain Dufresne (Ed.), *Handbook of nanocellulose cellulose nanocomposites* (Vol. 1, pp. 1-49): Wiley Online Library.

Karthik, T., & Murugan, R. (2013). Characterization and analysis of ligno-cellulosic seed fiber from Pergularia daemia plant for textile applications. *Fibers and Polymers, 14*(3), 465-472.

Karunakaran, G., Periyasamy, A. P., & Tehrani, A. (2023). Extraction of micro, nanocrystalline cellulose and textile fibers from coffee waste. *Journal of Testing and Evaluation, 51*(5), 3042-3056.

Katakojwala, R., & Mohan, S. V. (2020). Microcrystalline cellulose production from sugarcane bagasse: Sustainable process development and life cycle assessment. *Journal of Cleaner Production, 249*, 119342.

Kaur, P., Sharma, N., Munagala, M., Rajkhowa, R., Aallardyce, B., et al. (2021). Nanocellulose: resources, physio-chemical properties, current uses and future applications. *Frontiers in Nanotechnology, 3*, 747329.

Kaushik, M., Fraschini, C., Chauve, G., Putaux, J.-L., & Moores, A. (2015). *Transmission electron microscopy for the characterization of cellulose nanocrystals*: IntechOpen.

Kawaguchi, D., Nakayama, R., Koga, H., Totani, M., & Tanaka, K. (2023). Improvement of polymer adhesion by designing the interface layer. *Polymer, 265*, 125581.

Khan, S. U., Labonne, L., Ouagne, P., & Evon, P. (2021). Continuous mechanical extraction of fibres from linseed flax straw for subsequent geotextile applications. *Coatings, 11*(7), 852.

Kharine, A., Manohar, S., Seeton, R., Kolkman, R. G., Bolt, R. A., et al. (2003). Poly (vinyl alcohol) gels for use as tissue phantoms in photoacoustic mammography. *Physics in Medicine & Biology, 48*(3), 357.

Khouri, N. G., Bahú, J. O., Blanco-Llamero, C., Severino, P., Concha, V. O. C., et al. (2024). Polylactic acid (PLA): Properties, synthesis, and biomedical applications-A review of the literature. *Journal of Molecular Structure*, 138243.

Kian, L., Saba, N., Jawaid, M., & Sultan, M. (2019). A review on processing techniques of bast fibers nanocellulose and its polylactic acid (PLA) nanocomposites. *International Journal of Biological Macromolecules, 121*, 1314-1328.

Kiziltas, A., Nazari, B., Erbas Kiziltas, E., Gardner, D. J., Han, Y., et al. (2016). Method to reinforce polylactic acid with cellulose nanofibers via a polyhydroxybutyrate carrier system. *Carbohydrate Polymers, 140*, 393-399.

Komuraiah, A., Kumar, N. S., & Prasad, B. D. (2014). Chemical composition of natural fibers and its influence on their mechanical properties. *Mechanics of composite materials, 50*(3), 359-376.

Kong, Y., & Hay, J. N. (2002). The measurement of the crystallinity of polymers by DSC. *Polymer, 43*(14), 3873-3878.

Korolovych, V. F., Cherpak, V., Nepal, D., Ng, A., Shaikh, N. R., et al. (2018). Cellulose nanocrystals with different morphologies and chiral properties. *Polym, 145*, 334-347.

Koul, B., Yakoob, M., & Shah, M. P. (2022). Agricultural waste management strategies for environmental sustainability. *Environmental Research, 206*, 112285.

Kowalczyk, M., Piorkowska, E., Kulpinski, P., & Pracella, M. (2011). Mechanical and thermal properties of PLA composites with cellulose nanofibers and standard size fibers. *Composites Part A: Applied Science and Manufacturing, 42*(10), 1509-1514.

Kozłowski, R. M., Mackiewicz-Talarczyk, M., Wielgusz, K., Praczyk, M., & Allam, A. M. (2020). Bast fibres: flax. In R. M. Kozłowski & M. Mackiewicz-Talarczyk (Eds.), *Handbook of Natural Fibres (Second Edition)* (pp. 93-162): Woodhead Publishing.

Krajangsawasdi, N., Blok, L. G., Hamerton, I., Longana, M. L., Woods, B. K. S., et al. (2021). Fused Deposition Modelling of Fibre Reinforced Polymer Composites: A Parametric Review. *Journal of Composites Science, 5*(1), 29.

Kramer, O., Eikenbusch, J. K., Gheitasi, F., & Wu, J. (2024). Application of nanocellulose in food packaging-A SWOT analysis. *Detritus*(2023-Volume).

Kulshreshtha, S., & Ukaogo, P. O. (2021). Recent Advances in Mushroom Cultivation Technology and Its Application. *Bright Sky*.

Kumar, A., Negi, Y. S., Choudhary, V., & Bhardwaj, N. K. (2014a). Characterization of cellulose nanocrystals produced by acid-hydrolysis from sugarcane bagasse as agro-waste. *J. Mater. Phys. Chem., 2*(1), 1-8.

Kumar, A., Negi, Y. S., Choudhary, V., & Bhardwaj, N. K. (2014b). Characterization of cellulose nanocrystals produced by acid-hydrolysis from sugarcane bagasse as agro-waste. *J. Mater. Phys. Chem, 2*(1), 1-8.

Kumar, P., Shamim, Muztaba, M., Ali, T., Bala, J., et al. (2024). Fused Deposition Modeling 3D-Printed Scaffolds for Bone Tissue Engineering Applications: A Review. *Annals of Biomedical Engineering, 52*(5), 1184-1194.

Kumar, S. D., Venkadeshwaran, K., & Aravindan, M. (2020). Fused deposition modelling of PLA reinforced with cellulose nano-crystals. *Materials Today: Proceedings, 33*, 868-875.

La Gala, A., Ceretti, D. V., Fiorio, R., Cardon, L., & D'hooge, D. R. (2022). Comparing pellet-and filament-based additive manufacturing with conventional processing for ABS and PLA parts. *Journal of Applied Polymer Science, 139*(44), e53089.

Lamaming, J., Hashim, R., Leh, C. P., Sulaiman, O., Sugimoto, T., et al. (2015). Isolation and characterization of cellulose nanocrystals from parenchyma and vascular bundle of oil palm trunk (Elaeis guineensis). *Carbohydrate Polymers, 134*, 534-540.

Lani, N. S., Ngadi, N., Johari, A., & Jusoh, M. (2014). Isolation, characterization, and application of nanocellulose from oil palm empty fruit bunch fiber as nanocomposites. *Journal of Nanomaterials, 2014*, 13.

Lanzotti, A., Grasso, M., Staiano, G., & Martorelli, M. (2015). The impact of process parameters on mechanical properties of parts fabricated in PLA with an open-source 3-D printer. *Rapid Prototyping Journal, 21*(5), 604-617.

Laurindo, J. B. (2016). Barrier Properties of Films. In *Edible Films and Coatings* (pp. 71-82): CRC Press.

Le Gall, M., Davies, P., Martin, N., & Baley, C. (2018). Recommended flax fibre density values for composite property predictions. *Industrial crops and products, 114*, 52-58.

Le, T.-H., Le, V.-S., Dang, Q.-K., Nguyen, M.-T., Le, T.-K., et al. (2021). Microstructure evaluation and thermal–mechanical properties of abs matrix composite filament reinforced with multi-walled carbon nanotubes by a single screw extruder for fdm 3d printing. *Applied Sciences, 11*(19), 8798.

Lee, C. H., Khalina, A., Lee, S., & Liu, M. (2020). A Comprehensive Review on Bast Fibre Retting Process for Optimal Performance in Fibre-Reinforced Polymer Composites. *Advances in Materials Science and Engineering, 2020*(1), 6074063.

Lee, C. H., Padzil, F. N. B. M., Lee, S. H., Ainun, Z. M. A. a., & Abdullah, L. C. (2021). Potential for Natural Fiber Reinforcement in PLA Polymer Filaments for Fused Deposition Modeling (FDM) Additive Manufacturing: A Review. *Polymers, 13*(9), 1407.

Lee, H. V., Hamid, S. B. A., & Zain, S. K. (2014). Conversion of lignocellulosic biomass to nanocellulose: structure and chemical process. *Sci. World J., 2014*, 631013.

Lee, S.-Y., Mohan, D. J., Kang, I.-A., Doh, G.-H., Lee, S., et al. (2009). Nanocellulose reinforced PVA composite films: Effects of acid treatment and filler loading. *Fibers and Polymers, 10*(1), 77-82.

Leite, M., Fernandes, J., Deus, A. M., Reis, L., & Vaz, M. F. (2018). *Study of the influence of 3D printing parameters on the mechanical properties of PLA.* Paper presented at the Proceedings of the 3rd International Conference on Progress in Additive Manufacturing (Pro-AM 2018), Nanyang Technological University, Singapore.

Letcher, T., & Waytashek, M. (2014). *Material Property Testing of 3D-Printed Specimen in PLA on an Entry-Level 3D Printer.* Paper presented at the ASME 2014 International Mechanical Engineering Congress and Exposition.

Li, H., Wang, Z., Zhang, H., & Pan, Z. (2018). Nanoporous PLA/(chitosan nanoparticle) composite fibrous membranes with excellent air filtration and antibacterial performance. *Polymers, 10*(10), 1085.

Li, S., Xu, S., Liu, S., Yang, C., & Lu, Q. (2004). Fast pyrolysis of biomass in free-fall reactor for hydrogen-rich gas. *Fuel Processing Technology, 85*(8-10), 1201-1211.

Li, W., Wu, D., & Pan, F. (2012). A construction for doubly pandiagonal magic squares. *Discrete Mathematics, 312*(2), 479-485.

Li, W., Zhao, X., Huang, Z., & Liu, S. (2013). Nanocellulose fibrils isolated from BHKP using ultrasonication and their reinforcing properties in transparent poly (vinyl alcohol) films. *Journal of Polymer Research, 20*, 1-7.

Li, Y.-Y., Bai, Y.-R., Zhang, X.-Q., Liu, X., Dai, Z., et al. (2023). Preparation, Properties, and Mechanism of Anionic and Cationic Cellulose Nanocrystals/Waterborne Polyurethane Composite Films. *Bioresources, 18*(1).

Li, Y., Huang, L., Wang, X., Wang, Y., Lu, X., et al. (2023). Blending and functionalisation modification of 3D printed polylactic acid for fused deposition modeling. *Reviews on Advanced Materials Science, 62*(1), 20230140.

Ligon, S. C., Liska, R., Stampfl, J., Gurr, M., & Mülhaupt, R. (2017). Polymers for 3D printing and customized additive manufacturing. *Chemical reviews, 117*(15), 10212-10290.

Lim, W.-L., Gunny, A. A. N., Kasim, F. H., Gopinath, S. C., Kamaludin, N. H. I., et al. (2021). Cellulose nanocrystals from bleached rice straw pulp: acidic deep eutectic solvent versus sulphuric acid hydrolyses. *Cellulose, 28*(10), 6183-6199.

Lin, K.-H., Enomae, T., & Chang, F.-C. (2019). Cellulose nanocrystal isolation from hardwood pulp using various hydrolysis conditions. *Molecules, 24*(20), 3724.

Lin, L., Yan, R., Liu, Y., & Jiang, W. (2010). In-depth investigation of enzymatic hydrolysis of biomass wastes based on three major components: Cellulose, hemicellulose and lignin. *Bioresour Technol, 101*(21), 8217-8223.

Lin, N., & Dufresne, A. (2013). Physical and/or Chemical Compatibilization of Extruded Cellulose Nanocrystal Reinforced Polystyrene Nanocomposites. *Macromolecules, 46*(14), 5570-5583.

Lisha Zhang, L. (2013). *Pectin degradation by Botrytis cinerea: recognition of endopolygalacturonases by an Arabidopsis receptor and utilization of Dgalacturonic acid.* (PhD Dissertation), Wageningen University & Research, S.l. Retrieved from https://edepot.wur.nl/258044

Liu, D., Zhong, T., Chang, P. R., Li, K., & Wu, Q. (2010). Starch composites reinforced by bamboo cellulosic crystals. *Bioresource Technology, 101*(7), 2529-2536.

Lomelí-Ramírez, M. G., Valdez-Fausto, E. M., Rentería-Urquiza, M., Jiménez-Amezcua, R. M., Hernández, J. A., et al. (2018). Study of green nanocomposites based on corn starch and cellulose nanofibrils from Agave tequilana Weber. *Carbohydrate polymers, 201*, 9-19.

Lu, F., Yu, H., Yan, C., & Yao, J. (2016). Polylactic acid nanocomposite films with spherical nanocelluloses as efficient nucleation agents: effects on crystallization, mechanical and thermal properties. *RSC advances, 6*(51), 46008-46018.

Lu, P., & Hsieh, Y.-L. (2012). Preparation and characterization of cellulose nanocrystals from rice straw. *Carbohydrate Polymers, 87*(1), 564-573.

Lu, P., & Hsieh, Y.-L. (2010). Preparation and properties of cellulose nanocrystals: rods, spheres, and network. *Carbohydrate Polymers, 82*(2), 329-336.

Lu, S., Ma, T., Hu, X., Zhao, J., Liao, X., et al. (2022). Facile extraction and characterization of cellulose nanocrystals from agricultural waste sugarcane straw. *Journal of the Science of Food and Agriculture, 102*(1), 312-321.

Lu, T., Jiang, M., Jiang, Z., Hui, D., Wang, Z., et al. (2013). Effect of surface modification of bamboo cellulose fibers on mechanical properties of cellulose/epoxy composites. *Composites Part B: Engineering, 51*, 28-34.

Lyu, Y., Wu, J., Zhang, H., Brádaigh, C. M. Ó., & Yang, D. (2023). Effects of thermal process conditions on crystallinity and mechanical properties in material extrusion additive manufacturing of discontinuous carbon fibre reinforced polyphenylene sulphide composites. *Journal of Composite Materials, 57*(24), 3775-3787.

Ma, L., Zhang, Y., & Wang, S. (2017). Preparation and characterization of acrylonitrile-butadiene-styrene nanocomposites reinforced with cellulose nanocrystal via solution casting method. *Polymer Composites, 38*.

Magalhães da Silva, S. P., Antunes, T., Costa, M. E. V., & Oliveira, J. M. (2020). Cork-like filaments for Additive Manufacturing. *Additive Manufacturing, 34*, 101229.

Magunga, L., Magagula, S. I., Motloung, M. T., Lebelo, K., & Mochane, M. (2023). Cellulose reinforced polyamide composites: Effect of preparation method on composite properties. *Cellulose chemistry technology, 57*(9-10), 1087-1105.

Mahardika, M., Abral, H., Kasim, A., Arief, S., & Asrofi, M. (2018). Production of nanocellulose from pineapple leaf fibers via high-shear homogenization and ultrasonication. *Fibers, 6*(2), 28.

Maheswari, C. U., Reddy, K. O., Muzenda, E., Guduri, B., & Rajulu, A. (2012). Extraction and characterization of cellulose microfibrils from agricultural residue–Cocos nucifera L. *Biomass bioenergy, 46*, 555-563.

Mahjoub, R., Yatim, J. M., Mohd Sam, A. R., & Hashemi, S. H. (2014). Tensile properties of kenaf fiber due to various conditions of chemical fiber surface modifications. *Construction and Building Materials, 55*, 103-113.

Mahmoud, Y., Safidine, Z., & Belhaneche-Bensemra, N. (2021). Characterization of microcrystalline cellulose extracted from walnut and apricots shells by alkaline treatment. *Journal of the Serbian Chemical Society, 86*(5), 521-532.

Maiti, S., Jayaramudu, J., Das, K., Reddy, S. M., Sadiku, R., et al. (2013). Preparation and characterization of nano-cellulose with new shape from different precursor. *Carbohydrate Polymers, 98*(1), 562-567.

Majeed, K., Jawaid, M., Hassan, A., Bakar, A. A., Khalil, H. A., et al. (2013). Potential materials for food packaging from nanoclay/natural fibres filled hybrid composites. *Materials Design, 46*, 391-410.

Mamaye, M., Kiflie, Z., Feleke, S., & Yimam, A. (2020). Evaluation of soda delignification and single-stage hydrogen peroxide bleaching for the Ethiopian sugarcane bagasse for paper production. *Sugar Tech*, 1-12.

Manimaran, P., Sanjay, M., Senthamaraikannan, P., Yogesha, B., Barile, C., et al. (2018). A new study on characterization of Pithecellobium dulce fiber as composite reinforcement for light-weight applications. *Journal of Natural Fibers.*

Marano, S., Laudadio, E., Minnelli, C., & Stipa, P. (2022). Tailoring the barrier properties of PLA: a state-of-the-art review for food packaging applications. *Polymers, 14*(8), 1626.

Marcuello, C., Chabbert, B., Berzin, F., Bercu, N. B., Molinari, M., et al. (2023). Influence of surface chemistry of fiber and lignocellulosic materials on adhesion properties with polybutylene succinate at nanoscale. *Materials, 16*(6), 2440.

Marrot, L., Lefeuvre, A., Pontoire, B., Bourmaud, A., & Baley, C. (2013). Analysis of the hemp fiber mechanical properties and their scattering (Fedora 17). *Industrial Crops and Products, 51*, 317-327.

Martin, N., Mouret, N., Davies, P., & Baley, C. (2013). Influence of the degree of retting of flax fibers on the tensile properties of single fibers and short fiber/polypropylene composites. *Industrial Crops and Products, 49*, 755-767.

Martincic, M., Sandoval, S., Oró, J., & Tobías-Rossell, G. (2024). Thermal Stability and Purity of Graphene and Carbon Nanotubes: Key Parameters for Their Thermogravimetric Analysis (TGA). *Preprints, 1*, 2024060317.

Martínez-Sanz, M., Lopez-Rubio, A., & Lagaron, J. M. (2013). Nanocomposites of ethylene vinyl alcohol copolymer with thermally resistant cellulose nanowhiskers by melt compounding (I): Morphology and thermal properties. *J. Appl. Polym. Sci., 128*(5), 2666-2678.

Martínez-Sanz, M., Lopez-Rubio, A., & Lagaron, J. M. (2012). Optimization of the Dispersion of Unmodified Bacterial Cellulose Nanowhiskers into Polylactide via Melt Compounding to Significantly Enhance Barrier and Mechanical Properties. *Biomacromolecules, 13*(11), 3887-3899.

Martinsson, O. R., Nordin, A., & Tavčar, J. (2022). *Compounding composites from raw materials with extrusion directly on 3D printer*. Paper presented at the Proceedings of the Design Society.

Masood, S. H., & Song, W. Q. (2004). Development of new metal/polymer materials for rapid tooling using Fused deposition modelling. *Materials & Design, 25*(7), 587-594.

Masruchin, N. (2023). Nanocellulose, The Origin of Natural Reinforcement in Advanced Biocomposites. *Journal of Fibers Polymer Composites, 2*(1).

Mazian, B., Bergeret, A., Benezet, J.-C., & Malhautier, L. (2018). Influence of field retting duration on the biochemical, microstructural, thermal and mechanical properties of hemp fibres harvested at the beginning of flowering. *Industrial crops and products, 116*, 170-181.

Mazloumi, M., Johnston, L. J., & Jakubek, Z. J. (2018). Dispersion, stability and size measurements for cellulose nanocrystals by static multiple light scattering. *Cellulose, 25*, 5751-5768.

Md Salim, R., Asik, J., Sarjadi, M. S. J. W. S., & Technology. (2021). Chemical functional groups of extractives, cellulose and lignin extracted from native Leucaena leucocephala bark. *Wood Sci. Technol., 55*, 295-313.

Mehdi Jonoobi, M. J., Jalaluddin Harun, J. H., Paridah Md. Tahir, P. M. T., Lukmanul Hakim Zaini, L. H. Z., Syeed SaifulAzry, S. S., et al. (2010). Characteristics of nanofibers extracted from kenaf core. *BioResources, 5*(4), 2556-2566

Mehdi Jonoobi, M. J., Jalaludin Harun, J. H., Shakeri, A., Misra, M., & Oksman, K. (2009). Chemical composition, crystallinity, and thermal degradation of bleached and unbleached kenaf bast (Hibiscus cannabinus) pulp and nanofibers. *BioResources, 4*(2), 626-639.

Melikoğlu, A. Y., Bilek, S. E., & Cesur, S. (2019). Optimum alkaline treatment parameters for the extraction of cellulose and production of cellulose nanocrystals from apple pomace. *Carbohydrate Polymers, 215*, 330-337.

Meng, S., He, H., Jia, Y., Yu, P., Huang, B., et al. (2017). Effect of nanoparticles on the mechanical properties of acrylonitrile–butadiene–styrene specimens fabricated by fused deposition modeling. *Journal of Applied Polymer Science, 134*(7).

Miao, C., Mauran, D., & Hamad, W. Y. (2022). How hydrogen-bonding interactions and nanocrystal aspect ratios influence the morphology and mechanical performance of polymer nanocomposites reinforced with cellulose nanocrystals. *Soft Matter, 18*(24), 4572-4581.

Milosevic, M., Stoof, D., & Pickering, K. L. (2017). Characterizing the mechanical properties of fused deposition modelling natural fiber recycled polypropylene composites. *Journal of Composites Science, 1*(1), 7.

Ming, Y., Xin, Z., Zhang, J., Duan, Y., & Wang, B. (2020). Fabrication of continuous glass fiber-reinforced dual-cure epoxy composites via UV-assisted fused deposition modeling. *Composites Communications, 21*, 100401.

Mishra, R. K., Sabu, A., & Tiwari, S. K. (2018). Materials chemistry and the futurist eco-friendly applications of nanocellulose: Status and prospect. *Journal of Saudi Chemical Society, 22*(8), 949-978.

Mishra, S., Prabhakar, B., Kharkar, P. S., & Pethe, A. M. (2022). Banana peel waste: an emerging cellulosic material to extract nanocrystalline cellulose. *ACS omega, 8*(1), 1140-1145.

Missio, A. L., Otoni, C. G., Zhao, B., Beaumont, M., Khakalo, A., et al. (2022). Nanocellulose removes the need for chemical crosslinking in tannin-based rigid foams and enhances their strength and fire retardancy. *ACS Sustainable Chemistry Engineering, 10*(31), 10303-10310.

Mittal, M., & Chaudhary, R. (2018). Experimental study on the water absorption and surface characteristics of alkali treated pineapple leaf fiber and coconut husk fiber. *Int J Appl Eng Res, 13*(15), 12237-12243.

Mohammadi, M., Zolfagharian, A., Bodaghi, M., Xiang, Y., & Kouzani, A. Z. (2022). 4D printing of soft orthoses for tremor suppression. *Bio-Design Manufacturing, 5*(4), 786-807.

Mohammadpour-Haratbar, A., Boraei, S. B. A., Munir, M. T., Zare, Y., & Rhee, K. Y. (2024). A model for tensile strength of cellulose nanocrystals polymer nanocomposites. *Industrial Crops Products, 213*, 118458.

Mohite, A. S., Jagtap, A. R., Avhad, M. S., & More, A. P. (2022). Recycling of major agriculture crop residues and its application in polymer industry: A Review in the context of waste to energy nexus. *Energy Nexus, 7*, 100134.

Mohomane, S. M., Motloung, S. V., Koao, L. F., & Motaung, T. E. (2022). Effects of acid hydrolysis on the extraction of cellulose nanocrystals (CNCs): A review. *Cellul. Chem. Technol, 56*, 691-703.

Mokobia, K., Jonathan, E. M., Oyiborhoro, G., Maliki, M., & Ifijen, I. H. (2024). *Environmental degradation of polymer-based composite materials: challenges and mitigation strategies.* Paper presented at the TMS Annual Meeting & Exhibition.

Mondragon, G., Fernandes, S., Retegi, A., Peña, C., Algar, I., et al. (2014a). A common strategy to extracting cellulose nanoentities from different plants. *Ind. Crops Prod., 55*, 140-148.

Mondragon, G., Fernandes, S., Retegi, A., Peña, C., Algar, I., et al. (2014b). A common strategy to extracting cellulose nanoentities from different plants. *Industrial Crops and Products, 55*, 140-148.

Monfared, V., Bakhsheshi-Rad, H. R., Ramakrishna, S., Razzaghi, M., & Berto, F. (2021). A Brief Review on Additive Manufacturing of Polymeric Composites and Nanocomposites. *Micromachines, 12*(6).

Montoya-Escobar, N., Ospina-Acero, D., Velásquez-Cock, J. A., Gómez-Hoyos, C., Serpa Guerra, A., et al. (2022). Use of fourier series in X-ray diffraction (XRD) analysis and fourier-transform infrared spectroscopy (FTIR) for estimation of crystallinity in cellulose from different sources. *Polymers, 14*(23), 5199.

Morales, C., Giraldo, R., & Torres, M. (2021). Boxplot fences in proficiency testing. *Accreditation Quality Assurance, 26*(4), 193-200.

Morán, J. I., Alvarez, V. A., Cyras, V. P., & Vázquez, A. (2008). Extraction of cellulose and preparation of nanocellulose from sisal fibers. *Cellulose, 15*(1), 149-159.

Mostafa, K. G., Montemagno, C., & Qureshi, A. J. (2018). Strength to cost ratio analysis of FDM Nylon 12 3D Printed Parts. *Procedia Manufacturing, 26*, 753-762.

Mtibe, A., Linganiso, L. Z., Mathew, A. P., Oksman, K., John, M. J., et al. (2015). A comparative study on properties of micro and nanopapers produced from cellulose and cellulose nanofibres. *Carbohydrate Polymers, 118*, 1-8.

Mtibe, A., Motloung, M. P., Bandyopadhyay, J., & Ray, S. S. (2021). Synthetic biopolymers and their composites: Advantages and limitations—An overview. *Macromolecular rapid communications, 42*(15), 2100130.

Murphy, C. A., & Collins, M. N. (2018). Microcrystalline cellulose reinforced polylactic acid biocomposite filaments for 3D printing. *Polymer Composites, 39*(4), 1311-1320.

Murray-Smith, D. J. (2015). Testing and validation of computer simulation models. In D. J. Murray-Smith (Ed.), *Simulation Foundations, Methods Applications* (pp. 233-343): Springer Cham.

Musino, D., Rivard, C., Landrot, G., Novales, B., Rabilloud, T., et al. (2021). Hydroxyl groups on cellulose nanocrystal surfaces form nucleation points for silver nanoparticles of varying shapes and sizes. *Journal of colloid interface science, 584*, 360-371.

N'gatta, K. M., Belaid, H., El Hayek, J., Assanvo, E. F., Kajdan, M., et al. (2022a). 3D printing of cellulose nanocrystals based composites to build robust biomimetic scaffolds for bone tissue engineering. *Scientific Reports, 12*(1), 21244.

N'gatta, K. M., Belaid, H., El Hayek, J., Assanvo, E. F., Kajdan, M., et al. (2022b). 3D printing of cellulose nanocrystals based composites to build robust biomimetic scaffolds for bone tissue engineering. *Scientific Reports, 12*(1), 21244.

Nabipour, M., Akhoundi, B., & Bagheri Saed, A. (2020). Manufacturing of polymer/metal composites by fused deposition modeling process with polyethylene. *Journal of Applied Polymer Science, 137*(21), 48717.

Naduparambath, S., Jinitha, T., Shaniba, V., Sreejith, M., Balan, A. K., et al. (2018). Isolation and characterisation of cellulose nanocrystals from sago seed shells. *Carbohydrate polymers, 180*, 13-20.

Nair, G., Singh, A., Zimniewska, M., & Raghavan, V. (2013). Comparative Evaluation of Physical and Structural Properties of Water Retted and Non-retted Flax Fibers. *Fibers, 1*(3), 59-69.

Nakagaito, A. N., Fujimura, A., Sakai, T., Hama, Y., & Yano, H. (2009). Production of microfibrillated cellulose (MFC)-reinforced polylactic acid (PLA) nanocomposites from sheets obtained by a papermaking-like process. *Composites Science and Technology, 69*(7), 1293-1297.

Nanda, A., Mohapatra, B. B., Mahapatra, A. P. K., Mahapatra, A. P. K., & Mahapatra, A. P. K. (2021). Multiple comparison test by Tukey's honestly significant difference (HSD): Do the confident level control type I error. *International Journal of Statistics Applied Mathematics, 6*(1), 59-65.

Nang An, V., Chi Nhan, H. T., Tap, T. D., Van, T. T. T., Van Viet, P., et al. (2020). Extraction of high crystalline nanocellulose from biorenewable sources of Vietnamese agricultural wastes. *Journal of Polymers and the Environment, 28*, 1465-1474.

Nascimento, D. M., Almeida, J. S., Dias, A. F., Figueirêdo, M. C. B., Morais, J. P. S., et al. (2014). A novel green approach for the preparation of cellulose nanowhiskers from white coir. *Carbohydrate polymers, 110*, 456-463.

Nayak, S., & Mukherjee, A. K. (2015). Management of agricultural wastes using microbial agents. *Waste Manag. Chall. Threat. Oppor*, 65-91.

Nayak, S. Y., Heckadka, S. S., Seth, A., Prabhu, S., Sharma, R., et al. (2021). Effect of chemical treatment on the physical and mechanical properties of flax fibers: A comparative assessment. *Materials Today: Proceedings, 38*, 2406-2410.

Neciosup-Puican, A. A., Castañeda-Vía, J. A., Landauro, C. V., Quispe-Marcatoma, J., Samolski, I., et al. (2023). Synthesis of nanocellulose as mechanical reinforcement of thermoplastic starch. *MOMENTO*(67), 55-66.

Neelambaram, P., Thounchiyath, T., Narayan, R., & Chakrabarty, A. (2023). Cellulose nanofiber-incorporated high-solid siloxane acrylic latex by mini-emulsion polymerization for hydrophobic coating and wood adhesive. *Polymers for Advanced Technologies, 34*(12), 3859-3869.

Neena, P. (2023). Development of nanocomposite with LDPE and Graphene nanoparticles by means of melt extrusion method. *Materials Today: Proceedings*.

Nejatpour, M., Fallah, A., & Koc, B. (2024). An overview of 4D printing of smart multifunction continuous fiber-reinforced composites: recent advances and novel applications. *Advanced Composites and Hybrid Materials, 7*(5), 133.

Nepomuceno, N. C., Seixas, A. A. A., Medeiros, E. S., & Mélo, T. J. A. (2021). Evaluation of conductivity of nanostructured polyaniline/cellulose nanocrystals (PANI/CNC) obtained via in situ polymerization. *Journal of Solid State Chemistry, 302*, 122372.

Neto, W. P. F., Silvério, H. A., Dantas, N. O., Pasquini, D. J. I. C., & Products. (2013). Extraction and characterization of cellulose nanocrystals from agro-industrial residue–Soy hulls. *Ind. Crops Prod., 42*, 480-488.

Nevado, P., Lopera, A., Bezzon, V., Fulla, M., Palacio, J., et al. (2020). Preparation and in vitro evaluation of PLA/biphasic calcium phosphate filaments used for fused deposition modelling of scaffolds. *Materials Science Engineering: C, 114*, 111013.

Nezhad, I. S., Golzar, M., Behravesh, A., & Zare, S. (2021). Comprehensive Study on Shape Shifting Behaviors of Thermally Activated Hinges in FDM-based 4D Printing. *Research Square 1*.

Ng, H.-M., Sin, L. T., Bee, S.-T., Tee, T.-T., & Rahmat, A. (2017). Review of nanocellulose polymer composite characteristics and challenges. *Polymer-Plastics Technology Engineering, 56*(7), 687-731.

Ng, H.-M., Sin, L. T., Tee, T.-T., Bee, S.-T., Hui, D., et al. (2015a). Extraction of cellulose nanocrystals from plant sources for application as reinforcing agent in polymers. *Composites Part B: Engineering, 75*, 176-200.

Ng, H.-M., Sin, L. T., Tee, T.-T., Bee, S.-T., Hui, D., et al. (2015b). Extraction of cellulose nanocrystals from plant sources for application as reinforcing agent in polymers. *Composites Part B: Engineering, 75*, 176-200.

Nguyen, H. T. H., Qi, P., Rostagno, M., Feteha, A., & Miller, S. A. (2018). The quest for high glass transition temperature bioplastics. *Journal of Materials Chemistry A, 6*(20), 9298-9331.

Niendorf, K., & Raeymaekers, B. (2021). Additive manufacturing of polymer matrix composite materials with aligned or organized filler material: a review. *Advanced Engineering Materials, 23*(4), 2001002.

Nikzad, M., Masood, S. H., & Sbarski, I. (2011). Thermo-mechanical properties of a highly filled polymeric composites for Fused Deposition Modeling. *Materials & Design, 32*(6), 3448-3456.

Ning, F., Cong, W., Qiu, J., Wei, J., & Wang, S. (2015). Additive manufacturing of carbon fiber reinforced thermoplastic composites using fused deposition modeling. *Composites Part B: Engineering, 80*, 369-378.

Noori, A., Lu, Y., Saffari, P., Liu, J., Ke, J. J. C., et al. (2021). The effect of mercerization on thermal and mechanical properties of bamboo fibers as a biocomposite material: A review. *Constr Build Mater., 279*, 122519.

Noremylia, M., Hassan, M. Z., & Ismail, Z. (2022). Recent advancement in isolation, processing, characterization and applications of emerging nanocellulose: A review. *International Journal of Biological Macromolecules, 206*, 954-976.

Norrrahim, M. N. F., Kasim, N. A. M., Knight, V. F., Halim, N. A., Shah, N. A. A., et al. (2022). *A mini review on the mechanical performance of nanocellulose reinforced composites.* Paper presented at the AIP Conference Proceedings.

Norrrahim, M. N. F., Yasim-Anuar, T., Jenol, M., Nurazzi, N. M., Sapuan, S., et al. (2021). Performance evaluation of cellulose nanofiber reinforced polypropylene biocomposites for automotive applications. In *Biocomposite and synthetic composites for automotive applications* (pp. 199-215): Elsevier.

Nötzel, D., Eickhoff, R., & Hanemann, T. (2018). Fused filament fabrication of small ceramic components. *Materials, 11*(8), 1463.

Nurazzi, N., Abdullah, N., Norrrahim, M., Kamarudin, S., Ahmad, S., et al. (2022). Thermogravimetric analysis (TGA) and differential scanning calorimetry (DSC) of PLA/cellulose composites. In *Polylactic acid-based nanocellulose and cellulose composites* (pp. 145-164): CRC Press.

Nurazzi, N., Asyraf, M., Rayung, M., Norrrahim, M., Shazleen, S., et al. (2021). Thermogravimetric analysis properties of cellulosic natural fiber polymer composites: A review on influence of chemical treatments. *Polym, 13*(16), 2710.

Nurazzi, N., Asyraf, M., Rayung, M., Norrrahim, M., Shazleen, S., et al. (2021). Thermogravimetric analysis properties of cellulosic natural fiber polymer composites: A review on influence of chemical treatments. *Polymers, 13*(16), 2710.

Oksman, K., Mathew, A. P., Bondeson, D., & Kvien, I. (2006). Manufacturing process of cellulose whiskers/polylactic acid nanocomposites. *Composites Science and Technology, 66*(15), 2776-2784.

Okubo, K., Fujii, T., & Thostenson, E. T. (2009). Multi-scale hybrid biocomposite: Processing and mechanical characterization of bamboo fiber reinforced PLA with microfibrillated cellulose. *Composites Part A: Applied Science and Manufacturing, 40*(4), 469-475.

Omran, A. A. B., Mohammed, A. A. B. A., Sapuan, S. M., Ilyas, R. A., Asyraf, M. R. M., et al. (2021). Micro- and Nanocellulose in Polymer Composite Materials: A Review. *Polymers, 13*(2), 231.

Ono, Y., Funahashi, R., Saito, T., & Isogai, A. (2018). Investigation of stability of branched structures in softwood cellulose using SEC/MALLS/RI/UV and sugar composition analyses. *Cellulose 25*, 2667-2679.

Oun, A. A., & Rhim, J.-W. (2015). Effect of post-treatments and concentration of cotton linter cellulose nanocrystals on the properties of agar-based nanocomposite films. *Carbohydrate Polymers, 134*, 20-29.

Ovalle-Serrano, S., Gómez, F., Blanco-Tirado, C., & Combariza, M. (2018). Isolation and characterization of cellulose nanofibrils from Colombian fique decortication by-products. *Carbohydrate polymers, 189*, 169-177.

Oviedo, A., Puente, A., Bernal, C., & Pérez, E. (2020). Mechanical evaluation of polymeric filaments and their corresponding 3D printed samples. *Polymer Testing, 88*, 106561.

Owonubi, S. J., Agwuncha, S. C., Malima, N. M., Shombe, G. B., Makhatha, E. M., et al. (2021). Non-woody biomass as sources of nanocellulose particles: A review of extraction procedures. *Front. Energy Res, 9*, 608825.

Özsin, G., Kılıç, M., Kırbıyık Kurukavak, Ç., & Varol, E. (2023). Thermal characteristics, stability, and degradation of PVC composites and nanocomposites. In T. S. Akhina H (Ed.), *Poly (Vinyl Chloride) Based Composites and Nanocomposites* (pp. 293-318): Springer.

Pakdel, A. S., Niinivaara, E., Cranston, E. D., Berry, R. M., & Dubé, M. A. J. M. R. C. (2021). Cellulose nanocrystal (CNC)–latex nanocomposites: effect of CNC

hydrophilicity and charge on rheological, mechanical, and adhesive properties. *42*(3), 2000448.

Pan, S., Shen, H., & Zhang, L. (2021). Effect of carbon nanotube on thermal, tribological and mechanical properties of 3D printing polyphenylene sulfide. *Additive Manufacturing, 47*, 102247.

Panda, J., Mishra, A. K., Mohanta, Y. K., Patowary, K., Rauta, P. R., et al. (2024). Exploring biopolymer for food and pharmaceuticals application in the circular bioeconomy: an agro-food waste-to-wealth approach. *Waste Biomass Valorization, 15*(10), 5607-5637.

Pandey, R. (2016). Fiber Extraction from Dual-Purpose Flax. *Journal of Natural Fibers, 13*(5), 565-577.

Parameswaranpillai, J., & Jineesh, A. (2022). Nanocellulose: A Fundamental Material for Science and Technology Applications. *Molecules, 4*(27), 08032.

Paran, S. (2024). Nonlinear viscoelasticity and Payne effect of nanocellulose reinforced elastomer composites. In *Elastomeric Nanocellulose Composites* (pp. 301-317): Elsevier.

Pavan, M. V., Balamurugan, K., & Balamurugan, P. (2020). Compressive test Fractured Surface analysis on PLA-Cu composite filament printed at different FDM conditions. *IOP Conference Series: Materials Science and Engineering, 988*(1), 012019.

Peng, C., Yang, Q., Zhao, W., Ren, J., Yu, Q., et al. (2019). Relationship between interface chemistry and reinforcement in polybutadiene/cellulose nanocrystal nanocomposites. *Composites Science Technology, 177*, 103-110.

Peng, J., Ellingham, T., Sabo, R., Clemons, C. M., & Turng, L. S. (2015). Oriented polyvinyl alcohol films using short cellulose nanofibrils as a reinforcement. *Journal of Applied Polymer Science, 132*(48).

Perdoch, W., Cao, Z., Florczak, P., Markiewicz, R., Jarek, M., et al. (2022). Influence of nanocellulose structure on paper reinforcement. *Molecules, 27*(15), 4696.

Pereda, M., Dufresne, A., Aranguren, M. I., & Marcovich, N. E. (2014). Polyelectrolyte films based on chitosan/olive oil and reinforced with cellulose nanocrystals. *Carbohydrate Polymers, 101*, 1018-1026.

Pereira, A. L. S., Nascimento, D. M. d., Souza Filho, M. d. s. M., Morais, J. P. S., Vasconcelos, N. F., et al. (2014). Improvement of polyvinyl alcohol properties by adding nanocrystalline cellulose isolated from banana pseudostems. *Carbohydrate Polymers, 112*, 165-172.

Pervaiz, S., Qureshi, T. A., Kashwani, G., & Kannan, S. (2021). 3D printing of fiber-reinforced plastic composites using fused deposition modeling: a status review. *Materials, 14*(16), 4520.

Phaechamud, T., & Chitrattha, S. (2016). Pore formation mechanism of porous poly (dl-lactic acid) matrix membrane. *Materials Science Engineering: C, 61*, 744-752.

Picot-Allain, M. C. N., & Emmambux, M. N. J. F. R. I. (2023). Isolation, characterization, and application of nanocellulose from agro-industrial by-products: A review. *Food Reviews International 39*(2), 941-969.

Pirich, C. L., Picheth, G. F., Fontes, A. M., Delgado-Aguilar, M., & Ramos, L. P. (2020). Disruptive enzyme-based strategies to isolate nanocelluloses: a review. *Cellulose, 27*, 5457-5475.

Pirich, C. L., Picheth, G. F., Machado, J. P. E., Sakakibara, C. N., Martin, A. A., et al. (2019). Influence of mechanical pretreatment to isolate cellulose nanocrystals by sulfuric acid hydrolysis. *International Journal of Biological Macromolecules, 130,* 622-626.

Plymill, A., Minneci, R., Greeley, D. A., & Gritton, J. (2016). *Graphene and carbon nanotube PLA composite feedstock development for fused deposition modeling.* (MSc), University of Tennessee, University of Tennessee, Knoxville.

Poletto, M., Júnior, H. L. O., & Zattera, A. J. (2015). Thermal decomposition of natural fibers: kinetics and degradation mechanisms. *Reactions and mechanisms in thermal analysis of advanced materials,* 515-545.

Poletto, M., Ornaghi Junior, H. L., & Zattera, A. J. (2014). Native cellulose: structure, characterization and thermal properties. *Materials, 7*(9), 6105-6119.

Poletto, M., Zattera, A. J., Forte, M. M. C., & Santana, R. M. C. (2012). Thermal decomposition of wood: Influence of wood components and cellulose crystallite size. *Bioresource Technology, 109,* 148-153.

Prabhu, P., Fernandes, T., Chaubey, P., Kaur, P., Narayanan, S., et al. (2021). Mannose-conjugated chitosan nanoparticles for delivery of rifampicin to osteoarticular tuberculosis. *Drug Delivery and Translational Research*, 1-11.

Praczyk, M., & Wielgusz, K. (2021). Agronomic Assessment of Fibrous Flax and Linseed Advanced Breeding Lines as Potential New Varieties. *Agronomy, 11*(10), 1917.

Prakash, C., Senthil, P., & Sathies, T. (2021). Fused deposition modeling fabricated PLA dielectric substrate for microstrip patch antenna. *Materials Today: Proceedings, 39*, 533-537.

Preisner, M., Kulma, A., Zebrowski, J., Dymińska, L., Hanuza, J., et al. (2014). Manipulating cinnamyl alcohol dehydrogenase (CAD) expression in flax affects fibre composition and properties. *BMC plant biology, 14*, 1-18.

Priyadarshini, R. (2021). Thermal Characterization of Composites. In *Composite Materials* (pp. 149-154): CRC Press.

Proniewicz, L. M., Paluszkiewicz, C., Wesełucha-Birczyńska, A., Majcherczyk, H., Barański, A., et al. (2001). FT-IR and FT-Raman study of hydrothermally degradated cellulose. *Journal of Molecular Structure, 596*(1-3), 163-169.

Psochia, E. A., Delliere, P., Sanchez, R., Triantafyllidis, K. S., & Guigo, N. (2024). Sustainable alliance between nanocellulose and biobased polyfurfuryl alcohol. *Industrial Crops Products, 212,* 118346.

Qattawi, A., Alrawi, B., & Guzman, A. (2017). Experimental optimization of fused deposition modelling processing parameters: a design-for-manufacturing approach. *Procedia Manufacturing, 10,* 791-803.

Qazi, M. I., Akhtar, R., Abas, M., Khalid, Q. S., Babar, A. R., et al. (2020). An Integrated Approach of GRA Coupled with Principal Component Analysis for Multi-Optimization of Shielded Metal Arc Welding (SMAW) Process. *Materials, 13*(16), 3457.

Qin, Q., Zhang, X., Gao, B., Liu, W., Han, L., et al. (2024). Insight into the effect of different nanocellulose types on protein-based bionanocomposite film properties. *International Journal of Biological Macromolecules, 257*, 127944.

Qu, L. J., Zhu, S. F., Liu, M. J., & Wang, S. Y. (2005). The mechanism and technology parameters optimization of alkali-H2O2 one-bath cooking and bleaching of hemp. *Journal of Applied Polymer Science, 97*(6), 2279-2285.

Qureshi, S. S., Nizamuddin, S., Xu, J., Vancov, T., & Chen, C. (2024). Cellulose nanocrystals from agriculture and forestry biomass: synthesis methods, characterization and industrial applications. *Environmental Science and Pollution Research, 31*(49), 58745-58778.

Rahim, T. N. A. T., Abdullah, A. M., & Md Akil, H. (2019). Recent Developments in Fused Deposition Modeling-Based 3D Printing of Polymers and Their Composites. *Polymer Reviews, 59*(4), 589-624.

Rahim, T. N. A. T., Manaf, A. A., & and Md Akil, H. (2019). Recent Developments in Fused Deposition Modeling-Based 3D Printing of Polymers and Their Composites. *Polymer Reviews, 59*(4), 589-624.

Ramesh, M. (2016). Kenaf (Hibiscus cannabinus L.) fibre based bio-materials: A review on processing and properties. *Progress in Materials Science, 78*, 1-92.

Ramezani Dana, H., & Ebrahimi, F. (2023). Synthesis, properties, and applications of polylactic acid-based polymers. *Polymer Engineering Science 63*(1), 22-43.

Ranganagowda, R. P. G., Kamath, S. S., & Bennehalli, B. (2019). Extraction and Characterization of Cellulose from Natural Areca Fiber. *Material Science Research India, 16*(1), 86-93.

Ray, D. P., Banerjee, P., Ghosh, R. K., & Nag, D. (2015). Accelerated retting of jute for economic fibre yield. *Economic Affairs, 60*(4), 693.

Ray, R., Das, S. N., Mohapatra, A., & Das, H. C. (2020). Comprehensive characterization of a novel natural Bauhinia Vahlii stem fiber. *Polymer Composites, 41*(9), 3807-3816.

Rebouillat, S., & Pla, F. (2013). State of the art manufacturing and engineering of nanocellulose: a review of available data and industrial applications. *Journal of Biomaterials and Nanobiotechnology, 4*(2), 24.

Reddy, M. M., Vivekanandhan, S., Misra, M., Bhatia, S. K., & Mohanty, A. K. (2013). Biobased plastics and bionanocomposites: Current status and future opportunities. *Progress in polymer science, 38*(10-11), 1653-1689.

Reddy, N., & Yang, Y. (2005). Properties and potential applications of natural cellulose fibers from cornhusks. *Green Chemistry, 7*(4), 190-195.

Rejab, N. A., Akindayo, J. O., & Jaafar, M. (2022). Crystallinity of nanocellulose and its application in polymer composites: A short review. *Key Engineering Materials, 908*, 74-79.

Réquilé, S., Le Duigou, A., Bourmaud, A., & Baley, C. (2018). Peeling experiments for hemp retting characterization targeting biocomposites. *Industrial Crops and Products, 123*, 573-580.

Rezvani Ghomi, E., Khosravi, F., Saedi Ardahaei, A., Dai, Y., Neisiany, R. E., et al. (2021). The Life Cycle Assessment for Polylactic Acid (PLA) to Make It a Low-Carbon Material. *Polymers, 13*(11).

Rhim, J.-W., Reddy, J. P., & Luo, X. (2015). Isolation of cellulose nanocrystals from onion skin and their utilization for the preparation of agar-based bio-nanocomposites films. *Cellulose, 22*(1), 407-420.

Rinaldi, M., Ghidini, T., Cecchini, F., Brandao, A., & Nanni, F. (2018). Additive layer manufacturing of poly (ether ether ketone) via FDM. *Composites Part B: Engineering, 145*, 162-172.

Rivai, H., & Djamaan, A. (2016). Optimization of production and characterization of homolog vivacel from rice straw. *Der Pharmacia Lettre, 8*(19), 388-394.

Rizwan, M., Gilani, S. R., Durrani, A. I., & Naseem, S. J. I. J. o. B. M. (2021). Cellulose extraction of Alstonia scholaris: A comparative study on efficiency of different bleaching reagents for its isolation and characterization. *International Journal of Biological Macromolecules, 191*, 964-972.

Roman, M., & Winter, W. T. (2004). Effect of sulfate groups from sulfuric acid hydrolysis on the thermal degradation behavior of bacterial cellulose. *Biomacromolecules, 5*(5), 1671-1677.

Romanenko, V., & Nazarenko, O. (2024). Comparative analysis of modern technologies of additive production. *System Research in Energy*(2 (77)), 84-96.

Romão, S., Bettencourt, A., & Ribeiro, I. A. (2022). Novel features of cellulose-based films as sustainable alternatives for food packaging. *Polym, 14*(22), 4968.

Romruen, O., Karbowiak, T., Tongdeesoontorn, W., Shiekh, K., & Rawdkuen, S. (2022). Extraction and Characterization of Cellulose from Agricultural By-Products of Chiang Rai Province, Thailand. *Polym, 14*(9), 1830-1830.

Rosa, M. D. F., Medeiros, E., Malmonge, J. A., Gregorski, K. S., Wood, D. F., et al. (2010). Cellulose nanowhiskers from coconut husk fibers: Effect of preparation conditions on their thermal and morphological behavior. *Carbohydrate Polymers, 81*(1), 83-92.

Rosli, N. A., Ahmad, I., & Abdullah, I. (2013). Isolation and Characterization of Cellulose Nanocrystals from Agave angustifolia Fibre. *BioResources, 8*(2).

Rovera, C., Carullo, D., Bellesia, T., Büyüktaş, D., Ghaani, M., et al. (2023). Extraction of high-quality grade cellulose and cellulose nanocrystals from different lignocellulosic agri-food wastes. *Front. Sustain. Food Syst., 6*, 1087867.

Ruan, P., Raghavan, V., Gariepy, Y., & Du, J. (2015). Characterization of flax water retting of different durations in laboratory condition and evaluation of its fiber properties. *BioResources, 10*(2), 3553-3563.

Rude, T., Strait Jr, L., & Ruhala, L. (2000). Measurement of fiber density by helium pycnometry. *Journal of Composite Materials, 34*(22), 1948-1958.

Rudrapati, R., Assefa, B., Mitiku, G., Gena, R., Pydi, H. P., et al. (2023). *Optimization of wire electrical discharge machining processing conditions using Taguchi method.* Paper presented at the AIP Conference Proceedings.

Sachdev, S. (2024). Biofuel Production from Agricultural Residue: An Effective and Sustainable Approach for Management of Agro-waste. In P. Singh (Ed.), *Emerging*

Trends and Techniques in Biofuel Production from Agricultural Waste (pp. 131-145). Singapore: Springer Nature Singapore.

Sadan, M. K. (2023). Influence of adding different particles fillers on electrical conductivity and mechanical properties of high density polyethylene (HDPE) matrix composites. *Journal of Duhok University, 26*(2), 721-728.

Saha, S., & Ghosh, R. (2019). *Cellulose nanocrystals from lignocellulosic agro-waste: a comparative study on conventional and ultrasonic assisted preparation methods.* Paper presented at the Materialstoday Proceedings.

Sahakaro, K. (2017). Mechanism of reinforcement using nanofillers in rubber nanocomposites. In *Progress in rubber nanocomposites* (pp. 81-113): Elsevier.

Sain, M., & Panthapulakkal, S. (2006). Bioprocess preparation of wheat straw fibers and their characterization. *Industrial crops and products, 23*(1), 1-8.

Saleem, M. H., Ali, S., Hussain, S., Kamran, M., Chattha, M. S., et al. (2020). Flax (Linum usitatissimum L.): a potential candidate for phytoremediation? Biological and economical points of view. *Plants, 9*(4), 496.

Salifu, S., Desai, D., Ogunbiyi, O., & Mwale, K. (2022). Recent development in the additive manufacturing of polymer-based composites for automotive structures—A review. *The International Journal of Advanced Manufacturing Technology, 119*(11), 6877-6891.

Sanchez-Garcia, M. D., & Lagaron, J. M. (2010). On the use of plant cellulose nanowhiskers to enhance the barrier properties of polylactic acid. *Cellulose, 17*(5), 987-1004.

Santos, J., Escobar-Avello, D., Magalhães, P., Magalhães, F. D., Martins, J. M., et al. (2022). High-value compounds obtained from grape canes (Vitis vinifera L.) by steam pressure alkali extraction. *Food and Bioproducts Processing, 133*, 153-167.

Sapkota, J., Natterodt, J. C., Shirole, A., Foster, E. J., & Weder, C. (2017). Fabrication and Properties of Polyethylene/Cellulose Nanocrystal Composites. *Macromolecular Materials*

Engineering, 302, 1600300.

Saravanakumar, S., Kumaravel, A., Nagarajan, T., & Moorthy, I. G. (2014). Effect of chemical treatments on physicochemical properties of Prosopis juliflora fibers. *International Journal of Polymer Analysis and Characterization, 19*(5), 383-390.

Sargini, M., Masood, S., Palanisamy, S., Jayamani, E., & Kapoor, A. (2021). Additive manufacturing of an automotive brake pedal by metal fused deposition modelling. *Materials Today: Proceedings, 45*, 4601-4605.

Sarkar, S., Skalicky, M., Hossain, A., Brestic, M., Saha, S., et al. (2020). Management of crop residues for improving input use efficiency and agricultural sustainability. *Sustainability, 12*(23), 9808.

Sarno, B. J. (2020). Characterization of cellulose nanocrystals derived from umbrella plant (Cyperus alternifolius Linn). *Int. Res. J. Pure Appl. Chem., 21*(18), 33-42.

Sartika, D., Firmansyah, A. P., Junais, I., Arnata, I. W., Fahma, F., et al. (2023). High yield production of nanocrystalline cellulose from corn cob through a chemical-mechanical treatment under mild conditions. *International Journal of Biological Macromolecules, 240*, 124327.

Sastri, V. R. (2014). Polymer additives used to enhance material properties for medical device applications. *Plastics in medical devices*, 55-72.

Savadekar, N., & Mhaske, S. (2012). Synthesis of nano cellulose fibers and effect on thermoplastics starch based films. *Carbohydrate Polymers, 89*(1), 146-151.

Sawsen, C., Fouzia, K., Mohamed, B., & Moussa, G. (2014). Optimizing the formulation of flax fiber-reinforced cement composites. *Construction and building Materials, 54*, 659-664.

Scaffaro, R., Maio, A., Gulino, E. F., Alaimo, G., & Morreale, M. (2021). Green composites based on PLA and agricultural or marine waste prepared by FDM. *Polymers, 13*(9), 1361.

Seddiqi, H., Oliaei, E., Honarkar, H., Jin, J., Geonzon, L. C., et al. (2021). Cellulose and its derivatives: towards biomedical applications. *Cellulose, 28*(4), 1893-1931.

Segal, L., Creely, J. J., Martin Jr, A., & Conrad, C. (1959). An empirical method for estimating the degree of crystallinity of native cellulose using the X-ray diffractometer. *Text. Res. J., 29*(10), 786-794.

Segura Gonzalez, E. A., Olmos, D., González-Gaitano, G., Orgaz, B., & González-Benito, J. (2015). Effect of kaolin nanofiller and processing conditions on the structure, morphology, and biofilm development of polylactic acid. *Journal of Applied Polymer Science, 132*(42).

Selge, B., Gusovius, H.-J., & Ouagne, P. (2024). Processing of linseed straw: State-of-the-art and further perspectives. *Industrial crops and products, 222*, 119518.

Selulosa-Polivinilklorida, S. R. N., Sheltami, R. M., Kargarzadeh, H., & Abdullah, I. (2015). Effects of silane surface treatment of cellulose nanocrystals on the tensile properties of cellulose-polyvinyl chloride nanocomposite. *Sains Malays, 44*(6), 801-810.

Seraji, A. A., Goharpey, F., & Khademzadeh Yeganeh, J. (2022). Highly crystallized and tough polylactic acid through addition of surface modified cellulose nanocrystals. *Journal of Applied Polymer Science, 139*(37), e52871.

Seyni, A., Le Bolay, N., & Lamure, A. (2011). Matrix–filler interactions in a co-ground ecocomposite: Surface properties and behaviour in water. *Powder technology, 208*(2), 390-398.

Sezer, H. K., & Eren, O. (2019). FDM 3D printing of MWCNT re-inforced ABS nano-composite parts with enhanced mechanical and electrical properties. *Journal of manufacturing processes, 37*, 339-347.

Shaghaleh, H., Xu, X., & Wang, S. (2018). Current progress in production of biopolymeric materials based on cellulose, cellulose nanofibers, and cellulose derivatives. *RSC Adv, 8*(2), 825-842.

Shahabi-Ghahafarrokhi, I., Khodaiyan, F., Mousavi, M., & Yousefi, H. (2015). Preparation and characterization of nanocellulose from beer industrial residues using acid hydrolysis/ultrasound. *Fibers and Polymers, 16*(3), 529-536.

Shahi, N., Lee, E., Min, B., & Kim, D.-J. (2021). Rice husk-derived cellulose nanofibers: a potential sensor for water-soluble gases. *Sensors, 21*(13), 4415.

Shamsudin, S., Ali, A., Kamarudin, K., Al-Alimi, S., Altharan, Y. M., et al. (2023). *Biocompatibility and strength tests of PLA/SS316L composite material for*

orthopedic implant applications utilizing the 3D printing technique. Paper presented at the AIP Conference Proceedings.

Shang, G., & Sun, C. (2020). Effect of 3D printing technology on 3C product manufacturing. *World Journal of Engineering and Technology, 8*(4), 712-719.

Sheltami, R. M., Abdullah, I., Ahmad, I., Dufresne, A., & Kargarzadeh, H. (2012). Extraction of cellulose nanocrystals from mengkuang leaves (Pandanus tectorius). *Carbohydrate Polymers, 88*(2), 772-779.

Shemelya, C. M., Rivera, A., Perez, A. T., Rocha, C., Liang, M., et al. (2015). Mechanical, Electromagnetic, and X-ray Shielding Characterization of a 3D Printable Tungsten–Polycarbonate Polymer Matrix Composite for Space-Based Applications. *Journal of Electronic Materials, 44*(8), 2598-2607.

Shi, J., Shi, S. Q., Barnes, H. M., & Pittman, C. U. (2011). A chemical process for preparing cellulosic fibers hierarchically from kenaf bast fibers. *BioResources, 6*(1), 879-890.

Shin, H. K., Jeun, J. P., Kim, H. B., & Kang, P. H. (2012). Isolation of cellulose fibers from kenaf using electron beam. *Radiation Physics and Chemistry, 81*(8), 936-940.

Shmueli, Y., Lin, Y.-C., Zuo, X., Guo, Y., Lee, S., et al. (2020). In-situ X-ray scattering study of isotactic polypropylene/graphene nanocomposites under shear during fused deposition modeling 3D printing. *Composites Science Technology, 196*, 108227.

Shubham, P., Sikidar, A., & Chand, T. (2016). The influence of layer thickness on mechanical properties of the 3D printed ABS polymer by fused deposition modeling. *Key engineering materials, 706*, 63-67.

Silvério, H. A., Flauzino Neto, W. P., Dantas, N. O., & Pasquini, D. (2013). Extraction and characterization of cellulose nanocrystals from corncob for application as reinforcing agent in nanocomposites. *Industrial crops and products, 44*, 427-436.

Silvério, H. A., Neto, W. P. F., Dantas, N. O., & Pasquini, D. (2013a). Extraction and characterization of cellulose nanocrystals from corncob for application as reinforcing agent in nanocomposites. *Industrial crops and products, 44*, 427-436.

Silvério, H. A., Neto, W. P. F., Dantas, N. O., & Pasquini, D. (2013b). Extraction and characterization of cellulose nanocrystals from corncob for application as reinforcing agent in nanocomposites. *Industrial Crops Products, 44*, 427-436.

Silvério, H. A., Neto, W. P. F., Dantas, N. O., & Pasquini, D. (2013c). Extraction and characterization of cellulose nanocrystals from corncob for application as reinforcing agent in nanocomposites. *Ind. Crops Prod., 44*, 427-436.

Silviya, E., Varma, S., Unnikrishnan, G., & Thomas, S. (2009). Compounding and mixing of polymers. In S. T. a. Y. Weimin (Ed.), *Advances in Polymer Processing: From Macro- To Nano- Scales* (Vol. 2, pp. 71-105). UK: Woodhead publishing

Singh, R., Bedi, P., Fraternali, F., & Ahuja, I. P. S. (2016). Effect of single particle size, double particle size and triple particle size Al2O3 in Nylon-6 matrix on mechanical properties of feed stock filament for FDM. *Composites Part B: Engineering, 106*, 20-27.

Singhvi, M. S., Zinjarde, S. S., & Gokhale, D. V. (2019). Polylactic acid: synthesis and biomedical applications. *Journal of applied microbiology, 127*(6), 1612-1626.

Sinha, A., Martin, E. M., Lim, K.-T., Carrier, D. J., Han, H., et al. (2015). Cellulose Nanocrystals as Advanced. *Journal of Biosystems Engineering, 40*(4), 373-393.

Sinha, S. K. (2020). Additive manufacturing (AM) of medical devices and scaffolds for tissue engineering based on 3D and 4D printing. In *3D and 4D printing of polymer nanocomposite materials* (pp. 119-160): Elsevier.

Sinquefield, S., Ciesielski, P. N., Li, K., Gardner, D. J., & Ozcan, S. (2020). Nanocellulose dewatering and drying: current state and future perspectives. *ACS Sustain. Chem. Eng.. 8*(26), 9601-9615.

Sivaiah, P., & Chakradhar, D. (2019). Modeling and optimization of sustainable manufacturing process in machining of 17-4 PH stainless steel. *Measurement, 134*, 142-152.

Sodeifian, G., Ghaseminejad, S., & Yousefi, A. A. (2019). Preparation of polypropylene/short glass fiber composite as Fused Deposition Modeling (FDM) filament. *Results in Physics, 12*, 205-222.

Sola, A., & Trinchi, A. (2023). Recycling as a Key Enabler for Sustainable Additive Manufacturing of Polymer Composites: A Critical Perspective on Fused Filament Fabrication. *Polymers, 15*(21).

Soleimani, S., Heydari, A., & Fattahi. (2022). Isolation and characterization of cellulose nanocrystals from waste cotton fibers using sulfuric acid hydrolysis. *Studia archaeologica, 74*(11-12), 2200159.

Song, Y., Tashiro, K., Xu, D., Liu, J., & Bin, Y. (2013). Crystallization behavior of poly(lactic acid)/microfibrillated cellulose composite. *Polymer, 54*(13), 3417-3425.

Sow, S., Ranjan, S., Kumar, A., & Kumar, M. (2021). Improved retting methods of jute to enhance fibre quality and retting waste management. *Journal of Pharmacognosy Phytochemistry, 10*(1), 2614-2618.

Spagnol, C., Rodrigues, F. H. A., Pereira, A. G. B., Fajardo, A. R., Rubira, A. F., et al. (2012). Superabsorbent hydrogel composite made of cellulose nanofibrils and chitosan-graft-poly (acrylic acid). *Carbohydrate Polymers, 87*(3), 2038-2045.

Speri, M. (2011). *Insights on microbial and biochemical aspects of retting for bast fiber plant processing in a bioreactor.* (PhD Doctoral), Verona, Verona, Italy.

Sreenivasan, V., Somasundaram, S., Ravindran, D., Manikandan, V., & Narayanasamy, R. (2011). Microstructural, physico-chemical and mechanical characterisation of Sansevieria cylindrica fibres–An exploratory investigation. *Materials & Design, 32*(1), 453-461.

Srinivasan, R., Ruban, W., Deepanraj, A., Bhuvanesh, R., & Bhuvanesh, T. (2020). Effect on infill density on mechanical properties of PETG part fabricated by fused deposition modelling. *Materials Today: Proceedings, 27*, 1838-1842.

Srithep, Y., Ellingham, T., Peng, J., Sabo, R., Clemons, C., et al. (2013). Melt compounding of poly (3-hydroxybutyrate-co-3-hydroxyvalerate)/nanofibrillated cellulose nanocomposites.*Polymer Degradation Stability, 98*(8), 1439-1449.

Srithongkham, S., Vivitchanont, L., & Krongtaew, C. (2012). Starch/cellulose biocomposites prepared by high-shear homogenization/compression molding. *Journal of Materials Science Engineering B, 2*(4), 213-222.

Stamboulis, A., Baillie, C., & Peijs, T. (2001). Effects of environmental conditions on mechanical and physical properties of flax fibers. *Composites Part A: Applied Science and Manufacturing, 32*(8), 1105-1115.

Suaniti, N. M., & Adnyana, I. W. B. (2019). *Biodiesel Synthesis from Used frying Oil through Phosphoric Acid Refined and CaO Catalyzed Transesterification.* Paper presented at the IOP Conference Series: Materials Science and Engineering.

Sucinda, E. F., Abdul Majid, M. S., Ridzuan, M. J. M., Cheng, E. M., Alshahrani, H. A., et al. (2021). Development and characterisation of packaging film from Napier cellulose nanowhisker reinforced polylactic acid (PLA) bionanocomposites. *International Journal of Biological Macromolecules, 187*, 43-53.

Suryanegara, L., Nakagaito, A. N., & Yano, H. (2009). The effect of crystallization of PLA on the thermal and mechanical properties of microfibrillated cellulose-reinforced PLA composites. *Composites Science and Technology, 69*(7), 1187-1192.

Suryanegara, L., Nakagaito, A. N., & Yano, H. (2010). Thermo-mechanical properties of microfibrillated cellulose-reinforced partially crystallized PLA composites. *Cellulose, 17*(4), 771-778.

Suryanegara, L., Okumura, H., Nakagaito, A. N., & Yano, H. (2011). The synergetic effect of phenylphosphonic acid zinc and microfibrillated cellulose on the injection molding cycle time of PLA composites. *Cellulose, 18*(3), 689-698.

Swetha, T. A., Bora, A., Mohanrasu, K., Balaji, P., Raja, R., et al. (2023). A comprehensive review on polylactic acid (PLA)–Synthesis, processing and application in food packaging. *International Journal of Biological Macromolecules, 234*, 123715.

Syafri, E., Kasim, A., Abral, H., Sulungbudi, G. T., Sanjay, M., et al. (2018). Synthesis and characterization of cellulose nanofibers (CNF) ramie reinforced cassava starch hybrid composites. *International journal of biological macromolecules, 120*, 578-586.

Sztorch, B., Brząkalski, D., Pakuła, D., Frydrych, M., Špitalský, Z., et al. (2022). Natural and synthetic polymer fillers for applications in 3D printing—FDM technology area. *Solids, 3*(3), 508-548.

Tahir, D., Karim, M. R., Hu, H., Naseem, S., Rehan, M., et al. (2022). Sources, Chemical Functionalization, and Commercial Applications of Nanocellulose and Nanocellulose-Based Composites: A Review. *Polymers, 14*(21).

Tahir, P. M., Ahmed, A. B., SaifulAzry, S. O., & Ahmed, Z. (2011). Retting process of some bast plant fibres and its effect on fibre quality: a review. *BioResources, 6*(4).

Taib, N.-A. A. B., Rahman, M. R., Huda, D., Kuok, K. K., Hamdan, S., et al. (2023). A review on poly lactic acid (PLA) as a biodegradable polymer. *Polymer Bulletin, 80*(2), 1179-1213.

Tan, D. K., Maniruzzaman, M., & Nokhodchi, A. (2018). Advanced pharmaceutical applications of hot-melt extrusion coupled with fused deposition modelling (FDM) 3D printing for personalised drug delivery. *Pharmaceutics, 10*(4), 203.

Tan, J. C., & Low, H. Y. (2020). Multi-materials fused filament printing with embedded highly conductive suspended structures for compressive sensing. *Additive Manufacturing, 36,* 101551.

Tan, L. J., Zhu, W., & Zhou, K. (2020). Recent progress on polymer materials for additive manufacturing. *Advanced Functional Materials, 30*(43), 2003062.

Tang, J., Bao, L., Li, X., Chen, L., & Hong, F. F. (2015). Potential of PVA-doped bacterial nano-cellulose tubular composites for artificial blood vessels. *Journal of Materials Chemistry B, 3*(43), 8537-8547.

Tanpichai, S., Sampson, W. W., & Eichhorn, S. J. (2012). Stress-transfer in microfibrillated cellulose reinforced poly(lactic acid) composites using Raman spectroscopy. *Composites Part A: Applied Science and Manufacturing, 43*(7), 1145-1152.

TAPPI, S. (2020). Terms and their definition for cellulose nanomaterial in WI 3021.

Tarchoun, A. F., Trache, D., Hamouche, M. A., Abdelaziz, A., & Bessa, W. (2024). Extraction of nanocellulose—mechanical and chemical approaches. In *Elastomeric Nanocellulose Composites* (pp. 15-40): Elsevier.

Tareq, M. S., Rahman, T., Hossain, M., & Dorrington, P. (2021). Additive manufacturing and the COVID-19 challenges: An in-depth study. *Journal of Manufacturing systems, 60*, 787-798.

Tee, T.-T., Sin, L. T., Gobinath, R., Bee, S.-T., Hui, D., et al. (2013). Investigation of nano-size montmorillonite on enhancing polyvinyl alcohol–starch blends prepared via solution cast approach. *Composites Part B: Engineering, 47*, 238-247.

Teli, M., & Pandit, P. (2017). Novel method of ecofriendly single bath dyeing and functional finishing of wool protein with coconut shell extract biomolecules. *ACS Sustainable Chemistry & Engineering, 5*(9), 8323-8333.

Terekhina, S., Egorov, S., Tarasova, T., Skornyakov, I., Guillaumat, L., et al. (2022). In-nozzle impregnation of continuous textile flax fiber/polyamide 6 composite during FFF process. *Composites Part A: Applied Science Manufacturing, 153*, 106725.

Thakur, V., Guleria, A., Kumar, S., Sharma, S., & Singh, K. (2021). Recent advances in nanocellulose processing, functionalization and applications: A review. *Materials Advances, 2*(6), 1872-1895.

Timogarden. (2016). Ecological gardening and food processing. Retrieved from https://timogarden.wordpress.com/tag/flax-straw/

Tingaut, P., Eyholzer, C., & Zimmermann, T. (2011). Functional polymer nanocomposite materials from microfibrillated cellulose. In A. A. Hashim (Ed.), *Advances in Nanocomposite Technology*

(pp. 388). EMPA, Swizerland: BoD – Books on Demand, 2011.

Tirado-Garcia, I., Garcia-Gonzalez, D., Garzon-Hernandez, S., Rusinek, A., Robles, G., et al. (2021). Conductive 3D printed PLA composites: On the interplay of mechanical, electrical and thermal behaviours. *Composite Structures, 265*, 113744.

Tiwari, A., Niveditha, S. V., Mohan, C., & Bendi, A. (2024). Waste Management From Agricultural Field: Sustainable Practices and Framework. In C. Mohan, S. Jeet, S. Dixit, & S. A. C. Carabineiro (Eds.), *Exploring Waste Management in Sustainable Development Contexts* (pp. 154-169). Hershey, PA, USA: IGI Global.

Tolessa, A. (2023). Bioenergy potential from crop residue biomass resources in Ethiopia. *Heliyon, 9*(2).

Tonoli, G., Teixeira, E., Corrêa, A., Marconcini, J., Caixeta, L., et al. (2012). Cellulose micro/nanofibres from Eucalyptus kraft pulp: preparation and properties. *Carbohydrate polymers, 89*(1), 80-88.

Torrado, A. R., & Roberson, D. A. (2016). Failure analysis and anisotropy evaluation of 3D-printed tensile test specimens of different geometries and print raster patterns. *Journal of Failure Analysis and Prevention, 16*, 154-164.

Torrado Perez, A. R., Roberson, D. A., & Wicker, R. B. (2014). Fracture Surface Analysis of 3D-Printed Tensile Specimens of Novel ABS-Based Materials. *Journal of Failure Analysis and Prevention, 14*(3), 343-353.

Torrado Perez, A. R., Roberson, D. A., & Wicker, R. B. (2014). Fracture surface analysis of 3D-printed tensile specimens of novel ABS-based materials. *Journal of Failure Analysis Prevention, 14*, 343-353.

Trache, D., Hussin, M. H., Hui Chuin, C. T., Sabar, S., Fazita, M. R. N., et al. (2016). Microcrystalline cellulose: Isolation, characterization and Bio nanocomposites application—A review. *International Journal of Biological Macromolecules, 93*, 789-804.

Trache, D., Tarchoun, A. F., Derradji, M., Hamidon, T. S., Masruchin, N., et al. (2020a). Nanocellulose: from fundamentals to advanced applications. *Front Chem, 8*, 392.

Trache, D., Tarchoun, A. F., Derradji, M., Hamidon, T. S., Masruchin, N., et al. (2020b). Nanocellulose: from fundamentals to advanced applications. *Frontiers in Chemistry, 8*, 392.

Trembus, I., Syrotiuk, S., Cheropkina, R., & Deykun, I. (2022). Environmentally friendly technology for the production of microcrystalline cellulose from hemp fibers. *J. Chem. Technol. Metall., 57*(3), 480-486.

Trhlíková, L., Zmeskal, O., Psencik, P., & Florian, P. (2016). *Study of the thermal properties of filaments for 3D printing.* Paper presented at the AIP Conference Proceedings.

Trivedi, A. K., & Gupta, M. (2023). An efficient approach to extract nanocrystalline cellulose from sisal fibers: Structural, morphological, thermal and antibacterial analysis. *International Journal of Biological Macromolecules, 233*, 123496.

Trivedi, A. K., Gupta, M. K., & Singh, H. (2023). PLA based biocomposites for sustainable products: A review. *Advanced Industrial and Engineering Polymer Research, 6*(4), 382-395.

Trovatti, E., Fernandes, S. C., Rubatat, L., da Silva Perez, D., Freire, C. S., et al. (2012). Pullulan–nanofibrillated cellulose composite films with improved thermal and mechanical properties. *Composites Science Technology, 72*(13), 1556-1561.

Truong, M., Zhong, W., Boyko, S., & Alcock, M. (2009). A comparative study on natural fibre density measurement. *Journal of the Textile Institute, 100*(6), 525-529.

Tschan, M. J.-L., Gauvin, R. M., & Thomas, C. M. (2021). Controlling polymer stereochemistry in ring-opening polymerization: a decade of advances shaping the future of biodegradable polyesters. *Chemical Society Reviews, 50*(24), 13587-13608.

Tu, W., Wang, S., Deng, Q., Li, D., Zhang, Y., et al. (2024). Review on nanocellulose composites and CNFs assembled microfiber toward automotive applications. *Nanotechnology Reviews, 13*(1), 20240006.

Tuan Rahim, T. N. A., Abdullah, A. M., Md Akil, H., Mohamad, D., & Rajion, Z. A. (2015). Preparation and characterization of a newly developed polyamide composite utilising an affordable 3D printer. *Journal of Reinforced Plastics Composites Communications, 34*(19), 1628-1638.

Turku, I., & Kärki, T. (2014). The influence of different carbon type fillers on the mechanical and physical properties of co-extruded PP-based WPC. *Advanced Materials Research, 1025*, 200-207.

Ul-Islam, M., Wajid Ullah, M., Khan, S., Kamal, T., Ul-Islam, S., et al. (2016). Recent advancement in cellulose based nanocomposite for addressing environmental challenges. *Recent patents on nanotechnology, 10*(3), 169-180.

Vanderfleet, O. M., & Cranston, E. D. (2021). Production routes to tailor the performance of cellulose nanocrystals. *Nat. Rev. Mater., 6*(2), 124-144.

Vasile, G., & Paunescu, C. (2022). *Mechanical Characterization of Composite Materials with Polymeric Matrix*. Paper presented at the 2022 14th International Conference on Electronics, Computers and Artificial Intelligence (ECAI).

Vatandaş, B. B., Uşun, A., Guemruek, R., & Şimşek, C. (2023). The relationship between fiber bundle size and mechanical performance of additively manufactured continuous carbon fiber reinforced thermoplastic composites. *3D Printing Additive Manufacturing, 10*(6), 1190-1203.

Venkatachalam, S. (2016). Ultraviolet and visible spectroscopy studies of nanofillers and their polymer nanocomposites. *Spectroscopy of polymer nanocomposites*, 130-157.

Ventura-Cruz, S., Flores-Alamo, N., & Tecante, A. (2020). Preparation of microcrystalline cellulose from residual Rose stems (Rosa spp.) by successive delignification with alkaline hydrogen peroxide. *International Journal of Biological Macromolecules, 155*, 324-329.

Ventura-Cruz, S., & Tecante, A. (2021). Nanocellulose and microcrystalline cellulose from agricultural waste: Review on isolation and application as reinforcement in polymeric matrices. *Food Hydrocolloids, 118*, 106771.

Vieweger, D., Diel, S., Schweiger, H.-G., & Tetzlaff, U. (2024). Mechanical Properties of Raw Filaments and Printed Specimens: Effects of Fiber Reinforcements and Process Parameters. *Polymers, 16*(11), 1576.

Vilarinho, F., Stanzione, M., Buonocore, G., Barbosa-Pereira, L., Sendón, R., et al. (2021). Green tea extract and nanocellulose embedded into polylactic acid film: Properties and efficiency on retarding the lipid oxidation of a model fatty food. *Food Packaging Shelf Life, 27*, 100609.

Vishnu, R., & Revathi, R. (2019). Methods of isolation of nanocellulose from wood: A review. *J Pharmacogn Phytochem 8*(5), 2386-2392.

Völtz, L. R., Geng, S., Teleman, A., & Oksman, K. (2022). Influence of dispersion and orientation on polyamide-6 cellulose nanocomposites manufactured through liquid-assisted extrusion. *Nanomaterials, 12*(5), 818.

Voronova, M. I., Surov, O. V., Guseinov, S. S., Barannikov, V. P., & Zakharov, A. G. (2015). Thermal stability of polyvinyl alcohol/nanocrystalline cellulose composites. *Carbohydrate Polymers, 130*, 440-447.

Wada, M., & Okano, T. (2001). Localization of Iα and Iβ phases in algal cellulose revealed by acid treatments. *Cellulose, 8*, 183-188.

Wang, B., Chen, Y., Qu, T., & Li, F. (2021). Structure and properties of multi-walled carbon nanotube/acrylonitrile butadiene styrene nanocomposite specimens prepared by fused deposition modeling. *Journal of Macromolecular Science, Part B, 60*(2), 77-87.

Wang, B., Sain, M., & Oksman, K. (2007). Study of structural morphology of hemp fiber from the micro to the nanoscale. *Applied Composite Materials, 14*, 89-103.

Wang, D., Chen, D., & Chen, Z. (2020). Recent progress in 3D printing of bioinspired structures. *Frontiers in Materials, 7*, 286.

Wang, G., & Liu, L. (2023). Interfacial mechanics of polymer nanocomposites. *Composites Part A: Applied Science and Manufacturing, 141*, 106212.

Wang, P., Zou, B., Ding, S., Huang, C., Shi, Z., et al. (2020). Preparation of short CF/GF reinforced PEEK composite filaments and their comprehensive properties evaluation for FDM-3D printing. *Composites Part B: Engineering, 198*, 108175.

Wang, Q., Yao, Q., Liu, J., Sun, J., Zhu, Q., et al. (2019). Processing nanocellulose to bulk materials: A review. *Cellulose, 26*, 7585-7617.

Wang, T., & Drzal, L. T. (2012). Cellulose-Nanofiber-Reinforced Poly(lactic acid) Composites Prepared by a Water-Based Approach. *ACS Applied Materials & Interfaces, 4*(10), 5079-5085.

Wang, T., Li, N., Link, G., Jelonnek, J., Fleischer, J., et al. (2021). Load-dependent path planning method for 3D printing of continuous fiber reinforced plastics. *Composites Part A: Applied Science Manufacturing, 140*, 106181.

Wang, X., Guo, J., Ren, H., Jin, J., He, H., et al. (2023). Research progress of nanocellulose-based food packaging. *Trends in Food Science Technology*, 104289.

Wang, Z., Yao, Z., Zhou, J., He, M., Jiang, Q., et al. (2019). Improvement of polylactic acid film properties through the addition of cellulose nanocrystals isolated from waste cotton cloth. *International Journal of Biological Macromolecules, 129*, 878-886.

Wastemanaged. (2024, https://www.wastemanaged.co.uk/our-news/agriculture/agricultural-waste-guide/).Agricultural Waste Facts & Statistics. *Agricultural Waste Guide 2024*.

Weaver, A. (2017). *Mechanical and electrical properties of 3D-printed acrylonitrile butadiene styrene composites reinforced with carbon nanomaterials.* (Master of Science), Kansas State University,

Wei, X., Li, D., Jiang, W., Gu, Z., Wang, X., et al. (2015). 3D printable graphene composite. *Scientific Reports, 5*(1), 1-7.

Weishaupt, R., Siqueira, G., Schubert, M., Kämpf, M. M., Zimmermann, T., et al. (2017). A Protein-Nanocellulose Paper for Sensing Copper Ions at the Nano-to Micromolar Level. *Advanced Functional Materials, 27*(4), 1604291.

Weng, Z., Wang, J., Senthil, T., & Wu, L. (2016). Mechanical and thermal properties of ABS/montmorillonite nanocomposites for fused deposition modeling 3D printing. *Materials & Design, 102*, 276-283.

West, R. M. (2021). Best practice in statistics: Use the Welch t-test when testing the difference between two groups. *Annals of clinical biochemistry*, *58*(4), 267-269.

Widnyana, A., Rian, I. G., Surata, I. W., & Nindhia, T. G. T. (2020). Tensile Properties of coconut Coir single fiber with alkali treatment and reinforcement effect on unsaturated polyester polymer. *Materials Today: Proceedings*, *22*, 300-305.

Wiratma, O. (2021). *Fabrication and Characterization of PLA/Nanocrystalline Cellulose Nanocomposite Filaments for 3D Printing Application.* Paper presented at the IOP Conference Series: Materials Science and Engineering.

Wittbrodt, B., & Pearce, J. M. (2015). The effects of PLA color on material properties of 3-D printed components. *Additive Manufacturing*, *8*, 110-116.

Woigk, W., Fuentes, C. A., Rion, J., Hegemann, D., Van Vuure, A. W., et al. (2019). Interface properties and their effect on the mechanical performance of flax fibre thermoplastic composites. *Composites Part A: Applied Science and Manufacturing*, *122*, 8-17.

Wu, H., Liu, Y., Wu, H., Yuan, Y., & Zhang, J. (2023). Probing into the nucleation and reinforcing effects of poly (vinyl acetate) grafted cellulose nanocrystals in melt-processed poly (lactic acid) nanocomposites. *International Journal of Biological Macromolecules*, *231*, 123421.

Wu, Q., Meng, Y., Concha, K., Wang, S., Li, Y., et al. (2013). Influence of temperature and humidity on nano-mechanical properties of cellulose nanocrystal films made from switchgrass and cotton. *Industrial crops and products*, *48*, 28-35.

Wu, X., Liu, Y., Wu, H., Duan, Y., & Zhang, J. (2022). Melt-processed poly (L-lactic acid)/cellulose nanocrystals biocomposites for 3D printing: Improved melt processibility and inter-fuse adhesion. *Composites Science Technology*, *218*, 109135.

Wu, Y., Wu, J., Yang, F., Tang, C., & Huang, Q. (2019). Effect of H_2O_2 bleaching treatment on the properties of finished transparent wood. *Polym*, *11*(5), 776.

Wynn, M., Chen, K.-T., & Zobeiry, N. (2023). *Characterizing Thermal Degradation in Semi-Crystalline Thermoplastic Composites.* Paper presented at the Proceedings of The American Society For Composites-Thirty-Eighth Technical Conference, The University of Massachusetts Lowell, Hilton Boston-Woburn, Massachusetts, USA.

Xiao, H., Lu, W., & Yeh, J. T. (2009). Effect of plasticizer on the crystallization behavior of poly (lactic acid). *Journal of Applied Polymer Science*, *113*(1), 112-121.

Xiaoyong, S., Liangcheng, C., Honglin, M., Peng, G., Zhanwei, B., et al. (2017). *Experimental analysis of high temperature PEEK materials on 3D printing test.* Paper presented at the 2017 9th International conference on measuring technology and mechatronics automation (ICMTMA).

Xie, Y., Abdalkarim, S. Y. H., Ji, Z., Chen, Z., Wang, M., et al. (2023). Various-sized nanocelluloses induced stereocomplexes crystallization formation and its mechanism of stereoisomers poly (lactide acid) blend. *ACS Sustainable Chemistry Engineering*, *11*(35), 13164-13178.

Xing, L., Gu, J., Zhang, W., Tu, D., & Hu, C. (2018). Cellulose I and II nanocrystals produced by sulfuric acid hydrolysis of Tetra pak cellulose I. *Carbohydrate Polymers*, *192*, 184-192.

Xiong, R., Zhang, X., Tian, D., Zhou, Z., & Lu, C. (2012a). Comparing microcrystalline with spherical nanocrystalline cellulose from waste cotton fabrics. *Cellulose, 19*, 1189-1198.

Xiong, R., Zhang, X., Tian, D., Zhou, Z., & Lu, C. (2012b). Comparing microcrystalline with spherical nanocrystalline cellulose from waste cotton fabrics. *Cellulose, 19*, 1189-1198.

Yamamoto, B. E., Trimble, A. Z., Minei, B., & Ghasemi Nejhad, M. N. (2018). Development of multifunctional nanocomposites with 3-D printing additive manufacturing and low graphene loading. *Journal of Thermoplastic Composite Materials, 32*(3), 383-408.

Yang, L., Li, S., Zhou, X., Liu, J., Li, Y., et al. (2019). Effects of carbon nanotube on the thermal, mechanical, and electrical properties of PLA/CNT printed parts in the FDM process. *Synthetic Metals, 253*, 122-130.

Yang, L., Liu, X., Xiao, Y., Liu, B., Xue, Z., et al. (2023). Additive manufacturing of carbon nanotube/polylactic acid films with efficient electromagnetic interference shielding and electrical heating performance via fused deposition modeling. *Synthetic Metals, 293*, 117258.

Yang, W., Jiao, L., Liu, W., Deng, Y., & Dai, H. (2018). Morphology control for tunable optical properties of cellulose nanofibrils films. *Cellulose, 25*, 5909-5918.

Yao, T., Deng, Z., Zhang, K., & Li, S. (2019). A method to predict the ultimate tensile strength of 3D printing polylactic acid (PLA) materials with different printing orientations. *Composites Part B: Engineering, 163*, 393-402.

Yeo, J. C. C., Muiruri, J. K., Lee, P. S. K., Vijayakumar, R., Lin, T. T., et al. (2024). Sustainable poly (lactic acid) transformation: Leveraging agri-food waste—compatibilization strategies nexus for enhanced properties. *Advanced Composites Hybrid Materials, 7*(6), 190.

Yu, H., & Yu, C. (2010). Influence of various retting methods on properties of kenaf fiber. *Journal of the Textile Institute, 101*(5), 452-456.

Yu, S., Gan, M., Chen, Y., Hu, Z., Xie, Y., et al. (2022). Fabrication of lignin-containing cellulose Bio nanocomposite based on unbleached corncob and wheat straw pulp. *International Journal of Biological Macromolecules, 208*, 741-747.

Yuliasmi, S., Ginting, N., Wahyuni, H. S., Sigalingging, R. T., & Sibarani, T. (2019). The effect of alkalization on carboxymethil cellulose synthesis from stem and peel cellulose of banana. *Open Access Maced. J. Med. Sci., 7*(22), 3874.

Yuwawech, K., Wootthikanokkhan, J., & Tanpichai, S. (2015). Effects of two different cellulose nanofiber types on properties of poly (vinyl alcohol) composite films. *Journal of Nanomaterials, 2015*(1), 908689.

Zaini, L. H., Jonoobi, M., Tahir, P. M., & Karimi, S. (2013). Isolation and characterization of cellulose whiskers from kenaf (Hibiscus cannabinus L.) bast fibers. *Journal of Biomaterials and Nanobiotechnology, 4*(1).

Zainuddin, S. Y. Z., Ahmad, I., Kargarzadeh, H., Abdullah, I., & Dufresne, A. (2013). Potential of using multiscale kenaf fibers as reinforcing filler in cassava starch-kenaf biocomposites. *Carbohydrate Polymers, 92*(2), 2299-2305.

Zeleke, N. M., Sinha, D. K., & Mengesha, G. A. (2022). Chemical composition and extraction of micro crystalline cellulose from outer skin isolated coffee husk. *Adv. Mater. Sci. Eng., 2022*, 7163359.

Zerankeshi, M. M., Sayedain, S. S., Tavangarifard, M., & Alizadeh, R. (2022). Developing a novel technique for the fabrication of PLA-graphite composite filaments using FDM 3D printing process. *Ceramics International, 48*(21), 31850-31858.

Zhang, C., Zhang, P., Cheng, L., Li, J., Jian, R., et al. (2022). A strong, hydrophobic, transparent and biodegradable nano-lignocellulosic membrane from wheat straw by novel strategy. *J. Clean. Prod., 356*, 131879.

Zhang, L., Ruan, D., & Zhou, J. (2001). Structure and properties of regenerated cellulose films prepared from cotton linters in NaOH/urea aqueous solution. *Industrial & Engineering Chemistry Research, 40*(25), 5923-5928.

Zhang, M., Gao, Z., Hakobyan, K., Li, W., Gu, Z., et al. (2024). Rapid, Tough, and Trigger-Detachable Hydrogel Adhesion Enabled by Formation of Nanoparticles In Situ. *Small, 20*(26), 2310572.

Zhang, W., He, X., Li, C., Zhang, X., Lu, C., et al. (2014). High performance poly (vinyl alcohol)/cellulose nanocrystals nanocomposites manufactured by injection molding. *Cellulose, 21*(1), 485-494.

Zhang, W., Yang, X., Li, C., Liang, M., Lu, C., et al. (2011). Mechanochemical activation of cellulose and its thermoplastic polyvinyl alcohol ecocomposites with enhanced physicochemical properties. *Carbohydrate Polymers, 83*(1), 257-263.

Zhang, X., & Chen, L. (2020). Effects of laser scanning speed on surface roughness and mechanical properties of aluminum/Polylactic Acid (Al/PLA) composites parts fabricated by fused deposition modeling. *Polymer Testing, 91*, 106785.

Zhang, X., Chen, L., Mulholland, T., & Osswald, T. A. (2019). Effects of raster angle on the mechanical properties of PLA and Al/PLA composite part produced by fused deposition modeling. *Polymers for Advanced Technologies, 30*(8), 2122-2135.

Zhang, Y., Zhang, Y., Wei, Z., Guo, Z., Lei, W., et al. (2024). Single effect of filler spatial distribution states on the thermal conductivity of epoxy composites and their heat conduction mechanisms. *Composites Communications, 48*, 101902.

Zheng, W., Lv, R., Na, B., Liu, H., Jin, T., et al. (2017). Nanocellulose-mediated hybrid polyaniline electrodes for high performance flexible supercapacitors. *Journal of Materials Chemistry A, 5*(25), 12969-12976.

Zhong, W., Li, F., Zhang, Z., Song, L., & Li, Z. (2001). Short fiber reinforced composites for fused deposition modeling. *Materials Science and Engineering: A, 301*(2), 125-130.

Zhou, J., Fang, Z., Chen, K., Cui, J., Yang, D., et al. (2022). Improving the degree of polymerization of cellulose nanofibers by largely preserving native structure of wood fibers. *Carbohydrate Polymers, 296*, 119919.

Zhou, J., Zhang, L., & Cai, J. (2004). Behavior of cellulose in NaOH/urea aqueous solution characterized by light scattering and viscometry. *Journal of Polymer Science Part B: Polymer Physics, 42*(2), 347-353.

Zhu, S., Sun, H., Mu, T., Li, Q., & Richel, A. (2023). Preparation of cellulose nanocrystals from purple sweet potato peels by ultrasound-assisted maleic acid hydrolysis. *Food Chemistry, 403*, 134496.

Zhu, W., Han, M., Kim, D., Zhang, Y., Kwon, G., et al. (2022). Facile preparation of nanocellulose/Zn-MOF-based catalytic filter for water purification by oxidation process. *Environmental Research, 205*, 112417.

Zhu, Y., Zhao, Y., Zhang, X., Wang, L., Wang, X., et al. (2016). Metal filaments/nano-filler filled hybrid polymer fibers with improved conductive performance. *Materials Letters, 173*, 26-30.

Zhu, Z., Hao, M., & Zhang, N. (2018). Influence of contents of chemical compositions on the mechanical property of sisal fibers and sisal fibers reinforced PLA composites. *Journal of Natural Fibers, 17*(1), 101-112.

Zhu, Z., Wang, W., Wang, X., Zhao, X., Xia, N., et al. (2021). Easy way to prepare dispersible CNC dry powder by precipitation and conventional evaporation. *Cellulose, 28*, 9661-9676.

Ziemian, C. W., Sharma, M. M., & Ziemian, S. N. (2012). Anisotropic Mechanical Properties of ABS Parts Fabricated by Fused Deposition Modelling. In M. Gokcek (Ed.), *Mechanical Engineering* (pp. 684). Duke University, USA: BoD – Books on Demand, 2012.

Ziemian, C. W., Ziemian, R. D., & Haile, K. V. (2016). Characterization of stiffness degradation caused by fatigue damage of additive manufactured parts. *Materials Design, 109*, 209-218.

Ziemian, S., Okwara, M., & Ziemian, C. W. (2015). Tensile and fatigue behavior of layered acrylonitrile butadiene styrene. *Rapid Prototyping Journal*.

Zimmermann, M. V. G., Boakoski, D. G., Lavoratti, A., & Zattera, A. J. (2018). Influence of cellulose nanofiber content on the expansion of polystyrene nanocomposites expanded by supercritical CO2. *Polymer Bulletin, 75*(12), 5809-5824.

Zin, M. R. M., Mahendrasingam, A., Konkel, C., & Narayanan, T. (2021). Effect of D-isomer content on strain-induced crystallization behaviour of Poly (lactic acid) polymer under high speed uniaxial drawing. *Polymer, 216*, 123422.

Zinge, C., & Kandasubramanian, B. (2020). Nanocellulose based biodegradable polymers. *European Polymer Journal, 133*, 109758.

Zolfagharian, A., Khosravani, M. R., & Kaynak, A. (2020). Fracture Resistance Analysis of 3D-Printed Polymers. *Polymers, 12*(2), 302.

Zuk, M., Richter, D., Matuła, J., & Szopa, J. (2015). Linseed, the multipurpose plant. *Industrial Crops and Products, 75*, 165-177.

Zuo, Y., Gu, J., Tan, H., & Zhang, Y. (2015). Thermoplastic starch prepared with different plasticizers: Relation between degree of plasticization and properties. *Journal of Wuhan University of Technology-Mater. Sci. Ed., 30*(2), 423-428.

APPENDIX

Table 39 pH values of retted water at different retting time intervals

Sample	Retting Time (h)	pH				
		M_1	M_2	M_3	Mean	SD
R_0	0	6.8	7.3	6.9	7.00	0.26
R_1	48	5.7	5.65	6.1	5.82	0.25
R_2	96	5.53	5.48	5.62	5.54	0.07
R_3	144	5.03	5.34	5.21	5.19	0.16
R_4	168	5.01	4.95	4.91	4.96	0.05
R_5	192	4.91	4.73	5	4.88	0.14
R_6	216	4.7	4.93	4.94	4.86	0.14
R_7	240	5.1	4.9	5.02	5.01	0.10
R_8	264	5.23	5.14	4.72	5.03	0.27

Table 40 Stalk weight and water absorption percentage at different retting time intervals

Sample	Retting Time (h)	Stalk Weight (g)					Stalk Water Absorption (%)
		1	2	3	Mean	SD	
R_0	0	50	50	50	50.0	0.0	0
R_1	48	136.3	136.25	136.15	136.2	0.1	172.47
R_2	96	138.6	138.65	138.62	138.6	0.0	177.25
R_3	144	140.78	140.88	140.98	140.9	0.1	181.76
R_4	168	143.43	143.58	143.8	143.6	0.2	186.66
R_5	192	143.33	143.44	143.22	143.3	0.1	186.21
R_6	216	143.05	143.14	143.13	143.1	0.0	186.78
R_7	240	143.22	143.42	143.53	143.4	0.2	186.78
R_8	264	143.53	143.65	143.33	143.5	0.2	187.01

Table 41 Fiber yield and stalk weight loss percentages at different retting time intervals

Sample	Retting Time (h)	Fiber weight (g)					Fiber yield (%)	Stalk weight loss (g)	Stalk weight loss (%)
		1	2	3	Mean	SD			
R_0	0	7.85	7.73	7.89	7.82	0.08	15.65	0	0
R_1	48	6.9	6.84	7.63	7.12	0.44	14.25	2.87	5.74
R_2	96	6.9	6.96	6.95	6.94	0.03	13.87	3.1	6.2
R_3	144	6.35	6.38	6.31	6.35	0.04	12.69	5.02	10.04
R_4	168	6.33	6.29	6.36	6.33	0.04	12.65	6.15	12.3
R_5	192	6.27	6.41	6.37	6.35	0.07	12.70	6.23	12.46
R_6	216	6.39	6.28	6.34	6.34	0.06	12.67	6.3	12.6
R_7	240	6.37	6.42	6.25	6.35	0.09	12.69	6.1	12.2
R_8	264	6.31	6.35	6.29	6.32	0.03	12.63	6.03	12.06

Table 42 Single fiber properties under different degrees of retting

Fiber	Breaking force (cN)			Elongation at break (%)			Tenacity (cN/tex)			Diameter (μm)		
	R1	R2	R3	R1	R2	R3	R1	R2	R3	R1	R2	R3
1	187.7	220.4	200.9	2.3	2.1	1.5	42.9	57.8	58.7	107.42	104.64	100.06
2	187.7	301.6	146.5	2	1.6	1.8	36.2	62.7	50.6	90.30	102.00	98.34
3	114	297.6	198	1.9	1.5	1.8	48.8	61.9	54.8	138.43	96.04	76.85
4	316.1	352.2	253.3	2.9	2.3	1.8	40.8	73.2	57.9	146.65	91.72	83.38
5	381.1	264.1	192.4	2.7	2.4	1.5	41.5	54.9	53.3	110.24	120.98	86.31
6	223.2	184.2	151.2	1.8	2.1	1.8	43.6	38.3	51.9	130.04	103.85	85.32
7	234.8	337.6	232.8	1.9	2.6	1.8	45.5	70.2	56.8	82.66	97.20	88.32
8	244.7	170.5	191.3	2.1	1.5	1.8	34.1	35.4	53	116.28	88.27	90.78
9	129.8	298.8	237.3	2.1	2.1	1.9	35.7	62.1	53.4	183.10	76.35	93.06
10	111.6	357.1	130.1	1.5	2.4	1.6	47.5	74.2	56	137.47	109.73	87.00
11	-	-	-	-	-	-	-	-	-	116.22	140.87	98.12
12	-	-	-	-	-	-	-	-	-	179.87	124.20	96.83
Mean	213.07	278.41	193.38	2.12	2.06	1.73	41.66	59.07	54.64	128.22	104.65	90.36
SD	87.40	67.12	41.01	0.41	0.39	0.14	5.03	13.30	2.65	31.29	17.48	7.11

Table 43. Analysis of variance for means

Dewaxing process						
Source	**DF**	**Seq SS**	**Adj SS**	**Adj MS**	**F**	**P**
Concentration (%)	2	6.18380	6.18380	3.09190	30919.00	0.000
Temperature (℃)	2	0.17420	0.17420	0.08710	871.00	0.001
Time (min)	2	0.00020	0.00020	0.00010	1.00	0.500
Residual Error	2	0.00020	0.00020	0.00010		
Total	8	6.35840				
Alkalizing process						
Concentration (%)	2	35.2822	35.2822	17.6411	260.28	0.004
Temperature (℃)	2	19.2422	19.2422	9.6211	141.95	0.007
Time (min)	2	0.1622	0.1622	0.0811	1.20	0.455
Residual Error	2	0.1356	0.1356	0.0678		
Total	8	54.8222				
Bleaching process						
Concentration (%)	2	3.6038	3.6038	1.80190	23.95	0.040
Temperature (℃)	2	0.3125	0.3125	0.15623	2.08	0.325
Time (min)	2	0.4509	0.4509	0.22543	3.00	0.250
Residual Error	2	0.1505	0.1505	0.07523		
Total	8	4.5176				

Table 44. Analysis of variance for S/N ratios

Dewaxing process						
Source	**DF**	**Seq SS**	**Adj SS**	**Adj MS**	**F**	**P**
Concentration (%)	2	36.2155	36.2155	18.1077	1496.70	0.001
Temperature (°C)	2	1.0562	1.0562	0.5281	43.65	0.022
Time (min)	2	0.0195	0.0195	0.0098	0.81	0.554
Residual Error	2	0.0242	0.0242	0.0121		
Total	8	37.3154				
Alkalizing process						
Concentration (%)	2	14.2156	14.2156	7.10778	199.73	0.005
Temperature (°C)	2	7.0594	7.0594	3.52972	99.19	0.010
Time (min)	2	0.2752	0.2752	0.13760	3.87	0.205
Residual Error	2	0.0712	0.0712	0.03559		
Total	8	21.6214				
Bleaching process						
Concentration (%)	2	38.282	38.282	19.141	10.32	0.088
Temperature (°C)	2	5.699	5.699	2.850	1.54	0.394
Time (min)	2	7.388	7.388	3.694	1.99	0.334
Residual Error	2	3.710	3.710	1.855		
Total	8	55.080				

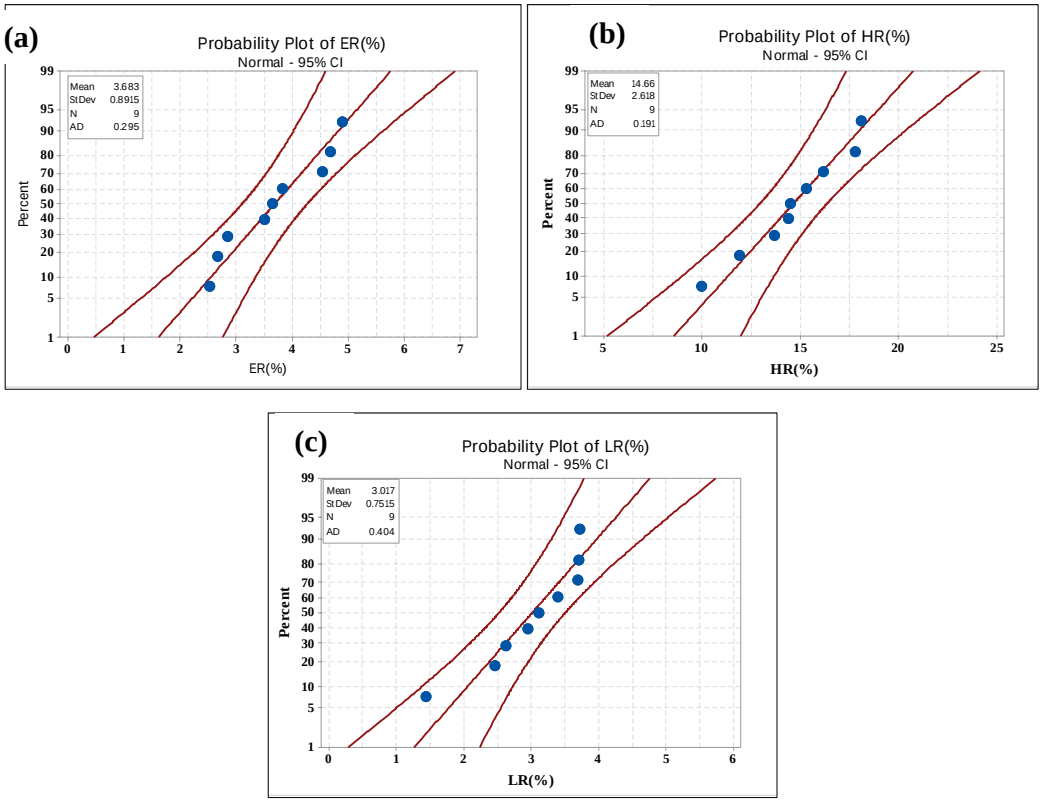

Figure 63. Normal probability plots of (a) ER (%) (b) HR (%) and (c) LR (%)

Table 45. Tensile test results of samples

Sample	Test 1	Test 2	Test 3	Mean	SD
TSF-PLA(MPa)	22.15	19.37	20.76	20.76	1.39
TSF-PLA/CNC (MPa)	27.49	21.91	24.70	24.70	2.79
TS3DP-PLA (MPa)	27.24	20.26	23.75	23.75	3.49
TS3DP-PLA/CNC (MPa)	30.13	23.31	26.72	26.72	3.41
EBF-PLA (%)	5.55	4.15	4.85	4.85	0.70
EBFPLA/CNC (%)	8.23	5.43	6.83	6.83	1.40
EB3DP/PLA (%)	4.94	3.24	4.09	4.09	0.85
EB3DP-PLA/CNC (%)	30.81	26.93	28.87	28.87	1.94
BFF-PLA (N)	43.53	36.47	40.00	40.00	3.53
BFF-PLA/CNC (N)	57.07	42.93	50.00	50.00	7.07
BF3DP-PLA (N)	1576.00	1320.00	1448.00	1448.00	128.00
BF3DP-PLA/CNC (N)	1812.00	1398.00	1605.00	1605.00	207.00
MF-PLA (MPa)	713.87	672.69	693.28	693.28	20.59
MF-PLA/CNC (MPa)	674.45	653.87	664.16	20.76	1.39
M3DP-PLA (MPa)	708.67	450.67	579.67	24.70	2.79
M3DP-PLA/CNC(MPa)	359.55	215.55	287.55	23.75	3.49

^{TS} Tensile strength, ^{EB} Elongation at break, ^{BF} breaking tensile force, ^{M} Elastic modulus

^{F} Filament sample, ^{3DP} 3D printed sample, ^{PLA} pure PLA sample, $^{PLA/CNC}$ composite sample

Table 8. Sources of FT–IR peaks and their assignments

Wavenumber (cm^{-1})	**Bond**	**Vibration**	**Sources**
3425	O–H	Stretching	Cellulose, hemicellulose, lignin and pectin
2917	C–H, $C–H_2$	Stretching	Cellulose, hemicellulose, lignin, pectin, wax and fats
2853	$C–H_2$	Symmetric stretching	wax
1731	C=O	Unconjugated	Hemicellulose, lignin
1636	O–H	Stretching	Absorbed water
1426	O–H, C–H	Bending	Cellulose, hemicellulose and lignin
1383	COO^-	Stretching	Hemicellulose
1157	C–O–C	Asymmetric Stretching	Cellulose, hemicellulose and lignin
1114	C–O	Stretching	Cellulose, hemicellulose and pectin
1032	C–O–C	Bending	Cellulose, hemicellulose, pectin, wax and fats
901	C–O–C	Stretching	Cellulose and hemicellulose
617	C–OH	Out–of–plane bending	Cellulose

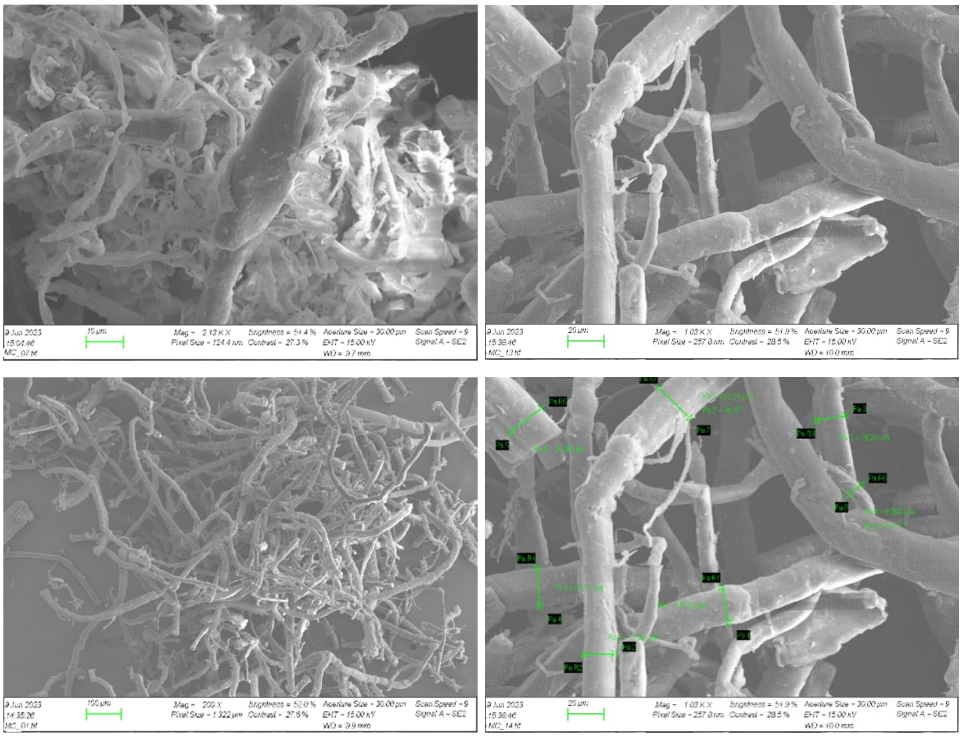

Figure 64. SEM images of MC

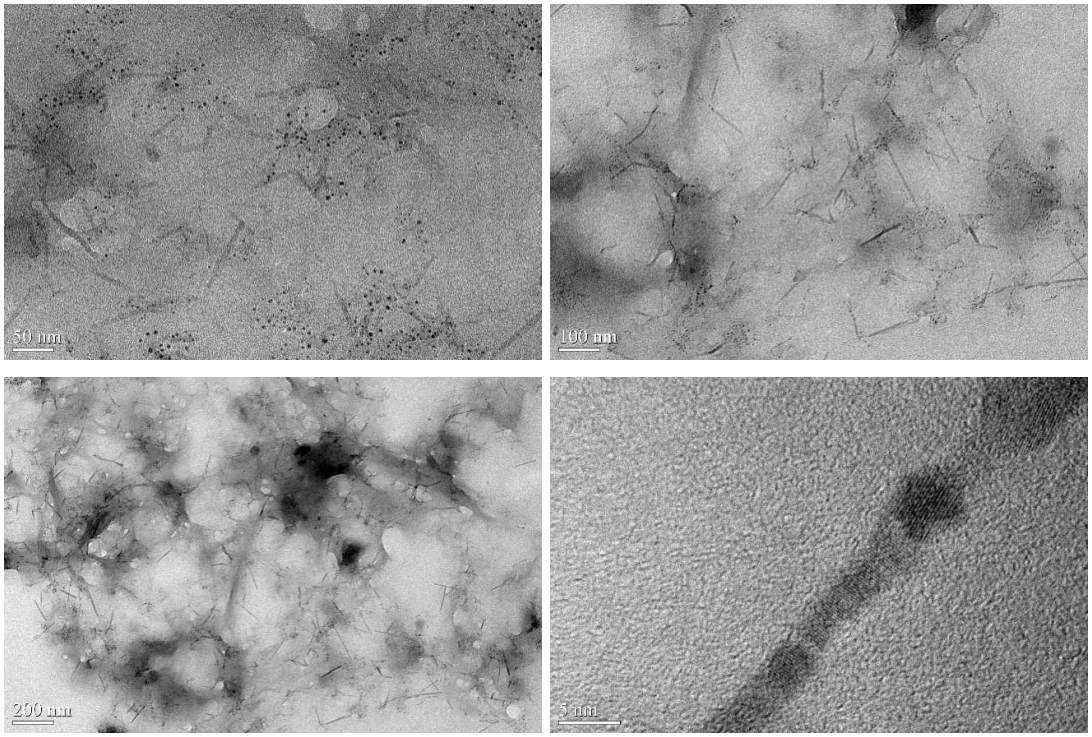

Figure 65. TEM and HRTEM images of CNC

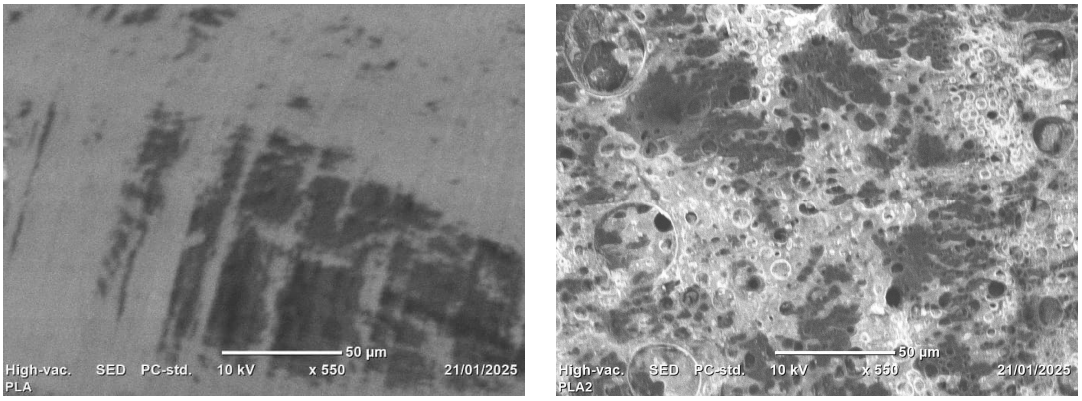

Figure 66. SEM images of pure PLA and PLA/CNC3% 3D printed samples surface morphology

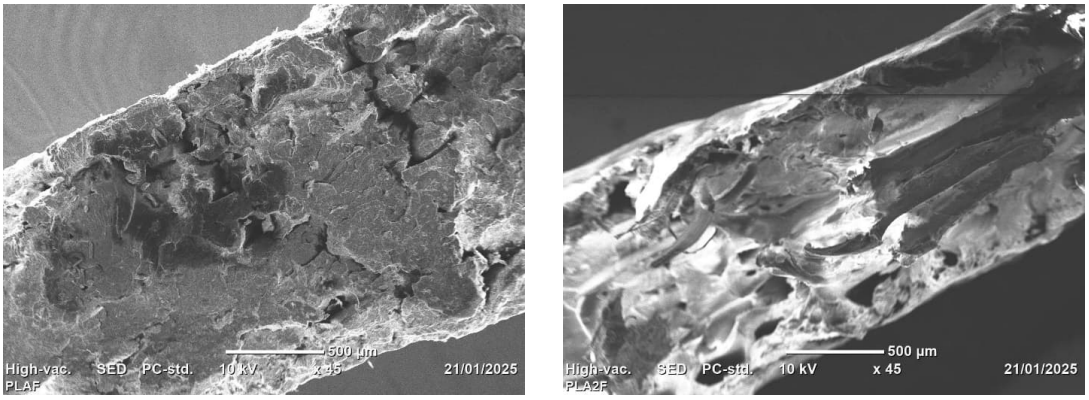

Figure 67. SEM images of pure PLA and PLA/CNC3% 3D printed samples fracture morphology

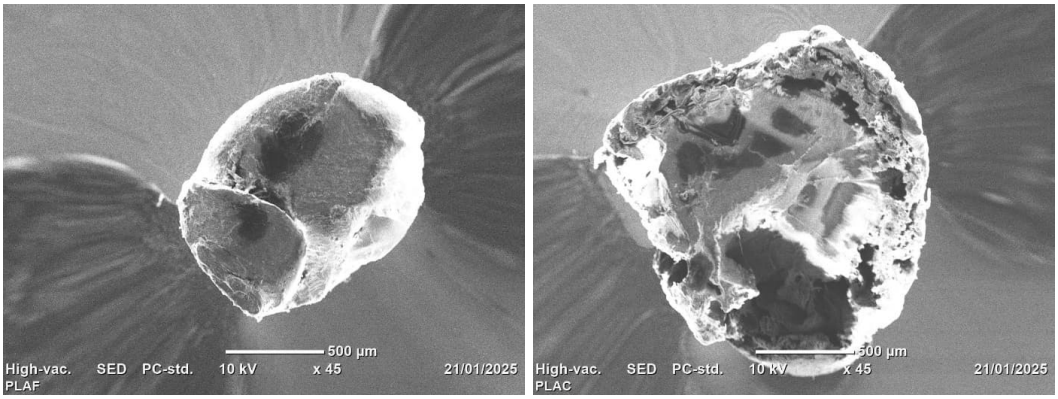

Figure 68. SEM images of pure PLA and PLA/CNC3% filament fracture morphology